DOKUZ EYLÜL UNIVERSITY GRADUATE SCHOOL OF NATURAL AND APPLIED SCIENCES

THE CALIBRATION OF HARDENING SOIL MODELS FOR NORTHERN İZMİR BAY AREA SOILS

by

Nihal BENLİ

November, 2008

İZMİR

THE CALIBRATION OF HARDENING SOIL MODELS FOR NORTHERN İZMİR BAY AREA SOILS

A Thesis Submitted to the
Graduate School of Natural and Applied Sciences of
Dokuz Eylül University
In Partial Fulfillment of the Requirements for
the Degree of Master of Science in Civil Engineering, Geotechnics Program

by
Nihal BENLİ

November, 2008
İZMİR

M.Sc THESIS EXAMINATION RESULT FORM

We have read the thesis entitled **"THE CALIBRATION OF HARDENING SOIL MODELS FOR NORTHERN İZMİR BAY AREA SOILS"** completed by **NİHAL BENLİ** under supervision of **ÖĞR. GÖR. DR. MEHMET KURUOĞLU** and we certify that in our opinion it is fully adequate, in scope and in quality, as a thesis for the degree of Master of Science.

Öğr. Gör. Dr. Mehmet KURUOĞLU

Supervisor

Doç. Dr. Gürkan ÖZDEN

(Jury Member)

Prof. Dr. M.Yalçın KOCA

(Jury Member)

Prof.Dr. Cahit HELVACI

Director

Graduate School of Natural and Applied Sciences

ACKNOWLEDGEMENTS

First, I want to thank my dear family for their help and continuous support; this thesis would never be finished without them. They mean everything for me. I thank to my supervisor Dr. Mehmet Kuruoğlu for helping me at my thesis on Geotechnics Program. I am also very thankful to Prof. Arif Şengün Kayalar because of his contributions, guidance and constructive criticisms for my thesis as my co-supervisor. Also, I am thankful to Asst. Prof. Dr. Gürkan Özden for teaching us new issues about geotechnics, so I could be knowledgeable about geotechnical studies in the world. In particular, I am grateful to Prof. Dr. Yalçın Koca for unlimited help, advice and support in my life.

In my life, I'm so grateful to Sultan Kaykanat, who is the teacher of my primary school, for earn my identity like other my whole classmates. The teachers and master of Şehit Konuk Primary school have always kept our idol in our life. Everytime, they believe us.

Especially, I wish to thank my friends for helping me. Without their help and support, I could not complete my thesis. For the editing, I am thankful to Sinem Partigöç and Murat Özkan who are students of City & Regional Planning and reseacher of Computer Engineering of İzmir Institute of Technology. When I came to the school, Sadık Can Girgin and Ezgi Aykoç were concerned and listened to me, so their friendness is very important for me. However, I'm grateful to Abdullah Özcan and Enver Yurdam for upon their copyroom's door, and also at their comprehension and tolerance. I cannot forget to thank my classmate Kubilay Öztürk for sharing his knowledge with me.

I wish to thank my friends in the Production Management Department, who called me for helping and building morale. Their names are Şeniz Yılmaz, Levent Ayvaz, Cem Acar, Gökhan Bilekdemir and Ayşe Koca. They are engineers in different departments. However, I'm grateful to Asst. Prof. Dr. Hüseyin Avunduk, who is my

supervisor of Production Management, for specializing me in material management and project management. I'm thankful to Asst. Prof. Dr. Ethem Duygulu for specializing us in management and organization. I want to thank other teachers in the Production Management Department, like Prof. Dr. Saime Oral, Prof. Dr. Oya Yıldırım, Prof. Dr. Berna Taner, Prof. Dr. Üzeyme Doğan, Prof. Dr. Ömer Baybars Tek, Prof. Dr. Muammer Doğan, Asst. Prof. Dr. Özlem İpekgil Doğan and Asst. Prof. Dr. Hilmi Yüksel. They believe us to be successful in our life.

Dr. Selim Baradan from Aegean University, Assoc. Prof. Dr. H. Murat Günaydın from İYTE Architecture Department, Civil Engineer Dr. Hüseyin Kırbaş –who has the master of production management program and doctor of geotechnic-, and General Manager of Soyak Company, Emre Çamlıbel have given me hope for accomplishing this thesis, I want to thank them for their guidance and support.

Moreover, people who helped me in my hardest times, are my sister Architect Nuray Benli, my cousin Funda Kaya, my cousin Zafer Kumran, Lawyer Özgür Deniz, Restorator Architect Bahar Sintaç and my sister Süheyla Partigöç are very important for me and I am thankful to them.

Nihal BENLİ

THE CALIBRATION OF HARDENING SOIL MODELS FOR NORTHERN İZMİR BAY AREA SOILS

ABSTRACT

Research for new models for expressing the real soil behaviour has been considered by scientists, because of the lack of accuracy of elastic or elasto-plastic models. The majority of these new models tend to define hyperbolical curve behaviour, which is also called “hardening soil model”.

In this study, the hardening characteristics of the sedimentary soils in Northern İzmir Bay area are investigated. The experimental data belong to the site investigation studies that were made for the site fill of the coastal road along Karşıyaka-Alaybey-Bostanlı route. The soil mechanics laboratory data was back analyzed using single hardening model of the Plaxis software so that model parameters are calibrated or classified to give the best fit with the odeometer test results.

Although effort has been spend on obtaining analysis results that were in good match with the test data, there were still some scattering in the results. The Janbu method within Plaxis yields a smooth parabolic curve from odeometer results while the data of Northern İzmir bay area resembles more like a detached parabola with two different slopes. Comments are made about the good match and scattering of the finite element analysis results, recommendations are made for future work.

Keywords: Hardening soil model, Finite elements method, Plaxis, Odeometer, Northern İzmir Bay

İZMİR KÖRFEZİ KUZEY KIYI ZEMİNLERİ İÇİN PEKLEŞEN

ZEMİN MODELLERİNİN KALİBRASYONU

ÖZ

Bilimadamları tarafından gerçek zemin davranışını tanımlamak için elastik veya elasto-plastik modeller eksik kalması sebebiyle yeni modellerin araştırması göz önünde tutulmaktadır. Bu yeni modellerin çoğunluğu, hiperbolik eğri davranışı gösteren zemin davranışını tanımlamaya yöneliktir; bu davranışa 'pekleşen zemin modeli' denir.

Bu çalışmada, İzmir körfezi kuzey kıyılarına ait tortul zeminler pekleşme karakterleri incelenmektedir. Karşıyaka – Alaybey – Bostanlı hattı üzerindeki sahil yoluna ait saha dolgusu için yapılan deney verilerine aittir. Zemin mekaniği laboratuvar verileri, Plaxis bilgisayar programının basit pekleşen zemin modeli anaizinin kaynağı olmuştur; böylece model parametreleri ödometre deney sonuçları vasıtasıyla en iyi uyumu veren kabrasyonun edilmektedir veya sınıflandırılması yapılmaktadır.

Deney verilerinin iyi gözlenmesinde elde edilen analiz sonuçları üzerinde, mevcut verilerle tam olarak uyum sağlamamıştır. Plaxis programı içindeki Janbu metodu, düzgün bir parabolik odeometre sonucu vermesine rağmen; İzmir körfezi kuzey kıyılarına ait veriler daha çok iki ayrı eğimden gelen kırıklı bir parabolu anımsatmaktadır. Sonlu eleman analiz sonuçlarının iyi gözlenmesi ve dağılımı hakkında yorumlar yapılmıştır, gelecek işler için yeniden değerlendirilmesi yapılmıştır.

Anahtar Sözcükler: Pekleşen zemin modeli, Sonlu elemanlar metodu, Plaxis, ödometre, Kuzey İzmir Körfezi

CONTENTS

Page

CHAPTER ONE

INTRODUCTION

Traditional constitutive models such as Mohr-Coulomb and Drucker-Prager usually fail to model the hardening behaviour of the soils during excavation. Therefore, researchers worked on this issue and they proposed the hardening model. Hardening model is associated with observing the incremental stress. There are several discussions and published literature about hardening soil models. Despite due effort, scientists still have not reached a common model. Applicability of non-associated hardening soil model is sought in this thesis to model hardening behavior of Northern İzmir Bay Area soils.

1.1 Objective and Scope

The aim of this research is to evaluate the behaviour of Northern İzmir Bay area soils in the framework of hardening soil models. The finite element method is used to solve the problem with advanced soil model. Among commercial software, PLAXIS is preferred for this purpose because it is commonly used in this area.

Database has been prepared from oedometer tests that were available in "The Report of Soil Experiments Belonging to the Coastal Road of Karşıyaka-Alaybey-Bostanlı Route", a site investigation study made for the Northern İzmir Bay Area in 1984. Firstly, soil behaviour in the experimental data was observed, and best applicable hardening model parameters expressing the test data as much as possible were obtained.

1.2 Outline of the Thesis

Chapter II contains the literature review and background about the constitutive models of materials and soil material. Various models, associated or non-associated, are briefly mentioned in the chapter. The use of the hardening soil model parameters in the Plaxis software is explained in detail.

Chapter III emphasizes the analysis of data of the oedometer tests in finite element analyses. The results of oedometer tests are expected to establish relations with PLAXIS analyses. When the research is introduced, the pre-assumption is given for initial point.

Chapter IV includes the conclusion of this research and recommendations for further development.

CHAPTER TWO

LITERATURE REVIEW AND BACKGROUND

2.1 Definition of Soil Models

Various soil constitutive models resulted from the desire to represent actual soil behaviour in finite element analyses as much as possible. Soil properties are generally named as soil texture, grain size and distribution, particle shape, Atterberg limits, soil classification and shear strength parameters. However, modeling of stress-strain behavior of the soils require definition of the stiffness properties in addition to the above (Huybrechts, De Vos, Whenham, 2004).

The principal properties of soil parameters that are placed in the utilized finite element software can be summarized as:

- The type of the modeled soil like clay or sand
- The soil stress-strain characteristics for a particular geotechnical problem like stiffness, deformation, strength, dilation, etc.
- The drainage conditions (i.e. undrained and drained)
- The availability of soil data from which the hardening parameters are derived.

In general, softwares support simple constitutive models for the illustration of soil behaviour. This is best reflected by the assumption of isotropic soil behavior, which is a major simplification over the usually anisotropic stress-strain characteristics of most soils.

2.2 Constitutive Models

In general, the soil behaviour is expected to be described using a model. So, many researchers intented to work on this issue and have developed several constitutive models which stipulate to reach approximately the experimental data about the real soil behaviour using models such as Von Mises model, Mohr-Coulomb model, Drucker-Praker model, Brisier-Pister model, Chen-Chen model, Hsieh-Ting-Chen model, Willam-Warnke model, Ottosen model and Hoek-Brown model. These models reach the failure condition in some manner and have different characteristics from each other (Chen, 1985) as shown in Figure 2.1.

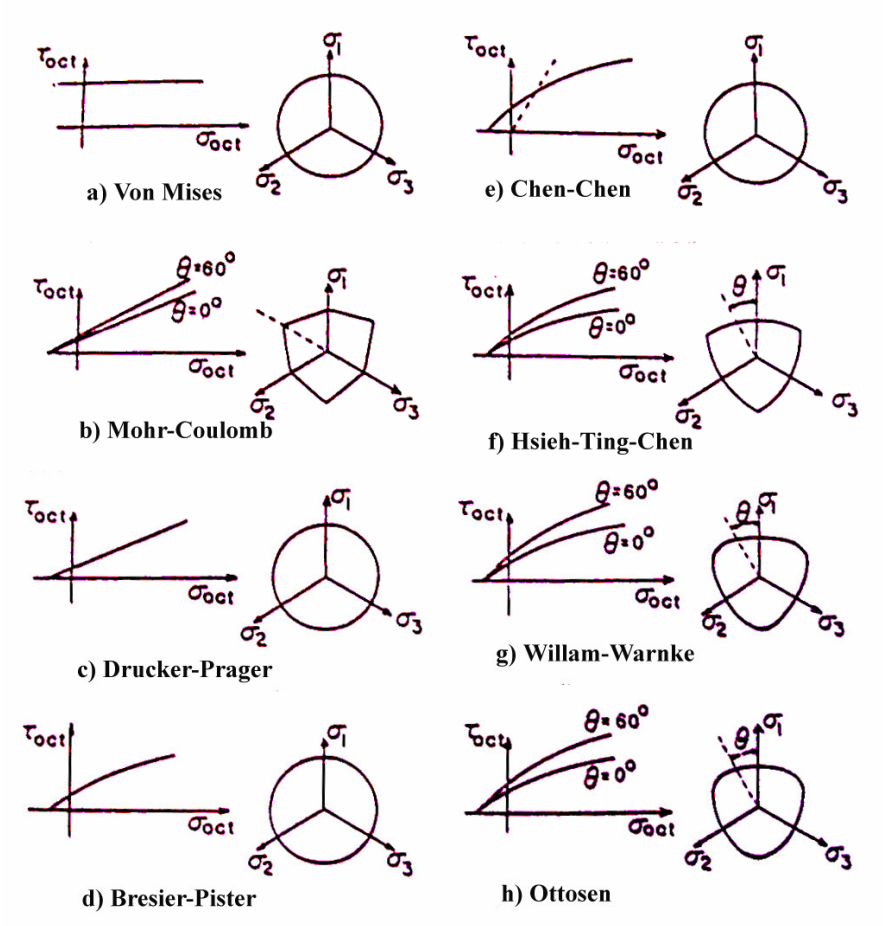

Figure 2.1 Failure Models (after Chen, 1985).

The above stated models are used in the stress space. Hydrostatic line is plotted on the principle stress axis that is shown by the red line in Figure 2.2. Therefore, hydrostatic line is represented by octahedral normal stress axis and the relationship between octahedral normal and shear stresses is established with these models. Newmark (1960) has suggested the usage of stresses and strains in octahedral plane for soils, who assumes a three-dimensional relationship between stress and strain. The idea about the three-dimensional relationship is developed for linear material that is not only homogenous and isotropic, but also extends and relations between stress and strain at a translated point in a homogeneous, isotropic and nonlinear material .

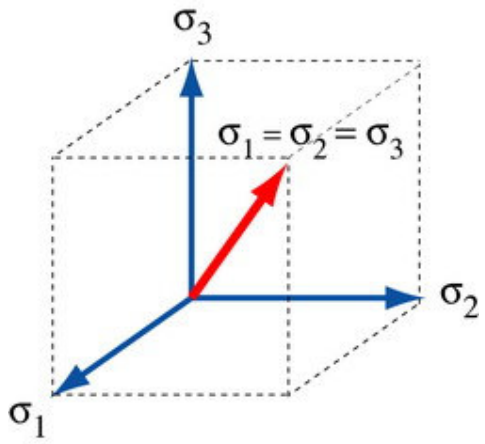

Figure 2.2 Hydrostatic Line

The octahedral normal and shear stresses are given as the measures of hydrostatic and deviatoric components of the state of stress;

$$\sigma_{oct} = \frac{\sigma_1 + \sigma_2 + \sigma_3}{3} \tag{2.1}$$

$$\tau_{oct} = \frac{1}{3}\sqrt{(\sigma_1 - \sigma_2)^2 + (\sigma_2 - \sigma_3)^2 + (\sigma_3 - \sigma_1)^2} \tag{2.2}$$

in which σ_{oct} and τ_{oct} represent the octahedral normal and shear stresses, respectively.

The octahedral components of strain are;

$$\varepsilon_{oct} = \frac{\varepsilon_1 + \varepsilon_2 + \varepsilon_3}{3} \tag{2.3}$$

in which ε_1 ε_2 and ε_3 are the principal strains. The octahedral γ_{oct} is a measure of distortion or the change in shape.

$$\frac{1}{2}\gamma_{oct} = \frac{1}{3}\sqrt{(\varepsilon_1 - \varepsilon_2)^2 + (\varepsilon_2 - \varepsilon_3)^2 + (\varepsilon_3 - \varepsilon_1)^2} \tag{2.4}$$

These formulations are valid for metal and concrete, but not for soils since soil, which is composed of solid particles, water, and air, experiences volume changes during shear deformation (Girijavallabhan & Reese, 1968).

Bell (1965) has shown a value difference of strain between one dimensional compression test and hydrostatic stress, which has elasticity at relationship of axial stress – strain diagram with using sand and acquired the experiment in Figure 2.3. The concave arm of the hydrostatic stress on the stress-strain curve is higher than the concave arm of the one dimensional compression on stress-strain curve. In other words, curve B have very little increase in the axial strain for higher values of the axial stress. In triaxial compression test, the cell pressure is accepted as a constant, and the axial stress is increased to arrange the test conditions. There are two important results of test. Firstly, a large deformation both axially and laterally at curve C occurs and secondly, the effect of deviatoric stress is calculated to be greater than the hydrostatic stresses' effect.

As another model study, the Mohr-Coulomb Model includes the general aspects of soil behaviour. However, the model has a characteristic which compromises an unrealistic prediction of the stress-strain relation for the geotechnical problems, especially under the undrained and partially drained conditions (Huybrechts, De Vos, Whenham, 2004).

Finally, the Constitutive Model provides the main path of these changes on the stress-strain relation and also imposes the upper / lower limits, like failures or yield surfaces .

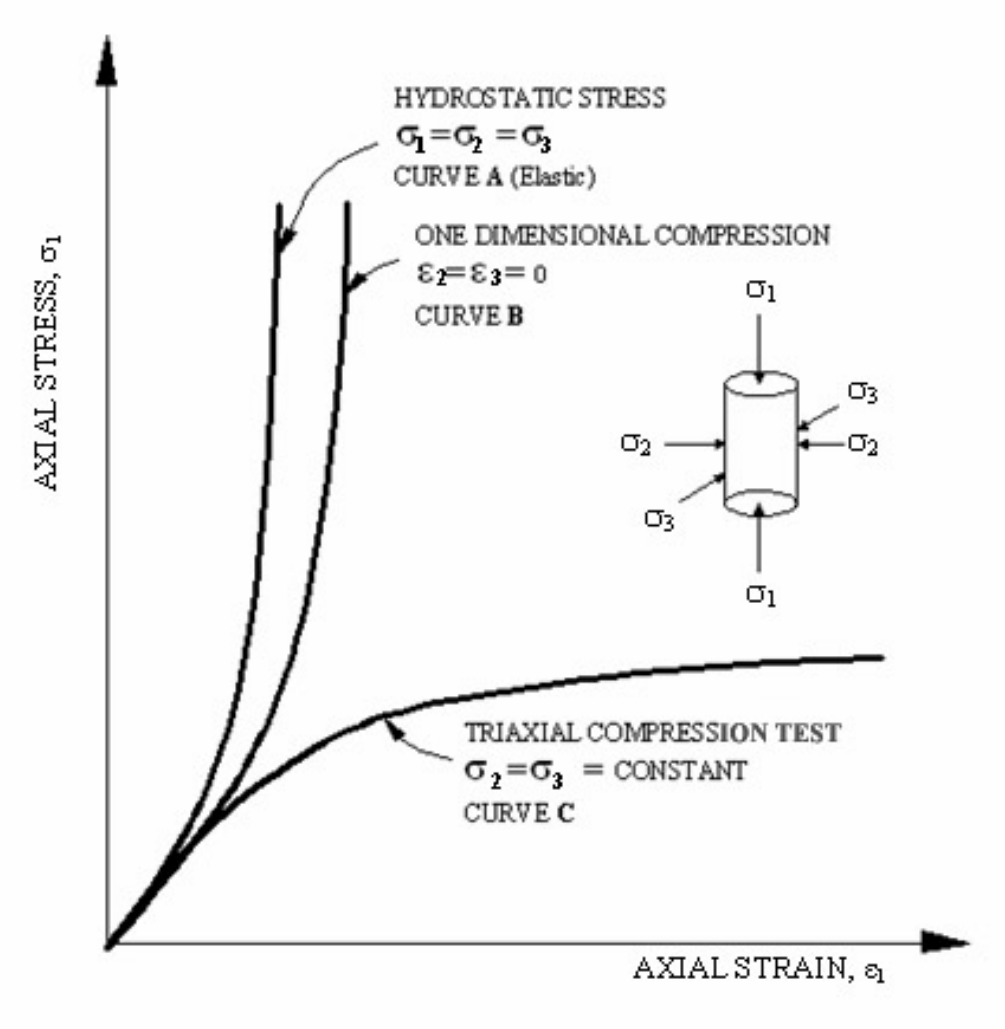

Figure 2.3 Axial stress – strain curves for soils under varied states of stress (After Girijavallabhan & Reese, 1968)

2.3 First Generation of Material Constitutive Models

The soil mechanics have based on the linear elasticity for the stress-strain analysis of soil mass under a footing or behind a retaining wall for a long time, so that the soil model have not a failure line. Failure problem is overcomen by elasto-plastic model (Al-Buraim, 1990).

2.3.1 Elastic Models

Robert Hooke had proposed a form in 1676. Hooke was concerned with springs instead of three-dimensional continuous bodies, and he simply stated that the force needed to extend the spring was a linear function of the amount of extention (Davis&Selvadurai, 1996). The law is known with his name. The general equation of Hooke's Law is;

$$\sigma = E\varepsilon \tag{2.5}$$

where σ is stress, E is modulus of elasticity, and ε is strain. The simplest relationship between stress and strain is described with 'the linear relation'.

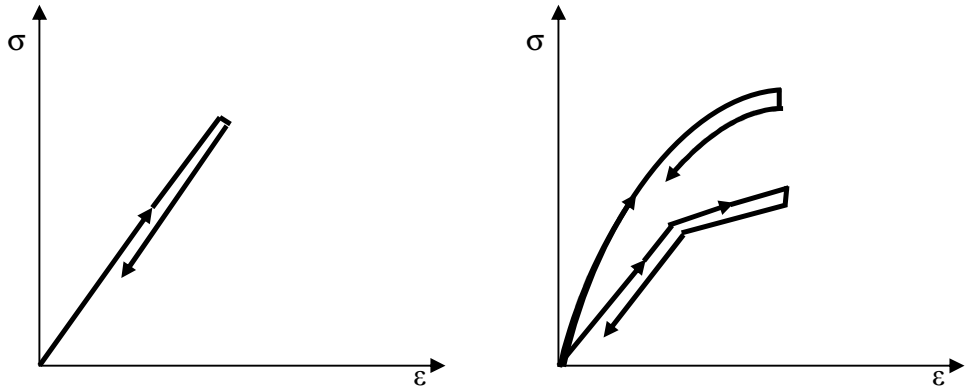

Figure 2.4 a) Linear elastic model, b) Non-linear elastic model (bilinear and hyperbolic)
(After Huybrechts, De Vos, Whenham, 2004)

Actually, instead of the linear models, the non- linear elastic models are better, according to the stress-strain behaviour of soil (see Fig.2.4). Only two are needed to fully describe the elastic behaviour of an isotropic body. They are modulus of elasticity (*E*) and Poisson's ratio (*v*). For example, for an isotropic body, lateral strains (ε_{yy} and ε_{zz}) are equal and linear functions of ε_{xx}. It is stated as;

$$\varepsilon_{yy} = \varepsilon_{zz} = -v\varepsilon_{xx} \tag{2.6}$$

It is substituted Hooke's law instead of ε_{xx} in Eq (2.6).

$$\varepsilon_{yy} = \varepsilon_{zz} = -\frac{v}{E}\sigma_{xx} \tag{2.7}$$

ε_{xx} is also written;

$$\varepsilon_{xx} = \frac{1}{E}\left[\sigma_{xx} - v\left(\sigma_{yy} + \sigma_{zz}\right)\right]. \tag{2.8}$$

2.3.2 The Elasto-Plastic Model

In general, soil undergoes both elastic and plastic deformations upon loading. A realistic constitutive model of soil behaviour must perform to distinguish between the elastic and plastic deformations.

By using the elasto-plastic, the failure problem which is translated from the initial linear elastic state to the ultimate state of the soil by plastic flow is concluded (Al-Buraim, 1990). Elastic-plastic models are based on the assumption that includes the principal directions of accumulated stress and incremental plastic strain (see Fig.2.5).

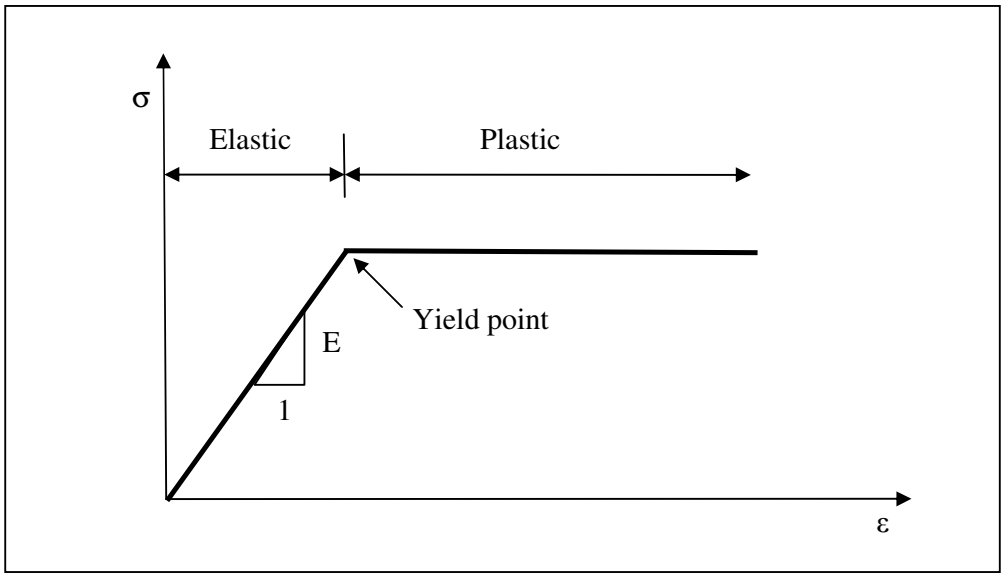

Figure 2.5 Elastic – Perfectly Plastic Model (After Huybrechts, De Vos, Whenham, 2004)

2.3.3 Second Generation of Material Constitutive Model

Figure 2.6 shows a typical uniaxial stress-strain diagram for plain concrete in the compression range. It's important to understand all constitutive models of materials. *A* point is limited to the linear elastic behaviour, and then the material structure weakens slowly towards *C* point. The curve, that lies between *A* and *C* points, exhibits the hardening behaviour. Also, the horizontal line between *C* and *D* represents the perfectly plastic behaviour. Ductile occurs at the *D* point. After the *D* point, the material passes to the softening behaviour to create the crushing. At the *B* point, the material's behaviour is represented under unload - reload conditions and total deformation is shown on the figure. The slope of line at the *B* point gives the elastic deformation, that is also called 'plastic deformation' and the total deformation is subtracted. According to the *B* point, which approaches to the *A* or *C* point, the amount of the plastic deformation is changed (Chen, 1985).

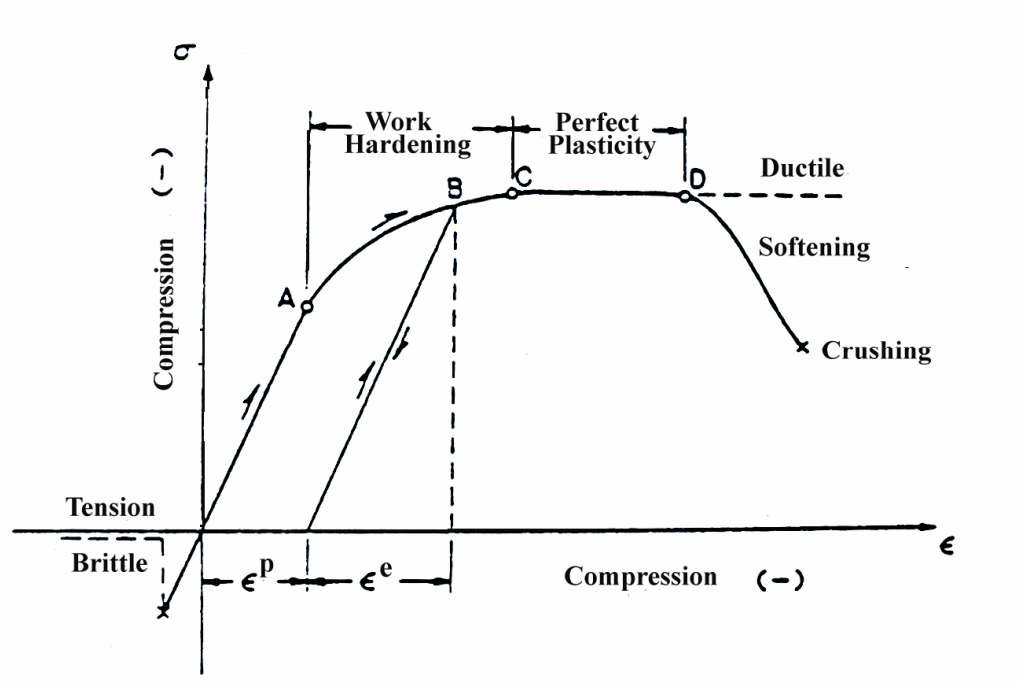

Figure 2.6 Schematic uniaxial stress-strain curve for plain concrete (After Chen, 1985)

Figure 2.7 illustrates the relation between the increases of stress and strain that is developed by Prager and his colleagues in 1950's. The relation involves the formal division of the strain rate ($\delta\varepsilon_T$) caused by changes in stress ($\delta\sigma_{ij}$) into elastic ($\delta\varepsilon_e$) and plastic ($\delta\varepsilon_p$) components.

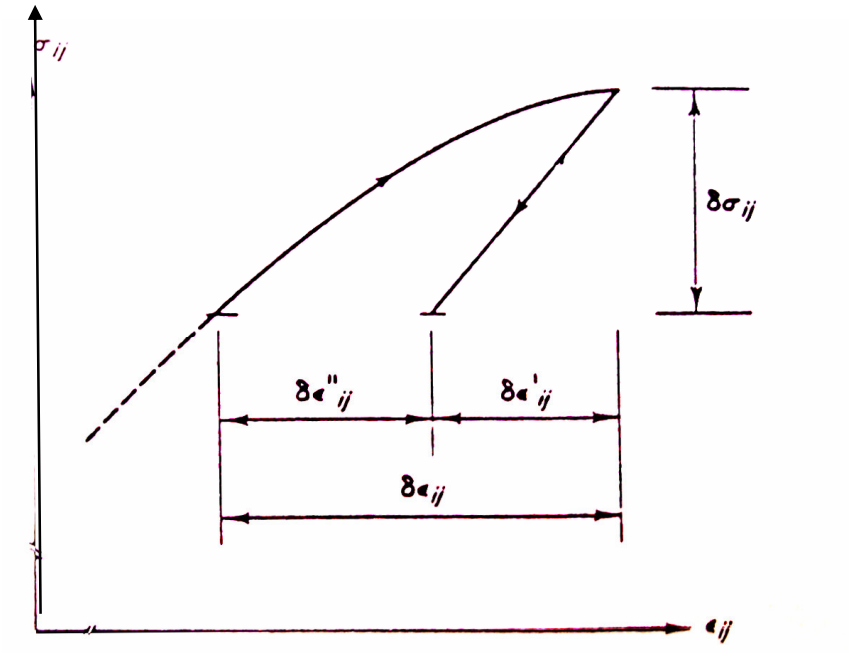

Figure 2.7 The decomposed of total strain (After Dougill, 1985)

As another notation about the strain of the basic Elastic-Plasticity Theory, the total strain rate ($\dot{\varepsilon}$) can be decomposed additively in an elastic (reversible) part ($\dot{\varepsilon}^e$) and a plastic (irreversible) part ($\dot{\varepsilon}^p$); (Amorosi, Boldini & Germano, 2007):

$$\dot{\varepsilon} = \dot{\varepsilon}^e + \dot{\varepsilon}^p$$

In the content of the Hooke's laws, the stress rate is related to the elastic strain rate in the total strain rate. Hooke's law applies as below:

$$\dot{\sigma}' = D^e.\dot{\varepsilon}^e = D^e.(\dot{\varepsilon} - \dot{\varepsilon}^p) \qquad (2.9)$$

where, D^e is the elastic stiffness matrix.

Soil undergoes both elastic and plastic deformation when subjected to load. The geotechnical problems include the bearing capacity of a shallow foundation, slope stability and tunnel stability. Bilinear elasto-plastic model is improved after elastic and elasto-plastic model.

At linear elastic–perfect plastic model, the first behaviour of a material have elastically linear relation until the yield point on stress-strain relation, afterwards the material shows continuous plastic yielding (plastic flow) under constant stress. There is no hardening behaviour (see Fig. 2.8.a). If plastic stiffness parameter of material is H, H will be zero. Another type of plastic behaviour is given on Figure 2.8.b, and first behaviour of the material is similar to the linear elasto–perfectly plastic model. After the yield point, if plastic stiffness H is greater than zero, it refers to the strain hardening. Another alternative is plastic stiffness, occurs when H is less than zero, its behaviour will be strain softening (Abed, 2008).

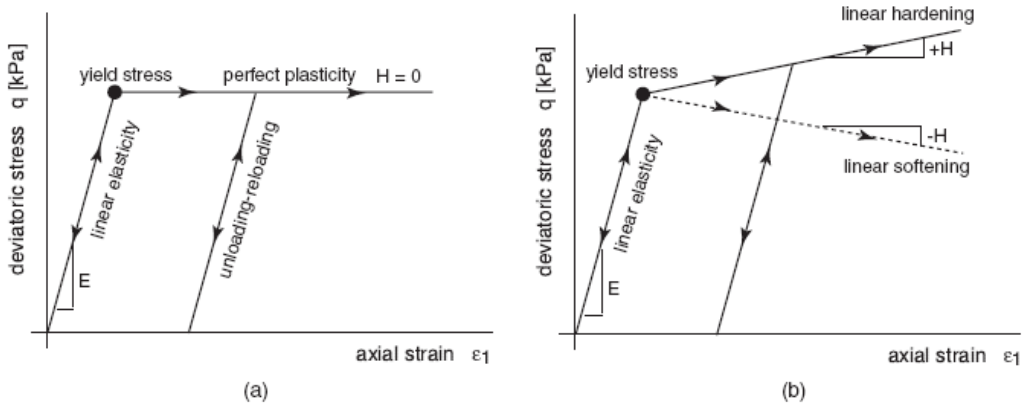

Figure 2.8 a) Perfect plasticity b) Linear strain hardening or softening plasticity (After Abed, 2008)

2.3.4 Simple Hyperbolic Model

David Wood has emphasized to 'Critical State Soil Mechanics' in his book called "Soil Behaviour and Critical State Soil Mechanics" (Boscan, 1998).

Firstly, Clough has developed appropriate non-linear or inelastic soil behaviour using high-speed computers and powerful numerical analytical technique, such as the

finite element method developed in 1960's. The non-linear analysis shows better performance than the analysis of the elasticity and the elastic-perfectly plastic models. Then, many studies of scientists who work on the soil behaviour are referenced to find the best definition of non-linear model for the stress-strain of all types of soil.

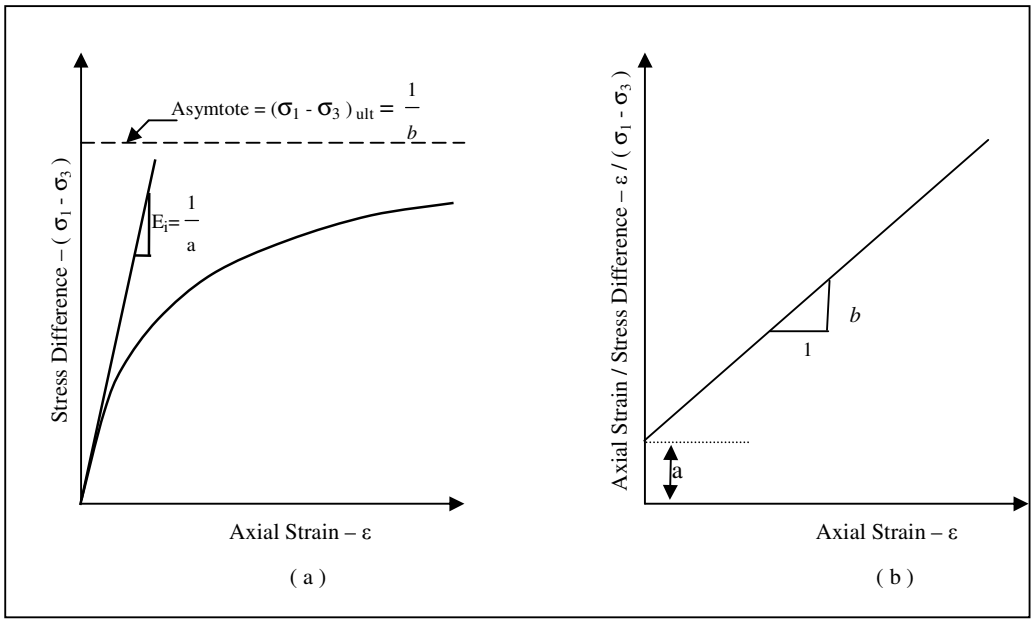

Figure 2.9 (a) Hyperbolic stress-strain curve (b)Transformed hyperbolic stress-strain curve (After Duncan & Chang, 1970)

Kondner and coworkers (1963) have focused on non-linear stress – strain curves of both clay and sand by developing a hyperbolic approach. The proposed hyperbolic equation is,

$$(\sigma_1 - \sigma_3) = \frac{\varepsilon}{a + b\varepsilon} \qquad (2.10)$$

in which σ_1 and σ_3 are respectively the major and minor principal stresses; ε is axial strain; and both a and b are constants which are visualized the physical measurements on the graphic of hyperbolic stress-strain curve. In Figure 9. a is illustrated as the reciprocal of initial tangent modulus, E_i; and constant b is the reciprocal of the asymptotic value of stress difference that is ultimate stress difference $(\sigma_1 - \sigma_3)_{ult}$ when the stress-strain curve approaches at infinite strain. The

hyperbolic equation is rewritten to plot a straight line for the constants a and b, on graphic in Figure 2.9 and the equation is shown in the following form:

$$\frac{\varepsilon}{(\sigma_1 - \sigma_3)} = a + b\varepsilon \tag{2.11}$$

Asymptotic value of the strength $(\sigma_1–\sigma_3)_{ult}$ is expected to decrease the value for closing to the compressive strength of the soil. Another constant is needed which includes R_f for determination of the stress difference at the failure.

$$(\sigma_1–\sigma_3)_f = R_f\,(\sigma_1–\sigma_3)_{ult} \tag{2.12}$$

where $(\sigma_1–\sigma_3)_f$ is stress difference at failure, $(\sigma_1–\sigma_3)_{ult}$ is the asymptotic value of stress difference, and R_f is the failure ratio which is always less than 1. The value of R_f stays between 0.75 and 1.00 and selected by importing to the confining pressure.

The constants a and b are defined by using initial tangent modulus (E_i) and the compressive strength. The equation can be rewritten as,

$$(\sigma_1 - \sigma_3) = \frac{\varepsilon}{\left[\frac{1}{E_i} + \frac{\varepsilon.R_f}{(\sigma_1 - \sigma_3)_f}\right]} \tag{2.13}$$

Moreover, Janbu (1963) has proved the relationship between the initial tangent modulus (E_i) and the confining pressure with experimental studies. It's expressed as;

$$E_i = K \cdot p_a \left(\frac{\sigma_3}{p_a}\right)^n \tag{2.14}$$

in which E_i is the initial tangent modulus; σ_3 is the minor principal stress; p_a is the atmospheric pressure expressed in the same pressure units as E_i and σ_3; K is a

modulus number; and n is the exponent determining for the rate of the variation of E_i with σ_3.

Actually, Duncan and Chang (1970) have used the formulation of Kondner and Janbu on their studies. A new non-linear model is developed by including the tangent modulus for using the finite element model from the experimental data.

2.3.5 Hardening Soil Model

The hardening soil model is an elasto-plastic type of the hyperbolic model. There are three types of hardening rules which are commonly used to define the behaviour of soil: Isotropic, kinematic, and mixed hardening. The isotropic hardening represents a uniform expansion of the yield surface in all direction, while the kinematic hardening symbolizes a simple means of accounting the plastic anisotropy, i.e., During the plastic flow, the yield surface is translated as a rigid body, with maintaining its size, shape and orientation. Finally, the mixed hardening means a combination of the isotropic and kinematic hardening. The available finite element code does not support the mixed hardening, so it is only limited to an isotropic hardening (Kempfert, & Gebreselassie, 2006).

The hardening soil model of cap that is closed to the Mohr-Coulomb type yield surface is allowed to expand during the plastic strain. Both the shear locus and the yield cap have the hexagonal shape of the classical Mohr-Coulomb failure surface.

The yield function defines stress as the material responses while it changes from elastic to plastic. In Figure 2.10, the elastic-plastic strain hardening model is illustrated, which resembles the soil behaviour in the oedometer test. The model deals with the swelling behaviour which happens during the elastic unload–reload loop.

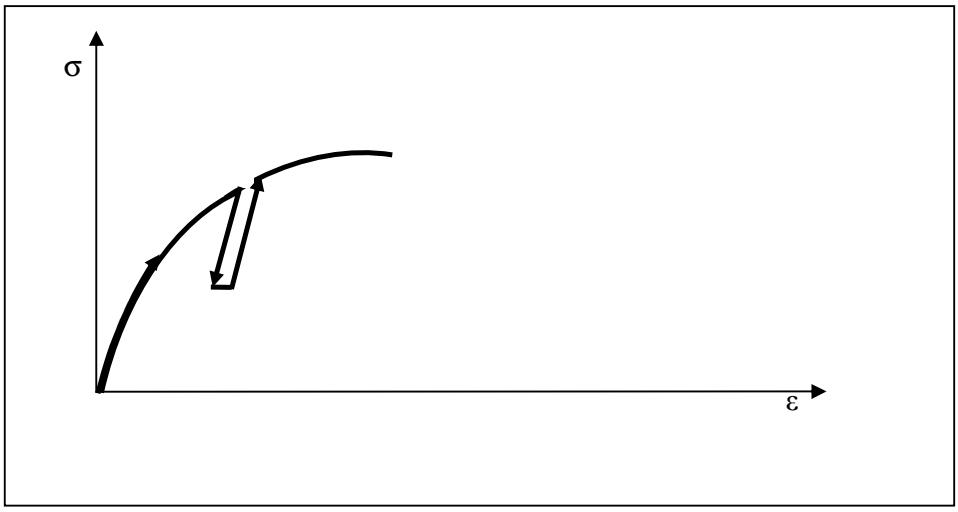

Figure 2.10 Elastic – plastic strain hardening model (After Huybrechts, De Vos, Whenham, 2004)

2.3.5.1 Isotropic Hardening Model

The deformation is explained with the decombination of reversible and irreversible. The definition is achieved using a well-defined curve known as the yield locus located in a shear stress – normal stress space. It is represented on the above Figure 2.7.

Hardening soil models are not based on the Mohr-Coulomb failure criterion, although the slope of the CSL can be correlated with angle of internal friction at the critical state. However, some of these models give a unique strain response to an increment of stress but do not give a unique stress response to an applied strain increment like cam-clay model.

Firstly, the yield surface on p-q axes is designated. Then the center of the ellipse is transported to center of axes and ellipse is rotated the smooth ellipse, as pointed out in Figure 2.11.

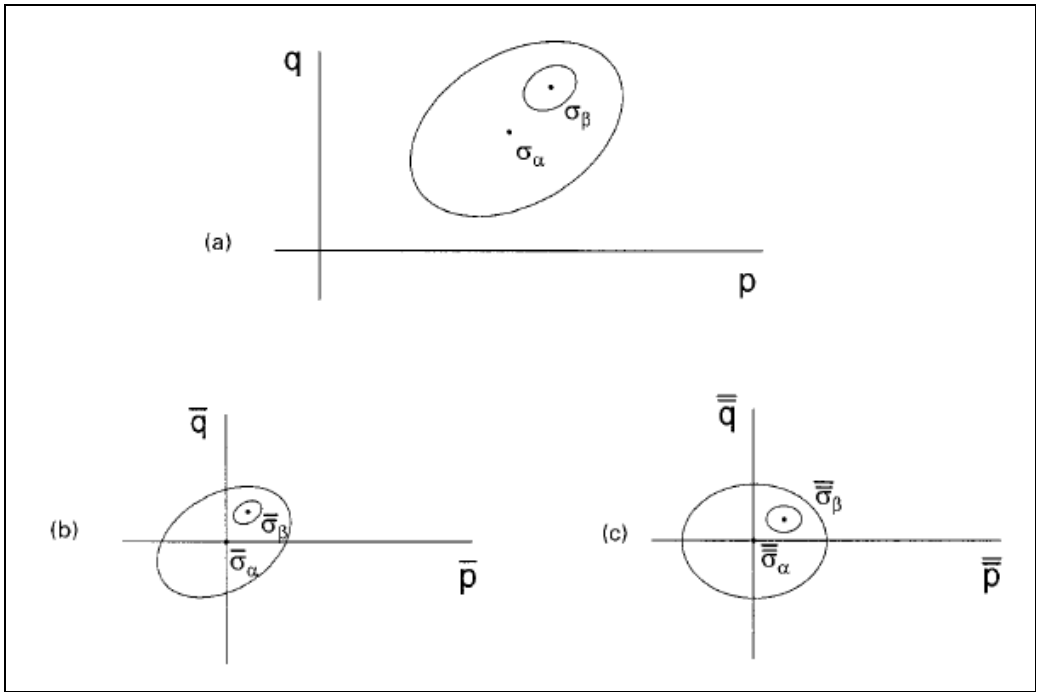

Figure 2.11 Schematic diagram of the (a) ‘real', (b) ‘intermediate normalized' and (c) ‘normalized' stress spaces in q-p plane (After Gajo & Muir Wood, 2001)

This process is called as ‘normalized’ stress in p-q plane. In Figure 2.12 also shows CLS and NCL criterions. CLS means ‘Critical Satete Line’. Its left side means softening, while its right side shows hardening. NCL is ‘Normal Compression Line’.

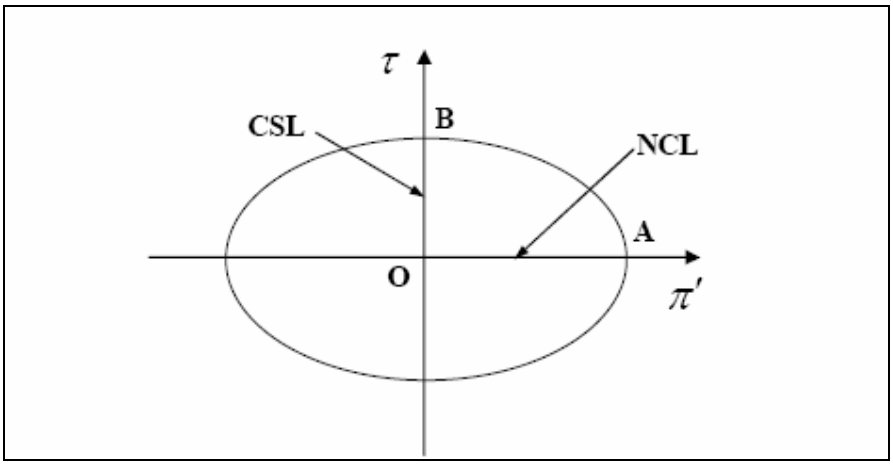

Figure 2.12 Yield locus in dissipative stress space (After Uchaipichat, 2005)

Another name of the isotropic hardening model is 'single hardening model'. it is illustrated on Figure 2.13. Then, the single hardening formulation is given by the following part:

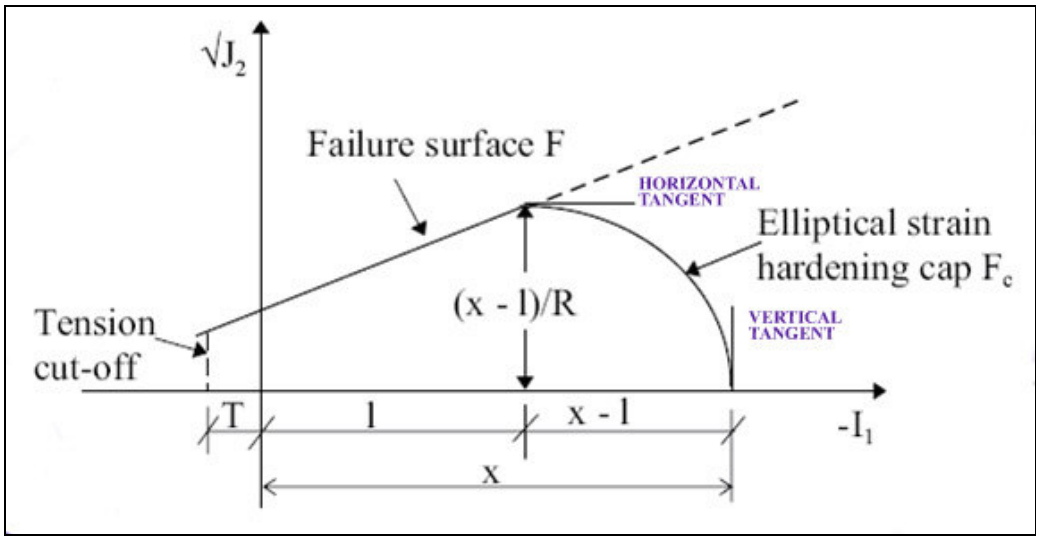

Figure 2.13 Cap model with elliptic hardening surface (After Kempfert & Gebreselassie, 2006)

$$\sqrt{J_2} + \alpha I_1 = k \tag{2.15}$$

And a strain-hardening cap takes the form of quarter of an ellipse,

$$F_c = (I_1 - l)^2 + R^2 . J_2 - (x - l)^2 \tag{2.16}$$

Where;

α, k = The material constant related to c, φ of Mohr-Coulomb criterion

l = The value of I_1 at the center of elliptic cap

R = The ratio of major / minor axis of elliptic cap or a constant aspect ratio of the cap

x = The hardening function that effectively controls the material compaction and/or dilatancy, which is stated as: (Chen, 1985)

$$x = x(\varepsilon_v^p) \tag{2.17}$$

2.3.5.2 Kinematic Hardening

Kinematic (or anisotropic as a more general term) evolution of the yield surface and plastic potential are considered as the key ingredients for the effects in a constitutive model. The center of ellipse is not at the center of $p' - q$ axes and it shifts to a vectorial length, so, "kinematic hardening" occurs. The cam clay model can be an example of kinematic hardening (see Fig.2.14).

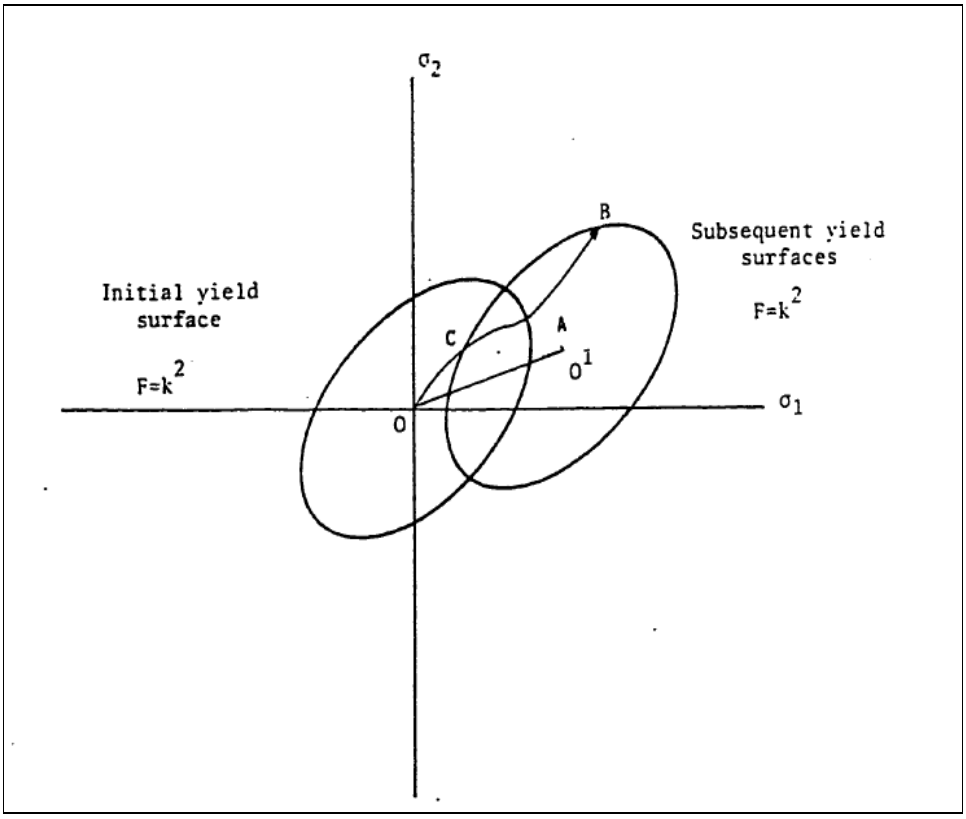

Figure 2.14 Schematic of subsequent yield surfaces for kinematic hardening (After Al-Bruim, 1990)

Furthermore, Figure 2.15 shows inner kinematic hardening behaviour. Three surfaces are similar in elliptical shape. The inner surfaces expand or contract with the outer surface. There is kinematic motion that depends on the stress state and stress history of the soil (Powrie, 2004). Its other name is 'bubble'.

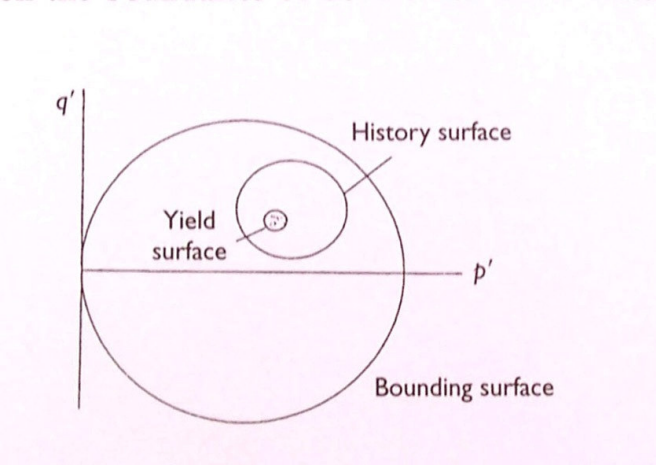

Figure 2.15 Inner kinematic hardening (After Powrie, 2004)

Combined hardening model contains both isotropic and kinematic hardening model by Al-Burium. The yield surface undergoes both uniform expansion with out rotation and distortion in all directions (see Fig.2.16) .The combined hardening model can be mixed with the other models.

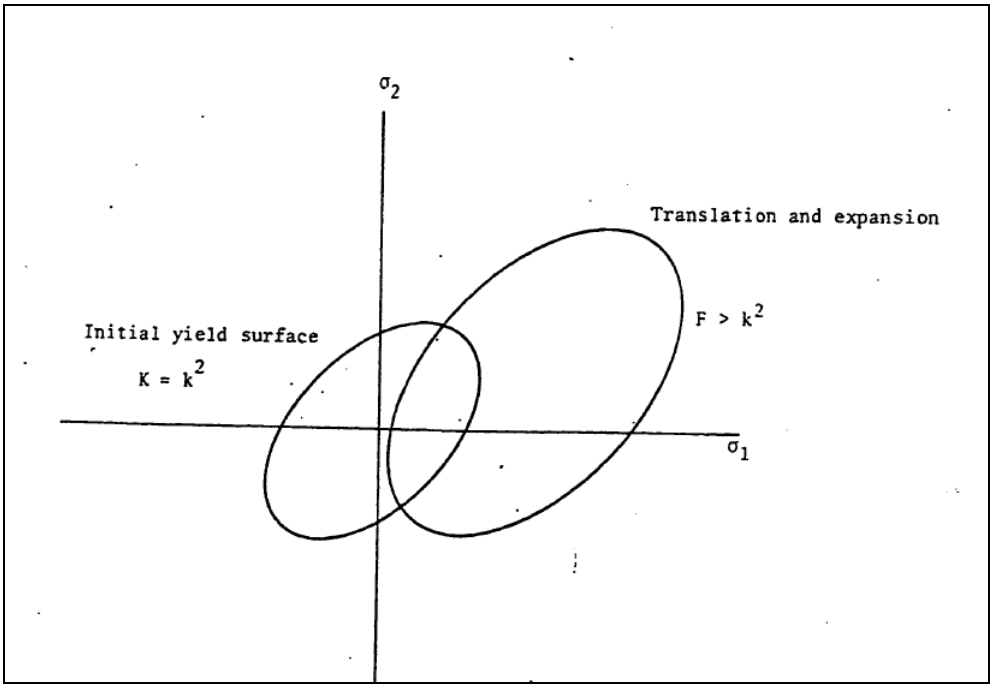

Figure 2.16 The schematic of loading surfaces for combined hardening rule (After Al-Burium, 1990)

2.3.5.3 The Cam Clay Model

The cam clay appears as the critical model which firstly describes the behaviour of soft soils, like clay. The models that are called 'the Cam-Clay (CC)' and 'Modified Cam-Clay (MCC)' are developed by the researchers at Cambridge University. To describe the soil behaviour, there are the three important properties, which are;

- Strength
- Compression or dilatancy (The change of volume that occurs with shearing)
- Critical state in which the soil elements can experience unlimited deformations without any change in stress or volume

The CC and MCC models are more realistic approaches for the cap of the plasticity models and also expressing the volume change. The state of a soil sample is characterized by three parameters of the critical state mechanics. These are;

- Effective main stress, p'
- Deviatoric (shear) stress, q', and
- Specific volume, υ

In general, under the stress conditions, the main stress (*p'*) and the deviator stress can be calculated in terms of the principal stresses (σ_1, σ_2 and σ_3) such that;

$$p' = \frac{1}{3}(\sigma_1' + \sigma_2' + \sigma_3'), \tag{2.18}$$

$$q' = \frac{1}{\sqrt{2}}\sqrt{(\sigma_1' - \sigma_2')^2 + (\sigma_2' - \sigma_3')^2 + (\sigma_3' - \sigma_1')^2} \tag{2.19}$$

The models assumes that when a soft soil sample is slowly compressed under the isotropic stress conditions and perfectly drained conditions; the relationship between specific volume (υ) and effective mean stress (ln *p'*) consists of a straight virgin consolidation line (or normal consolidation line) and a set of straight swelling lines (or un-/reloading lines).

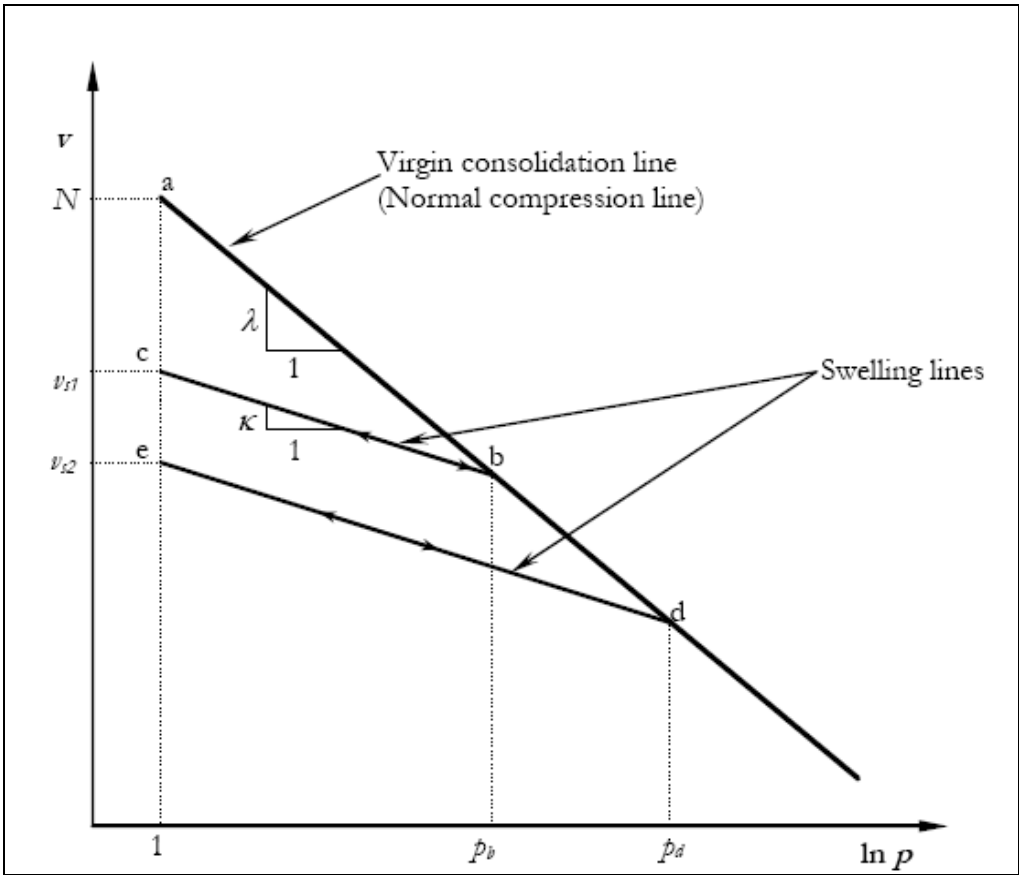

Figure 2.17 Behaviour of soil sample under isotropic compression (CamClay, n.d.).

At Figure 2.17, the virgin consolidation line is defined with the equation,

$$\upsilon = N - \lambda \ln p' \tag{2.20}$$

while the equation for a swelling line is,

$$\upsilon = \upsilon_s - \kappa \ln p' \tag{2.21}$$

where, λ is the slope of the normal compression line in -ln *p'* space, while κ is slope of the swelling line in υ- ln *p'* space. N is the specific volume of the normal compression line at a unit pressure.

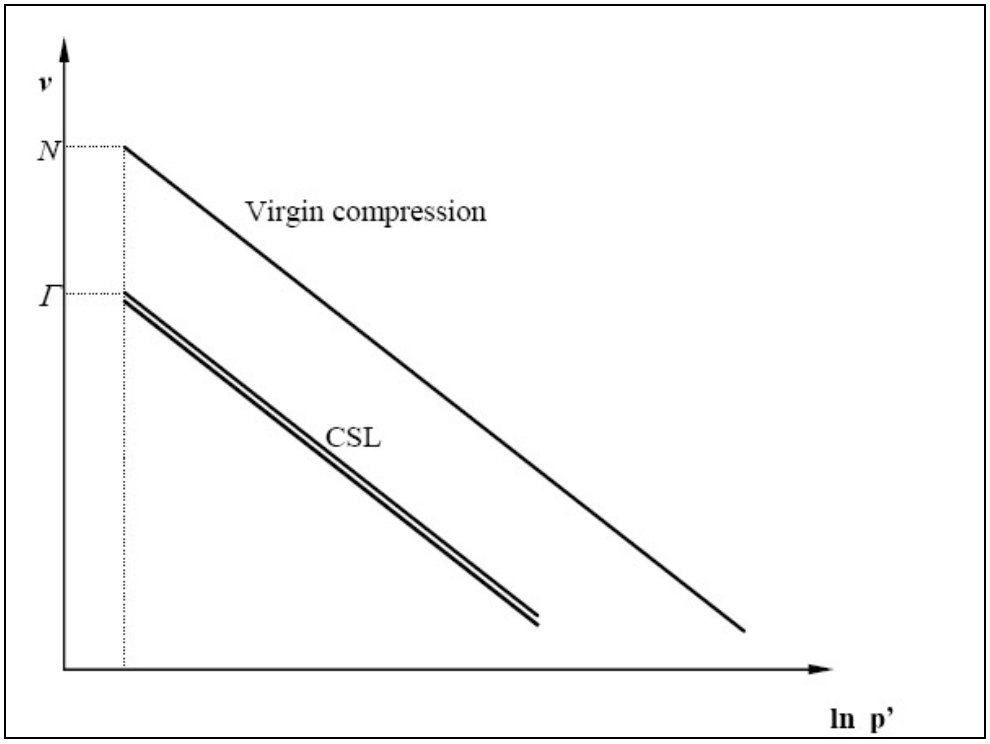

Figure 2.18 Location of CLS relative to virgin compression line (CamClay, n.d.).

2.3.5.3.1. Yield Function at The CC and MCC Model. The yield function of Cam-Clay is represented as:

$$q + Mp' \ln\left(\frac{p'}{p'_o}\right) = 0 \tag{2.22}$$

and also, the yield function of Modified Cam-Clay is defined as:

$$\frac{q^2}{p'^2} + M\left(1 - \frac{p'_o}{p'}\right) = 0 \tag{2.23}$$

Where, p'_o parameter defines the size of the yield surface, the M parameter is the slope of the CLS (Critical Line State) in *p'-q* space. CLS is a key characteristic that intersects the yield curve at the point at the maximum value of *q.* (See Figure 2.18).

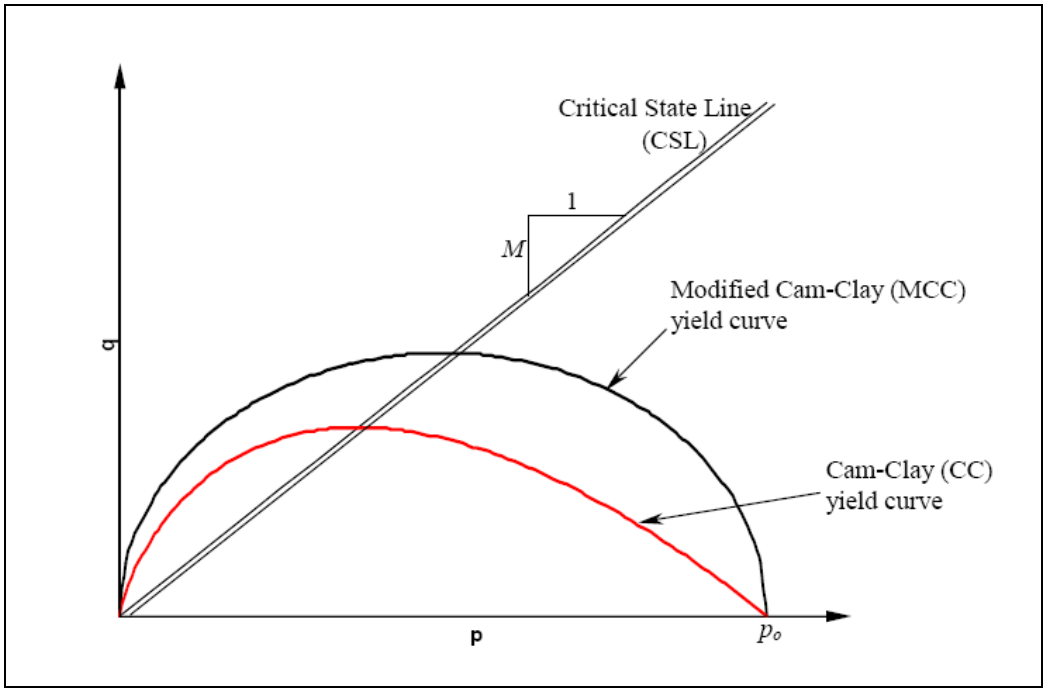

Figure 2.19 Cam-Clay and Modified Cam-Clay yield surfaces (in "p–q) space. The parameter M is the slope of the CSL (CamClay, n.d.).

The slope M of the CLS in q-p' space can be calculated with the friction angle (φ') of the Mohr-Coulomb yield criterion in triaxial compression test,

$$M = \frac{6\sin\varphi'}{3-\sin\varphi'} \tag{2.24}$$

The slopes λ and κ of the normal compression and swelling lines in v-ln p' space are related to the compression index (C_c) and swelling index (C_s), respectively, which are measured by oedometer tests. Also, κ is chosen within range of $\frac{1}{5}\lambda$ to $\frac{1}{3}\lambda$.

$$\lambda = \frac{C_c}{\ln 10}; \qquad \kappa = \frac{C_s}{\ln 10} \tag{2.25) and (2.26}$$

2.3.5.3.2. Hardening Behaviour at the CC and MCC Model. If yielding occurs at right side of the intersection of the CLS and the yield surface that is called "the wet or subcritical side" at Figure 2.20, the soil material shows the hardening behaviour. When a sample is sheared, the material behaves elastically until it hits the initial yield surface. Then, the soil material shows the hardening behaviour until it gets to point C which is the yield surface at critical state. The hardening stress-strain curve for the wet side loading is shown on Figure 2.21.

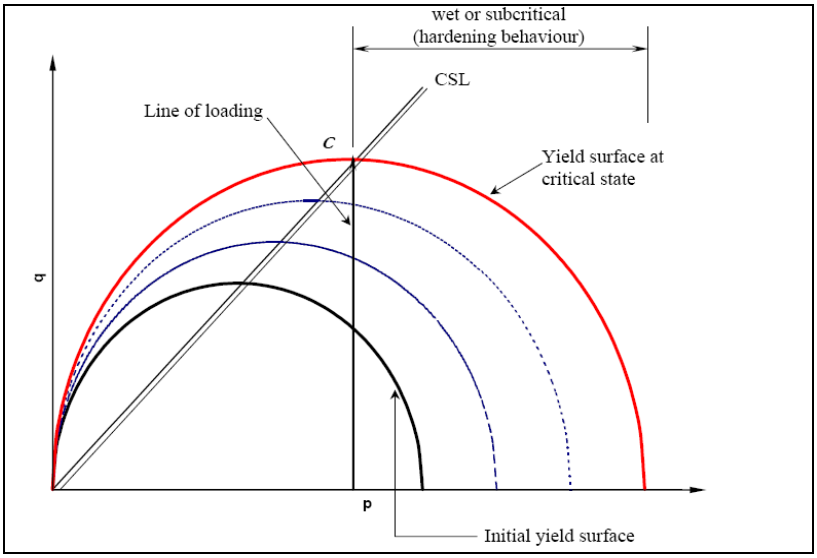

Figure 2.20 Evolution of the yield curve on the wet side of Modified Cam-Clay under simple shearing (CamClay, n.d.)

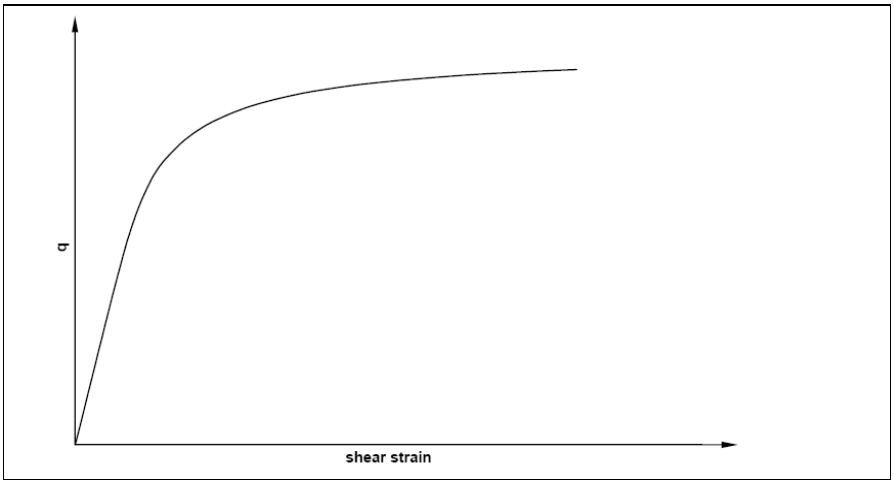

Figure 2.21 Hardening stress-strain response on wet side of Modified Cam-Clay material under simple shearing (CamClay, n.d.)

2.3.5.3.3. Softening Behaviour at the CC and MCC Model. If yielding occurs on the left of the intersection of the CLS and yield surface which is called "the dry or supercritical side" on Figure 2.22, the soil material shows the softening behaviour. At the dry side, the yield stress curve bends after the stress state contacts the initial surface. The softening stress-strain curve for the dry side loading is shown on Figure 2.23.

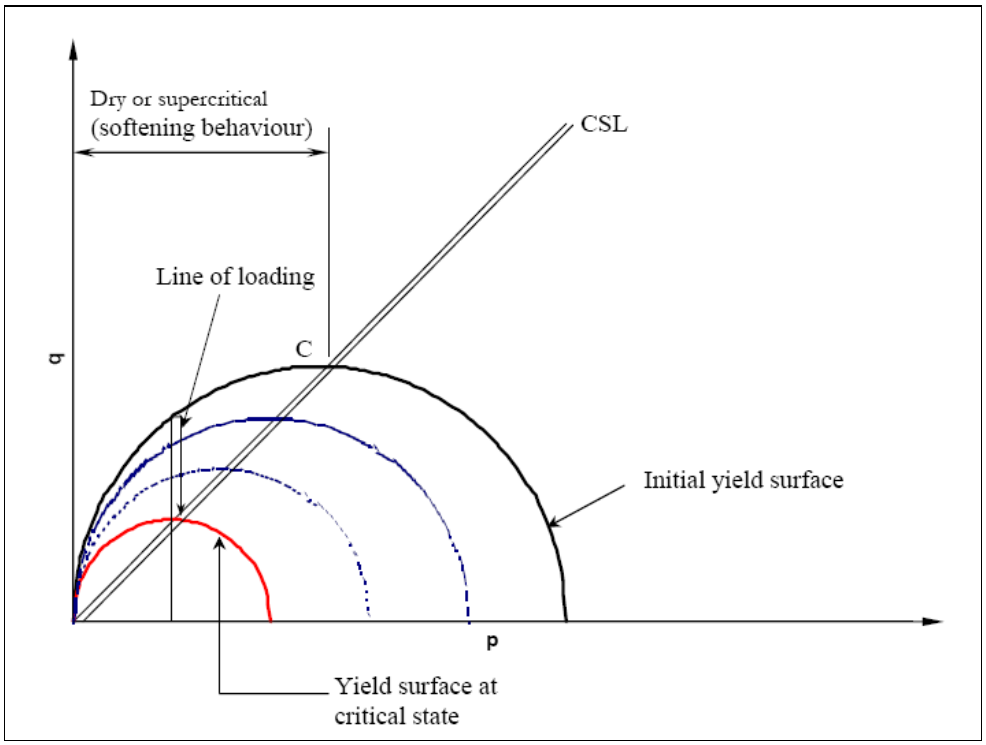

Figure 2.22 Evaluations of the yield curve on the dry side of Modified Cam-Clay under simple shearing (CamClay, n.d.).

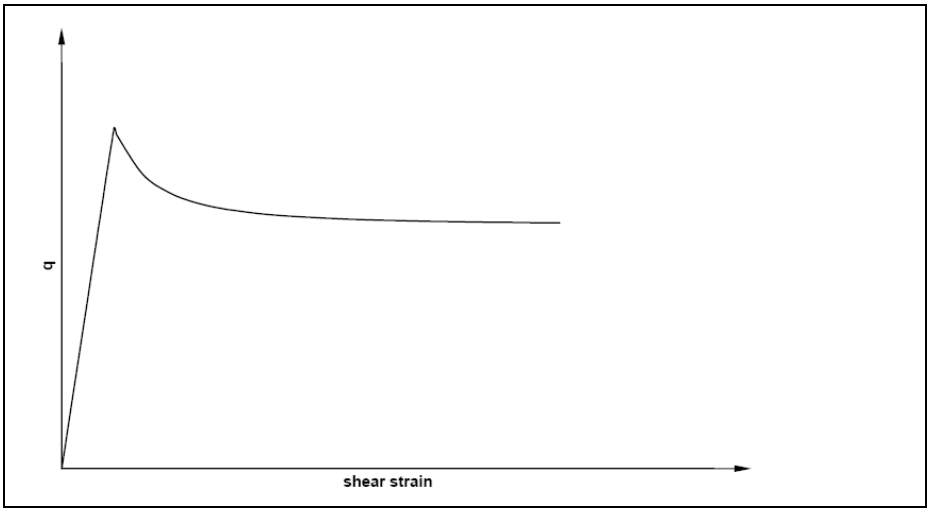

Figure 2.23 Softening stress-strain response on dry side of Modified Cam-Clay material under simple shearing (CamClay, n.d.).

In Figure 2.24, if a model (such as Cam Clay) is taken into account with a symmetrical shape, according to *p'* axis, it can also be called "double hardening model". However, the figure obviously illustrates that the Cam Clay Model changes the volume strain in instability, stability or rigidity situations (Schofield & Wroth, 1968).

Therefore, Figure 2.25 shows Modified Cam Clay yield surface in principal stress space. Its shape is prolate spheroid. The model is used in soft soil material type in PLAXIS. It's only yield surface of cap model. This issue deals with the model at the end of this chapter.

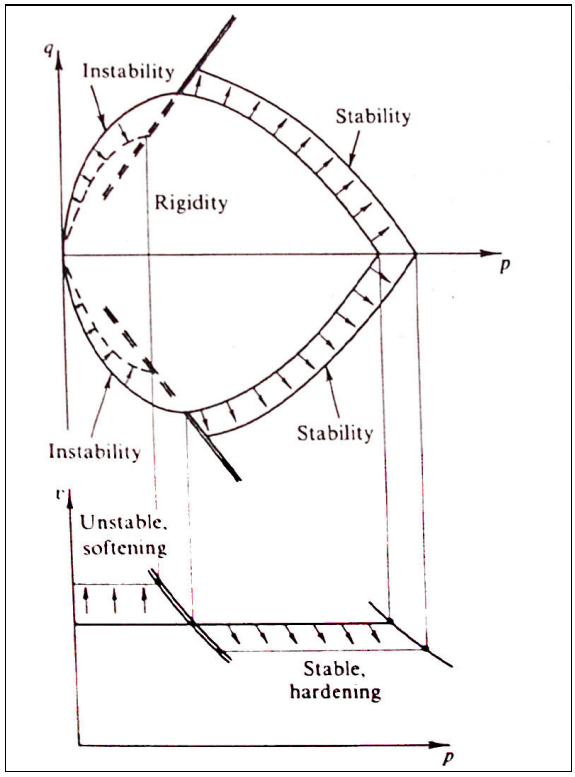

Figure 2.24 Rigidity, stability, and instability (After Schofield & Wroth, 1968)

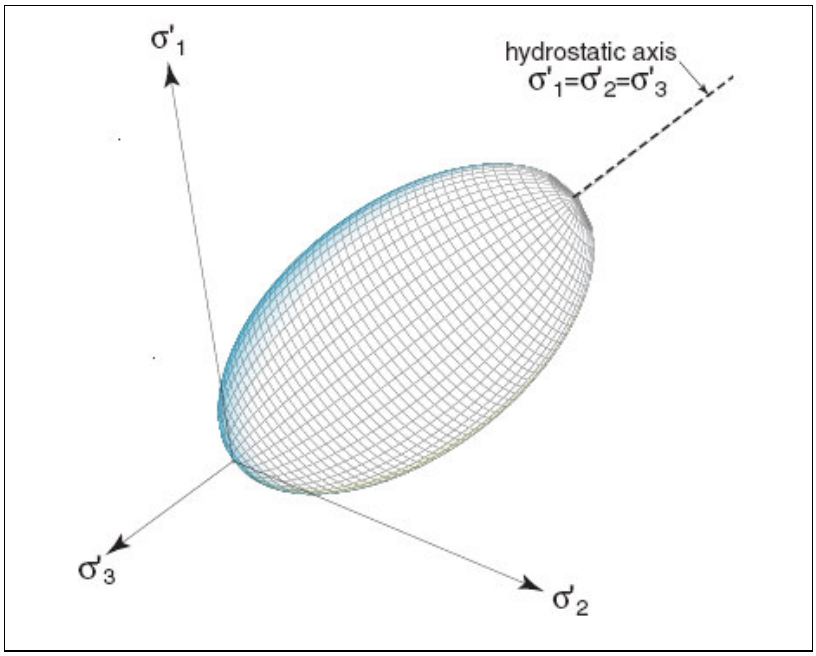

Figure 2.25 Modified Cam Clay yield surface in principal stress space (After Abed, 2008)

2.4 The Current Studies of Scientists During The Quarter Period

The capillary and saturated degree affect the soil behaviour and model that involve an advanced and realistic characteristic for the retention curve with the usage of instance of kinematic hardening and capillary hysteresis (Laloui & Nuth 2008).

The 'hardening' term means that the yield surface changes in size, location and/or shape with the loading history. So, this kind of particular change in the yield surface is only due to an irreversible phenomenon, related to a given plastic work, for instance the plastic rearrangement of particles.

Lade and others (2008) work on the plastic potential surface for the single hardening model determined for the Santa Monica Beach sand. The experiments indicate that the non-associated flow is required to observe model behaviour and the 'torsion' criterion is added to their studies (See Figure 2.26).

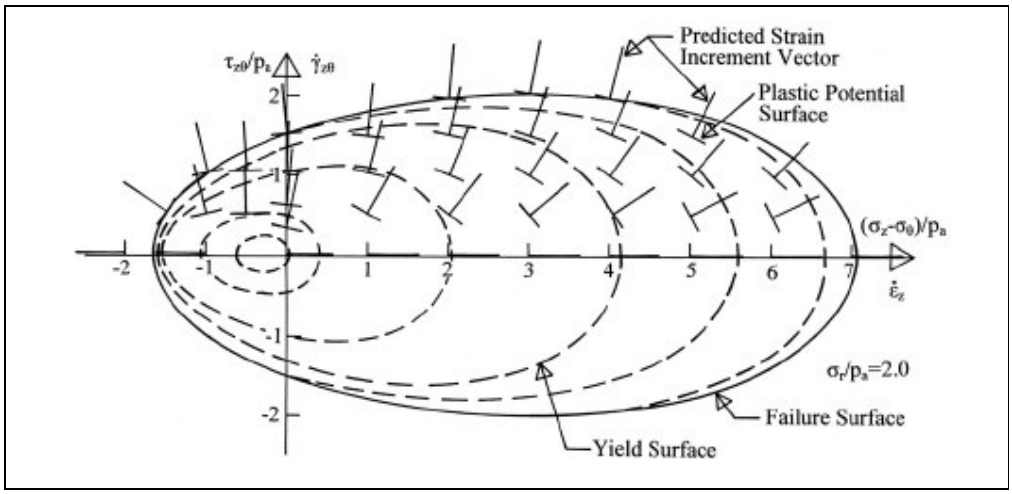

Figure 2.26 Inclinations of strain increment vectors from non-associated plastic potential surface shown at various points in $(\sigma_z-\sigma_\theta) - \tau_{z\theta}$ diagram (After Lade P.V. and others, 2008)

Nova (2005) has summarized to the hardening model in "A Simple Elasto-Plastic Model for Soils and Soft Rocks" differently. He has categorized soils and soft rocks into the four criterions. There is a model structure including the soils without any cement, the predictions for sand and the remolded clay, the model type for bonded

soils and soft rocks, and finally the model type for bonded soils with chemical degradation. For example; Tamagnini, Castellanza, and Nova (2002) have emphasized a model that describes the mechanical behaviour of the cemented soils and the weak rocks undergoing mechanical and non - mechanical degradation processes, like these processes associated with chemical weathering phenomena.

A simple elastic plastic strain-hardening model (as cam clay) that is kind of an associated model has four criteria. These criteria are:

- Plastic potential, (g)
- Yield function, (f)
- Hardening rule
- Elastic law (For unloading-reloading)

In Figure 2.27, the plastic potential effects to the strain increment vector. Thereby, the direction of extension is defined.

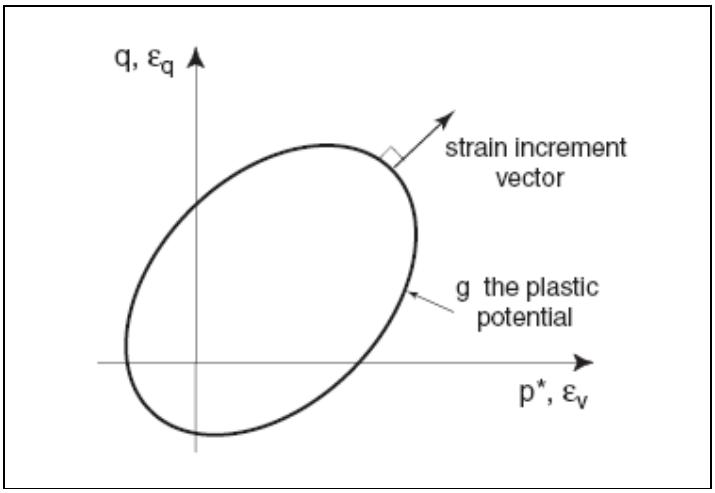

Figure 2.27 Strain increment direction (After Abed, 2008)

If the yield surface keeps its initial shape during plastic flow and only extends that is named isotropic hardening. Hardening which causes yield surface rotation is called rotational hardening (See Fig.2.28).

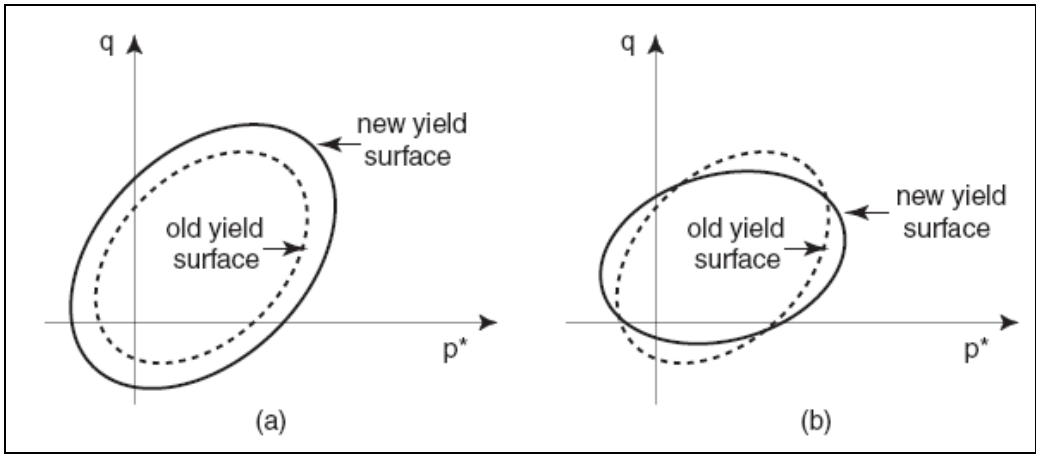

Figure 2.28 Examples of hardening (a) isotropic hardening (b) rotational hardening (After Abed, 2008)

2.4.1 The Developed Hyperbolic Models by Tatsuoka

'Deformation and Strength Characteristics of Granular Materials: From the experimental research for last 35 years by a geotechnical engineering researcher III-1' that is operated by Department of Civil Engineering Tokyo University of Science, consists of a part of non - linear stress - strain relationship. The relation's part which is mentioned has three main groups. These are the original hyperbolic, the modified hyperbolic and the genera hyperbolic (see Fig 2.29).

The original hyperbolic equation is:

$$y = \frac{x}{1+x} \tag{2.27}$$

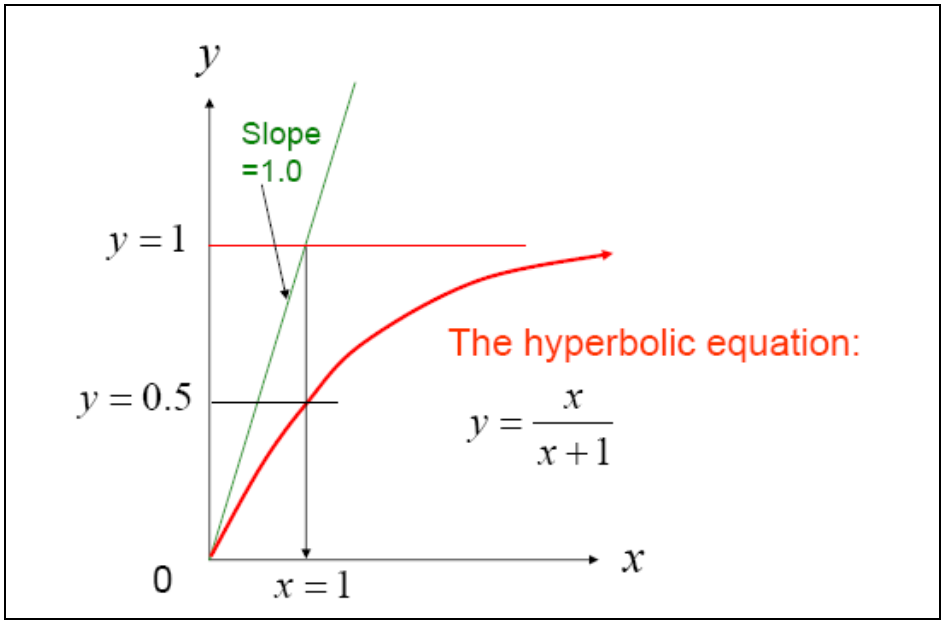

Figure 2.29 Original hyperbolic model (After Tatsuoka, 2007)

The original hyperbolic equation is simplified using the normalized stress and strain (see Fig. 2.30). The equation of original hyperbolic is:

$$\frac{x}{y} = x + 1 \tag{2.28}$$

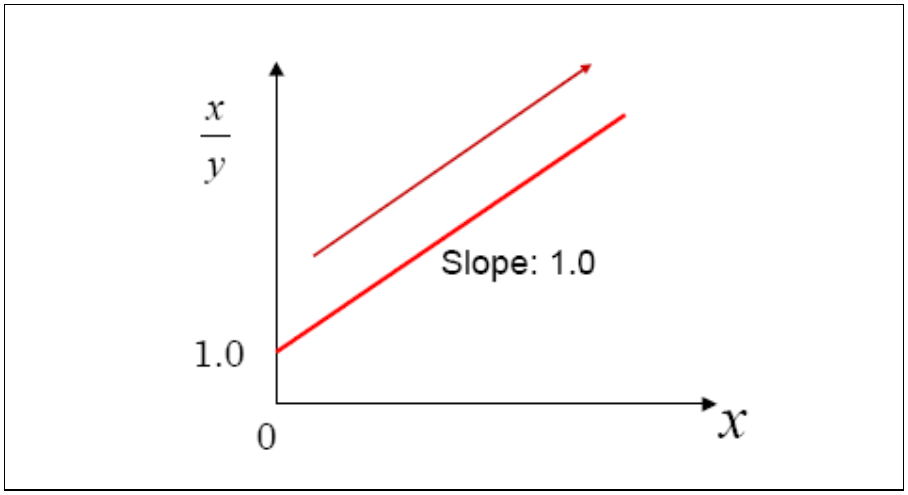

Figure 2.30 The original hyperbolic equation in terms of normalized stress and strain, y-x. (After Tatsuoka, 2007)

The model is developed to fit the hyperbolic model using given triaxial compression test data.

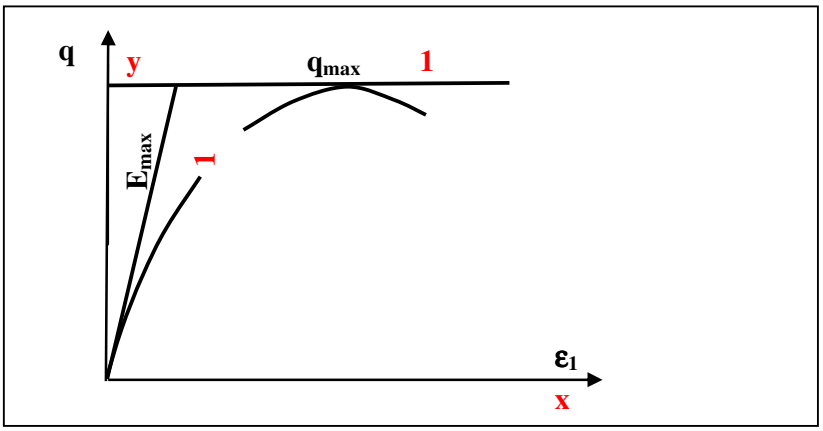

Figure 2.31 Fitting hyperbolic of given TC test data (After Tatsuoka, 2007)

$$q = \frac{\varepsilon_1}{\frac{1}{c_1.E_{\max}} + \frac{\varepsilon_1}{c_2.q_{\max}}} \tag{2.29}$$

which is used for the new assumptions that $E_{\max}$ and $q_{\max}$ are constant during the loading to simplify the equation 2.29. Then, the constants are substituted in the equation (see Fig.2.31).

$$y = \frac{q}{q_{\max}}, \tag{2.30}$$

$$x = \frac{\varepsilon_1}{(\varepsilon_1)_r}, \tag{2.31}$$

$$(\varepsilon_1)_r = \frac{q_{\max}}{E_{\max}}; \tag{2.32}$$

$$\frac{q}{q_{\max}} = \frac{\frac{\varepsilon_1}{(\varepsilon_1)_r}}{\frac{1}{c_1} + \frac{\varepsilon_1}{c_2.(\varepsilon_1)_r}} \xrightarrow{translation} y = \frac{x}{\frac{1}{c_1} + \frac{x}{c_2}} \tag{2.33}$$

in which, c_1 and c_2 are the coefficient of fitting the hyperbolic model with triaxial compression test data.

The relation between the stress and strain can be explained with other approaches that include the different coefficients or equations. There is the comparison of measured stress-strain relations with the several different hyperbolic models at table 2.1. Table 2.1 consists of the analysis of the Figure 2.32.

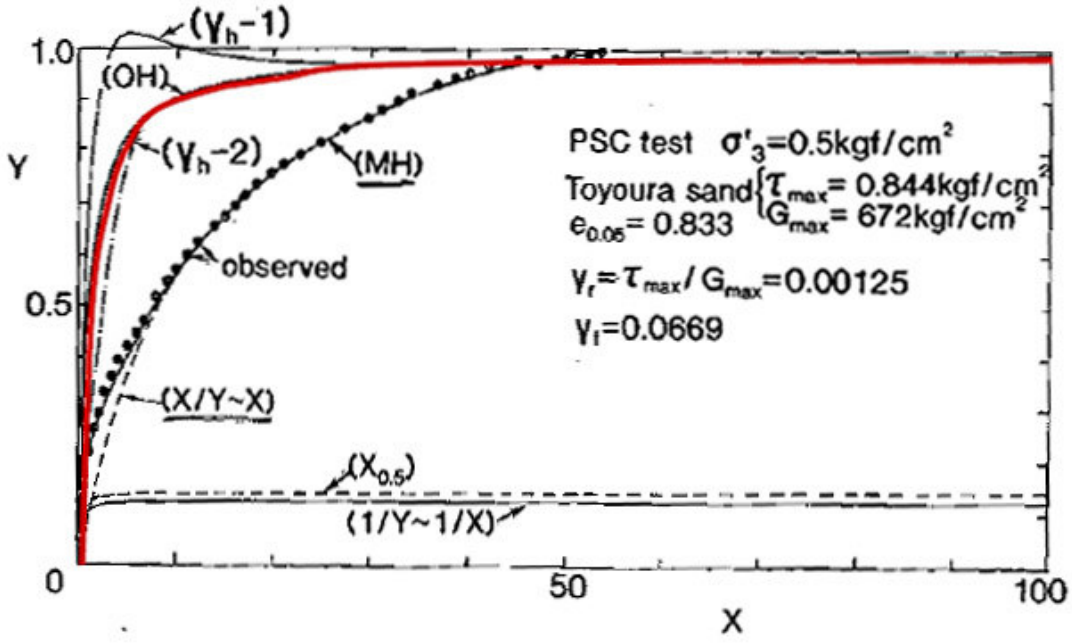

Figure 2.32 The modified the original hyperbolic equation to fit better the experiment (After Tatsuoka, 2007)

Table 2.1 The several methods for determining the correction factors c_1 and c_2 (After Tatsuoka, 2007)

c_1 =1.00, c_2 = 1.00	: Original Hyperbolic	(OH)
c_1 =0.10, c_2 = 1.24	: From x/y – x fitting (Kondner's method)	(X/Y X)
c_1 =1.00, c_2 = 0.125	: From 1/y 1/x fitting	(1/Y X)
c_1 =1.00, c_2 = 0.140	: c_2 = x when y/x = 0.5	($X_{0.5}$)
c_1 =1.00, c_2 = 1/(1 – 0.5.exp(-0.160.x))	: Hardin and Drneviech (1972)	(γ_h 1)
c_1 =1.00, c_2 = 1/(1 – 6.04.exp(-0.824.x))	: Hardin and Drneviech (1972)	(γ_h 2)
c_1 = f(x), c_2 = g(x)	: A proposed method	(MH)

As another model, Konder's Method assigns the suitable results at large strains and does not fit the curve at small strain or the elastic behaviour.

Moreover, Tatsuoka (2007) has proposed a new method for Toyoura sand. The method is called "the genera hyperbolic" and developed by Tatsuoka and Shibuya in 1992. c_1 and c_2 are shown in graphics at Figure 2.33. The relation of stress – strain is reached at Y/X Y axis (See Figure 2.34).

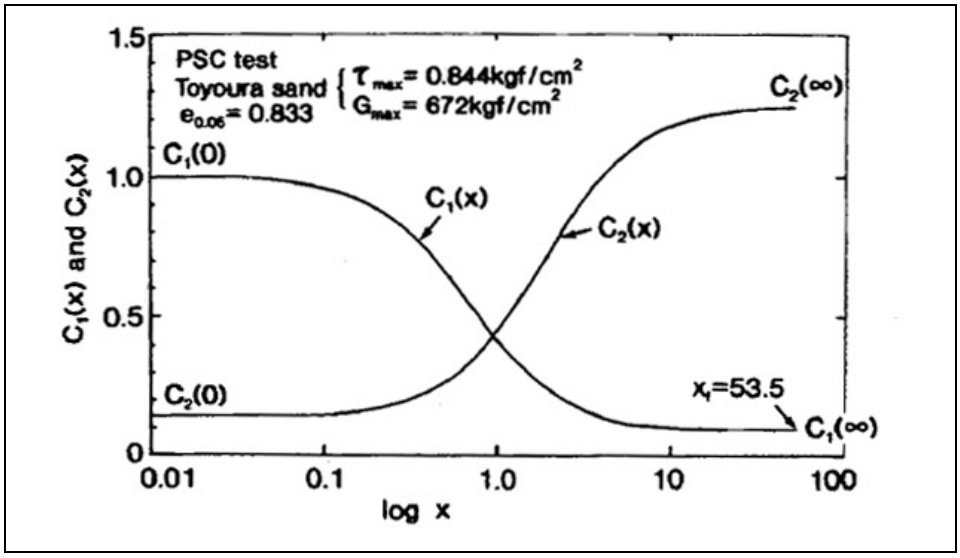

Figure 2.33 Functions' graphic of coeffection c_1 and c_2 (After Tatsuoka, 2007)

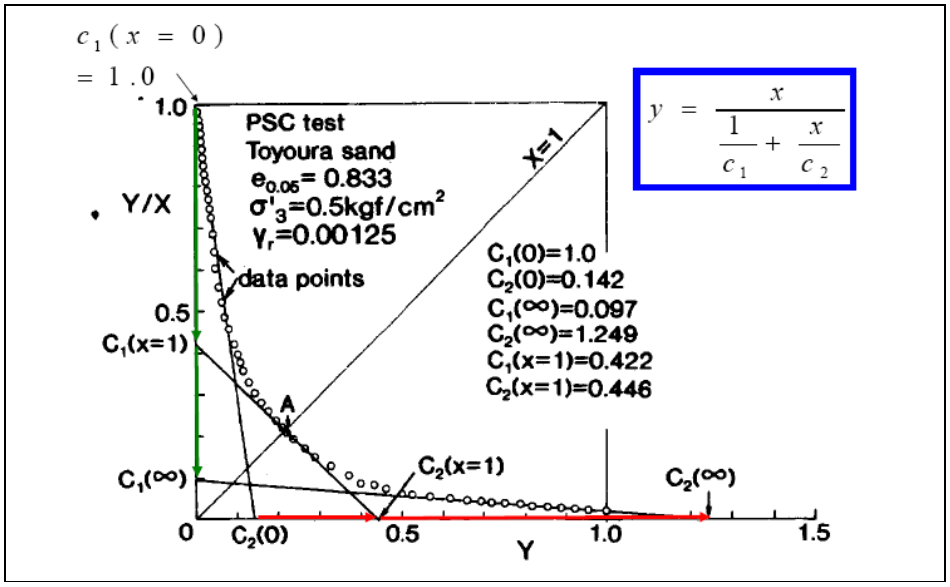

Figure 2.34 Simplified the relation of stress and strain according to Tatsuoka (After Tatsuoka, 2007)

2.4.2 The Investigations on the Structure of Hardening Soil Model

Modaressi and Laloui (1997) are studied on "a thermo-viscoplastic constitutive model for clays" The effect of heat on clay behaviour is characterized by non-linearity and irreversibility. Due to the complex influence of temperature, thermomechanical factors have to be taken into account for the numerical simulation of the behaviour of such materials (see Fig.2.35).

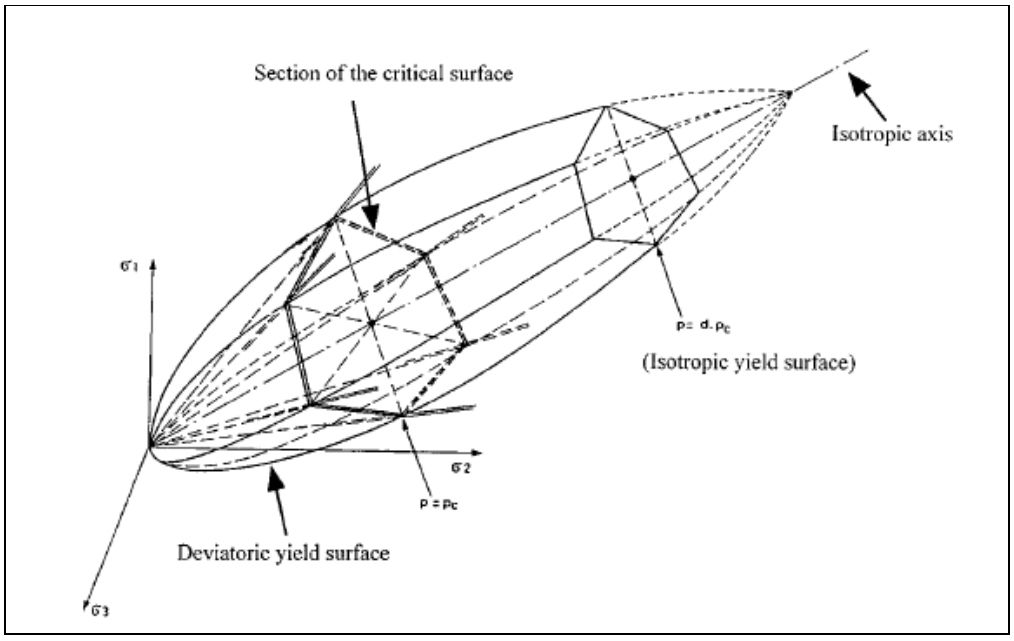

Figure 2.35 Presentation of yield surfaces (deviatoric and isotropic) in σ_1, σ_2 and σ_3 plane (After Modaressi & Laloui, 1997)

The new studies deal with finding a unified constitutive model for both clay and sand with hardening parameter. About this issue, Yao, Sun and Matsuoka (2007) assert five parameters to transform the many models, but the concept is not associated. Gajo and Muir Wood (2001) have another study, which is about the general formulation and simulations natural and reconstituted clay behaviour. Their proposal is using the coefficients to transform from isotropic hardening to kinematic hardening and rotational hardening that relates to plastic strain.

2.5 The Software Programs Related to Geotechnical Modelling

The commonly used software programs in geotechnical market elevate the finite-element method. The known programs of the first group are for soil models: ABAQUS, ADINA, ANSYS/LS-DYNA, DYNA3D, LIRA, NASTRAN, etc. All software packages have difference; because of the analytical programs that include the physical equations or models for the material. The programs used in geotechnics are ANSYS CivilFEM, GEO-SLOPE, PLAXIS, SAGE CRISP, Z_SOIL, etc. Most of programs quote the parameters or constants for the description of materials' models; except ABAQUS and CRISP. The deformations and stresses are defined with the elastic behaviour, the elastoplastic behaviour with hardening, and the elastoplastic behaviour with softening of material type when the static or kinematic force is loaded. In Table 2.2, the evaluation of soil model in the different software packages is available (Boldyrev, Idrisov, & Valeev, 2006).

Table 2.2 The evaluation of soil model in the different software packages (After Boldyrev, Idrisov, & Valeev, 2006)

Types of models	Software packages					
	Abaqus	Ansys	Ls-Dyna	Crisp	Plaxis	Z-Soil
Deformation	nonlinearly elastic (Mises)	nonlinearly elastic (Mises, Drucker-Prager)	nonlinearly elastic (Krieg)	Duncan-Chang	modified Duncan-Chang	elastic
Elasto-plastic	Modernized Drucker- Prager Modernized Mohr-Coulomb Cap (Drucker-Prager) Modernized Cam-Clay	Drucker-Prager elasto-ideally plastic	Cap (Drucker-Prager) Drucker-Prager elasto-ideally plastic	Elasto-ideally plastic (Mises, Tresca, Mohr-Coulomb, Drucker-Prager) Modernized elasto-ideally plastic (Mohr-Coulomb) Cap-Clay Three-surface with kinematic hardening	Mohr-Coulomb with hardening Cap (Mohr-Coulomb) Soft-Soil (Mohr-Coulomb)	Elasto-ideally plastic (Mohr-Coulomb, Drucker-Prager) Cap (Drucker-Prager) Modified Mohr-Coulomb Modified Cam-Clay

The numerical codes to study about the geotechnical problems have developed greatly over the past 30 years; however, very simple soil constitutive models are implemented in these programs. The available elasto-plastic constitutive models include both isotropic and kinematic hardening has been implemented in a FEM code. Programs affect the analysis for different situations that are developed for one,

two, and three-dimensional problems. The simple soil constitutive models are implemented in these commercial codes; like elastic-linear, elastic-perfectly plastic Mohr-Coulomb or Drucker-Prager, Cam-Clay, etc. The geotechnical constitutive models deal with the following materials: cam clay material, elastic-perfectly plastic Drucker-Prager material modified to include an elliptical cap hardening, elastic-perfectly plastic Mohr-Coulomb material and elastic linear material. (Abate, Caruso, Massimino,& Maugeri, 2006)

2.5.1 PLAXIS Software Program

PLAXIS is used as a main model that assimilates the Mohr-Coulomb model. The Mohr-Coulomb model represents a first-order approach for the soil or rock behaviours.

PLAXIS is intended to improve the advance of the soil models. As a general second-order model, an elasto-plastic type of hyperbolic model is called the 'hardening soil model'. In the model, the total strains are calculated using a stress-dependent stiffness, being different for the virgin loading and un-/reloading. The plastic strains are calculated to establish with a multi-surface yield criterion. The hardening is assumed to be isotropic, depends on both the plastic shear and volumetric strain. (Schanz and others, 1999).

The hardening soil stiffness is described using different inputs for stiffness, like the triaxial loading stiffness, E_{50}, the triaxial unloading stiffness, E_{ur} and the oedometer loading stiffness, E_{oed}. The basic parameters for the Mohr-Coulomb and the hardening soil model are:

Table 2.3 Comparing to inputs of Hardening soil model and Mohr-coulomb model at PLAXIS

Mohr-Coulomb model	**Hardening Soil model**
1. Failure parameter a. φ; Friction Angle b. c; cohesion c. ψ; Dilation Angle	**1. Failure parameters as in the MC model** a. φ; Friction Angle b. c; cohesion c. ψ; Dilation Angle
2. Stiffness parameters: a. E; Young's Modulus b. ν; Poisson's Ratio	**2. Hyperbolic stiffness parameters:** a. E_{ref}^{50} ; Secant stiffness in standard triaxial test at p_{ref} b. E_{ref}^{oed} ; Tangent Stiffness for primary oedometer loading at p_{ref} c. m; Power for stress level dependency of stiffness d. E_{ref}^{ur} ; Unloading/reloading stiffness e. ν_{ur} ; Poisson's Ratio for unloading-reloading f. p_{ref} ; Reference Stress for stiffness g. R_f; Failure ratio

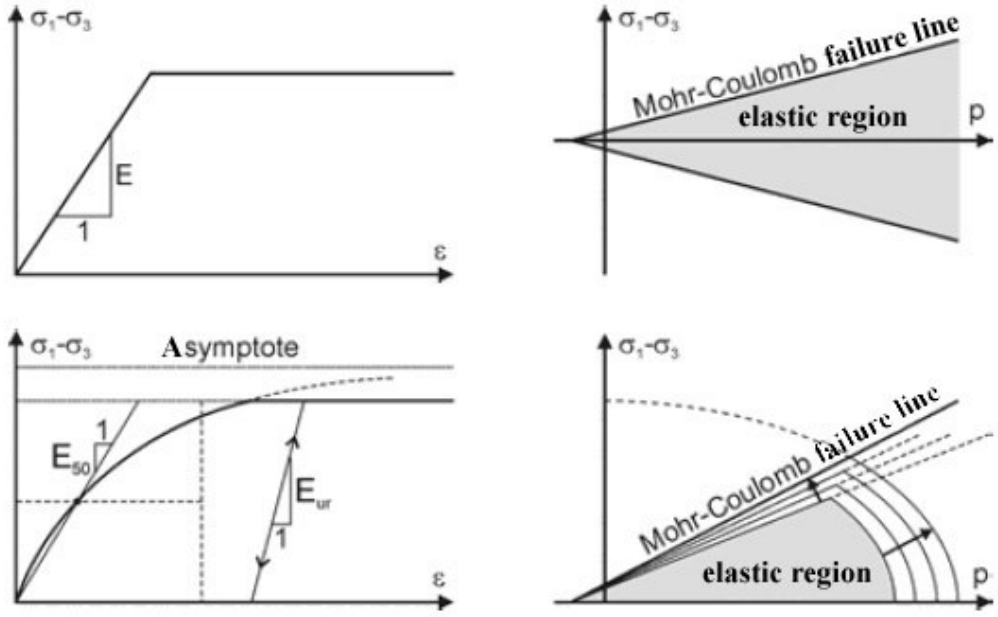

Figure 2.36 Comparing to inputs of Hardening soil model and Mohr-coulomb model at PLAXIS (After Wehnert &Vermeer, 2004a).

Kodner and Zelasko (1963) have observed a new relationship between the axial strain and the deviatoric stress in the case of a drained triaxial loading and a

hyperbola can be a suitable representation of relation. In PLAXIS, the hyperbolic yield curve of triaxial test is calculated by: (see Figure 2.36)

$$\varepsilon_1 = \frac{q_a}{2E_{50}} \frac{(\sigma_1 - \sigma_3)}{q_a(\sigma_1 - \sigma_3)} \tag{2.34}$$

The equation is valid for $q<q_f$; in which, q_f is the ultimate deviatoric stress and q_a is quantity stress.

$$q_f = \frac{6\sin\varphi_p}{3-\sin\varphi_p}\left(p + c\cot\varphi_p\right) \tag{2.35}$$

$$q_a = \frac{q_f}{R_f} \tag{2.36}$$

The relationship on above for q_f is derived from the Mohr-Coulomb failure criterion that involves the strength parameters c and φ_p. The ratio between q_f and q_a is given with the failure ratio (R_f) and often is taken into account as 0.9.

$$E_{50} = E_{50}^{ref}\left(\frac{\sigma_3' + c\cot\varphi_p}{\sigma^{ref} + c\cot\varphi_p}\right)^m \tag{2.37}$$

E_{50} is a reference of stiffness modulus corresponding to the reference stress (σ_{ref}). The amount of stress dependency is given with the power m. The actual stiffness depends on the minor principal stress (σ_3'), that is effective confining pressure in a triaxial test. The power should be taken equal to 1.0 for soft clays. The second modulus (E_{50}^{ref}) is determined from a triaxial stress-strain curve for a mobilization of 50% of the advised maximum shear strength (q_f).

$$E_{ur} = E_{ur}^{ref}\left(\frac{\sigma_3 + c\cot\varphi_p}{\sigma^{ref} + c\cot\varphi_p}\right)^m \tag{2.38}$$

E_{ur}^{ref} is a reference of Young's modulus for un/reloading, corresponding to the reference pressure (σ_{ref}).

$$E_{oed} = E_{oed}^{ref}\left(\frac{\sigma_1 + c\cot\varphi_p}{\sigma^{ref} + c\cot\varphi_p}\right)^m \tag{2.39}$$

The elasticity modulus E_{ur}^{ref} can be determined directly from a triaxial test or indirectly with the oedometer results. The unloading modulus from the oedometer test is denoted as E_{oed}^{ur} and according to the isotropic linear elasticity, the following relationship holds;

$$E_{ur} = (1-2v_{ur})\frac{1+v_{ur}}{1-v_{ur}}E_{oed}^{ur} \tag{2.40}$$

Hence the estimation of value of Poisson's ratio (v_{ur}), E_{ur} can be calculated from E_{oed}^{ur} (Vermeer, Marcher, and Ruse, 2002) (See Figure 2.37).

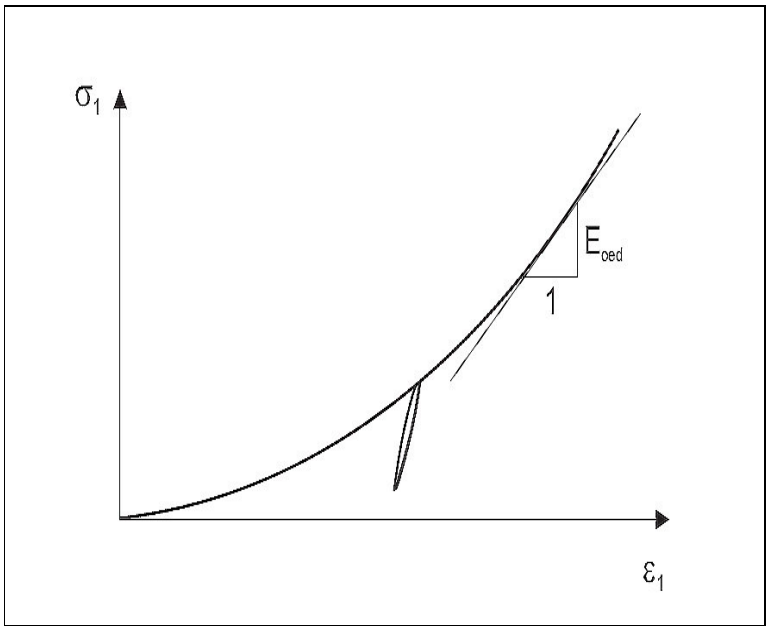

Figure 2.37 Characteristic curve of an oedometer test (After Moeller, 2006)

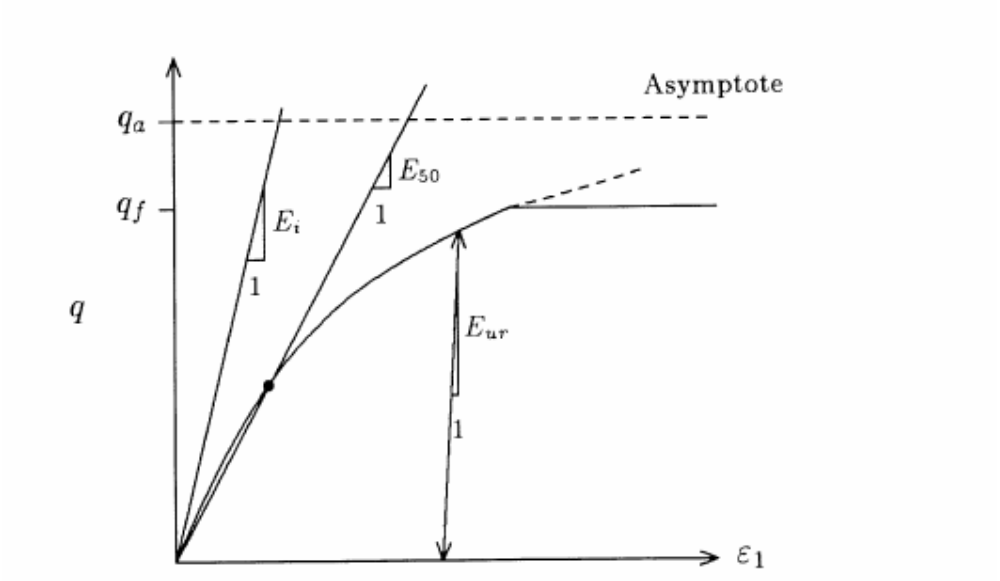

Figure 2.38 Hyperbolic stress-strain relation in primary loading for a standard drained triaxial test (After Schanz and others, 1999)

In the reference manual which is the part of PLAXIS manual, the over consolidation ratio affects to choose the hardening soil model or the soft soil model to describe the soil behaviour. The over consolidation ratio (OCR) is defined by the ratio between the isotropic reconsolidation stress (p_p) and current equivalent isotropic stress (p^{eq}).

$$\text{OCR} = \frac{p_p}{p^{eq}} \tag{2.41}$$

where,

$$p^{eq} = p' + \frac{q^2}{M^2\sqrt{p' + c\cot\varphi'}} \quad \text{(for Soft Soil / Creep Model)} \tag{2.42}$$

$$p^{eq} = \sqrt{(p')^2 + q^2/M^2} \quad \text{(for Hardening Soil Model)} \tag{2.43}$$

The isotropic reconsolidation stress (p_p) determines at the initial position of a cap type yield surface in the advanced soil model.

2.5.1.1 Formulation of the Mohr-Coulomb Model

The Mohr-Coulomb model is formulated by five parameters that are given in the previous part. The formulation of perfect plasticity decomposes strain rate ($\dot{\varepsilon}$) into elastic ($\dot{\varepsilon}^e$) and a plastic part ($\dot{\varepsilon}^p$):

$$\dot{\varepsilon} = \dot{\varepsilon}^e + \dot{\varepsilon}^p . \tag{2.44}$$

Elastic stress-strain relationship is given by;

$$\dot{\sigma}' = D^e \dot{\varepsilon}^e \ , \tag{2.45}$$

Plastic part of stress-strain relationship represents;

$$\dot{\sigma}' = D^e (\dot{\varepsilon} - \dot{\varepsilon}^p). \tag{2.46}$$

Using the plastic potential functions in PLAXIS, The non-associated plasticity is adopted and the plastic strain rates are formulated as;

$$\dot{\varepsilon}^p = \lambda_1 \frac{\partial g_1}{\partial \sigma'} + \lambda_2 \frac{\partial g_2}{\partial \sigma'} + \lambda_3 \frac{\partial g_3}{\partial \sigma'}, \tag{2.47}$$

where λ_1, λ_2 and λ_3 are the plastic multipliers. (Moeller, 2006)

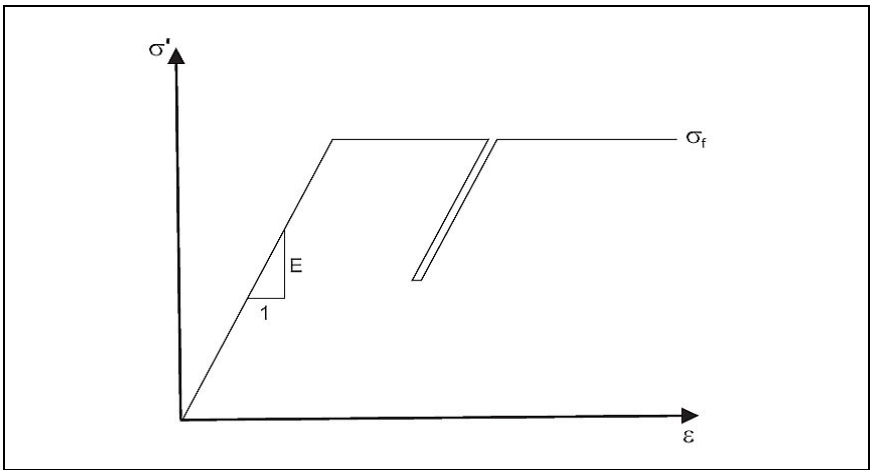

Figure 2.39 Linear elastic perfectly plastic material behaviour (After Moeller, 2006)

The Mohr-Coulomb yield conditions consist of six yield function at the principal stresses:

$$f_{1a} = \frac{1}{2}(\sigma'_2 - \sigma'_3) + \frac{1}{2}(\sigma'_2 + \sigma'_3).\sin\varphi - \mathrm{c}.\cos\varphi \le 0 \quad (2.48.1a)$$

$$f_{1b} = \frac{1}{2}(\sigma'_3 - \sigma'_2) + \frac{1}{2}(\sigma'_3 + \sigma'_2).\sin\varphi - \mathrm{c}.\cos\varphi \le 0 \quad (2.48.1b)$$

$$f_{2a} = \frac{1}{2}(\sigma'_3 - \sigma'_1) + \frac{1}{2}(\sigma'_3 + \sigma'_1).\sin\varphi - \mathrm{c}.\cos\varphi \le 0 \quad (2.48.2a)$$

$$f_{2b} = \frac{1}{2}(\sigma'_1 - \sigma'_3) + \frac{1}{2}(\sigma'_1 + \sigma'_3).\sin\varphi - \mathrm{c}.\cos\varphi \le 0 \quad (2.48.2a)$$

$$f_{3a} = \frac{1}{2}(\sigma'_1 - \sigma'_2) + \frac{1}{2}(\sigma'_1 + \sigma'_2).\sin\varphi - \mathrm{c}.\cos\varphi \le 0 \quad (2.48.3a)$$

$$f_{3b} = \frac{1}{2}(\sigma'_2 - \sigma'_1) + \frac{1}{2}(\sigma'_2 + \sigma'_1).\sin\varphi - \mathrm{c}.\cos\varphi \le 0 \quad (2.48.3b)$$

where, c is the cohesion and φ is the friction angle. These yield functions are illustrated as hexagonal cones in the principal stress space in the Figure 2.40.

The six plastic potential functions are defined for the Mohr-Coulomb model:

$$g_{1a} = \frac{1}{2}(\sigma'_2 - \sigma'_3) + \frac{1}{2}(\sigma'_2 + \sigma'_3).\sin\psi \quad (2.49.1a)$$

$$g_{1b} = \frac{1}{2}(\sigma'_3 - \sigma'_2) + \frac{1}{2}(\sigma'_3 + \sigma'_2).\sin\psi \quad (2.49.1b)$$

$$g_{2a} = \frac{1}{2}(\sigma'_3 - \sigma'_1) + \frac{1}{2}(\sigma'_3 + \sigma'_1).\sin\psi \quad (2.49.2a)$$

$$g_{2b} = \frac{1}{2}(\sigma'_1 - \sigma'_3) + \frac{1}{2}(\sigma'_1 + \sigma'_3).\sin\psi \quad (2.49.2b)$$

$$g_{3a} = \frac{1}{2}(\sigma'_1 - \sigma'_2) + \frac{1}{2}(\sigma'_1 + \sigma'_2).\sin\psi \quad (2.49.3a)$$

$$g_{3b} = \frac{1}{2}(\sigma'_2 - \sigma'_1) + \frac{1}{2}(\sigma'_2 + \sigma'_1).\sin\psi \quad (2.49.3b)$$

where, ψ is the dilatancy angle.

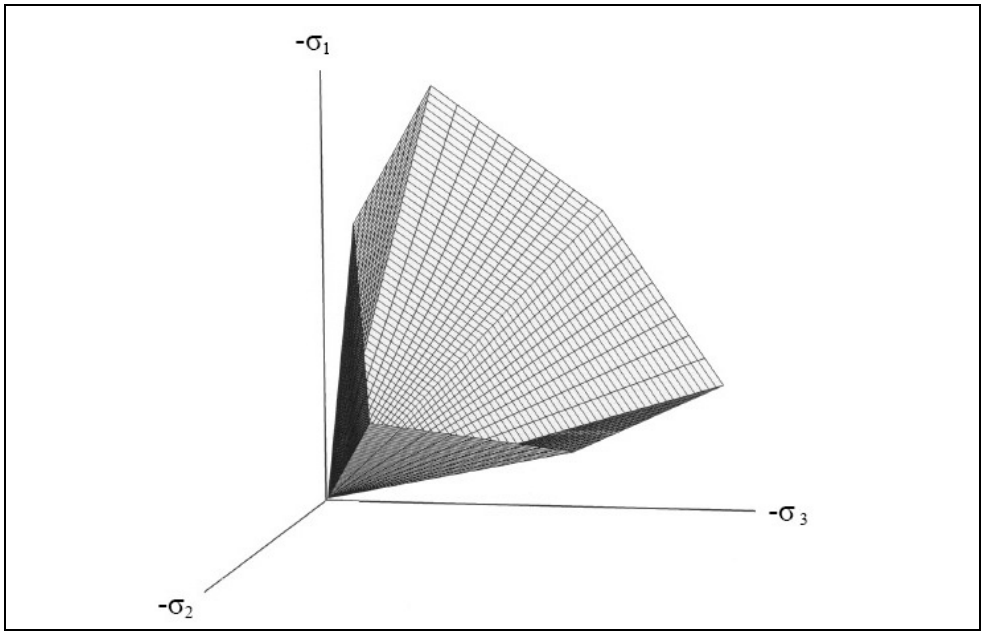

Figure 2.40 The Mohr-Coulomb yield surface in principal stress space (c=0) (After PLAXIS Manual)

Figure 2.40 can be illustrated with Figure 2.41. Figure 2.41(a) and Figure 2.40 have similarity and Figure 2.41(b) is the ground plan of the Mohr-Coulomb yield surface that also is given compression part and extention part.

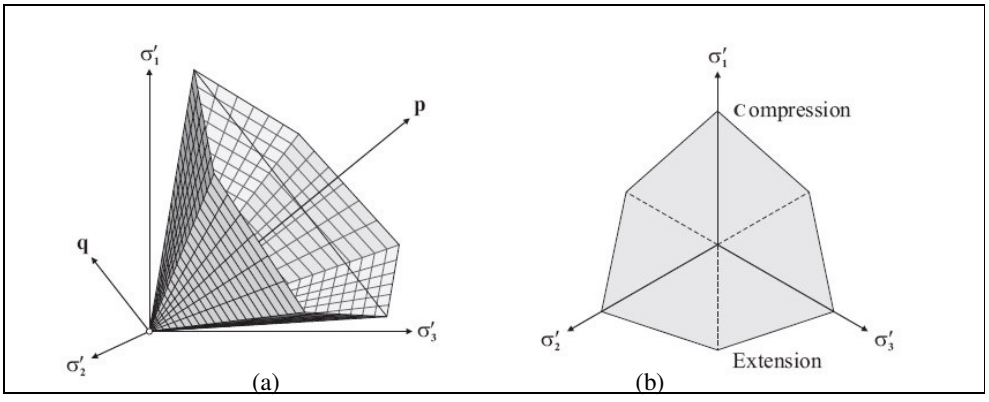

Figure 2.41 The Mohr-Coulomb yield surface in principal stress space with hydrostatic line (After Wehnert, 2006)

2.5.1.2 The Hardening Soil Model on the Cap Yield Surface

In the material models manual which is a part of PLAXIS manual, a cap type yield surface is formulated with the independent input of both E_{50}^{ref} and E_{oed}^{ref}. E_{50}^{ref} determines the elastic yield surface area in the hardening soil model. E_{oed}^{ref} effects to occur the cap yield surface with the other factors, and especially, it is a very important factor of all factors.

In PLAXIS, the cap yield surface is described as;

$$f^c = \frac{\tilde{q}^{\,2}}{\alpha^2} + p^2 - p_p^2 \tag{2.50}$$

where, α is the auxiliary model parameter which is also related with the K_0^{nc}; however, we have $p = -(\sigma_1+\sigma_2+\sigma_3)/3$ and $\tilde{q} = \sigma_1 + (\delta - 1)\sigma_2 - \delta\sigma_3$ with $\delta = (3+\sin\varphi)/(3-\sin\varphi)$. $\tilde{q}$ is a special stress measure for deviatoric stresses. Triaxial compression's case is $(-\sigma_1 > -\sigma_2 = -\sigma_3)$, which yields $\tilde{q} = -(\sigma_1 - \sigma_3)$ and for triaxial extension is $(-\sigma_1 = -\sigma_2 > -\sigma_3)$, $\tilde{q}$ reduces to $\tilde{q} = -\delta(\sigma_1 - \sigma_3)$. p_p is the reconsolidation stress, which is used to determine the magnitude of the yield cap. The hardening law p_p is related to the volumetric cap strain;

$$\varepsilon_v^{pc} = \frac{\beta}{1-m}\left(\frac{p_p}{p^{ref}}\right)^{1-m} \tag{2.51}$$

The volumetric cap strain is the plastic volumetric strain in the isotropic compression. Both α and β are the cap parameters, but they are not used as the direct input parameters. The input parameters are respectively K_0^{nc} and E_{oed}^{ref}, instead of α and β.

The shape of the yield cap with an ellipse can be realized in p-$\tilde{q}$ plane, like the Figure 2.42. The ellipse has a length p_p on p-axis and αp_p on the $\tilde{q}$-axis. While pp determines its magnitude, α determines its aspect ratio. High values of α lead to

steep caps underneath the Mohr-Coulomb line, whereas the small α-values define the caps that are pointed around the p-axis. The ellipse is used both for yield surface and for a plastic potential. Hence,

$$\dot{\underline{\varepsilon}}^{pc} = \lambda \frac{\partial f^{c}}{\partial \underline{\sigma}} \tag{2.51}$$

where;

$$\lambda = \frac{\beta}{2p}\left(\frac{p_p}{p^{ref}}\right)^{m} \frac{\dot{p}_p}{p^{ref}} \tag{2.52}$$

The expression for λ is derived from the yield condition and the volumetric cap strain (ε_v^{pc}) for p_p. p_p values provide the input data on the initial stage with PLAXIS procedure for initial stresses.

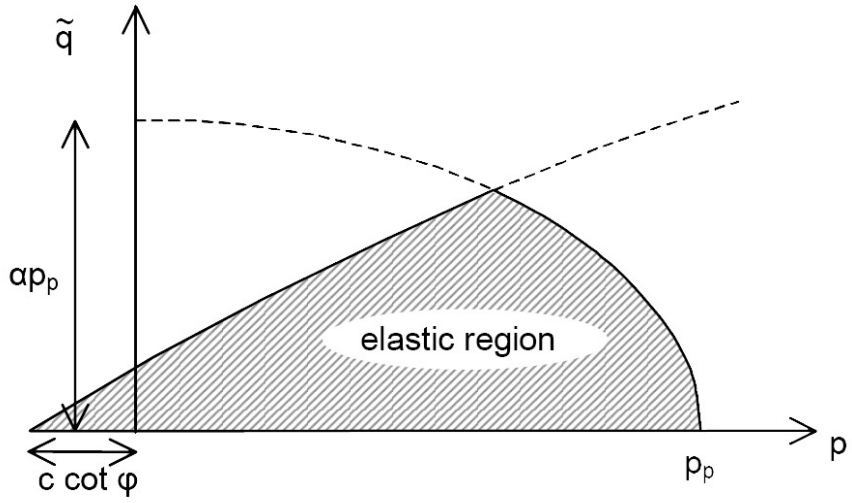

Figure 2.42 Yield surface of hardening-soil model in p- $\tilde{q}$ plane. (After Brinkgrever, 2002)

Figure 2.42 illustrates to a simple yield lines. Here, the line originates from the classical Mohr-Coulomb envelope and the arc is a quarter of the ellipse which is a yield function. The arc and line intersects at a point. The point where the intersection occurs is represented to change the yield function. In other words, the Mohr-Coulomb model ends and isotropic hardening model begins at this specific point. The

elastic region, which represents the shaded area at the Figure 2.43, is described with the contouring yield line.

The yield surfaces are mentioned in the principal stress space in Figure 2.44. The hexagonal shape is formed by the Mohr-Coulomb failure criterion, and then the cap surface expands as a function of pre-consolidation stress $p_{p.}$ Furthermore, the figure shows the behaviour of the strain increment vector in terms of defining at the cap of the hardening soil model in PLAXIS.

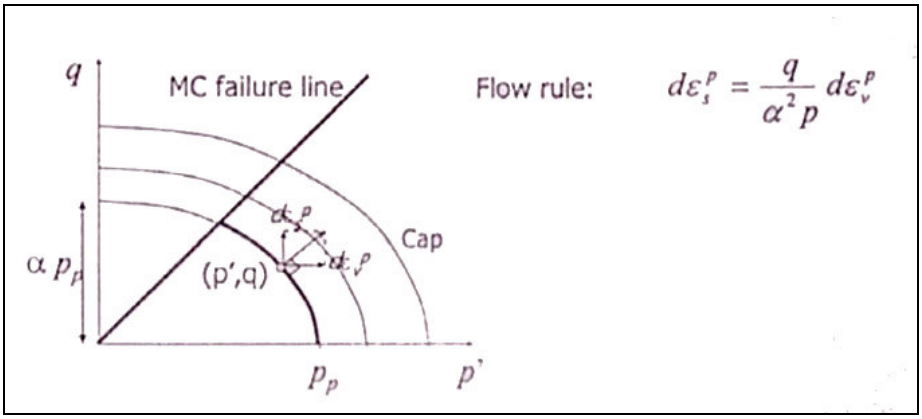

Figure 2.43 Density hardening in HS Model (After Brinkgrever, 2007)

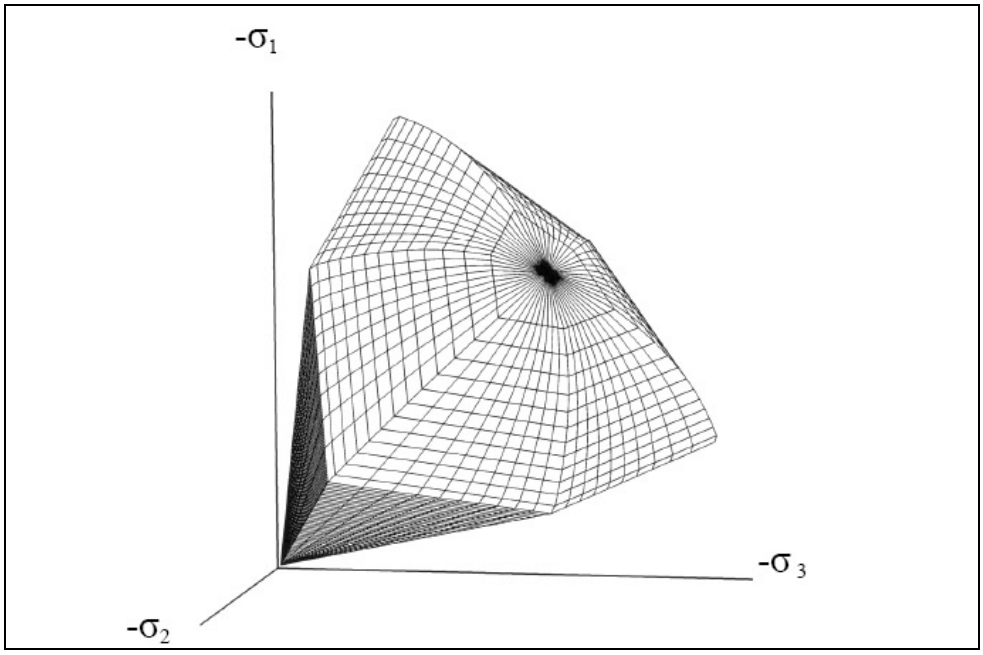

Figure 2.44 Representation of total yield contour of the Hardening-Soil model in principal stress space for the cohensionless soils (PLAXIS Manual)

The yield surface of PLAXIS's hardening model is similar to yield surface of Drucker Prager model, when the small strain is taken into account. The real soil behaviour is represented by approximating Drucker Prager model. In the ground plan of the developed hardening soil model in Figure 2.45, the yield surface relates to the friction angle that is obtained with Mutsuoka-Nakai criterion.

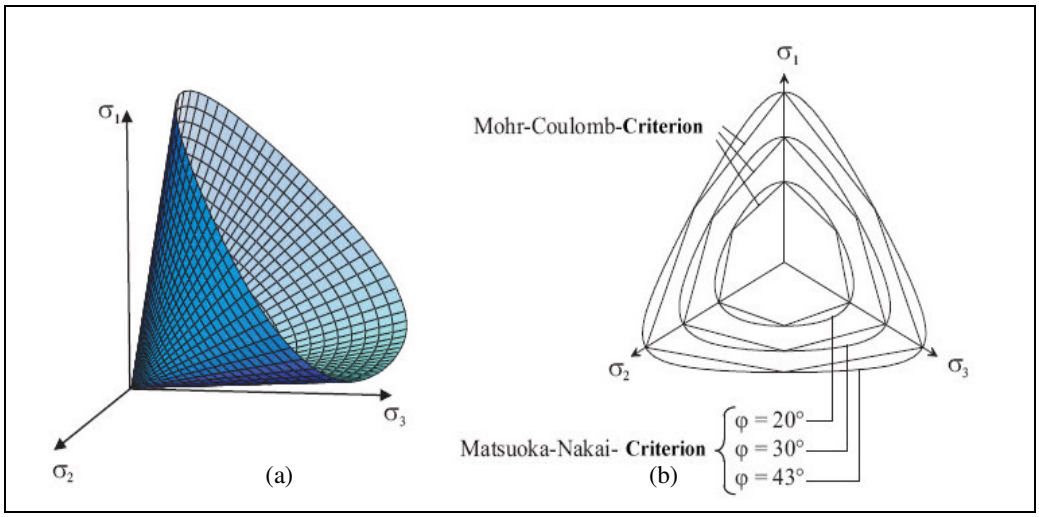

Figure 2.45 Hardening soil model with taking small strain into account (After Hintner, 2008)

CHAPTER THREE

ANALYSIS OF THE OEDOMETER TEST DATA

USING PLAXIS SOFTWARE

3.1 The materials and the selection of materials' properties by using hardening soil parameters at PLAXIS

In this research, the results of "the report of soil experiments belong to the coast road of Karşıyaka – Alaybey - Bostanlı route" are used to calibrate with Northern Izmir bay area soils using the hardening soil models at PLAXIS program. The report is written in 1984. In the report, the experiments especially are focus on the results of oedometer tests which are presented very detailed.

In terms of the results ranked in the report, firstly, all oedometer tests results are given a specimen name, according to the borehole name and the oedometer's order. The oedometer tests are transferred to the computer using MS Excel which are included in Appendix-A. All of the study is arranged according to the specimens' names.

The tests' results are pointed and fitted the most suitable curve and plotted with the degree of reliability in MATLAB program. At the end of a long research, the *cubic spline model* is made a decision on the most suitable curve for the relation of axial stress-axial strain according to the illustrated parabolic arm at PLAXIS manual. Appendix – B is involved these graphics of axial stress-axial strain that are prepared on MATLAB program. E_{oed}^{ref} is assigned by PLAXIS and corresponds to p_{ref} which is equal to 100kN/m^2 from the curve of load-axial strain at oedemeter tests.

Secondly, E_{ur}^{ref} and E_{50}^{ref} are the parameters of the hardening soil material type in PLAXIS and defined as the representation of soil properties of Northern İzmir Bay

area. Also, m and v_{ur} are the variables of hardening model to determine in the second step. c is equal to zero for normally consolidated clay. If below part of the curve of PLAXIS can approach the curve of oedometer test in means by these variables, for resembling above of the curves, variable ψ is taken to differ from zero.

The new approach is aimed to modify with using these parameters to represent the Northern İzmir Bay area in this study. So, the available studies are researched and eliminated. At seminar note of PLAXIS, the perfect model describes to be "the cam clay model"; but it can be explained the cam clay model with the parameters of the hardening soil model as;

- $E_{oed}^{ref} = 0.5 * E_{50}^{ref}$
- $E_{ur}^{ref} = 3 * E_{50}^{ref}$
- m=1
- $v_{ur} = 0.2$.

The variables are given for alluvial and volcanic deposits of Columbia riverland in the thesis of Kevin Abraham (2007) as;

- $E_{oed}^{ref} = 0.8 * E_{50}^{ref}$
- $E_{ur}^{ref} = 3 * E_{50}^{ref}$
- m=0.8
- $v_{ur} = 0.2$.

PLAXIS program limits m parameter between greater than 0.5 and less than 1. Moreover, in the PLAXIS manual, E_{ur}^{ref} sets $3\,E_{50}^{ref}$ to equal. Though, φ is taken from the chart of correlation between Ip and φ in Bowles's book which is called "Foundation Analysis and Design".Also, it is given in Appendix-C. c is assumed zero, because of the existence of normal clay under consolidated drained condition in the specimens. However, E_{50}^{ref} is greater than E_{oed}^{ref} for the representation of the soft soil in Krepfret's book which is called "Excavations and Foundations in soft soils".

Hardening parameters for clays are given like: v is between 0.30 and 0.38, v_{ur} is between 0.15 and 0.20, m is near to 1. However, in the Mohr-Coulomb model, v is accepted in range between 0.3 and 0.4, and for un-/ reload conditions, v_{ur} is range between 0.15 and 0.25 in one dimensional compression (Huybrechts, De Vos, Whenham, 2004).

E_{oed}^{ref} lies in MATLAB, so that E_{oed}^{ref} is accepted as constant for this study when E_{oed}^{ref} is used for the soil classification on the Table 3.1. (Huybrechts, De Vos, Whenham, 2004).

Table 3.1 Elastic moduli according to soil classification (After Huybrechts, De Vos, Whenham,2004).

Elastic Modul	**(kN/m²)**
Clay	
very soft	500 – 5000
soft	5000 – 20000
medium	20000 – 50000
stiff clay, silty clay	50000 – 100000
sandy clay	25000 – 200000
clay shale	100000 – 200000
Sand	
loose sand	10000 – 25000
dense sand	25000 – 100000
dense sand and gravel	100000 – 200000
silty sand	25000 – 200000

Twenty specimens stand in a part of the soil classification which are the very soft clay like: B02-2, B10-2, B14-1, B15-1, B16-1, B16-2, B17-1, B18-1, B18-2, B19-1, B20-1, B24-1.

Nineteen specimens exist in a part of the soil classification which are the soft clay as: B01-2, B03-1, B07-1, B08-1, B09-1, B09-2, B10-1, B11-1, B11-2, B12-1, B12-2, B13-1, B13-2, B17-2, B20-2, B21-1, B23-1, B25-1, B26-1.

B05-1 is a specimen of medium clay, B02-1 is specimen of loose sand, B01-1 is another specimen of dense sand in the soil classification, according to table 3.1.

3.2 The New Developments on PLAXIS

The University of Glasgow (UK), Helsinki University of Technology (Finland), The University of Stuttgart (Germany),The Graz University of Technology (Austria) and The Norwegian University of Science and Technology, Trondheim (Norway) study in a research training network on Soft Clay Modelling for Engineering Practice (SCMEP) by European Community during four years between 2000 – 2004 years.

These universities focus on three main issues about the soft clay, which include anisotropy, destructuration and time-dependency/creep (Wheeler and others, 2003). PLAXIS is made in the University of Stuttgart, so the program is developed with adding the soft soil model, the soft soil creep model and the jointed rock model. PLAXIS involves the linear elastic model, the Morh-coulomb model and the hardening soil model before the beginning of the research above.

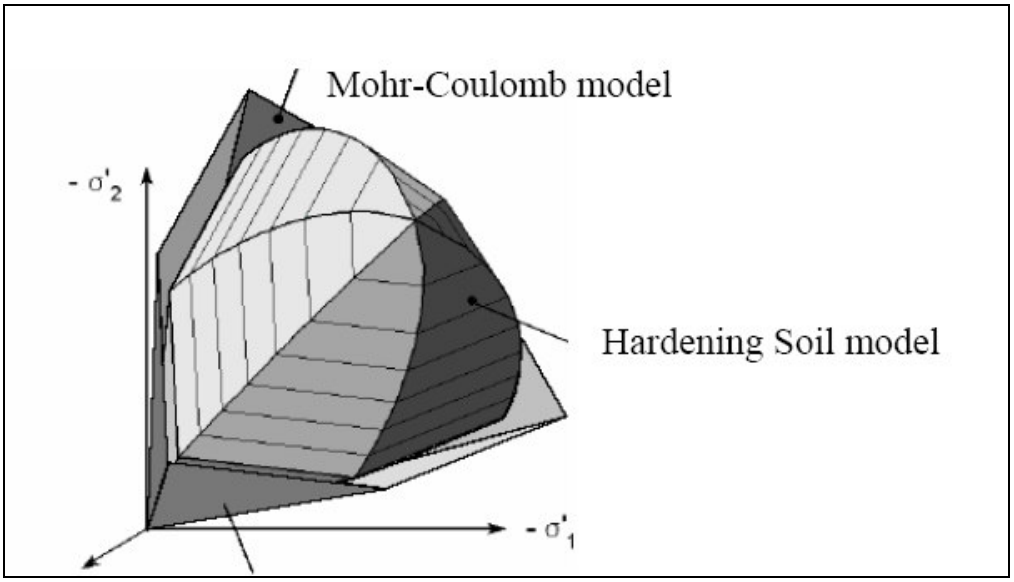

Figure 3.1 Mohr-Coulomb and Hardening Soil failure criterion in the principal stress space (After Meißner and others., 2006)

Mohr– Coulomb model can be extended by introducing strain hardening/softening plasticity (see Fig. 3.1). The cap of hardening soil model is involved Cam clay and modified cam clay models are based on the critical state theory (Huybrechts, De Vos, Whenham, 2004).

This model is occurred parameters of the hardening soil model. There are E_{50}^{ref}, E_{oed}^{ref} and E_{ur}^{ref}. All of them have the different influences. The parameter E_{50}^{ref} is purely shear hardening parameter (shear yield surface), while the parameter E_{oed}^{ref} is purely a compression hardening parameter (cap yield surface). E_{ur}^{ref} is a common parameter to both yield surfaces. E_{50}^{ref} is more noticeable in the first part of the curve. The amount of decreasing in E_{oed}^{ref} results in more compressibility of the soil (Kempfert, & Gebreselassie, 2006).

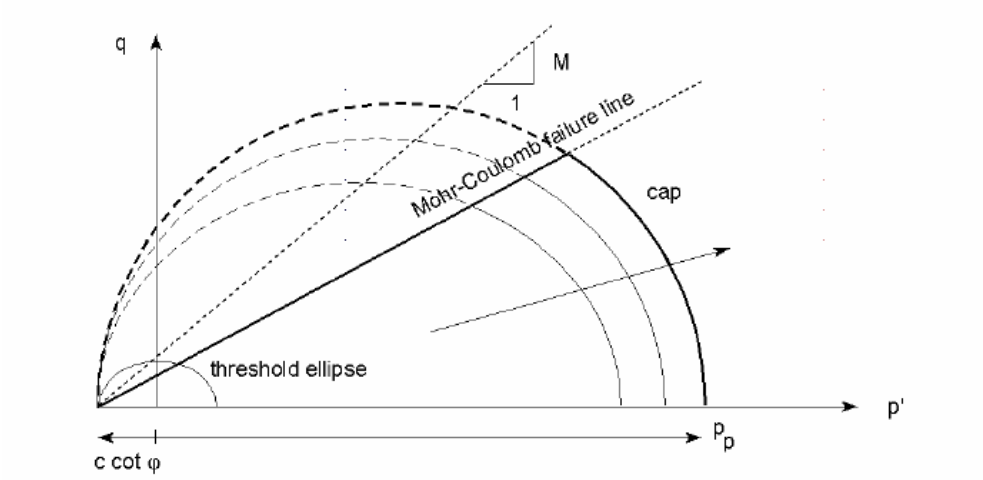

Figure 3.2 Yield surface of the soft soil model in $p' - q$ plane (After Brinkgrever, 2002).

The soft soil model is developed with using the cam clay model at PLAXIS program. The ellipse of the soft soil model occurs a half of ellipse on Figure 3.2. When the ellipse and Mohr-coulomb intersect, the cap of soft soil model occurs, which is greater than cap of hardening soil model type of PLAXIS. Therefore, the cap of soft soil model is more swollen than the cap of hardening soil model (see Fig.3.3).

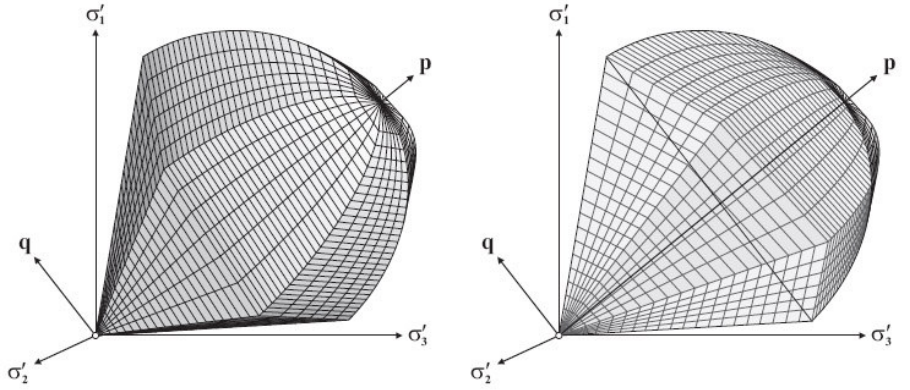

Figure 3.3 Yield surface of soft soil model in principal stress space.(After Wehnert, 2006)

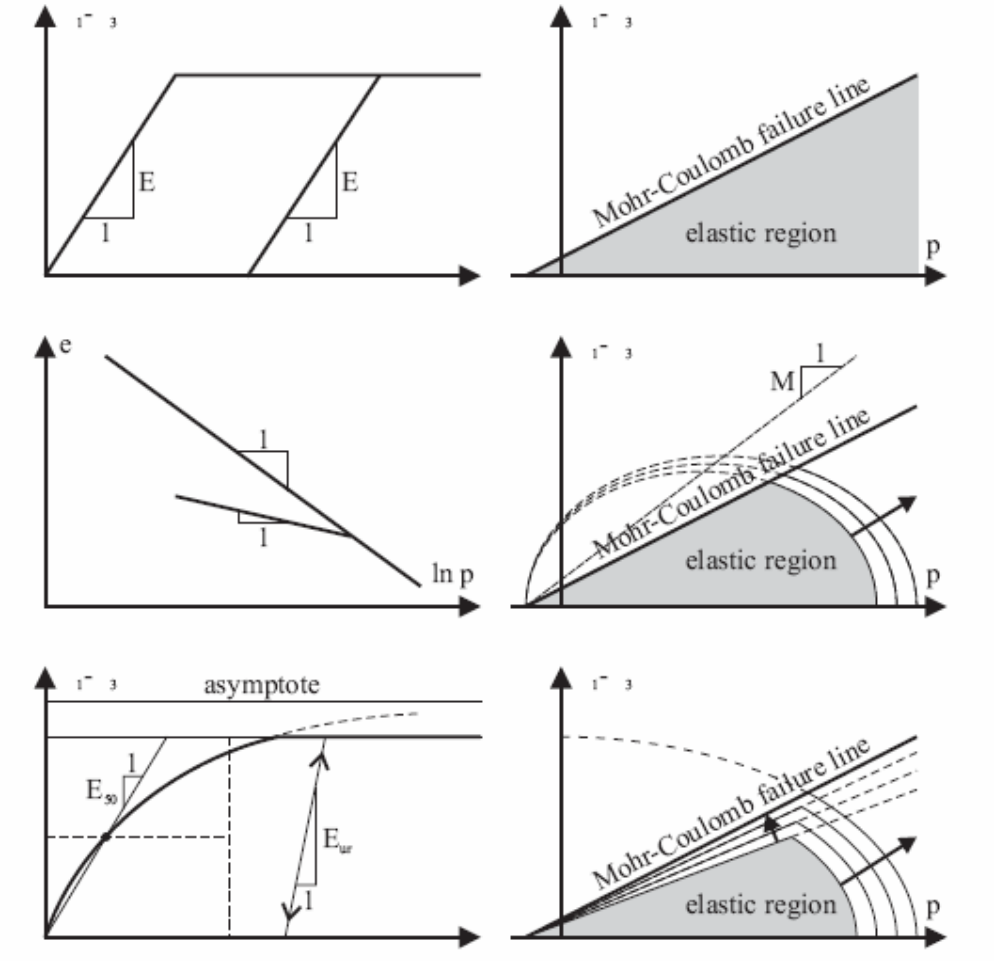

Figure 3.4 Basic ideas of MC (at top),the SS(at middle) and HS (at bottom) model; p'=1/3($\sigma'_1 + \sigma'_2 + \sigma'_3$); (After Wehnert & Vermeer,2004b)

In Figure 3.4, the comparison and explanation of some models are given in PLAXIS. In the first row, elastic model is available and E, Elastisite modulus is emphasized. The second row has soft soil model and there are the slopes λ and κ of the normal compression and swelling lines in e-ln p' space. The last row has hardening soil model, while whole studies of thesis use the model.

The Soft soil model includes a linear stress dependency. While plotting a stress-stiffness curve from an oedometer test, a line of the form E_{oed} = σ/λ* is formed. This condition leads to the logarithmic relationship between the volumetric strain ε_v and the mean effective stress p' in the Soft Soil model

$$\varepsilon_v - \varepsilon_{vo} = \lambda^* \ln\left(\frac{p'}{p'_o}\right) \tag{3.1}$$

Because of the usage of the volumetric strain (ε_v), instead of the void ratio (e); the equation 3.1 involves the modified compression index (λ*), instead of the compression index (λ) (Burland, 1965). The modified swelling index (κ*) determines the elastic behaviour during the unloading and reloading processes (Wehnert & Vermeer,2004b).

$$\varepsilon_v - \varepsilon_{vo} = \kappa^* \ln\left(\frac{p'}{p'_o}\right) \tag{3.2}$$

3.3 The Analysis of the Oedometer Tests' Data on PLAXIS

The model of the oedometer test in PLAXIS program explains to establish with the soil material type that is hardening soil model at Appendix – E.

The results of oedemeter tests are evaluated at the following table:

Table 3.2 The variables of derived models

Model name	**E_eod**	**E_50**	**E_ur (E_50*3)**	**φ**	**m**	v_{ur}	**ψ**	**c**
—	**(kN/m²)**	**(kN/m²)**	**(kN/m²)**	**(°)**	**—**	**—**	**—**	**—**
E models								
E5	E_oed_c	(E_oed*(1/0,5))	3*E_50	φ_c	1	0.20	0	0.005
E6	E_oed_c	(E_oed*(1/0,6))	3*E_50	φ_c	1	0.20	0	0.005
E7	E_oed_c	(E_oed*(1/0,7))	3*E_50	φ_c	1	0.20	0	0.005
E8	E_oed_c	(E_oed*(1/0,8))	3*E_50	φ_c	1	0.20	0	0.005
A models								
A1	E_oed_c	(E_oed*(1/0,8))	3*E_50	φ_c	0.8	0.20	0	0.005
A2	E_oed_c	(E_oed*(1/0,8))	3*E_50	φ_c	0.9	0.20	0	0.005
A3	E_oed_c	(E_oed*(1/0,8))	3*E_50	φ_c	0.7	0.20	0	0.005
A4	E_oed_c	(E_oed*(1/0,8))	3*E_50	φ_c	1	0.20	0	0.005
A5	E_oed_c	(E_oed*(1/0,8))	3*E_50	φ_c	1	0.15	0	0.005

*_c means constant value that for specimens' own value at Appendix - D

The E models begin with the definition of cam clay model at PLAXIS manual. E5 model represents it. The others of E models are derived from E5 model using to increase 0.1 at ratio $E_{oed}^{ref} / E_{50}^{ref}$, but in results of E models, a little influence visualizes on odeometer test results, whereas the book of "Excavations and Foundations in Soft Soils" by Kempfert and Gebreselassie emphasizes to the change in stiffness parameters E_{ur}^{ref} , E_{50}^{ref} and E_{oed}^{ref} on the stress-strain behaviour.

The A models are a more successful approach than the E models. The A1 model is similar to soil behaviour at B16-1, B17-1, B19-1 and B20-1. The A2 model is similar to soil behaviour at B02-2, B03-1, B14-1, B16-2, B18-1, B18-2, B20-2 and B24-1. The A3 model is similar to soil behaviour at B10-2 and B15-1. The A4 model is similar to soil behaviour at B10-1 and B17-2. The A5 model is similar to soil behaviour at B09-2.

The variables in the analysis of A models, which are the m and v_{ur}, cause the visible change in the schematics of analysis. The schemas are given in Appendix - H.

Figure 3.5 illustrates soil behaviours of Northern İzmir Bay areas by specimens of oedometer tests. Most of the curves are in a range between B09-1 and B12-1. This condition is assumed to be boundary value for the representation of Northern İzmir Bay areas.

Under this condition, the analyses are repeated. When this process begins, ψ is taken into account to be in a range between 0° and 8° from "Numerical investigation into stress and strain development around a displacement pile in sand" which is written by Dijkstra, Broere and van Tol. ψ is affected by arm of parabola. The upward arm of parabola begins to rotates clockwise according to increasion at the value of ψ. ψ, dilatancy angle's effection is neglected in my study because the different is very little. It may caused the degree of φ, friction angle that is less than 30.

Second approach is investigated to provide a general curve of the most of soil specimens that are represented. Before the general curve is researched, the boundary limits are plotted according to involved the most of values of soil specimens that contain through the new boundary curves. There are initial curve and final curve. The slope of initial curve is near to 4000 kN/m^2. The slope of final curve is near to 5000 kN/m^2 at which reference pressure is 100 kN/m^2. Start point is cam clay model's parameters. Figure 3.6 is involved the curve of specimens and M5 model. Diffirent models are set with change the parameters of program by trial and error method and M5 is best of the models. Figure 3.7 illustrates the models. Table of the parameters are given in Appendix - H.

M19 is given an amazing result, M19 has differed a parameter from M18. E_{ur}^{ref} is nearly to double of E_{ur}^{ref} of M18. PLAXIS seminer note or PLAXIS manual are

emphasized to the cap model that occurs with only E_{oed}^{ref}, but it can see E_{ur}^{ref} that make more stiff to soil model.

Third approach is limits of parameters that are determined:

- $0.5 < m < 1$,
- $0.15 < \nu_{ur} < 0.25$ for odeometer's results,
- 4000 kN/m^2 < E_{oed}^{ref} < 5000 kN/m^2 for only this study.

They can easily change parameters and occur great influence than others.

The follow path is trail and error method again and derived models. G model series is set. Figure 3.9 show the whole G models. ν_{ur} is selected 0.15 for providing big change. E_{ur}^{ref} is prefer to be least value of G3 which is accepted on PLAXIS. Then only parameter m is increased step by step. Figure 3.10 is illustrated the multi-altenative solution.

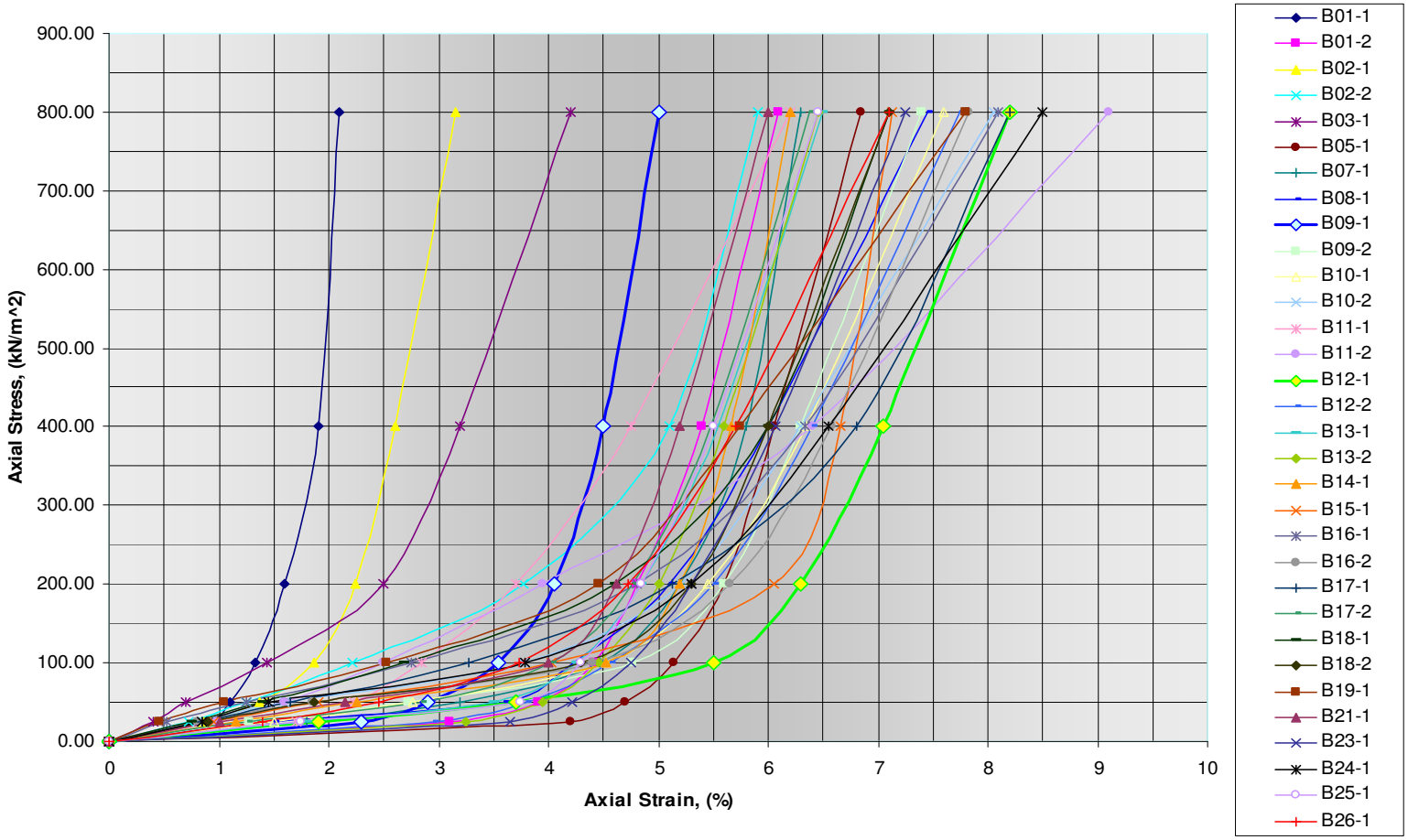

Figure 3.5 The plotting odeometer test results of the soil experiments belong to the coast road of Karşıyaka – Alaybey - Bostanlı route

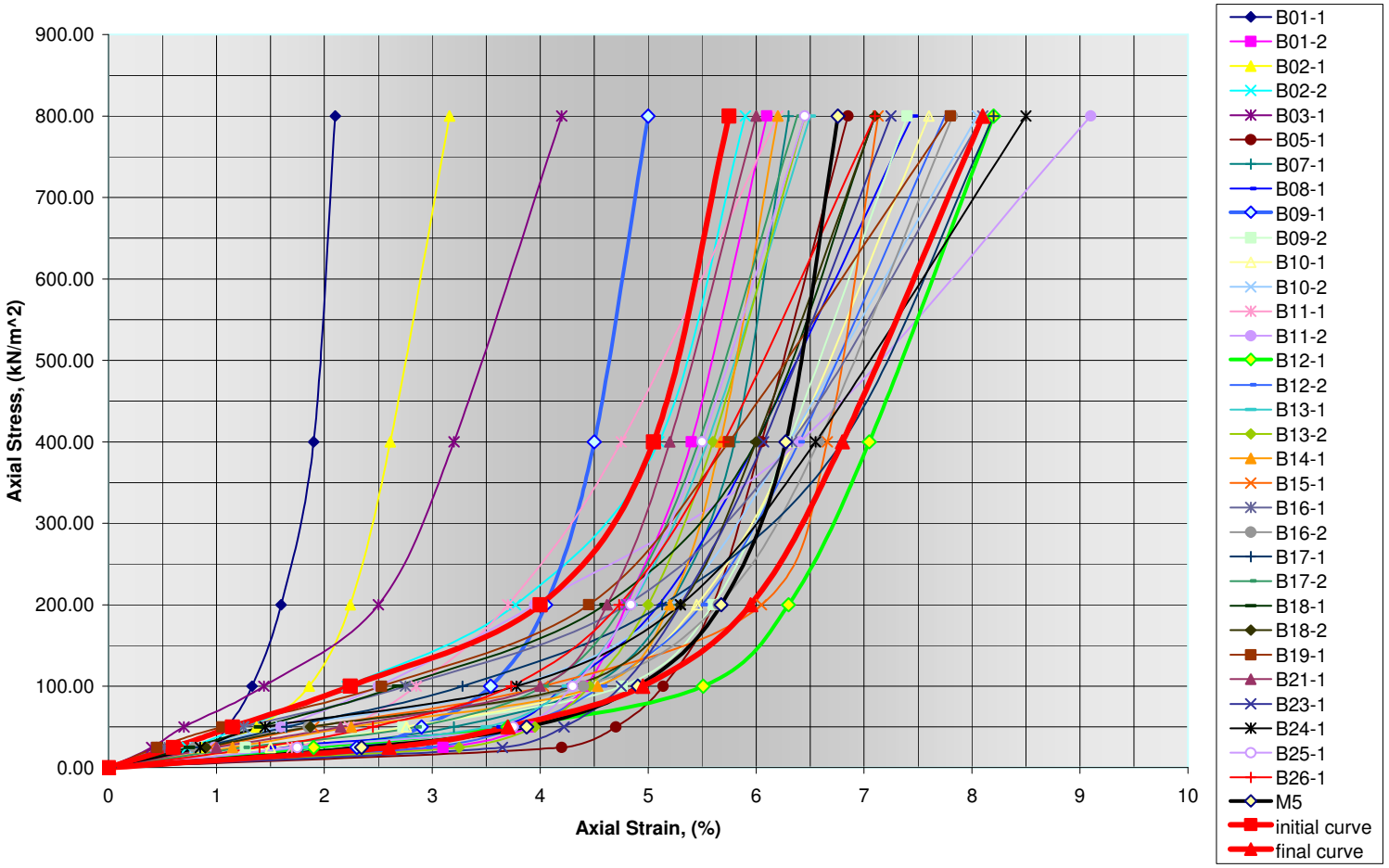

Figure 3.6 Determination of the boundary curves and finding a general model (M5) of deformation

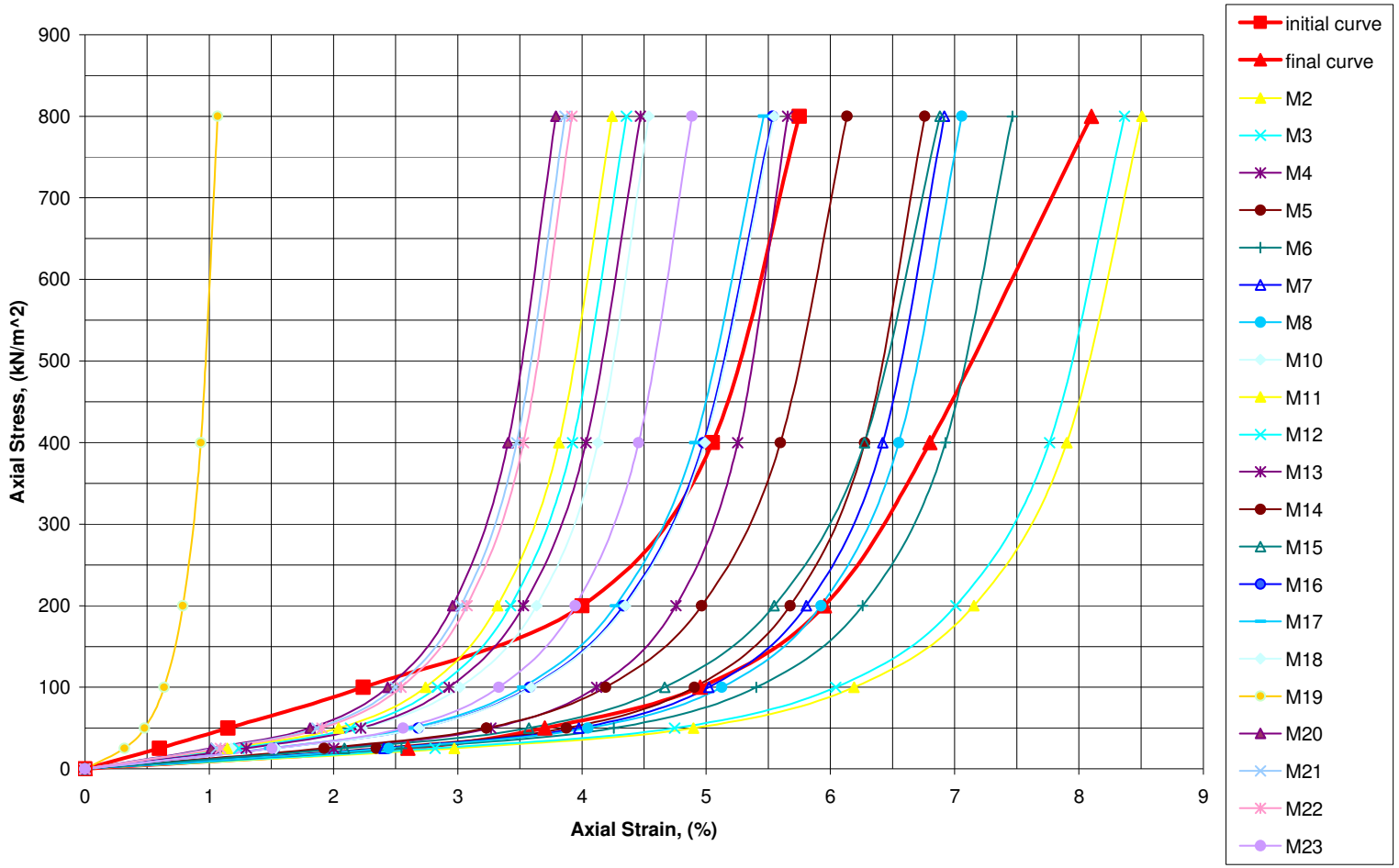

Figure 3.7 The representation of the whole M models

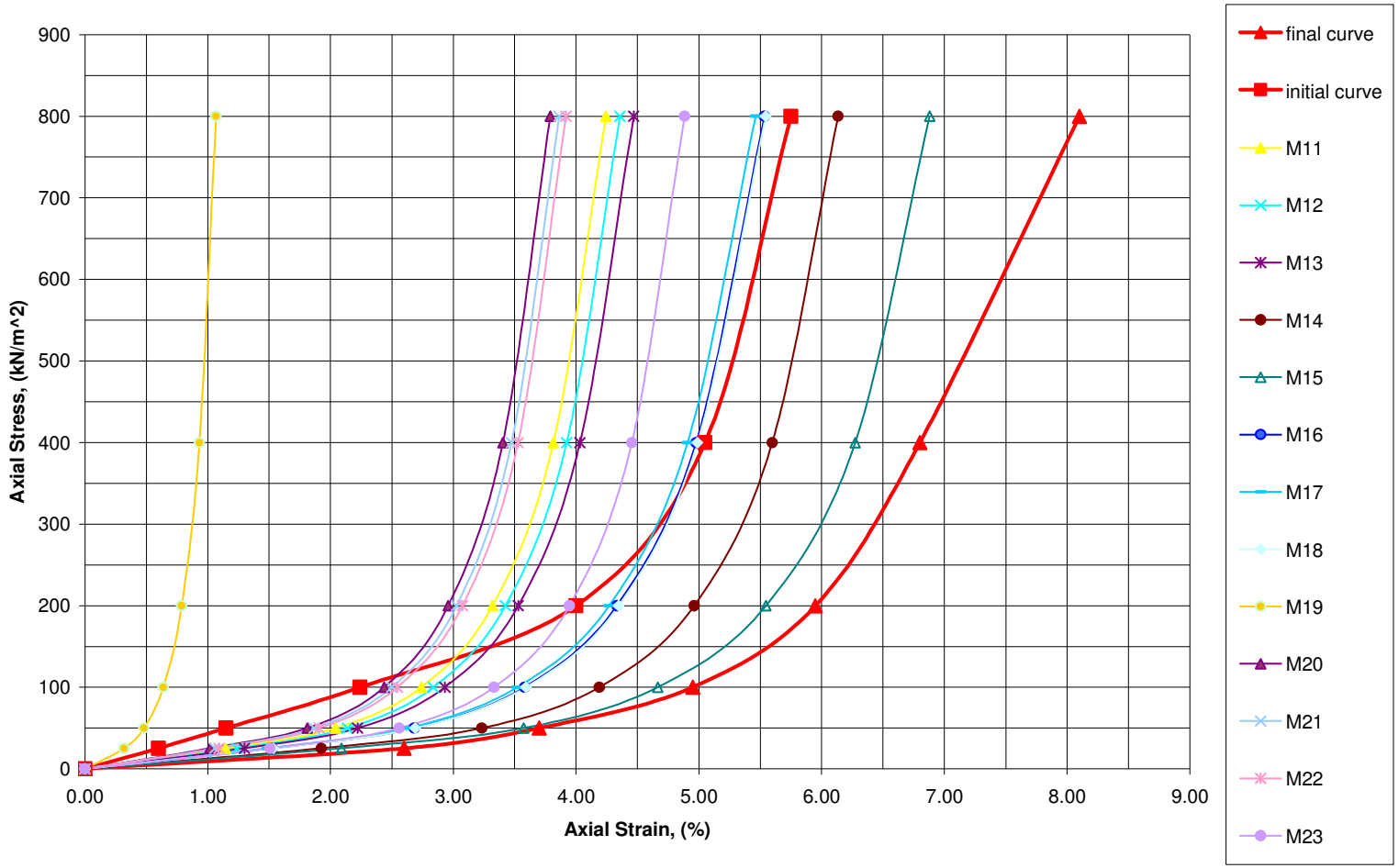

Figure 3.8 The representation of the some M models that have better results.

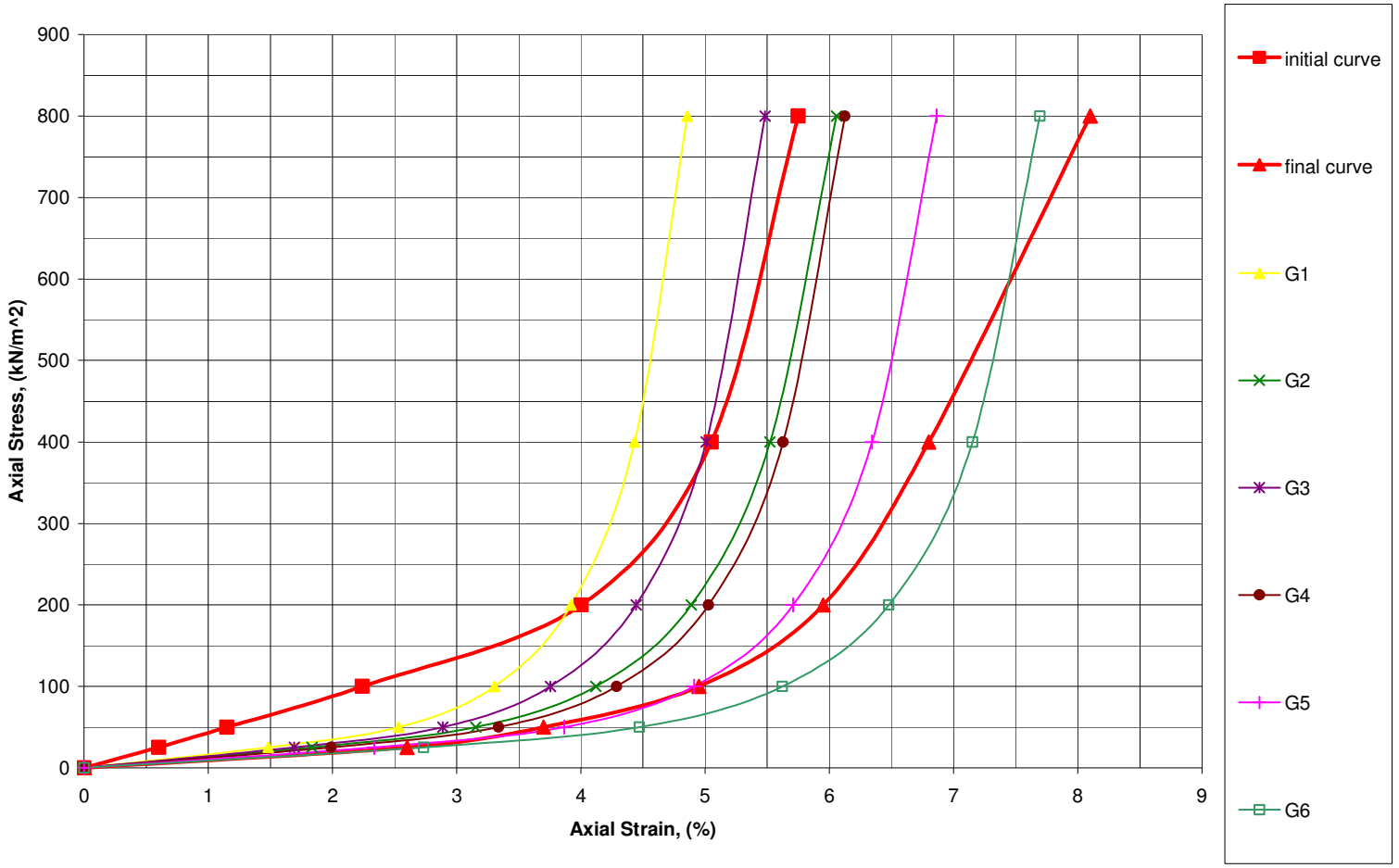

Figure 3.9 The representation of the whole G models

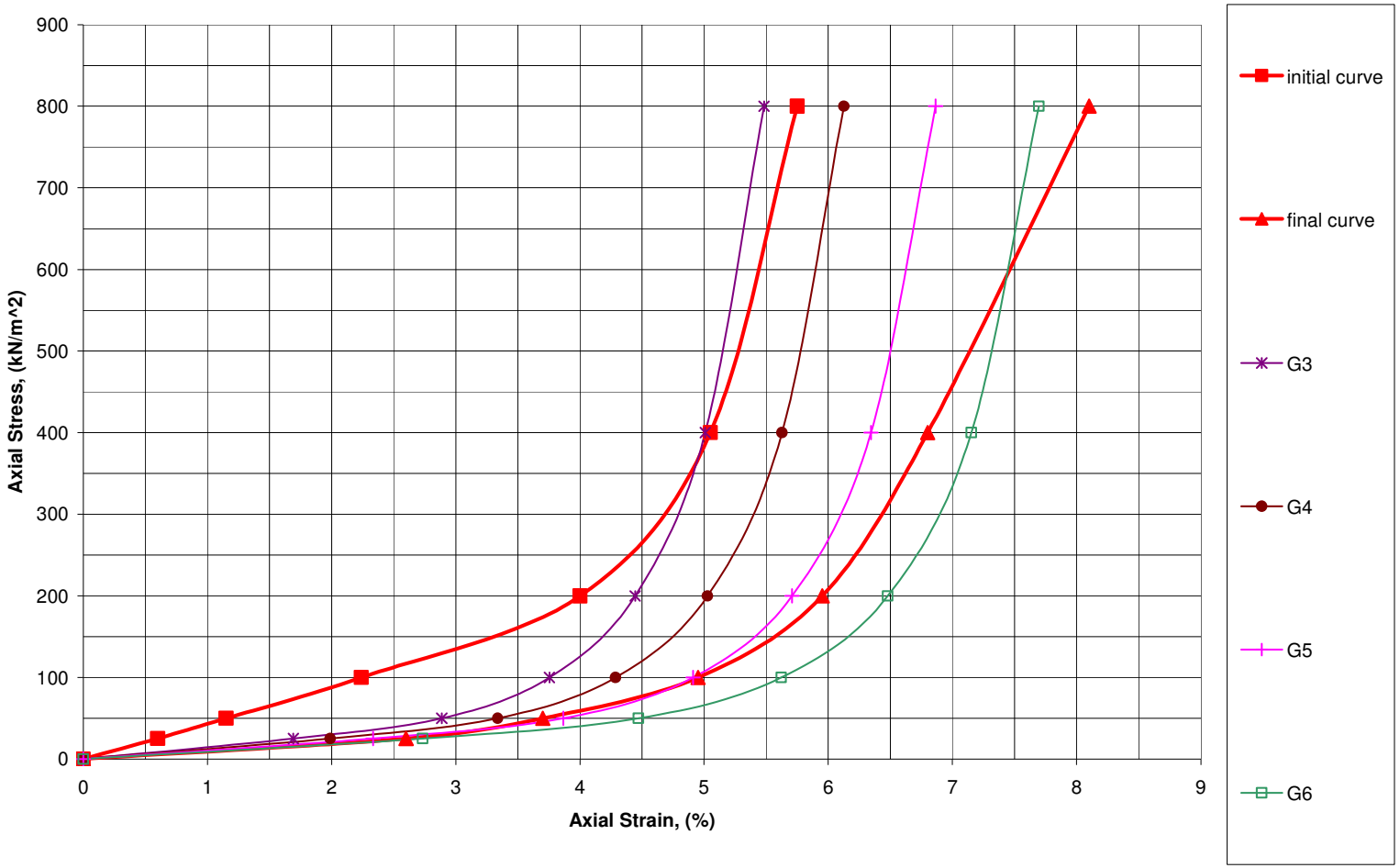

Figure 3.10 The representation of a relationship between soils of Northern İzmir bay areas and the G models

3.4 The Effects of PLAXIS Parameters on Test Results

In the oedometer model at PLAXIS program, some variables of soil material type are evaluated how to draw under a condition that all of variables are same, but each of them only takes different values.

The change in PLAXIS parameters causes some effections. The arm of parabola is greater than the arm of former parabola,

- when m is increasing,
- when v_{ur} is decreasing,
- or when E_{50}^{ref} is decreasing.(See Fig.3.11)

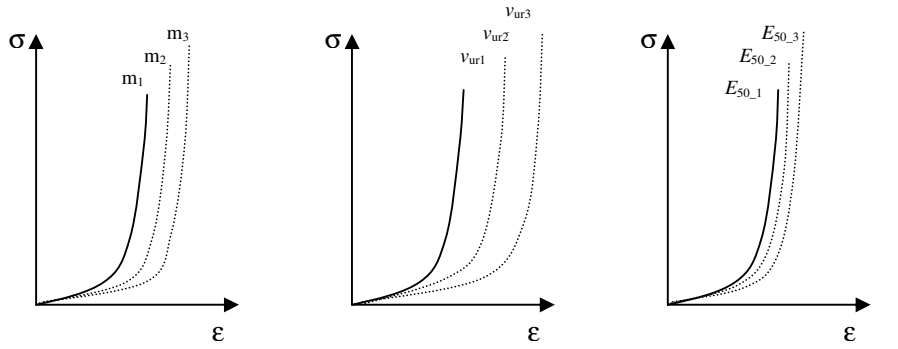

a) $m_1<m_2<m_3$ b) $v_{ur1}> v_{ur2}> v_{ur3}$ c) $E_{50\_1}> E_{50\_2}> E_{50\_3}$

Figure 3.11 The relationship of the parameters of the hardening soil model at PLAXIS

CHAPTER FOUR

CONCLUSIONS AND RECOMMENDATIONS

4.1 Conclusions

The aim of this thesis is to investigate the behaviour of Northern İzmir Bay area soils in the framework of hardening soil models using finite element method. In the scope of this thesis study, the oedometer test results of Northern İzmir Bay Area soils belonging to a site investigation study titled as "The Report of Soil Experiments Belongs to the Coastal Road of Karşıyaka-Alaybey-Bostanlı Route, 1984" were utilized. The data reduction of oedometer tests were made using MATLAB mathematics software suit by obtaining the best fit curve using *cubic spline model* as shown in Figure 2.37.

Firstly, all of the oedometer tests were evaluated individually. This approach has resulted in the A and E models. These curves, however, failed to model the original data completely. Therefore, some readings on the tails of the original curves were eliminated. Then, lower and upper limit curves were determined for further data analyses. After having E_{oed}^{ref} determined, the slopes of the lower limit and upper limit curves were found to be approximately 4000 kN/m^2 and 5000 kN/m^2, respectively.

The second step was to develop an average model that can represent the entire data. The determination of the parameters were made using cam clay model parameters as suggested in the seminar notes of Plaxis (Brinkgreve, 2007) following the trial and error method. The best fit parameters of M models for representation of the average model is given by Model # M5.

Finally, the experience gained in the trials using regular ranges given in the Plaxis manual and cam-clay parameter fitting analyses a final attempt has been made to obtain the best correlating finite element hardening model parameters. This approach may be called as the multi-alternative solution. This approach has resulted in the so-called G Models. In this approach firstly two curves are obtained for the lower and upper limits of the test data. These curves are named as G3 and G6, respectively. They represent the best fit curves to the limit values. It is believed that the multi-alternative solution is the best approach in this thesis study. The engineer willing to apply this model to his/her analysis is expected to choose the best applicable curve to the problem among available curves presented in this study.

4.2 Recommendations

In PLAXIS, application of the hardening soil model to the Northern İzmir Bay area soils requires considerably hard work since it is almost impossible to represent the real soil behavior by choosing the original hardening model parameters as given in the Plaxis Manual. It appears that soft soil model may better represent the regional soil characteristics provided that satisfactory test data are available.

The complexity of the microstructure of the soil and influence of the environmental factors such as temperature are expected to insert a considerable scattering of the best-fit models established to represent the test data using Plaxis hardening model. This aspect of the hardening model was pronounced by various researchers in the past (Tamagnini, Castellanza, and Nova , 2002; Nova, 2005).

The lower-upper boundary limiting values approach is a frequently followed engineering analysis method in daily geotechnical project and design studies. The geotechnical engineer decides for the best representing analysis result after having several runs using lower and upper limit soil parameters. In this respect, the G Models of this thesis study can be applied to engineering problems of the region. It is suggested that future studies are made depending on comprehensive oedometer and triaxial test data including the unloading-reloading soil stiffness, E_{ur}^{ref} .

REFERENCES

Abate, G., Caruso, C., Massimino, M. R. &Maugeri, M. (2006). Validation of a new soil constitutive model for cyclic loading by FEM analysis. *Soil Stress-Strain Behaviour: Measurement, Modeling and Analysis Geotechnical Symposium in Roma, March 16 & 17, 2006,* (759–768). Retrieved June 3, 2008, from Springer.

Abed, A. A.(February 2008). *Numerical modeling of expansive soil behaviour.* PhD Thesis, University of Stuttgart, Baden, Germany, Retrieved June 5, 2008, from http://www.uni-stuttgart.de/igs/content/publications/Diss_Abed_Online.pdf.

Abraham, K. (May,2007). *Three dimensional behaviour of retaining wall systems* PhD Thesis, university of Louisiana, Louisiana, USA. Retrieved November 28, 2007, from http://etd.lsu.edu/docs/available/etd-04092007-161907/unrestricted/-Abraham_dis.pdf.

Airey, D.,(2006). *Stress-Strain Behaviour of Soils.* Retrieved November 23, 2007 from www.civil.usyd.edu.au/courses/civl2410/smb2.ppt.

Al-Buraim, I. M.,(May, 1990). St*udying the behaviour of Dhahran Dune sand using the 3rd invariant stress dependent combined hardening cap model.* MA. Thesis, King Fahd University of Petroleum & Minerals, Dhahran, Arabia. Retrieved August 3, 2008, from https://eprints.kfupm.edu.sa/9815/1/9815.pdf.

Amorosi, A., Boldini, D.& Germano, V. (2007). Implicit Integration of A mixed Isotropic-Kinematic Hardening Plasticity Model for Structured Clays*. Int. J. Numer. Anal. Meth. Geomech.,* DOI:10.1002/nag.663, 1-31, Retrieved November 23, 2007, from Wiley database.

Bell, J. M., (1965). *Stress-strain characteristics of cohensionless granular materials subjected to statically applied homogeneous loads in an open system.* PhD Thesis, university of California Institute of Technology, Pasadena, California, USA.

Boldyrev, G. G., Idrisov, I. Kh. & Valeev D. N. (2006). Determination of parameters for soil models. *Soil Mechanics and Foundation Engineering,* 43(3), 101-108. Retrieved June 3, 2008, from Springer database.

Boscan, O., (August 2004). *Experimental and computational modeling of granular materials.* PhD Thesis, university of Louisiana State, USA. Retrieved November 28, 2007, from http://etd.lsu.edu/docs/available/etd-07072004-211420/-unrestricted/Boscan_thesis.pdf.

Bowles, J. E., (1997). *Foundation analysis and design*.(5th Ed.) Singapore: The McGraw-Hill comp.Part-2.

Brinkgreve, R.B.J. (Ed.). (2002). *Manual of PLAXIS 2-D – version 8.2*. Netherlands: A.A Balkema Publishers.

Brinkgreve, R.B.J. (2007). *Seminar note of PLAXIS manual,* Plaxis bv & Delft University of Technology.

CamClay,*Description of Cam-Clay and Modified-Cam-Clay Critical State Strength Models* (n.d.) Retrieved November 27, 2007, from http://www-.rocscience.com/downloads/phase2/WebHelp/pdf_files/theory/CamClay.pdf.

Chen, W. F., (1985). Constitutive Relations for Concrete, Rocks and Soils: Discusser's Report. In Bazant, Z. P. (Ed). (1990). *Mechanics of Geomaterials: Rocks, Concretes, Soils* (2nd ed), (65 – 86). University Microfilms International, Michigan: UMI Print.

Clough, R. W., (1960). The finite element method in plane stress analysis. Proceedings, *ASCE, Conference on electronic computation*, Pittsburg, USA.

Davis, R. O. & Selvadurai, A. P. S.,(1996). *Elasticity and geomechanics*. NewYork, USA: Cambridge Uni.press.

Dijkstra, J., Broere, W. & van Tol, A.F. (2006). Numerical investigation into stress and strain development around a displacement pile in sand. *6th NUMGE Conference*, Granz, Austria, September 2006, 6th -8th . Retrieved by August 4,

2008 from http://www.geo.citg.tudelft.nl/broere/pdf/dijkstra_numerical_pi_-numge2006.pdf.

Dougill, J. W. (1985). Constitutive Relations for Concrete and Rock: Applications and Extensions of Elasticity and Plasticity Theory. In Bazant, Z. P. (Ed). (1990). *Mechanics of Geomaterials: Rocks, Concretes, Soils* (2nd ed), (21 – 46). University Microfilms International, Michigan: UMI Print.

Duncan, J. M., Chang, C. Y., (1970). Nonlinear analysis of stress and strain in soils. Proceedings, *ASCE, Journal of The Soil Mechanics and Foundations Division,* 5, 1629 – 1953.

Gajo, A. & Muir Wood, D., (2001). A new approach to anisotropic, bounding surface plasticity: general formulation and simulations of natural and reconstituted clay behaviour. *Int. J. Numer. Anal. Meth. Geomech.* 25 (207-241). Retrieved June 3, 2008, from Wiley database.

Girijavallabhan, C. V., Reese, L. C., (1968). Finite – element method for problems in soil mechanics, Proceedings, *ASCE, Journal of the Soil Mechanics and Foundations Division,* 2, 473 – 496.

Hintner, J., (April, 2008). *Analyse der Fundamentverschiebungen İnfolge Vertikaler und Geneigter Belastung*. PhD Thesis, University of Stuttgart, Baden, Germany, Retrieved September 01, 2008 from http://www.uni-stuttgart.de/igs-/content/publications/Diss_Hintner-57.pdf.

Huybrechts, N., De Vos, M., Whenham, V. (Eds.).(December,2004). *WP3: design tools; part1: use of finite element method in geotechnical design*, Retrieved August 02, 2006, from http://www-.geotechnet.org/upload/documents/wp3/WP3-final.pdf.

Janbu, N.,(1963). Soil compressibility as determined by oedometer and triaxial tests. *European conference on soil mechanics & foundations engineering,* Wiesbaden, Germany, 1, 19-25.

Karmakar, S., Sharma, J. and Kushwaha, R.L.,(2004). Critical state elasto-plastic constitutive models for soil failure in tillage – A review, *Canadian biosystems engineering* 46, (2.19-2.23) Retrieved August 05, 2008, from http://engrwww-.usask.ca/oldsite/societies/-csae/protectedpapers/c0346.pdf.

Kayalar, A. Ş., Yılmaz, R., (1984). *Karşıyaka Alaybey-Bostanlı Arası Sahil Yolu Zemin Deneyleri*. Uni.of Dokuz Eylül, İzmir, Türkiye.

Kempfert, H. G.,& Gebreselassie B., (2006). *Excavations and Foundations in Soft Soils* Netherlands: Springer-Verlag Berlin Heidelberg, Germany. Retrieved July 12, 2008, from Springer database.

Lade, P. V., Nam, J., Hong, W. P.,(2008). Interpretation of strains in torsion shear tests. *Computers and Geotechnics, doi:10.1016/j.compgeo.2008.02.001,* 1-15, Retrieved July 7,2008, from Elsiver database.

Laloui, L.,& Nuth, M., (2008). On the use of the generalised effective stress in the constitutive modeling of unsaturated soils. *Computers and Geotechnics*, doi:10.1016/j.compgeo.2008.03.002, 1-4. Retrieved July 7,2008, from Elsiver database.

Meißner, S., Quick, H., Arslan, U. & Zimmer, C. Displacement behaviour of shallow foundations under cyclic loading, *The 19th international conference on Magnetically levitated systems and linear drives*, Dresden, Germany. September 2006, 13.-15. from http://www.maglev2006.com/145_Meissner/145_meissner_-ok.pdf.

Modaressi, H. & Laloui, L. (1997). A thermo-viscoplastic constitutive model for clays. *Int. J. Numer. Anal. Meth. Geomech.,* vol. 21, 313-335. Retrieved July 07, 2008, from http://lmswww.epfl.ch/en/rech/thermo/LTVP%20model.pdf.

Moeller, S. C., (June, 2006). *Characteristic curve of an oedometer*. PhD Thesis, University of Stuttgart, Baden, Germany, Retrieved September 01, 2008, from http://www.uni-stuttgart.de/igs/content/publications/Doctoral_Thesis_Sven_-Moeller.pdf.

Newmark, N. M., (1960). Failure hypothesis for soils. Proceedings, *ASCE Research Conference On Soil Mechanics And Foundation Engineering*, 1, 162-178.

Nova, R., (2005). *A simple elasto-plastic model for soils and soft rocks.* Milan University of Technology, Baltimore, Retrieved November 28, 2007.from http://www.ce.jhu.edu/rajah/My%20Web%20Page/NSF%20Workshop%202005/Presentations/Session%202/Nova.pdf.

Powrie, W., (2004). *Soil Mechanics: Concept & Application*, (2nd ed.) NewYork, USA: Spon Press.

Schanz, T., Vermeer, P. A., Bonnier, P. G., (1999). The hardening soil model:Formulation and verification. *Beyond 2000 in computational Geotechnics-10 years of PLAXIS*. Balkema, Rotterdam, Retrieved November 28, 2007, from http://www.uni-stuttgart.de/igs/content/publications/40.pdf.

Schofield, A. & Wroth., (1968). *Critical State Soil Mechanics*. London, England: McGraw-Hill.

Tamagnini, C., Castellanza, R., and Nova, R., (2002). *A Generalized Backward Euler algorithm for the numerical integration of an isotropic hardening elastoplastic model for mechanical and chemical degradation of bonded geomaterials*. International Journal for Numerical and Analytical Methods in Geomechanics, 26, 963–1004, Retrieved December 12, 2007, from Wiley database.

Tatsuoka, F.,(2007). *Deformation and Strength Characteristics of Granular Materials: from experimental research for the last 35 years by a geotechnical engineering researcher III-1.* Department of Civil Engineering, Tokyo University of Science. Retrieved November 28, 2007, from http://soil.iis.u-tokyo.ac.jp/-HP2007/Lecture/winter_tatsuoka/3-1%20Nonlinear%20and%20Yield%20locus-2007.pdf.

Uchaipichat, A.,(July, 2005). *Experimental investigation and constitutive modeling of thermo-hydro mechanical coupling in unsaturated soil*. PhD Thesis, university of New South Wales, Sydney, NSW, Australia.

Vermeer, P. A., Marcher, T., and Ruse, N.,(2002). On the Ground Response Curve, *FELSBAU 20, 6,* 1-8*,* Retrieved November 28, 2007, from http://www.uni-stuttgart.de/igs/content/publications/68.pdf.

Wehnert, M., (March, 2006). *Ein Beitrag Zur Drainierten und undrainierten Analyse in der Geotechnik*. PhD Thesis, University of Stuttgart, Baden, Germany, Retrieved July 28, 2008, from http://www.uni-stuttgart.de/igs/content-/publications/Diss_Benz.pdf.

Wehnert, M., Vermeer, P. A.,(2004a). Numerische simulation von probebelastungen an Großhohrpfählen, Proceedings of *the 4th Kolloquiuni Bauen in Boden und Fels, Ostjildern,* TAE: 555-565, Retrieved July 28, 2008, from http://www.uni-stuttgart.de/igs/content/publications/93.pdf.

Wehnert, M., Vermeer, P. A.,(2004b). Numerical Analyses of load tests on board piles. NUMOG (9^{th}), 25-27 August 2004, Ottawa, Canada, Retrieved July 28, 2008, from http://www.uni-stuttgart.de/igs/content/publications/100.pdf.

Wheeler, S.J., Cudny, M., Neher, H.P., Wiltafsky, C., (2003). *Some developments in constitutive modelling of soft clays*. Int. Workshop on Geotechnics of Soft Soils-Theory and Practice, Retrieved July 28, 2008, from http://www.uni-stuttgart.de-/igs/content/publications/81.pdf.

Yao, Y.P., Sun, D.A.& Matsuoka, H., (2007). A unified constitutive model for both clay and sand with hardening parameter independent on stress path. *Int. J. Comput. Geotech.* 4.3 (1-13), Retrieved November 23, 2007 from ScienceDirect database.

APPENDICES

Appendix A: The Results of Oedometer Tests on MS EXCEL

Table A. 1 The result of oedometer test of specimen B01-1

Borehole no:	1	Specimen No:	T1	Depth(m):	3.00-3.45
Diameter(cm):	7	Wet weight(gr):	139,260	Natural unit weight (gr/cm^3)	1,905
Height(cm):	1,9	Dry weight(gr):	108,450	Dry unit weight (gr/cm^3)	1,483
Area (cm^2):	38,484	Water weight(gr):	30,810	Water content, (%)	0,284
Volume (cm^3):	73,120	Specific gravity	2,610	Initial void ratio, e_0	0,760

Pressure, σ (kg/cm^2)	0-0,25	0,25-0,50	0,50-1,00	1,00-2,00	2,00-4,00	4,00-8,00
Final pressure, σ_f (kg/cm^2)	0,25	0,50	1,00	2,00	4,00	8,00
Change in Pressure, Δσ (kg/cm^2)	0,25	0,25	0,50	1,00	2,00	4,00
Initial dial reading, Di (-)	420	770	875	1002	1155	1335
Final dial reading, Df (-)	770	875	1002	1155	1335	1538
Dial reading, ΔD (-)	350	105	127	153	180	203
Change in Height of solid, ΔH (cm)	0,07	0,021	0,025	0,031	0,036	0,041
Initial Height of solids, Hi (cm)	1,900	1,830	1,809	1,784	1,753	1,717
Final Height of solids, Hf (cm)	1,83	1,809	1,784	1,753	1,717	1,676
Average of Height of solids; Hav (cm)	1,865	1,820	1,796	1,768	1,735	1,697
Drainage of Height of solids, H dr (cm)	0,933	0,910	0,898	0,884	0,868	0,848
Change in void ratio, Δe (-)	0,065	0,019	0,024	0,028	0,033	0,038
Void ratio, e (-)	0,695	0,676	0,652	0,624	0,590	0,553
Avarage of void ratio, e_{av} (-)	0,728	0,685	0,664	0,638	0,607	0,572
Coefficient of compressibility, ∂V (cm2 /kg)	0,259	0,078	0,047	0,028	0,017	0,009
Coefficient of volume compressibility, mv (cm^2 / kg)	0,150	0,046	0,028	0,017	0,010	0,006

Table A. 2 The result of oedometer test of specimen B01-2

Borehole no:	1	Specimen No:	T7	Depth(m):	13.50-13.95
Diameter(cm):	7	Wet weight(gr):	119,930	Natural unit weight (gr/cm^3)	1,640
Height(cm):	1,9	Dry weight(gr):	74,910	Dry unit weight (gr/cm^3)	1,024
Area (cm^2):	38,484	Water weight(gr):	45,020	Water content, (%)	0,601
Volume (cm^3):	73,120	Specific gravity	2,620	Initial void ratio, e_0	1,557

Pressure, σ (kg/cm^2)	0-0,25	0,25-0,50	0,50-1,00	1,00-2,00	2,00-4,00	4,00-8,00
Final pressure, σ_f (kg/cm^2)	0,25	0,50	1,00	2,00	4,00	8,00
Change in Pressure, Δσ (kg/cm^2)	0,25	0,25	0,50	1,00	2,00	4,00
Initial dial reading, Di (-)	400	950	1282	1722	2236	2813
Final dial reading, Df (-)	950	1282	1722	2236	2813	3345
Dial reading, ΔD (-)	550	332	440	514	577	532
Change in Height of solid, ΔH (cm)	0,110	0,066	0,088	0,103	0,115	0,106
Initial Height of solids, Hi (cm)	1,900	1,790	1,724	1,636	1,533	1,417
Final Height of solids, Hf (cm)	1,790	1,724	1,636	1,533	1,417	1,311
Average of Height of solids; Hav (cm)	1,845	1,757	1,680	1,584	1,475	1,364
Drainage of Height of solids, H dr (cm)	0,923	0,878	0,840	0,792	0,738	0,682
Change in void ratio, Δe (-)	0,148	0,089	0,118	0,138	0,155	0,143
Void ratio, e (-)	1,409	1,320	1,201	1,063	0,908	0,764
Avarage of void ratio, e_{av} (-)	1,483	1,364	1,260	1,132	0,985	0,836
Coefficient of compressibility, ∂V (cm2 /kg)	0,592	0,357	0,237	0,138	0,078	0,036
Coefficient of volume compressibility, mv (cm^2 / kg)	0,238	0,151	0,105	0,065	0,039	0,019

Table A. 3 The result of oedometer test of specimen B02-1

Borehole no:	2	Specimen No:	T2	Depth(m):	4.50–4.95
Diameter(cm):	7	Wet weight(gr):	141,500	Natural unit weight (gr/cm^3)	1,935
Height(cm):	1,9	Dry weight(gr):	106,500	Dry unit weight (gr/cm^3)	1,456
Area (cm^2):	38,484	Water weight(gr):	35,000	Water content, (%)	0,329
Volume (cm^3):	73,120	Specific gravity	2,600	Initial void ratio, e_0	0,785

Pressure, σ (kg/cm^2)	0-0,25	0,25-0,50	0,50-1,00	1,00-2,00	2,00-4,00	4,00-8,00
Final pressure, σ_f (kg/cm^2)	0,25	0,500	1,00	2,00	4,00	8,00
Change in Pressure, Δσ (kg/cm^2)	0,25	0,25	0,50	1,00	2,00	4,00
Initial dial reading, Di (-)	555	930	1060	1237	1450	1698
Final dial reading, Df (-)	930	1060	1237	1450	1698	1998
Dial reading, ΔD (-)	375	130	177	213	248	300
Change in Height of solid, ΔH (cm)	0,075	0,026	0,035	0,043	0,050	0,060
Initial Height of solids, Hi (cm)	1,900	1,825	1,799	1,764	1,721	1,671
Final Height of solids, Hf (cm)	1,825	1,799	1,764	1,721	1,671	1,611
Average of Height of solids; Hav (cm)	1,863	1,812	1,781	1,742	1,696	1,641
Drainage of Height of solids, H dr (cm)	0,931	0,906	0,891	0,871	0,848	0,821
Change in void ratio, Δe (-)	0,070	0,024	0,033	0,040	0,047	0,056
Void ratio, e (-)	0,715	0,690	0,657	0,617	0,570	0,514
Avarage of void ratio, e_{av} (-)	0,750	0,702	0,673	0,637	0,594	0,542
Coefficient of compressibility, ∂V (cm2 /kg)	0,282	0,098	0,067	0,040	0,023	0,014
Coefficient of volume compressibility, mv (cm^2 / kg)	0,161	0,057	0,040	0,024	0,015	0,009

Table A. 4 The result of oedometer test of specimen B02-2

Borehole no:	2	Specimen No:	T10	Depth(m):	16.50-16.95
Diameter(cm):	7	Wet weight(gr):	128,880	Natural unit weight (gr/cm^3)	1,763
Height(cm):	1,9	Dry weight(gr):	90,130	Dry unit weight (gr/cm^3)	1,233
Area (cm^2):	38,484	Water weight(gr):	38,750	Water content, (%)	0,430
Volume (cm^3):	73,120	Specific gravity	2,820	Initial void ratio, e_0	1,288

Pressure, σ (kg/cm^2)	0-0,25	0,25-0,50	0,50-1,00	1,00-2,00	2,00-4,00	4,00-8,00
Final pressure, σ_f (kg/cm^2)	0,25	0,50	1,00	2,00	4,00	8,00
Change in Pressure, Δσ (kg/cm^2)	0,25	0,25	0,50	1,00	2,00	4,00
Initial dial reading, Di (-)	475	655	775	986	1325	1821
Final dial reading, Df (-)	655	775	986	1325	1821	2375
Dial reading, ΔD (-)	180	120	211	339	496	554
Change in Height of solid, ΔH (cm)	0,036	0,024	0,042	0,068	0,099	0,111
Initial Height of solids, Hi (cm)	1,900	1.864	1.840	1.798	1.730	1.631
Final Height of solids, Hf (cm)	1,864	1,840	1,798	1,730	1,631	1,520
Average of Height of solids; Hav (cm)	1,882	1,852	1,819	1,764	1,680	1,575
Drainage of Height of solids, H dr (cm)	0,941	0,926	0,909	0,882	0,840	0,788
Change in void ratio, Δe (-)	0,043	0,029	0,051	0,082	0,119	0,133
Void ratio, e (-)	1,245	1,216	1,165	1,083	0,964	0,830
Avarage of void ratio, e_{av} (-)	1,266	1,230	1,190	1,124	1,024	0,897
Coefficient of compressibility, ∂V (cm2 /kg)	0,173	0,116	0,102	0,082	0,060	0,033
Coefficient of volume compressibility, mv (cm^2 / kg)	0,077	0,052	0,046	0,038	0,030	0,018

Table A. 5 The result of oedometer test of specimen B03-1

Borehole no:	3	Specimen No:	T10	Depth(m):	18.50-18.95
Diameter(cm):	7	Wet weight(gr):	141,560	Natural unit weight (gr/cm^3)	1,936
Height(cm):	1,9	Dry weight(gr):	109,600	Dry unit weight (gr/cm^3)	1,499
Area (cm^2):	38,484	Water weight(gr):	31,960	Water content, (%)	0,292
Volume (cm^3):	73,120	Specific gravity	2,630	Initial void ratio, e_0	0,755

Pressure, σ (kg/cm^2)	0-0,25	0,25-0,50	0,50-1,00	1,00-2,00	2,00-4,00
Final pressure, σ_f (kg/cm^2)	0,5	1,00	2,00	4,00	8,00
Change in Pressure, Δσ (kg/cm^2)	0,5	0,50	1,00	2,00	4,00
Initial dial reading, Di (-)	350	620	750	987	1295
Final dial reading, Df (-)	620	750	987	1295	1695
Dial reading, ΔD (-)	270	130	237	308	400
Change in Height of solid, ΔH (cm)	0,054	0.026	0.047	0.062	0.080
Initial Height of solids, Hi (cm)	1.900	1.846	1.820	1.773	1.711
Final Height of solids, Hf (cm)	1,846	1,820	1,773	1,711	1,631
Average of Height of solids; Hav (cm)	1,873	1,833	1,796	1,742	1,671
Drainage of Height of solids, H dr (cm)	0,937	0,917	0,898	0,871	0,836
Change in void ratio, Δe (-)	0,050	0,024	0,044	0,057	0,074
Void ratio, e (-)	0,705	0,681	0,637	0,580	0,507
Avarage of void ratio, e_{av} (-)	0,730	0,693	0,659	0,609	0,543
Coefficient of compressibility, ∂V (cm2 /kg)	0,100	0,048	0,044	0,028	0,018
Coefficient of volume compressibility, mv (cm^2 / kg)	0,058	0,028	0,026	0,018	0,012

Table A. 6 The result of oedometer test of specimen B05-1

Borehole no:	5	Specimen No:	T1	Depth(m):	6.45-6.90
Diameter(cm):	7	Wet weight(gr):	119,100	Natural unit weight (gr/cm^3)	1,629
Height(cm):	1,9	Dry weight(gr):	70,700	Dry unit weight (gr/cm^3)	0,967
Area (cm^2):	38,484	Water weight(gr):	48,400	Water content, (%)	0,685
Volume (cm^3):	73,120	Specific gravity	2,620	Initial void ratio, e_0	1,710

Pressure, σ (kg/cm^2)	0-0,25	0,25-0,50	0,50-1,00	1,00-2,00	2,00-4,00	4,00-8,00
Final pressure, σ_f (kg/cm^2)	0,25	0,50	1,00	2,00	4,00	8,00
Change in Pressure, Δσ (kg/cm^2)	0,25	0,25	0,50	1,00	2,00	4,00
Initial dial reading, Di (-)	720	1280	1655	2183	2760	3350
Final dial reading, Df (-)	1280	1655	2183	2760	3350	3930
Dial reading, ΔD (-)	560	375	528	577	590	580
Change in Height of solid, ΔH (cm)	0.112	0.075	0.106	0.115	0.118	0.116
Initial Height of solids, Hi (cm)	1.900	1.788	1.713	1.607	1.492	1.374
Final Height of solids, Hf (cm)	1,788	1,713	1,607	1,492	1,374	1,258
Average of Height of solids; Hav (cm)	1,844	1,751	1,660	1,550	1,433	1,316
Drainage of Height of solids, H dr (cm)	0,922	0,875	0,830	0,775	0,717	0,658
Change in void ratio, Δe (-)	0,160	0,107	0,151	0,165	0,168	0,165
Void ratio, e (-)	1,550	1,443	1,293	1,128	0,960	0,794
Avarage of void ratio, e_{av} (-)	1,630	1,497	1,368	1,210	1,044	0,877
Coefficient of compressibility, ∂V (cm2 /kg)	0,639	0,428	0,301	0,165	0,084	0,041
Coefficient of volume compressibility, mv (cm^2 / kg)	0,243	0,171	0,127	0,074	0,041	0,022

Table A. 7 The result of oedometer test of specimen B07-1

Borehole no:	7	Specimen No:	T4	Depth(m):	18.5-18.95
Diameter(cm):	7	Wet weight(gr):	119,430	Natural unit weight (gr/cm^3)	1,633
Height(cm):	1,9	Dry weight(gr):	75,360	Dry unit weight (gr/cm^3)	1,031
Area (cm^2):	38,484	Water weight(gr):	44,070	Water content, (%)	0,585
Volume (cm^3):	73,120	Specific gravity	2,570	Initial void ratio, e_0	1,494

Pressure, σ (kg/cm^2)	0-0,25	0,25-0,50	0,50-1,00	1,00-2,00	2,00-4,00	4,00-8,00
Final pressure, σ_f (kg/cm^2)	0,25	0,50	1,00	2,00	4,00	8,00
Change in Pressure, Δσ (kg/cm^2)	0,25	0,25	0,50	1,00	2,00	4,00
Initial dial reading, Di (-)	200	671	971	1390	1880	2432
Final dial reading, Df (-)	671	971	1390	1880	2432	3034
Dial reading, ΔD (-)	471	300	419	490	552	602
Change in Height of solid, ΔH (cm)	0.094	0.060	0.084	0.098	0.110	0.120
Initial Height of solids, Hi (cm)	1.900	1.806	1.746	1.662	1.564	1.454
Final Height of solids, Hf (cm)	1,806	1,746	1,662	1,564	1,454	1,333
Average of Height of solids; Hav (cm)	1,8529	1,776	1,704	1,613	1,509	1,393
Drainage of Height of solids, H dr (cm)	0,926	0,888	0,852	0,807	0,754	0,697
Change in void ratio, Δe (-)	0,124	0,079	0,110	0,129	0,145	0,158
Void ratio, e (-)	1,370	1,292	1,182	1,053	0,908	0,750
Avarage of void ratio, e_{av} (-)	1,432	1,331	1,237	1,117	0,980	0,829
Coefficient of compressibility, ∂V (cm2 /kg)	0,495	0,315	0,220	0,129	0,072	0,040
Coefficient of volume compressibility, mv (cm^2 / kg)	0,203	0,135	0,098	0,061	0,037	0,022

Table A. 8 The result of oedometer test of specimen B08-1

Borehole no:	8	Specimen No:	T1	Depth(m):	6.00-6.45
Diameter(cm):	7	Wet weight(gr):	123,400	Natural unit weight (gr/cm^3)	1,688
Height(cm):	1,9	Dry weight(gr):	78,000	Dry unit weight (gr/cm^3)	1,067
Area (cm^2):	38,484	Water weight(gr):	45,400	Water content, (%)	0,582
Volume (cm^3):	73,120	Specific gravity	2,640	Initial void ratio, e_0	1,475

Pressure, σ (kg/cm^2)	0-0,25	0,25-0,50	0,50-1,00	1,00-2,00	2,00-4,00	4,00-8,00
Final pressure, σ_f (kg/cm^2)	0,25	0,50	1,00	2,00	4,00	8,00
Change in Pressure, Δσ (kg/cm^2)	0,25	0,25	0,50	1,00	2,00	4,00
Initial dial reading, Di (-)	815	1017	1234	1670	2263	2873
Final dial reading, Df (-)	1017	1234	1670	2263	2873	3400
Dial reading, ΔD (-)	202	217	436	593	610	527
Change in Height of solid, ΔH (cm)	0.040	0.043	0.087	0.119	0.122	0.105
Initial Height of solids, Hi (cm)	1.900	1.860	1.816	1.729	1.610	1.488
Final Height of solids, Hf (cm)	1,860	1,816	1,729	1,610	1,488	1,383
Average of Height of solids; Hav (cm)	1,8798	1,838	1,773	1,670	1,549	1,436
Drainage of Height of solids, H dr (cm)	0,940	0,919	0,886	0,835	0,775	0,718
Change in void ratio, Δe (-)	0,053	0,057	0,114	0,154	0,159	0,137
Void ratio, e (-)	1,422	1,366	1,252	1,098	0,939	0,802
Avarage of void ratio, e_{av} (-)	1,449	1,394	1,309	1,175	1,018	0,870
Coefficient of compressibility, ∂V (cm2 /kg)	0,211	0,226	0,227	0,154	0,079	0,034
Coefficient of volume compressibility, mv (cm^2 / kg)	0,086	0,094	0,098	0,071	0,039	0,018

Table A. 9 The result of oedometer test of specimen B09-1

Borehole no:	9	Specimen No:	T1	Depth(m):	5,50-5,95
Diameter(cm):	7	Wet weight(gr):	126,890	Natural unit weight (gr/cm^3)	1,735
Height(cm):	1,9	Dry weight(gr):	84,020	Dry unit weight (gr/cm^3)	1,149
Area (cm^2):	38,484	Water weight(gr):	42,870	Water content, (%)	0,510
Volume (cm^3):	73,120	Specific gravity	2,590	Initial void ratio, e_0	1,254

Pressure, σ (kg/cm^2)	0-0,25	0,25-0,50	0,50-1,00	1,00-2,00	2,00-4,00	4,00-8,00
Final pressure, σ_f (kg/cm^2)	0,25	0,50	1,00	2,00	4,00	8,00
Change in Pressure, Δσ (kg/cm^2)	0,25	0,25	0,50	1,00	2,00	4,00
Initial dial reading, Di (-)	610	1123	1393	1782	2130	2563
Final dial reading, Df (-)	1123	1393	1782	2130	2563	3025
Dial reading, ΔD (-)	513	270	389	348	433	462
Change in Height of solid, ΔH (cm)	0,103	0,054	0,078	0,070	0,087	0,092
Initial Height of solids, Hi (cm)	1,900	1,797	1,743	1,666	1,596	1,509
Final Height of solids, Hf (cm)	1,797	1,743	1,666	1,596	1,509	1,417
Average of Height of solids; Hav (cm)	1,849	1,770	1,705	1,631	1,553	1,463
Drainage of Height of solids, H dr (cm)	0,924	0,885	0,852	0,815	0,776	0,732
Change in void ratio, Δe (-)	0,122	0,064	0,092	0,083	0,103	0,110
Void ratio, e (-)	1,132	1,068	0,976	0,893	0,791	0,681
Avarage of void ratio, e_{av} (-)	1,193	1,100	1,022	0,935	0,842	0,736
Coefficient of compressibility, ∂V (cm2 /kg)	0,487	0,256	0,185	0,083	0,051	0,027
Coefficient of volume compressibility, mv (cm^2 / kg)	0,222	0,122	0,091	0,043	0,028	0,016

Table A. 10 The result of oedometer test of specimen B09-2

Borehole no:	9	Specimen No:	T4	Depth(m):	18,00-18,45
Diameter(cm):	7	Wet weight(gr):	119,600	Natural unit weight (gr/cm^3)	1,636
Height(cm):	1,9	Dry weight(gr):	74,100	Dry unit weight (gr/cm^3)	1,013
Area (cm^2):	38,484	Water weight(gr):	45,500	Water content, (%)	0,614
Volume (cm^3):	73,120	Specific gravity	2,600	Initial void ratio, e_0	1,566

Pressure, σ (kg/cm^2)	0-0,25	0,25-0,50	0,50-1,00	1,00-2,00	2,00-4,00	4,00-8,00
Final pressure, σ_f (kg/cm^2)	0,25	0,50	1,00	2,00	4,00	8,00
Change in Pressure, Δσ (kg/cm^2)	0,25	0,25	0,50	1,00	2,00	4,00
Initial dial reading, Di (-)	400	790	1047	1394	2005	2615
Final dial reading, Df (-)	790	1047	1394	2005	2615	3265
Dial reading, ΔD (-)	390	257	347	611	610	650
Change in Height of solid, ΔH (cm)	0,078	0,051	0,069	0,122	0,122	0,130
Initial Height of solids, Hi (cm)	1,900	1,822	1,771	1,701	1,579	1,457
Final Height of solids, Hf (cm)	1,822	1,771	1,701	1,579	1,457	1,327
Average of Height of solids; Hav (cm)	1,861	1,796	1,736	1,640	1,518	1,392
Drainage of Height of solids, H dr (cm)	0,931	0,898	0,868	0,820	0,759	0,696
Change in void ratio, Δe (-)	0,105	0,069	0,094	0,165	0,165	0,176
Void ratio, e (-)	1,461	1,391	1,298	1,132	0,968	0,792
Avarage of void ratio, e_{av} (-)	1,513	1,426	1,344	1,215	1,050	0,880
Coefficient of compressibility, ∂V (cm2 /kg)	0,421	0,278	0,187	0,165	0,082	0,044
Coefficient of volume compressibility, mv (cm^2 / kg)	0,168	0,114	0,080	0,075	0,040	0,023

Table A. 11 The result of oedometer test of specimen B10-1

Borehole no:	10	Specimen No:	T1	Depth(m):	8,00–8,45
Diameter(cm):	7	Wet weight(gr):	108,750	Natural unit weight (gr/cm^3)	1,487
Height(cm):	1,9	Dry weight(gr):	75,000	Dry unit weight (gr/cm^3)	1,026
Area (cm^2):	38,484	Water weight(gr):	33,750	Water content, (%)	0,450
Volume (cm^3):	73,120	Specific gravity	2,640	Initial void ratio, e_0	1,574

Pressure, σ (kg/cm^2)	0-0,25	0,25-0,50	0,50-1,00	1,00-2,00	2,00-4,00	4,00-8,00
Final pressure, σ_f (kg/cm^2)	0,25	0,50	1,00	2,00	4,00	8,00
Change in Pressure, Δσ (kg/cm^2)	0,25	0,25	0,50	1,00	2,00	4,00
Initial dial reading, Di (-)	510	850	1065	1408	1825	2330
Final dial reading, Df (-)	850	1065	1408	1825	2330	2875
Dial reading, ΔD (-)	340	215	343	417	505	545
Change in Height of solid, ΔH (cm)	0,068	0,043	0,069	0,083	0,101	0,109
Initial Height of solids, Hi (cm)	1,900	1,832	1,789	1,720	1,637	1,536
Final Height of solids, Hf (cm)	1,832	1,789	1,720	1,637	1,536	1,427
Average of Height of solids; Hav (cm)	1,866	1,811	1,755	1,679	1,587	1,482
Drainage of Height of solids, H dr (cm)	0,933	0,905	0,877	0,839	0,793	0,741
Change in void ratio, Δe (-)	0,092	0,058	0,093	0,113	0,137	0,148
Void ratio, e (-)	1,482	1,424	1,331	1,218	1,081	0,933
Avarage of void ratio, e_{av} (-)	1,528	1,453	1,377	1,274	1,149	1,007
Coefficient of compressibility, ∂V (cm2 /kg)	0,368	0,233	0,186	0,113	0,068	0,037
Coefficient of volume compressibility, mv (cm^2 / kg)	0,146	0,095	0,078	0,050	0,032	0,018

Table A. 12 The result of oedometer test of specimen B10-2

Borehole no:	10	Specimen No:	T3	Depth(m):	15,00-15,45
Diameter(cm):	7	Wet weight(gr):	122,430	Natural unit weight (gr/cm^3)	1,674
Height(cm):	1,9	Dry weight(gr):	77,940	Dry unit weight (gr/cm^3)	1,066
Area (cm^2):	38,484	Water weight(gr):	44,490	Water content, (%)	0,571
Volume (cm^3):	73,12	Specific gravity	2,670	Initial void ratio, e_0	1,505

Pressure, σ (kg/cm^2)	0-0,25	0,25-0,50	0,50-1,00	1,00-2,00	2,00-4,00	4,00-8,00
Final pressure, σ_f (kg/cm^2)	0,25	0,50	1,00	2,00	4,00	8,00
Change in Pressure, Δσ (kg/cm^2)	0,25	0,25	0,50	1,00	2,00	4,00
Initial dial reading, Di (-)	200	447	605	885	1420	2105
Final dial reading, Df (-)	447	605	885	1420	2105	2777
Dial reading, ΔD (-)	247	158	280	535	685	672
Change in Height of solid, ΔH (cm)	0,049	0,032	0,056	0,107	0,137	0,134
Initial Height of solids, Hi (cm)	1,900	1,851	1,819	1,763	1,656	1,519
Final Height of solids, Hf (cm)	1,851	1,819	1,763	1,656	1,519	1,385
Average of Height of solids; Hav (cm)	1,875	1,835	1,791	1,710	1,588	1,452
Drainage of Height of solids, H dr (cm)	0,938	0,917	0,896	0,855	0,794	0,726
Change in void ratio, Δe (-)	0,065	0,042	0,074	0,141	0,181	0,177
Void ratio, e (-)	1,440	1,398	1,324	1,183	1,003	0,825
Avarage of void ratio, e_{av} (-)	1,472	1,419	1,361	1,254	1,093	0,914
Coefficient of compressibility, ∂V (cm2 /kg)	0,261	0,167	0,148	0,141	0,090	0,044
Coefficient of volume compressibility, mv (cm^2 / kg)	0,105	0,069	0,063	0,063	0,043	0,023

Table A. 13 The result of oedometer test of specimen B11-1

Borehole no:	11	Specimen No:	T1	Depth(m):	10,50-10,95
Diameter(cm):	7	Wet weight(gr):	124,760	Natural unit weight (gr/cm^3)	1,706
Height(cm):	1,9	Dry weight(gr):	84,000	Dry unit weight (gr/cm^3)	1,149
Area (cm^2):	38,484	Water weight(gr):	40,760	Water content, (%)	0,485
Volume (cm^3):	73,120	Specific gravity	2,610	Initial void ratio, e_0	1,272

Pressure, σ (kg/cm^2)	0-0,25	0,25-0,50	0,50-1,00	1,00-2,00	2,00-4,00	4,00-8,00
Final pressure, σ_f (kg/cm^2)	0,25	0,500	1,00	2,00	4,00	8,00
Change in Pressure, Δσ (kg/cm^2)	0,25	0,25	0,50	1,00	2,00	4,00
Initial dial reading, Di (-)	500	880	1090	1357	1708	2218
Final dial reading, Df (-)	880	1090	1357	1708	2218	2750
Dial reading, ΔD (-)	380	210	267	351	510	532
Change in Height of solid, ΔH (cm)	0,076	0,042	0,053	0,070	0,102	0,106
Initial Height of solids, Hi (cm)	1,900	1,824	1,782	1,729	1,658	1,556
Final Height of solids, Hf (cm)	1,824	1,782	1,729	1,658	1,556	1,450
Average of Height of solids; Hav (cm)	1,862	1,803	1,755	1,694	1,607	1,503
Drainage of Height of solids, H dr (cm)	0,931	0,902	0,878	0,847	0,804	0,752
Change in void ratio, Δe (-)	0,091	0,050	0,064	0,084	0,122	0,127
Void ratio, e (-)	1,181	1,131	1,067	0,983	0,861	0,734
Avarage of void ratio, e_{av} (-)	1,227	1,156	1,099	1,025	0,922	0,798
Coefficient of compressibility, ∂V (cm2 /kg)	0,364	0,201	0,128	0,084	0,061	0,032
Coefficient of volume compressibility, mv (cm^2 / kg)	0,163	0,093	0,061	0,041	0,032	0,018

Table A. 14 The result of oedometer test of specimen B11-2

Borehole no:	11	Specimen No:	T3	Depth(m):	15,00-15,45
Diameter(cm):	7	Wet weight(gr):	120,160	Natural unit weight (gr/cm^3)	1,643
Height(cm):	1,9	Dry weight(gr):	75,060	Dry unit weight (gr/cm^3)	1,027
Area (cm^2):	38,484	Water weight(gr):	45,100	Water content, (%)	0,601
Volume (cm^3):	73,120	Specific gravity	2,660	Initial void ratio, e_0	1,591

Pressure, σ (kg/cm^2)	0-0,25	0,25-0,50	0,50-1,00	1,00-2,00	2,00-4,00	4,00-8,00
Final pressure, σ_f (kg/cm^2)	0,25	0,50	1,00	2,00	4,00	8,00
Change in Pressure, Δσ (kg/cm^2)	0,25	0,25	0,50	1,00	2,00	4,00
Initial dial reading, Di (-)	420	790	960	1218	1553	2287
Final dial reading, Df (-)	790	960	1218	1553	2287	3044
Dial reading, ΔD (-)	370	170	258	335	734	757
Change in Height of solid, ΔH (cm)	0,074	0,034	0,052	0,067	0,147	0,151
Initial Height of solids, Hi (cm)	1,900	1,826	1,792	1,740	1,673	1,527
Final Height of solids, Hf (cm)	1,826	1,792	1,740	1,673	1,527	1,375
Average of Height of solids; Hav (cm)	1,863	1,809	1,766	1,707	1,600	1,451
Drainage of Height of solids, H dr (cm)	0,932	0,905	0,883	0,853	0,800	0,725
Change in void ratio, Δe (-)	0,101	0,046	0,070	0,091	0,200	0,206
Void ratio, e (-)	1,490	1,444	1,373	1,282	1,082	0,875
Avarage of void ratio, e_{av} (-)	1,541	1,467	1,409	1,328	1,182	0,979
Coefficient of compressibility, ∂V (cm2 /kg)	0,404	0,185	0,141	0,091	0,100	0,052
Coefficient of volume compressibility, mv (cm^2 / kg)	0,159	0,075	0,058	0,039	0,046	0,026

Table A. 15 The result of oedometer test of specimen B12-1

Borehole no:	12	Specimen No:	T1	Depth(m):	8,00-8,45
Diameter(cm):	7	Wet weight(gr):	115,400	Natural unit weight (gr/cm^3)	1,578
Height(cm):	1,9	Dry weight(gr):	67,800	Dry unit weight (gr/cm^3)	0,927
Area (cm^2):	38,484	Water weight(gr):	47,600	Water content, (%)	0,702
Volume (cm^3):	73,120	Specific gravity	2,670	Initial void ratio, e_0	1,880

Pressure, σ (kg/cm^2)	0-0,25	0,25-0,50	0,50-1,00	1,00-2,00	2,00-4,00	4,00-8,00
Final pressure, σ_f (kg/cm^2)	0,25	0,50	1,00	2,00	4,00	8,00
Change in Pressure, Δσ (kg/cm^2)	0,25	0,25	0,50	1,00	2,00	4,00
Initial dial reading, Di (-)	250	650	1025	1442	2105	2810
Final dial reading, Df (-)	650	1025	1442	2105	2810	3095
Dial reading, ΔD (-)	400	375	417	663	705	285
Change in Height of solid, ΔH (cm)	0,080	0,075	0,083	0,133	0,141	0,057
Initial Height of solids, Hi (cm)	1,900	1,820	1,745	1,662	1,529	1,388
Final Height of solids, Hf (cm)	1,820	1,745	1,662	1,529	1,388	1,331
Average of Height of solids; Hav (cm)	1,860	1,783	1,703	1,595	1,459	1,360
Drainage of Height of solids, H dr (cm)	0,930	0,891	0,852	0,798	0,729	0,680
Change in void ratio, Δe (-)	0,121	0,114	0,126	0,201	0,214	0,086
Void ratio, e (-)	1,759	1,645	1,519	1,318	1,104	1,018
Avarage of void ratio, e_{av} (-)	1,819	1,702	1,582	1,418	1,211	1,061
Coefficient of compressibility, ∂V (cm2 /kg)	0,485	0,455	0,253	0,201	0,107	0,022
Coefficient of volume compressibility, mv (cm^2 / kg)	0,172	0,168	0,098	0,083	0,048	0,010

Table A. 16 The result of oedometer test of specimen B12-2

Borehole no:	12	Specimen No:	T3	Depth(m):	18,00-18,45
Diameter(cm):	7	Wet weight(gr):	117,430	Natural unit weight (gr/cm^3)	1,606
Height(cm):	1,9	Dry weight(gr):	70,230	Dry unit weight (gr/cm^3)	0,960
Area (cm^2):	38,484	Water weight(gr):	47,200	Water content, (%)	0,672
Volume (cm^3):	73,120	Specific gravity	2,670	Initial void ratio, e_0	1,780

Pressure, σ (kg/cm^2)	0-0,25	0,25-0,50	0,50-1,00	1,00-2,00	2,00-4,00	4,00-8,00
Final pressure, σ_f (kg/cm^2)	0,25	0,50	1,00	2,00	4,00	8,00
Change in Pressure, Δσ (kg/cm^2)	0,25	0,25	0,50	1,00	2,00	4,00
Initial dial reading, Di (-)	160	590	873	1307	1913	2535
Final dial reading, Df (-)	590	873	1307	1913	2535	3185
Dial reading, ΔD (-)	430	283	434	606	622	650
Change in Height of solid, ΔH (cm)	0.086	0.057	0.087	0.121	0.124	0.130
Initial Height of solids, Hi (cm)	1.9	1.814	1.757	1.671	1.549	1.425
Final Height of solids, Hf (cm)	1.814	1.757	1.671	1.549	1.425	1.295
Average of Height of solids; Hav (cm)	1.857	1.786	1.714	1.610	1.487	1.360
Drainage of Height of solids, H dr (cm)	0.929	0.893	0.857	0.805	0.744	0.680
Change in void ratio, Δe (-)	0.126	0.083	0.127	0.177	0.182	0.190
Void ratio, e (-)	1.654	1.571	1.444	1.267	1.085	0.895
Avarage of void ratio, e_{av} (-)	1.717	1.613	1.508	1.356	1.176	0.990
Coefficient of compressibility, ∂V (cm2 /kg)	0.503	0.331	0.254	0.177	0.091	0.048
Coefficient of volume compressibility, mv (cm^2 / kg)	0.185	0.127	0.101	0.075	0.042	0.024

Table A. 17 The result of oedometer test of specimen B13-1

Borehole no:	13	Specimen No:	T2	Depth(m):	12,00-12,45
Diameter(cm):	7	Wet weight(gr):	122,550	Natural unit weight (gr/cm^3)	1,676
Height(cm):	1,9	Dry weight(gr):	76,700	Dry unit weight (gr/cm^3)	1,049
Area (cm^2):	38,484	Water weight(gr):	45,850	Water content, (%)	0,598
Volume (cm^3):	73,120	Specific gravity	2,550	Initial void ratio, e_0	1,431

Pressure, σ (kg/cm^2)	0-0,25	0,25-0,50	0,50-1,00	1,00-2,00	2,00-4,00	4,00-8,00
Final pressure, σ_f (kg/cm^2)	0,25	0,50	1,00	2,00	4,00	8,00
Change in Pressure, Δσ (kg/cm^2)	0,25	0,25	0,50	1,00	2,00	4,00
Initial dial reading, Di (-)	530	921	1140	1515	2020	2565
Final dial reading, Df (-)	921	1140	1515	2020	2565	3150
Dial reading, ΔD (-)	391	219	375	505	545	585
Change in Height of solid, ΔH (cm)	0,078	0,044	0,075	0,101	0,109	0,117
Initial Height of solids, Hi (cm)	1,900	1,822	1,778	1,703	1,602	1,493
Final Height of solids, Hf (cm)	1,822	1,778	1,703	1,602	1,493	1,376
Average of Height of solids; Hav (cm)	1,861	1,800	1,741	1,653	1,548	1,435
Drainage of Height of solids, H dr (cm)	0,930	0,900	0,870	0,826	0,774	0,717
Change in void ratio, Δe (-)	0,100	0,056	0,096	0,129	0,139	0,150
Void ratio, e (-)	1,331	1,275	1,179	1,050	0,910	0,761
Avarage of void ratio, e_{av} (-)	1,381	1,303	1,227	1,114	0,980	0,835
Coefficient of compressibility, ∂V (cm2 /kg)	0,400	0,224	0,192	0,129	0,070	0,037
Coefficient of volume compressibility, mv (cm^2 / kg)	0,168	0,097	0,086	0,061	0,035	0,020

Table A. 18 The result of oedometer test of specimen B13-1

Borehole no:	13	Specimen No:	T4	Depth(m):	17,00-17,45
Diameter(cm):	7	Wet weight(gr):	118,460	Natural unit weight (gr/cm^3)	1,620
Height(cm):	1,9	Dry weight(gr):	73,350	Dry unit weight (gr/cm^3)	1,003
Area (cm^2):	38,484	Water weight(gr):	45,110	Water content, (%)	0,615
Volume (cm^3):	73,120	Specific gravity	2,590	Initial void ratio, e_0	1,582

Pressure, σ (kg/cm^2)	0-0,25	0,25-0,50	0,50-1,00	1,00-2,00	2,00-4,00	4,00-8,00
Final pressure, σ_f (kg/cm^2)	0,25	0,50	1,00	2,00	4,00	8,00
Change in Pressure, Δσ (kg/cm^2)	0,25	0,25	0,50	1,00	2,00	4,00
Initial dial reading, Di (-)	500	940	1230	1650	2183	2715
Final dial reading, Df (-)	940	1230	1650	2183	2715	3295
Dial reading, ΔD (-)	440	290	420	533	532	580
Change in Height of solid, ΔH (cm)	0,088	0,058	0,084	0,107	0,106	0,116
Initial Height of solids, Hi (cm)	1,900	1,812	1,754	1,670	1,563	1,457
Final Height of solids, Hf (cm)	1,812	1,754	1,670	1,563	1,457	1,341
Average of Height of solids; Hav (cm)	1,856	1,783	1,712	1,617	1,510	1,399
Drainage of Height of solids, H dr (cm)	0,928	0,892	0,856	0,808	0,755	0,700
Change in void ratio, Δe (-)	0,120	0,079	0,114	0,145	0,145	0,158
Void ratio, e (-)	1,462	1,384	1,269	1,125	0,980	0,822
Avarage of void ratio, e_{av} (-)	1,522	1,423	1,327	1,197	1,052	0,901
Coefficient of compressibility, ∂V (cm2 /kg)	0,478	0,315	0,228	0,145	0,072	0,039
Coefficient of volume compressibility, mv (cm^2 / kg)	0,190	0,130	0,098	0,066	0,035	0,021

Table A. 19 The result of oedometer test of specimen B14-1

Borehole no:	14	Specimen No:	T4	Depth(m):	17,00-17,45
Diameter(cm):	7	Wet weight(gr):	123,000	Natural unit weight (gr/cm^3)	1,682
Height(cm):	1,9	Dry weight(gr):	78,210	Dry unit weight (gr/cm^3)	1,070
Area (cm^2):	38,484	Water weight(gr):	44,790	Water content, (%)	0,573
Volume (cm^3):	73,120	Specific gravity	2,620	Initial void ratio, e_0	1,450

Pressure, σ (kg/cm^2)	0-0,25	0,25-0,50	0,50-1,00	1,00-2,00	2,00-4,00	4,00-8,00
Final pressure, σ_f (kg/cm^2)	0,25	0,50	1,00	2,00	4,00	8,00
Change in Pressure, Δσ (kg/cm^2)	0,25	0,25	0,50	1,00	2,00	4,00
Initial dial reading, Di (-)	320	653	873	1272	1822	2350
Final dial reading, Df (-)	653	873	1272	1822	2350	2915
Dial reading, ΔD (-)	333	220	399	550	528	565
Change in Height of solid, ΔH (cm)	0,067	0,044	0,080	0,110	0,106	0,113
Initial Height of solids, Hi (cm)	1,900	1,833	1,789	1,710	1,600	1,494
Final Height of solids, Hf (cm)	1,833	1,789	1,710	1,600	1,494	1,381
Average of Height of solids; Hav (cm)	1,867	1,811	1,750	1,655	1,547	1,438
Drainage of Height of solids, H dr (cm)	0,933	0,906	0,875	0,827	0,773	0,719
Change in void ratio, Δe (-)	0,086	0,057	0,103	0,142	0,136	0,146
Void ratio, e (-)	1,364	1,307	1,204	1,063	0,926	0,781
Avarage of void ratio, e_{av} (-)	1,407	1,336	1,256	1,134	0,995	0,854
Coefficient of compressibility, ∂V (cm2 /kg)	0,344	0,227	0,206	0,142	0,068	0,036
Coefficient of volume compressibility, mv (cm^2 / kg)	0,143	0,097	0,091	0,066	0,034	0,020

Table A. 20 The result of oedometer test of specimen B15-1

Borehole no:	15	Specimen No:	T1	Depth(m):	6,50-6,95
Diameter(cm):	7	Wet weight(gr):	119,260	Natural unit weight (gr/cm^3)	1,631
Height(cm):	1,9	Dry weight(gr):	70,660	Dry unit weight (gr/cm^3)	0,966
Area (cm^2):	38,484	Water weight(gr):	48,600	Water content, (%)	0,688
Volume (cm^3):	73,120	Specific gravity	2,580	Initial void ratio, e_0	1,670

Pressure, σ (kg/cm^2)	0-0,25	0,25-0,50	0,50-1,00	1,00-2,00	2,00-4,00	4,00-8,00
Final pressure, σ_f (kg/cm^2)	0,25	0,50	1,00	2,00	4,00	8,00
Change in Pressure, Δσ (kg/cm^2)	0,25	0,25	0,50	1,00	2,00	4,00
Initial dial reading, Di (-)	400	717	893	1277	1835	2477
Final dial reading, Df (-)	717	893	1277	1835	2477	3150
Dial reading, ΔD (-)	317	176	384	558	642	673
Change in Height of solid, ΔH (cm)	0,063	0,035	0,077	0,112	0,128	0,135
Initial Height of solids, Hi (cm)	1,900	1,837	1,801	1,725	1,613	1,485
Final Height of solids, Hf (cm)	1,837	1,801	1,725	1,613	1,485	1,350
Average of Height of solids; Hav (cm)	1,868	1,819	1,763	1,669	1,549	1,417
Drainage of Height of solids, H dr (cm)	0,934	0,910	0,882	0,834	0,774	0,709
Change in void ratio, Δe (-)	0,089	0,049	0,108	0,157	0,180	0,189
Void ratio, e (-)	1,581	1,531	1,424	1,267	1,086	0,897
Avarage of void ratio, e_{av} (-)	1,625	1,556	1,477	1,345	1,176	0,992
Coefficient of compressibility, ∂V (cm2 /kg)	0,356	0,198	0,216	0,157	0,090	0,047
Coefficient of volume compressibility, mv (cm^2 / kg)	0,136	0,077	0,087	0,067	0,041	0,024

Table A. 21 The result of oedometer test of specimen B16-1

Borehole no:	16	Specimen No:	T2	Depth(m):	11,5-11,95
Diameter(cm):	7	Wet weight(gr):	125,100	Natural unit weight (gr/cm^3)	1,711
Height(cm):	1,9	Dry weight(gr):	81,270	Dry unit weight (gr/cm^3)	1,111
Area (cm^2):	38,484	Water weight(gr):	43,830	Water content, (%)	0,539
Volume (cm^3):	73,120	Specific gravity	2,620	Initial void ratio, e_0	1,357

Pressure, σ (kg/cm^2)	0-0,25	0,25-0,50	0,50-1,00	1,00-2,00	2,00-4,00	4,00-8,00
Final pressure, σ_f (kg/cm^2)	0,25	0,50	1,00	2,00	4,00	8,00
Change in Pressure, Δσ (kg/cm^2)	0,25	0,25	0,50	1,00	2,00	4,00
Initial dial reading, Di (-)	100	305	430	641	1113	1800
Final dial reading, Df (-)	305	430	641	1113	1800	2500
Dial reading, ΔD (-)	205	125	211	472	687	700
Change in Height of solid, ΔH (cm)	0,041	0,025	0,042	0,094	0,137	0,140
Initial Height of solids, Hi (cm)	1,900	1,859	1,834	1,792	1,697	1,560
Final Height of solids, Hf (cm)	1,859	1,834	1,792	1,697	1,560	1,420
Average of Height of solids; Hav (cm)	1,880	1,847	1,813	1,745	1,629	1,490
Drainage of Height of solids, H dr (cm)	0,940	0,923	0,906	0,872	0,814	0,745
Change in void ratio, Δe (-)	0,051	0,031	0,052	0,117	0,170	0,174
Void ratio, e (-)	1,306	1,275	1,223	1,106	0,935	0,762
Avarage of void ratio, e_{av} (-)	1,332	1,291	1,249	1,164	1,020	0,848
Coefficient of compressibility, ∂V (cm2 /kg)	0,203	0,124	0,105	0,117	0,085	0,043
Coefficient of volume compressibility, mv (cm^2 / kg)	0,087	0,054	0,047	0,054	0,042	0,023

Table A. 22 The result of oedometer test of specimen B16-2

Borehole no:	16	Specimen No:	T3	Depth(m):	17,50-17,95
Diameter(cm):	7	Wet weight(gr):	120,300	Natural unit weight (gr/cm^3)	1,645
Height(cm):	1,9	Dry weight(gr):	86,430	Dry unit weight (gr/cm^3)	1,182
Area (cm^2):	38,484	Water weight(gr):	33,870	Water content, (%)	0,392
Volume (cm^3):	73,120	Specific gravity	2,510	Initial void ratio, e_0	1,123

Pressure, σ (kg/cm^2)	0-0,25	0,25-0,50	0,50-1,00	1,00-2,00	2,00-4,00	4,00-8,00
Final pressure, σ_f (kg/cm^2)	0,25	0,50	1,00	2,00	4,00	8,00
Change in Pressure, Δσ (kg/cm^2)	0,25	0,25	0,50	1,00	2,00	4,00
Initial dial reading, Di (-)	470	751	907	1240	1852	2520
Final dial reading, Df (-)	751	907	1240	1852	2520	3185
Dial reading, ΔD (-)	281	156	333	612	668	665
Change in Height of solid, ΔH (cm)	0,056	0,031	0,067	0,122	0,134	0,133
Initial Height of solids, Hi (cm)	1,900	1,844	1,813	1,746	1,624	1,490
Final Height of solids, Hf (cm)	1,844	1,813	1,746	1,624	1,490	1,357
Average of Height of solids; Hav (cm)	1,872	1,828	1,779	1,685	1,557	1,424
Drainage of Height of solids, H dr (cm)	0,936	0,914	0,890	0,842	0,778	0,712
Change in void ratio, Δe (-)	0,063	0,035	0,074	0,137	0,149	0,149
Void ratio, e (-)	1,060	1,025	0,951	0,814	0,665	0,516
Avarage of void ratio, e_{av} (-)	1,092	1,043	0,988	0,883	0,740	0,591
Coefficient of compressibility, ∂V (cm2 /kg)	0,251	0,139	0,149	0,137	0,075	0,037
Coefficient of volume compressibility, mv (cm^2 / kg)	0,120	0,068	0,075	0,073	0,043	0,023

Table A. 23 The result of oedometer test of specimen B17-1

Borehole no:	17	Specimen No:	T1	Depth(m):	6,5-6,95
Diameter(cm):	7	Wet weight(gr):	119,100	Natural unit weight (gr/cm^3)	1,629
Height(cm):	1,9	Dry weight(gr):	73,460	Dry unit weight (gr/cm^3)	1,005
Area (cm^2):	38,484	Water weight(gr):	45,640	Water content, (%)	0,621
Volume (cm^3):	73,120	Specific gravity	2,540	Initial void ratio, e_0	1,528

Pressure, σ (kg/cm^2)	0-0,25	0,25-0,50	0,50-1,00	1,00-2,00	2,00-4,00	4,00-8,00
Final pressure, σ_f (kg/cm^2)	0,25	0,50	1,00	2,00	4,00	8,00
Change in Pressure, Δσ (kg/cm^2)	0,25	0,25	0,50	1,00	2,00	4,00
Initial dial reading, Di (-)	440	667	820	1117	1760	2527
Final dial reading, Df (-)	667	820	1117	1760	2527	3225
Dial reading, ΔD (-)	227	153	297	643	767	698
Change in Height of solid, ΔH (cm)	0,045	0,031	0,059	0,129	0,153	0,140
Initial Height of solids, Hi (cm)	1,900	1,855	1,824	1,765	1,636	1,483
Final Height of solids, Hf (cm)	1,855	1,824	1,765	1,636	1,483	1,343
Average of Height of solids; Hav (cm)	1,877	1,839	1,794	1,700	1,559	1,413
Drainage of Height of solids, H dr (cm)	0,939	0,920	0,897	0,850	0,780	0,706
Change in void ratio, Δe (-)	0,060	0,041	0,079	0,171	0,204	0,186
Void ratio, e (-)	1,468	1,427	1,348	1,177	0,973	0,787
Avarage of void ratio, e_{av} (-)	1,498	1,447	1,387	1,262	1,075	0,880
Coefficient of compressibility, ∂V (cm2 /kg)	0,242	0,163	0,158	0,171	0,102	0,046
Coefficient of volume compressibility, mv (cm^2 / kg)	0,097	0,067	0,066	0,076	0,049	0,025

Table A. 24 The result of oedometer test of specimen B17-2

Borehole no:	17	Specimen No:	T3	Depth(m):	17,50-17,95
Diameter(cm):	7	Wet weight(gr):	123,300	Natural unit weight (gr/cm^3)	1,686
Height(cm):	1,9	Dry weight(gr):	76,460	Dry unit weight (gr/cm^3)	1,046
Area (cm^2):	38,484	Water weight(gr):	46,840	Water content, (%)	0,613
Volume (cm^3):	73,120	Specific gravity	2,530	Initial void ratio, e_0	1,420

Pressure, σ (kg/cm^2)	0-0,25	0,25-0,50	0,50-1,00	1,00-2,00	2,00-4,00	4,00-8,00
Final pressure, σ_f (kg/cm^2)	0,25	0,500	1,000	2,000	4,000	8,000
Change in Pressure, Δσ (kg/cm^2)	0,25	0,250	0,500	1,000	2,000	4,000
Initial dial reading, Di (-)	370	742	945	1273	1783	2315
Final dial reading, Df (-)	742	945	1273	1783	2315	2885
Dial reading, ΔD (-)	372	203	328	510	532	570
Change in Height of solid, ΔH (cm)	0,074	0,041	0,066	0,102	0,106	0,114
Initial Height of solids, Hi (cm)	1,9	1,826	1,785	1,719	1,617	1,511
Final Height of solids, Hf (cm)	1,826	1,785	1,719	1,617	1,511	1,397
Average of Height of solids; Hav (cm)	1,863	1,805	1,752	1,668	1,564	1,454
Drainage of Height of solids, H dr (cm)	0,931	0,903	0,876	0,834	0,782	0,727
Change in void ratio, Δe (-)	0,095	0,052	0,084	0,130	0,136	0,145
Void ratio, e (-)	1,325	1,274	1,190	1,060	0,925	0,779
Avarage of void ratio, e_{av} (-)	1,373	1,299	1,232	1,125	0,992	0,852
Coefficient of compressibility, ∂V (cm2 /kg)	0,379	0,207	0,167	0,130	0,068	0,036
Coefficient of volume compressibility, mv (cm^2 / kg)	0,160	0,090	0,075	0,061	0,034	0,020

Table A. 25 The result of oedometer test of specimen B18-1

Borehole no:	18	Specimen No:	T2	Depth(m):	12,5-12,95
Diameter(cm):	7	Wet weight(gr):	124,000	Natural unit weight (gr/cm^3)	1,696
Height(cm):	1,9	Dry weight(gr):	78,700	Dry unit weight (gr/cm^3)	1,076
Area (cm^2):	38,484	Water weight(gr):	45,300	Water content, (%)	0,576
Volume (cm^3):	73,120	Specific gravity	2,600	Initial void ratio, e_0	1,416

Pressure, σ (kg/cm^2)	0-0,25	0,25-0,50	0,50-1,00	1,00-2,00	2,00-4,00	4,00-8,00
Final pressure, σ_f (kg/cm^2)	0,25	0,50	1,00	2,00	4,00	8,00
Change in Pressure, Δσ (kg/cm^2)	0,25	0,25	0,50	1,00	2,00	4,00
Initial dial reading, Di (-)	365	555	690	943	1373	1998
Final dial reading, Df (-)	555	690	943	1373	1998	2630
Dial reading, ΔD (-)	190	135	253	430	625	632
Change in Height of solid, ΔH (cm)	0,038	0,027	0,051	0,086	0,125	0,126
Initial Height of solids, Hi (cm)	1,900	1,862	1,835	1,784	1,698	1,573
Final Height of solids, Hf (cm)	1,862	1,835	1,784	1,698	1,573	1,447
Average of Height of solids; Hav (cm)	1,881	1,849	1,810	1,741	1,636	1,510
Drainage of Height of solids, H dr (cm)	0,941	0,924	0,905	0,871	0,818	0,755
Change in void ratio, Δe (-)	0,048	0,034	0,064	0,109	0,159	0,161
Void ratio, e (-)	1,368	1,333	1,269	1,160	1,001	0,840
Avarage of void ratio, e_{av} (-)	1,392	1,351	1,301	1,214	1,080	0,920
Coefficient of compressibility, ∂V (cm2 /kg)	0,193	0,137	0,129	0,109	0,079	0,040
Coefficient of volume compressibility, mv (cm^2 / kg)	0,081	0,058	0,056	0,049	0,038	0,021

Table A. 26 The result of oedometer test of specimen B18-2

Borehole no:	18	Specimen No:	T3	Depth(m):	19,00-19,45
Diameter(cm):	7	Wet weight(gr):	120,790	Natural unit weight (gr/cm^3)	1,652
Height(cm):	1,9	Dry weight(gr):	76,660	Dry unit weight (gr/cm^3)	1,048
Area (cm^2):	38,484	Water weight(gr):	44,130	Water content, (%)	0,576
Volume (cm^3):	73,120	Specific gravity	2,640	Initial void ratio, e_0	1,518

Pressure, σ (kg/cm^2)	0-0,25	0,25-0,50	0,50-1,00	1,00-2,00	2,00-4,00	4,00-8,00
Final pressure, σ_f (kg/cm^2)	0,25	0,50	1,00	2,00	4,00	8,00
Change in Pressure, Δσ (kg/cm^2)	0,25	0,25	0,50	1,00	2,00	4,00
Initial dial reading, Di (-)	435	682	848	1215	1740	2365
Final dial reading, Df (-)	682	848	1215	1740	2365	2985
Dial reading, ΔD (-)	247	166	367	525	625	620
Change in Height of solid, ΔH (cm)	0,049	0,033	0,073	0,105	0,125	0,124
Initial Height of solids, Hi (cm)	1,900	1,851	1,817	1,744	1,639	1,514
Final Height of solids, Hf (cm)	1,851	1,817	1,744	1,639	1,514	1,390
Average of Height of solids; Hav (cm)	1,875	1,834	1,781	1,692	1,577	1,452
Drainage of Height of solids, H dr (cm)	0,938	0,917	0,890	0,846	0,788	0,726
Change in void ratio, Δe (-)	0,065	0,044	0,097	0,139	0,166	0,164
Void ratio, e (-)	1,453	1,409	1,311	1,172	1,006	0,842
Avarage of void ratio, e_{av} (-)	1,485	1,431	1,360	1,242	1,089	0,924
Coefficient of compressibility, ∂V (cm2 /kg)	0,262	0,176	0,195	0,139	0,083	0,041
Coefficient of volume compressibility, mv (cm^2 / kg)	0,105	0,072	0,082	0,062	0,040	0,021

Table A. 27 The result of oedometer test of specimen B19-1

Borehole no:	19	Specimen No:	T4	Depth(m):	16,5-16,95
Diameter(cm):	7	Wet weight(gr):	125,430	Natural unit weight (gr/cm^3)	1,715
Height(cm):	1,9	Dry weight(gr):	81,160	Dry unit weight (gr/cm^3)	1,110
Area (cm^2):	38,484	Water weight(gr):	44,270	Water content, (%)	0,545
Volume (cm^3):	73,120	Specific gravity	2,530	Initial void ratio, e_0	1,279

Pressure, σ (kg/cm^2)	0-0,5	0,50-1,00	1,00-2,00	2,00-4,00	4,00-8,00
Final pressure, σ_f (kg/cm^2)	0,5	1,00	2,00	4,00	8,00
Change in Pressure, Δσ (kg/cm^2)	0,5	0,50	1,00	2,00	4,00
Initial dial reading, Di (-)	380	466	665	1157	1835
Final dial reading, Df (-)	466	665	1157	1835	2470
Dial reading, ΔD (-)	86	199	492	678	635
Change in Height of solid, ΔH (cm)	0,017	0,040	0,098	0,136	0,127
Initial Height of solids, Hi (cm)	1,900	1,883	1,843	1,745	1,609
Final Height of solids, Hf (cm)	1,883	1,843	1,745	1,609	1,482
Average of Height of solids; Hav (cm)	1,891	1,863	1,794	1,677	1,546
Drainage of Height of solids, H dr (cm)	0,946	0,931	0,897	0,838	0,773
Change in void ratio, Δe (-)	0,021	0,048	0,118	0,163	0,152
Void ratio, e (-)	1,258	1,211	1,093	0,930	0,778
Avarage of void ratio, e_{av} (-)	1,269	1,234	1,152	1,011	0,854
Coefficient of compressibility, ∂V (cm2 /kg)	0,041	0,095	0,118	0,081	0,038
Coefficient of volume compressibility, mv (cm^2 / kg)	0,018	0,043	0,055	0,040	0,021

Table A. 28 The result of oedometer test of specimen B20-1

Borehole no:	20	Specimen No:	T1	Depth(m):	11,00-11,45
Diameter(cm):	7	Wet weight(gr):	121,840	Natural unit weight (gr/cm^3)	1,666
Height(cm):	1,9	Dry weight(gr):	78,330	Dry unit weight (gr/cm^3)	1,071
Area (cm^2):	38,484	Water weight(gr):	43,510	Water content, (%)	0,555
Volume (cm^3):	73,120	Specific gravity	2,640	Initial void ratio, e_0	1,464

Pressure, σ (kg/cm^2)	0-0,25	0,25-0,50	0,50-1,00	1,00-2,00	2,00-4,00	4,00-8,00
Final pressure, σ_f (kg/cm^2)	0,25	0,50	1,00	2,00	4,00	8,00
Change in Pressure, Δσ (kg/cm^2)	0,25	0,25	0,50	1,00	2,00	4,00
Initial dial reading, Di (-)	370	585	708	898	1432	2095
Final dial reading, Df (-)	585	708	898	1432	2095	2760
Dial reading, ΔD (-)	215	123	190	534	663	665
Change in Height of solid, ΔH (cm)	0,043	0,025	0,038	0,107	0,133	0,133
Initial Height of solids, Hi (cm)	1,900	1,857	1,832	1,794	1,688	1,555
Final Height of solids, Hf (cm)	1,857	1,832	1,794	1,688	1,555	1,422
Average of Height of solids; Hav (cm)	1,879	1,845	1,813	1,741	1,621	1,489
Drainage of Height of solids, H dr (cm)	0,939	0,922	0,907	0,871	0,811	0,744
Change in void ratio, Δe (-)	0,056	0,032	0,049	0,139	0,172	0,172
Void ratio, e (-)	1,408	1,376	1,327	1,189	1,017	0,844
Avarage of void ratio, e_{av} (-)	1,436	1,392	1,352	1,258	1,103	0,930
Coefficient of compressibility, ∂V (cm2 /kg)	0,223	0,128	0,099	0,139	0,086	0,043
Coefficient of volume compressibility, mv (cm^2 / kg)	0,092	0,053	0,042	0,061	0,041	0,022

Table A. 29 The result of oedometer test of specimen B20-2

Borehole no:	20	Specimen No:	T4	Depth(m):	21,00-21,45
Diameter(cm):	7	Wet weight(gr):	124,590	Natural unit weight (gr/cm^3)	1,704
Height(cm):	1,9	Dry weight(gr):	81,430	Dry unit weight (gr/cm^3)	1,114
Area (cm^2):	38,484	Water weight(gr):	43,160	Water content, (%)	0,530
Volume (cm^3):	73,120	Specific gravity	2,570	Initial void ratio, e_0	1,308

Pressure, σ (kg/cm^2)	0-0,25	0,25-0,50	0,50-1,00	1,00-2,00	2,00-4,00	4,00-8,00
Final pressure, σ_f (kg/cm^2)	0,25	0,50	1,00	2,00	4,00	8,00
Change in Pressure, Δσ (kg/cm^2)	0,25	0,25	0,50	1,00	2,00	4,00
Initial dial reading, Di (-)	115	365	542	847	1310	1807
Final dial reading, Df (-)	365	542	847	1310	1807	2370
Dial reading, ΔD (-)	250	177	305	463	497	563
Change in Height of solid, ΔH (cm)	0,050	0,035	0,061	0,093	0,099	0,113
Initial Height of solids, Hi (cm)	1,9	1,850	1,815	1,754	1,661	1,562
Final Height of solids, Hf (cm)	1,850	1,815	1,754	1,661	1,562	1,449
Average of Height of solids; Hav (cm)	1,875	1,832	1,784	1,707	1,611	1,505
Drainage of Height of solids, H dr (cm)	0,938	0,916	0,892	0,854	0,806	0,753
Change in void ratio, Δe (-)	0,061	0,043	0,074	0,112	0,121	0,137
Void ratio, e (-)	1,247	1,204	1,130	1,018	0,897	0,760
Avarage of void ratio, e_{av} (-)	1,278	1,226	1,167	1,074	0,957	0,829
Coefficient of compressibility, ∂V (cm2 /kg)	0,243	0,172	0,148	0,112	0,060	0,034
Coefficient of volume compressibility, mv (cm^2 / kg)	0,107	0,077	0,068	0,054	0,031	0,019

Table A. 30 The result of oedometer test of specimen B21-1

Borehole no:	21	Specimen No:	T3	Depth(m):	15,50-15,95
Diameter(cm):	7	Wet weight(gr):	127,300	Natural unit weight (gr/cm^3)	1,741
Height(cm):	1,9	Dry weight(gr):	83,500	Dry unit weight (gr/cm^3)	1,142
Area (cm^2):	38,484	Water weight(gr):	43,800	Water content, (%)	0,525
Volume (cm^3):	73,120	Specific gravity	2,700	Initial void ratio, e_0	1,364

Pressure, σ (kg/cm^2)	0-0,25	0,25-0,50	0,50-1,00	1,00-2,00	2,00-4,00	4,00-8,00
Final pressure, σ_f (kg/cm^2)	0,25	0,50	1,00	2,00	4,00	8,00
Change in Pressure, Δσ (kg/cm^2)	0,25	0,25	0,50	1,00	2,00	4,00
Initial dial reading, Di (-)	400	720	911	1224	1685	2180
Final dial reading, Df (-)	720	911	1224	1685	2180	2740
Dial reading, ΔD (-)	320	191	313	461	495	560
Change in Height of solid, ΔH (cm)	0,064	0,038	0,063	0,092	0,099	0,112
Initial Height of solids, Hi (cm)	1,900	1,836	1,798	1,735	1,643	1,544
Final Height of solids, Hf (cm)	1,836	1,798	1,735	1,643	1,544	1,432
Average of Height of solids; Hav (cm)	1,868	1,817	1,767	1,689	1,594	1,488
Drainage of Height of solids, H dr (cm)	0,934	0,908	0,883	0,845	0,797	0,744
Change in void ratio, Δe (-)	0,080	0,048	0,078	0,115	0,123	0,139
Void ratio, e (-)	1,284	1,237	1,159	1,044	0,921	0,782
Avarage of void ratio, e_{av} (-)	1,324	1,261	1,198	1,102	0,983	0,851
Coefficient of compressibility, ∂V (cm2 /kg)	0,319	0,190	0,156	0,115	0,062	0,035
Coefficient of volume compressibility, mv (cm^2 / kg)	0,137	0,084	0,071	0,055	0,031	0,019

Table A. 31 The result of oedometer test of specimen B23-1

Borehole no:	23	Specimen No:	T1	Depth(m):	9,50-9,95
Diameter(cm):	7	Wet weight(gr):	116,960	Natural unit weight (gr/cm^3)	1,600
Height(cm):	1,9	Dry weight(gr):	70,900	Dry unit weight (gr/cm^3)	0,970
Area (cm^2):	38,484	Water weight(gr):	46,060	Water content, (%)	0,650
Volume (cm^3):	73,120	Specific gravity	2,600	Initial void ratio, e_0	1,681

Pressure, σ (kg/cm^2)	0-0,25	0,25-0,50	0,50-1,00	1,00-2,00	2,00-4,00	4,00-8,00
Final pressure, σ_f (kg/cm^2)	0,25	0,50	1,00	2,00	4,00	8,00
Change in Pressure, Δσ (kg/cm^2)	0,25	0,25	0,50	1,00	2,00	4,00
Initial dial reading, Di (-)	340	762	1032	1507	2060	2680
Final dial reading, Df (-)	762	1032	1507	2060	2680	3288
Dial reading, ΔD (-)	422	270	475	553	620	608
Change in Height of solid, ΔH (cm)	0,084	0,054	0,095	0,111	0,124	0,122
Initial Height of solids, Hi (cm)	1,900	1,816	1,762	1,667	1,556	1,432
Final Height of solids, Hf (cm)	1,816	1,762	1,667	1,556	1,432	1,310
Average of Height of solids; Hav (cm)	1,858	1,789	1,714	1,611	1,494	1,371
Drainage of Height of solids, H dr (cm)	0,929	0,894	0,857	0,806	0,747	0,686
Change in void ratio, Δe (-)	0,119	0,076	0,134	0,156	0,175	0,172
Void ratio, e (-)	1,562	1,486	1,352	1,196	1,021	0,849
Avarage of void ratio, e_{av} (-)	1,621	1,524	1,419	1,274	1,108	0,935
Coefficient of compressibility, ∂V (cm2 /kg)	0,476	0,305	0,268	0,156	0,087	0,043
Coefficient of volume compressibility, mv (cm^2 / kg)	0,182	0,121	0,111	0,069	0,041	0,022

Table A. 32 The result of oedometer test of specimen B24-1

Borehole no:	24	Specimen No:	T2	Depth(m):	10,0-10,45
Diameter(cm):	7	Wet weight(gr):	123,500	Natural unit weight (gr/cm^3)	1,689
Height(cm):	1,9	Dry weight(gr):	79,000	Dry unit weight (gr/cm^3)	1,080
Area (cm^2):	38,484	Water weight(gr):	44,500	Water content, (%)	0,563
Volume (cm^3):	73,120	Specific gravity	2,680	Initial void ratio, e_0	1,481

Pressure, σ (kg/cm^2)	0-0,25	0,25-0,50	0,50-1,00	1,00-2,00	2,00-4,00	4,00-8,00
Final pressure, σ_f (kg/cm^2)	0,25	0,50	1,00	2,00	4,00	8,00
Change in Pressure, Δσ (kg/cm^2)	0,25	0,25	0,50	1,00	2,00	4,00
Initial dial reading, Di (-)	370	568	700	911	1530	2200
Final dial reading, Df (-)	568	700	911	1530	2200	2870
Dial reading, ΔD (-)	198	132	211	619	670	670
Change in Height of solid, ΔH (cm)	0,040	0,026	0,042	0,124	0,134	0,134
Initial Height of solids, Hi (cm)	1,900	1,860	1,834	1,792	1,668	1,534
Final Height of solids, Hf (cm)	1,860	1,834	1,792	1,668	1,534	1,400
Average of Height of solids; Hav (cm)	1,880	1,847	1,813	1,730	1,601	1,467
Drainage of Height of solids, H dr (cm)	0,940	0,924	0,906	0,865	0,801	0,734
Change in void ratio, Δe (-)	0,052	0,034	0,055	0,162	0,175	0,175
Void ratio, e (-)	1,429	1,395	1,340	1,178	1,003	0,828
Avarage of void ratio, e_{av} (-)	1,455	1,412	1,367	1,259	1,091	0,916
Coefficient of compressibility, ∂V (cm2 /kg)	0,207	0,138	0,110	0,162	0,087	0,044
Coefficient of volume compressibility, mv (cm^2 / kg)	0,084	0,057	0,047	0,072	0,042	0,023

Table A. 33 The result of oedometer test of specimen B25-1

Borehole no:	25	Specimen No:	T1	Depth(m):	5,50-5,95
Diameter(cm):	7	Wet weight(gr):	122,180	Natural unit weight (gr/cm^3)	1,671
Height(cm):	1,9	Dry weight(gr):	77,230	Dry unit weight (gr/cm^3)	1,056
Area (cm^2):	38,484	Water weight(gr):	44,950	Water content, (%)	0,582
Volume (cm^3):	73,120	Specific gravity	2,740	Initial void ratio, e_0	1,594

Pressure, σ (kg/cm^2)	0-0,25	0,25-0,50	0,50-1,00	1,00-2,00	2,00-4,00	4,00-8,00
Final pressure, σ_f (kg/cm^2)	0,25	0,50	1,00	2,00	4,00	8,00
Change in Pressure, Δσ (kg/cm^2)	0,25	0,25	0,50	1,00	2,00	4,00
Initial dial reading, Di (-)	425	734	955	1358	1890	2418
Final dial reading, Df (-)	734	955	1358	1890	2418	2980
Dial reading, ΔD (-)	309	221	403	532	528	562
Change in Height of solid, ΔH (cm)	0,062	0,044	0,081	0,106	0,106	0,112
Initial Height of solids, Hi (cm)	1,900	1,838	1,794	1,713	1,607	1,501
Final Height of solids, Hf (cm)	1,838	1,794	1,713	1,607	1,501	1,389
Average of Height of solids; Hav (cm)	1,869	1,816	1,754	1,660	1,554	1,445
Drainage of Height of solids, H dr (cm)	0,935	0,908	0,877	0,830	0,777	0,723
Change in void ratio, Δe (-)	0,084	0,060	0,110	0,145	0,144	0,153
Void ratio, e (-)	1,510	1,449	1,339	1,194	1,050	0,896
Avarage of void ratio, e_{av} (-)	1,552	1,479	1,394	1,267	1,122	0,973
Coefficient of compressibility, ∂V (cm2 /kg)	0,337	0,241	0,220	0,145	0,072	0,038
Coefficient of volume compressibility, mv (cm^2 / kg)	0,132	0,097	0,092	0,064	0,034	0,019

Table A. 34 The result of oedometer test of specimen B26-1

Borehole no:	26	Specimen No:	T4	Depth(m):	13,50-13,95
Diameter(cm):	7	Wet weight(gr):	121,300	Natural unit weight (gr/cm^3)	1,659
Height(cm):	1,9	Dry weight(gr):	75,770	Dry unit weight (gr/cm^3)	1,036
Area (cm^2):	38,484	Water weight(gr):	45,530	Water content, (%)	0,601
Volume (cm^3):	73,120	Specific gravity	2,700	Initial void ratio, e_0	1,606

Pressure, σ (kg/cm^2)	0-0,25	0,25-0,50	0,50-1,00	1,00-2,00	2,00-4,00	4,00-8,00
Final pressure, σ_f (kg/cm^2)	0,25	0,50	1,00	2,00	4,00	8,00
Change in Pressure, Δσ (kg/cm^2)	0,25	0,25	0,50	1,00	2,00	4,00
Initial dial reading, Di (-)	480	803	1036	1390	1838	2596
Final dial reading, Df (-)	803	1036	1390	1838	2596	3271
Dial reading, ΔD (-)	323	233	354	448	758	675
Change in Height of solid, ΔH (cm)	0,065	0,047	0,071	0,090	0,152	0,135
Initial Height of solids, Hi (cm)	1,900	1,835	1,789	1,718	1,628	1,477
Final Height of solids, Hf (cm)	1,835	1,789	1,718	1,628	1,477	1,342
Average of Height of solids; Hav (cm)	1,868	1,812	1,753	1,673	1,553	1,409
Drainage of Height of solids, H dr (cm)	0,934	0,906	0,877	0,837	0,776	0,705
Change in void ratio, Δe (-)	0,089	0,064	0,097	0,123	0,208	0,185
Void ratio, e (-)	1,517	1,453	1,356	1,233	1,026	0,840
Avarage of void ratio, e_{av} (-)	1,562	1,485	1,405	1,295	1,130	0,933
Coefficient of compressibility, ∂V (cm2 /kg)	0,354	0,256	0,194	0,123	0,104	0,046
Coefficient of volume compressibility, mv (cm^2 / kg)	0,138	0,103	0,081	0,054	0,049	0,024

Appendix B: The MATLAB studies about drawing a suitable curve

Table B. 1 The Editor File of The MATLAB for Fitting The Curve

```
load alım
 % transfering the experiment data
B=[0 0.25 0.5 1 2 4 8]
clear A h1 h2 h3 h4  x yp B1 xa ya xb yb
e=edeg(26,:)
A=e
%set team of axis
grid on
propertyeditor('on')
hold on;
axis on
% axis are occured
z2=max(A)
z4=max(B)
z5=max(z2,z4)
z1=min(A)
z3=min(B)
axis([z1 z5 z3 z5])
xl=xlabel('\epsilon-strain,(%)')
yl=ylabel('\sigma-stress,(kg/cm^2)')
h1=plot(A,B,'b.')
set(h1, 'markersize', 20)
A1=[A(1) A(3:6)]
B1=[B(1) B(3:6)]
h2=plot(A1,B1,'m.')
set(h2, 'markersize',15)
```

```
if p==1.00
 % dark green
set(h3,'color',[0.2 0.5 0.3])
set(h4,'color',[0.2 0.5 0.3])
elseif p>=0.95 & p<1.00
 % orange
set(h3,'color',[1 0.6 0])
set(h4,'color',[1 0.6 0])
else
 % red
set(h3,'color',[1 0 0])
set(h4,'color',[1 0 0])
end
 % input the legend
legend('\sigma-\epsilon of experiment','\sigma-
\epsilon for calculate',' combinated value of
\sigma-\epsilon by reliability is %70','cubic
spline')
d=fnval(csaps(ypp,x,p),1)
xa=[0 d]
ya=[1 1]
xb=[d d]
yb=[1 0]
h5=plot(xa,ya,'k-')
set(h5,'linewidth',1.5)
h6=plot(xb,yb,'k-')
set(h6,'linewidth',1.5)
```

Table B. 2 The curve model at MATLAB program

Fitting curve model ⟶ Cubic spline model

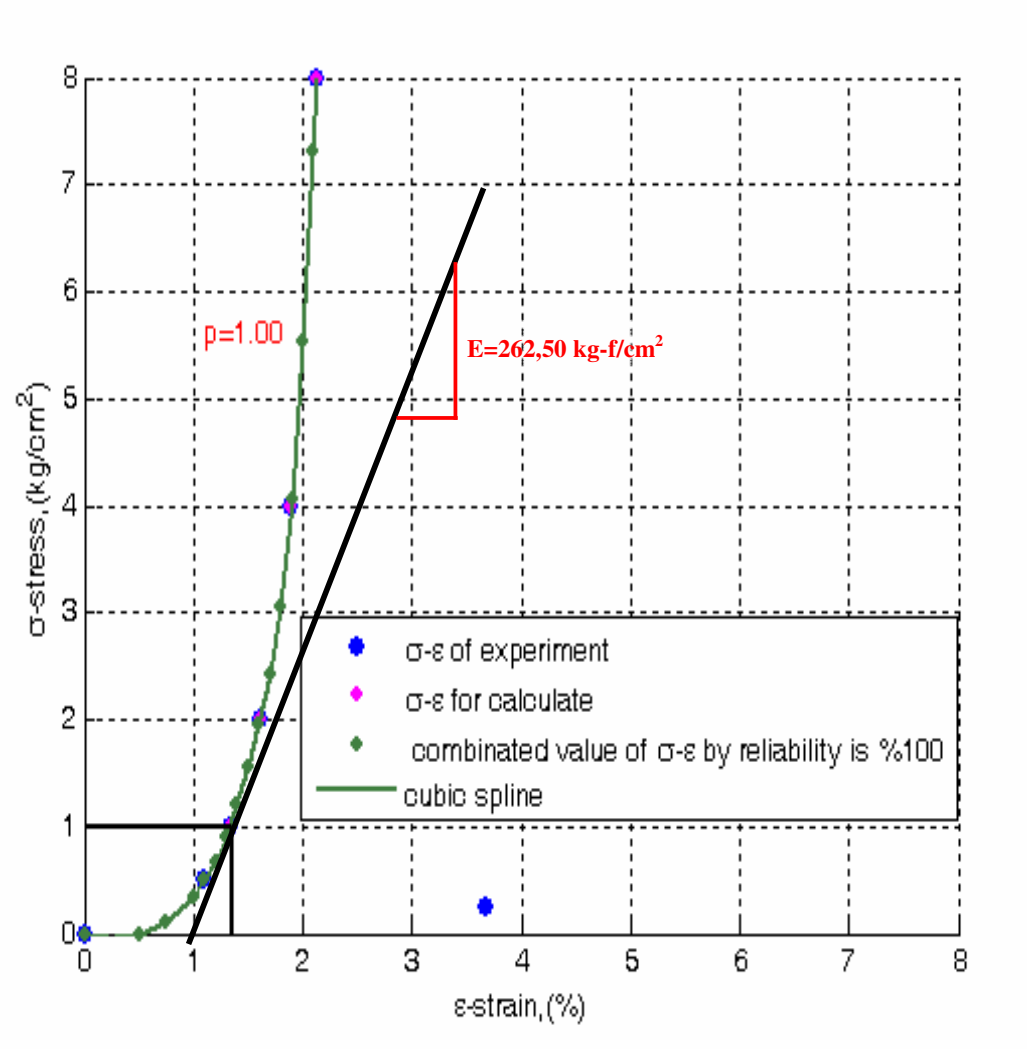

Figure B.2. 1 The oedometer test of B.01-1 is evaluated to find the E_{oed}^{ref} by the MATLAB, for translating the PLAXİS.

Table B.2. 1 The new values of evaluated odeometer test of specimen B01-1.

B.01-1		
Loading (kN/ m^2)	**Found ε (%) by Experiment**	**Found ε (%) by Matlab**
0	0.00	0.00
25	3.68	0.90
50	1.11	1.10
100	1.34	1.33
200	1.61	1.60
400	1.89	1.90
800	2.14	2.10

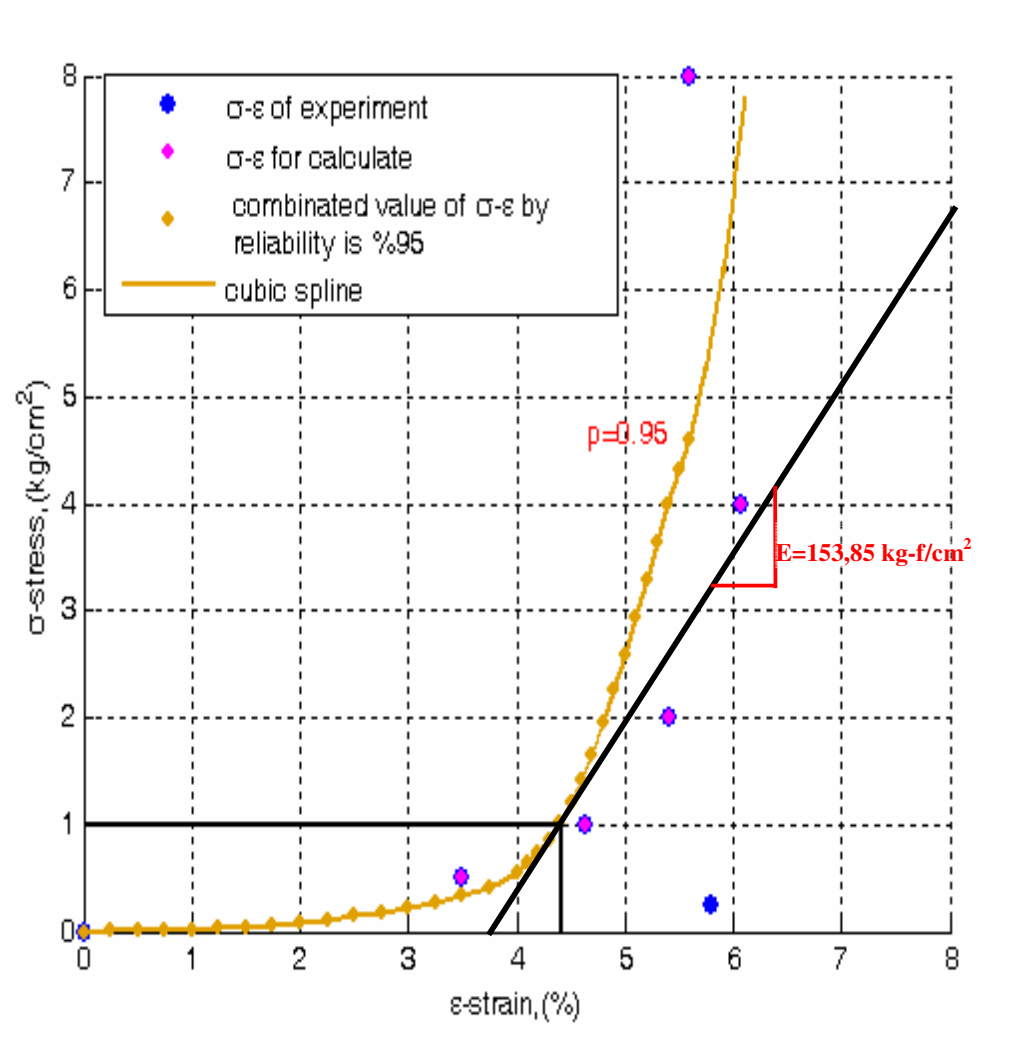

Figure B.2. 2 The oedometer test of B.01-2 is evaluated to find the E_{oed}^{ref} by the MATLAB, for translating the PLAXİS.

Table B.2. 2 The new values of evaluated odeometer test of specimen B01-2.

B.01-2		
Loading (kN/ m^2)	**Found ε (%) by Experiment**	**Found ε (%) by Matlab**
0	0.00	0.00
25	5.79	3.10
50	3.49	3.90
100	4.63	4.42
200	5.41	4.80
400	6.07	5.40
800	5.60	6.10

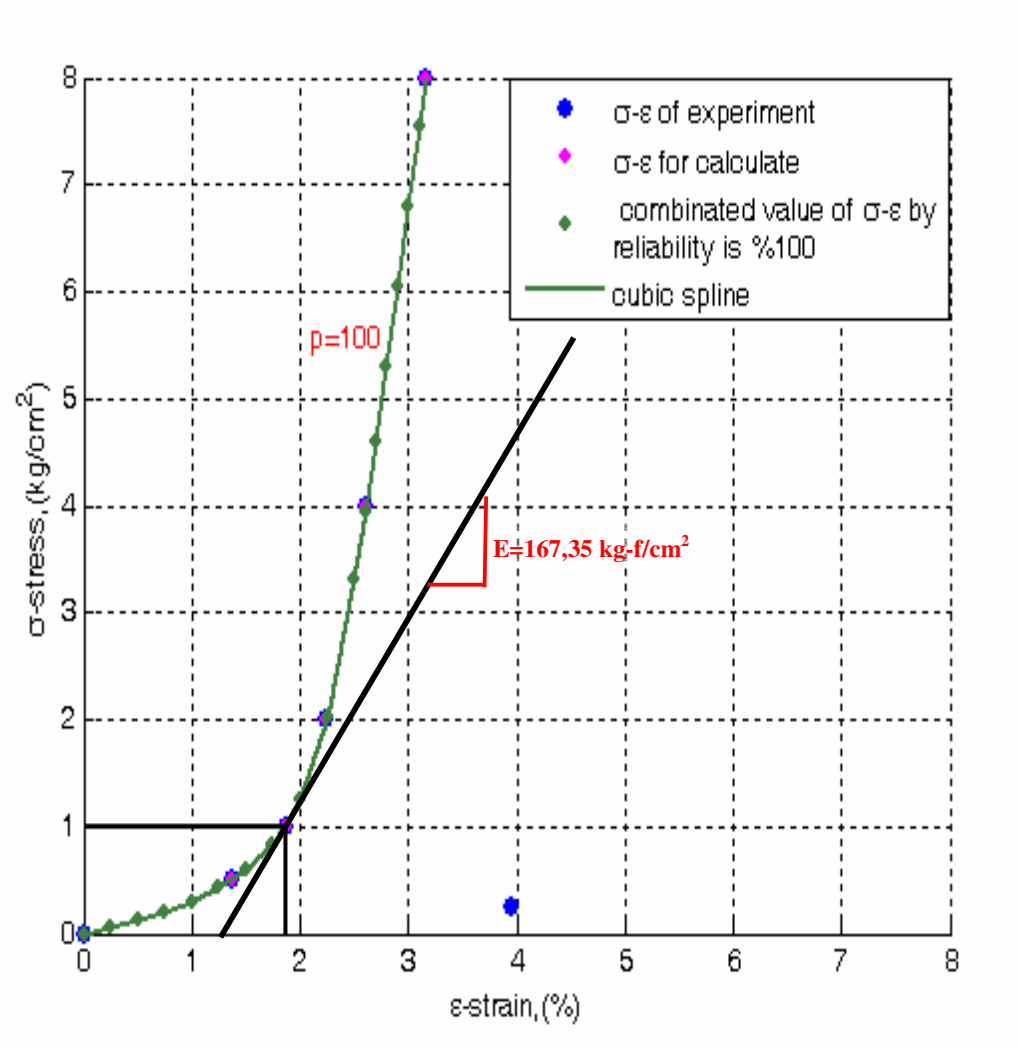

Figure B.2. 3 The oedometer test of B.02-1 is evaluated to find the E_{oed}^{ref} by the MATLAB, for translating the PLAXİS.

Table B.2. 3 The new values of evaluated odeometer test of specimen B02-1.

B.02-1		
Loading (kN/ m^2)	**Found ε (%) by Experiment**	**Found ε (%) by Matlab**
0	0.00	0.00
25	3.95	0.86
50	1.37	1.37
100	1.86	1.86
200	2.24	2.24
400	2.61	2.61
800	3.16	3.16

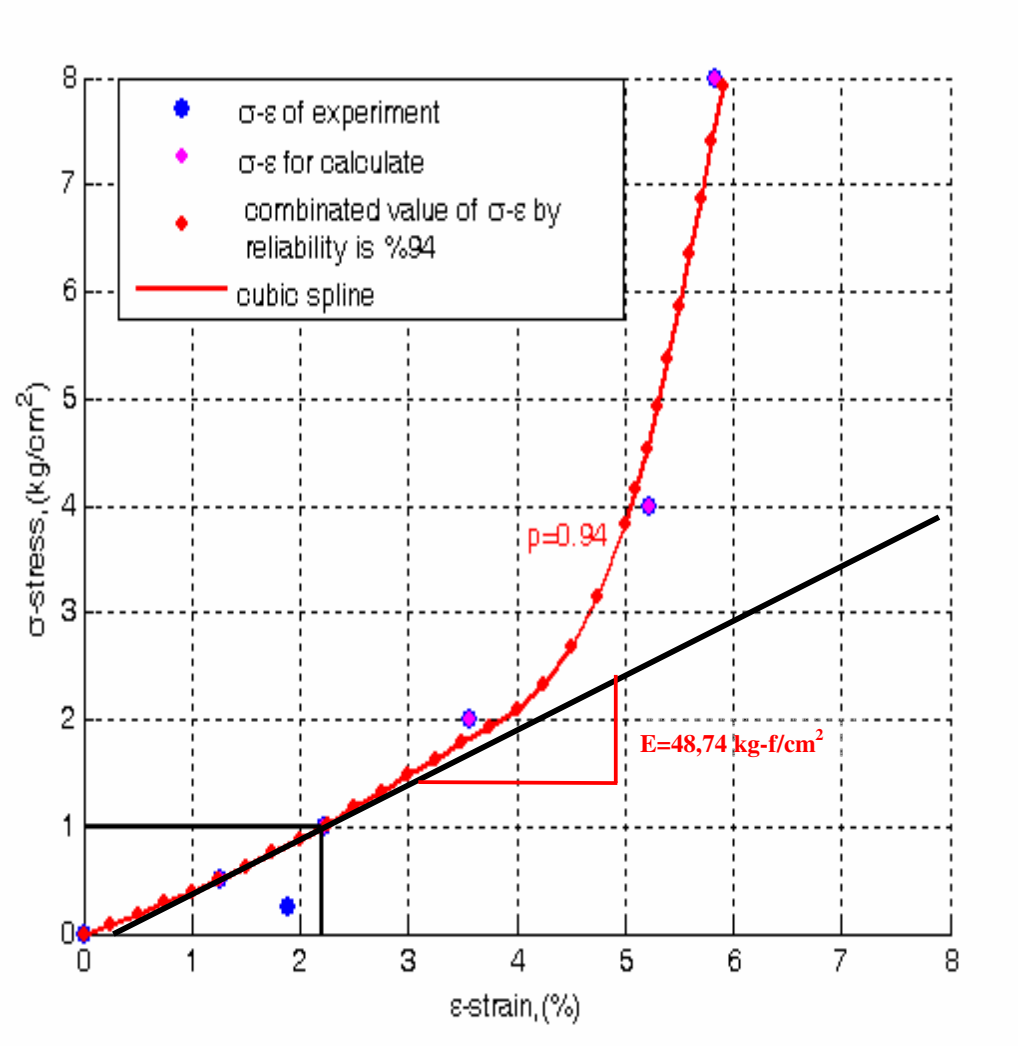

Figure B.2. 4 The oedometer test of B.02-2 is evaluated to find the E_{oed}^{ref} by the MATLAB, for translating the PLAXİS.

Table B.2. 4 The new values of evaluated odeometer test of specimen B02-2.

B.02-2		
Loading (kN/ m^2)	**Found ε (%) by Experiment**	**Found ε (%) by Matlab**
0	0.00	0.00
25	1.89	0.73
50	1.26	1.25
100	2.22	2.21
200	3.57	3.77
400	5.22	5.10
800	5.83	5.90

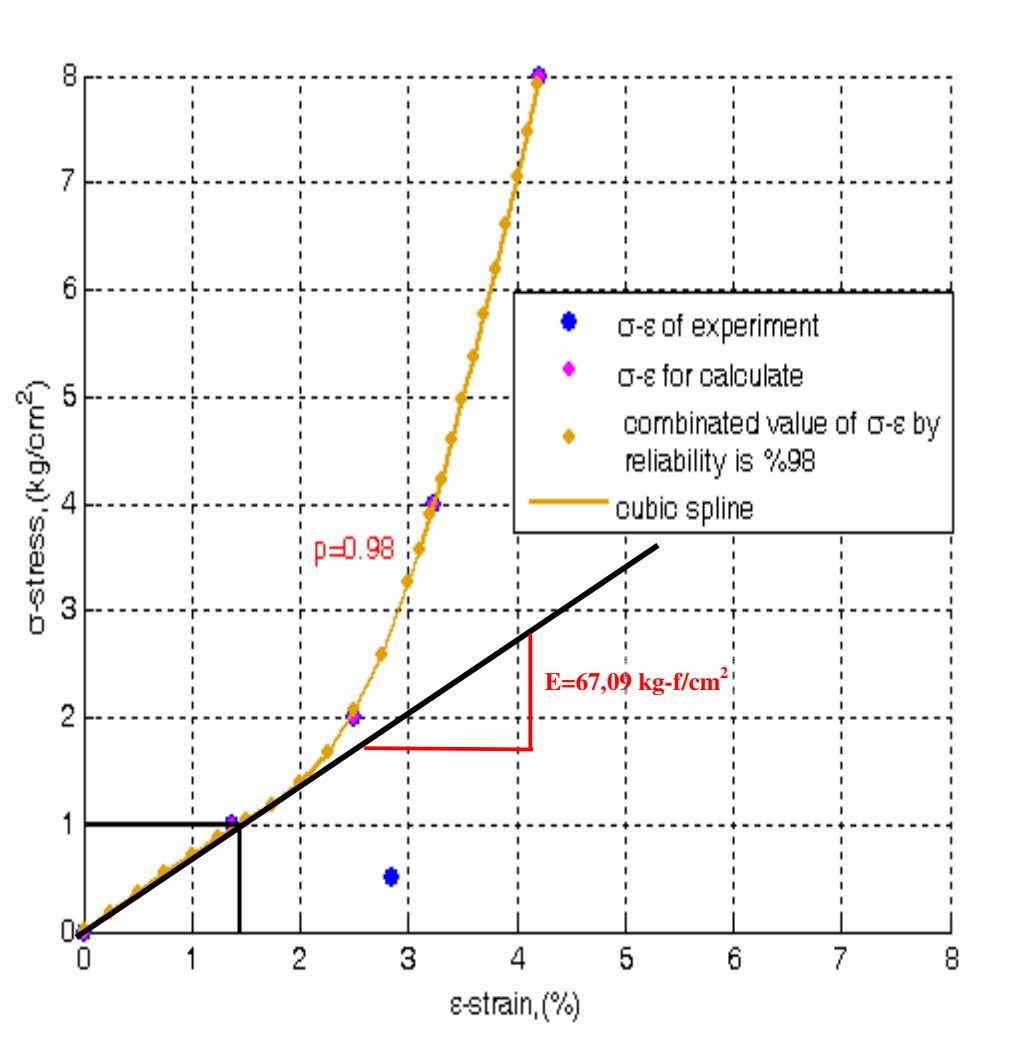

Figure B.2. 5 The oedometer test of B.03-1 is evaluated to find the E_{oed}^{ref} by the MATLAB, for translating the PLAXİS.

Table B.2. 5 The new values of evaluated odeometer test of specimen B03-1.

B.03-1		
Loading (kN/ m²)	**Found ε (%) by Experiment**	**Found ε (%) by Matlab**
0	0.00	0
25	0.00	0.4
50	2.84	0.7
100	1.37	1.44
200	2.49	2.5
400	3.24	3.2
800	4.21	4.2

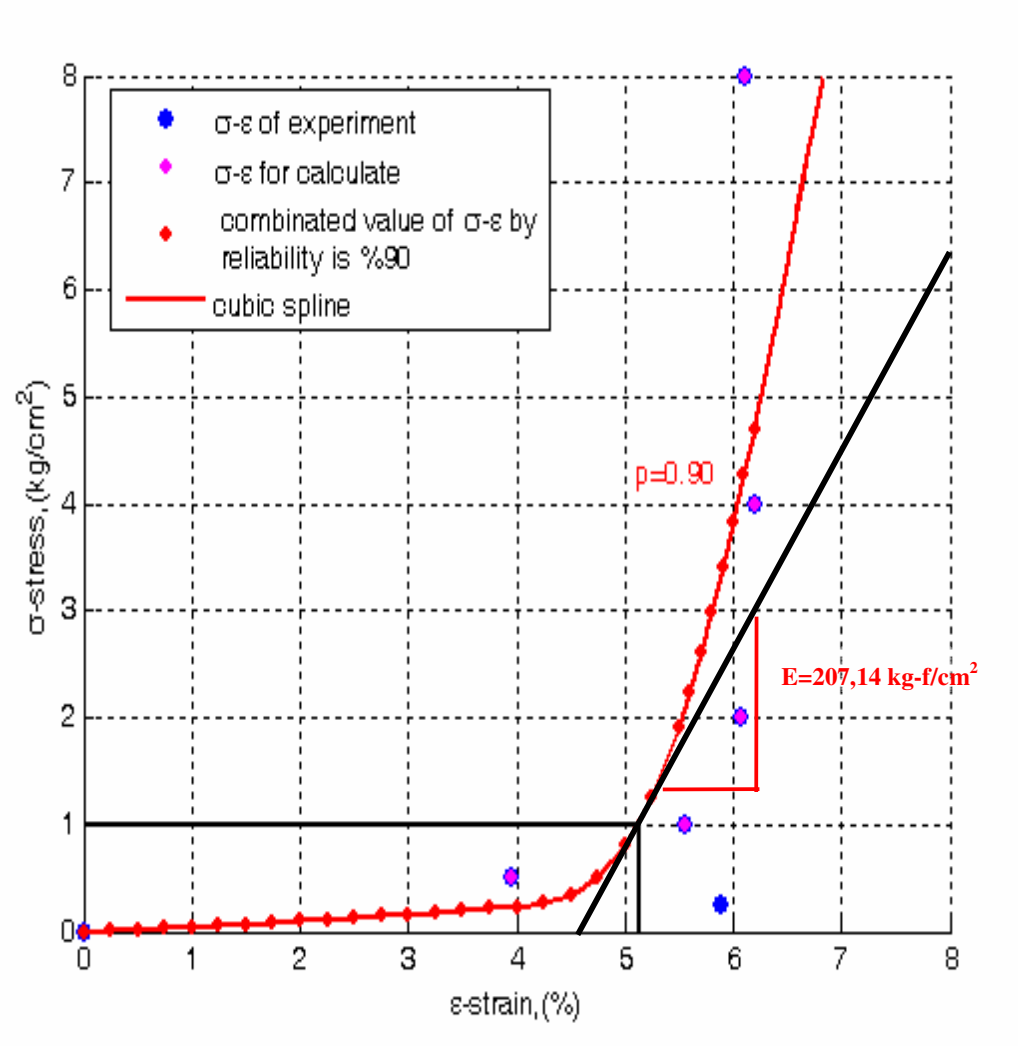

Figure B.2. 6 The oedometer test of B.05-1 is evaluated to find the E_{oed}^{ref} by the MATLAB, for translating the PLAXİS.

Table B.2. 6 The new values of evaluated odeometer test of specimen B05-1.

B.05-1		
Loading (kN/ m^2)	**Found ε (%) by Experiment**	**Found ε (%) by Matlab**
0	0.00	0.00
25	5.89	4.20
50	3.95	4.70
100	5.56	5.14
200	6.07	5.60
400	6.21	6.05
800	6.11	6.85

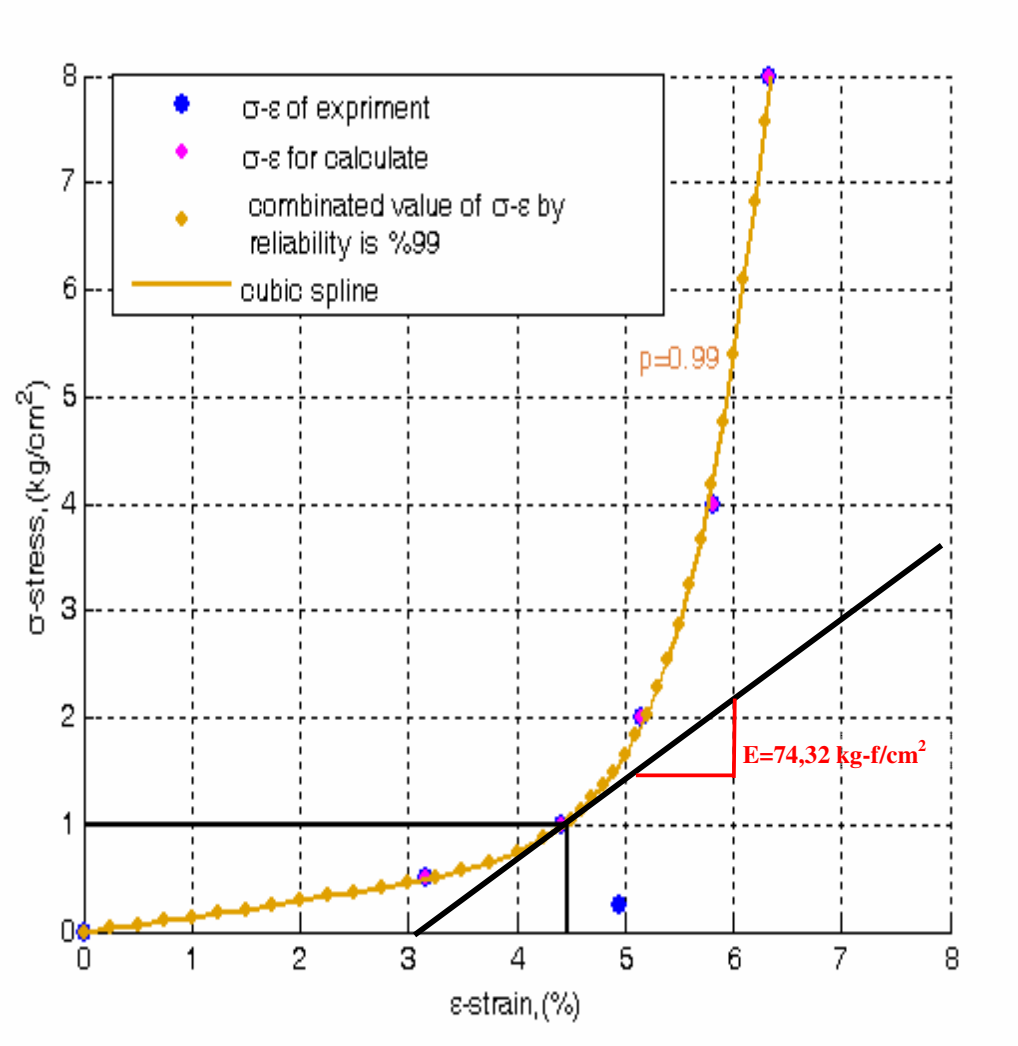

Figure B.2. 7 The oedometer test of B.07-1 is evaluated to find the E_{oed}^{ref} by the MATLAB, for translating the PLAXİS.

Table B.2. 7 The new values of evaluated odeometer test of specimen B07-1.

B.07-1		
Loading (kN/ m^2)	**Found ε (%) by Experiment**	**Found ε (%) by Matlab**
0	0.00	0.00
25	4.96	1.80
50	3.16	3.20
100	4.41	4.47
200	5.16	5.20
400	5.81	5.80
800	6.34	6.30

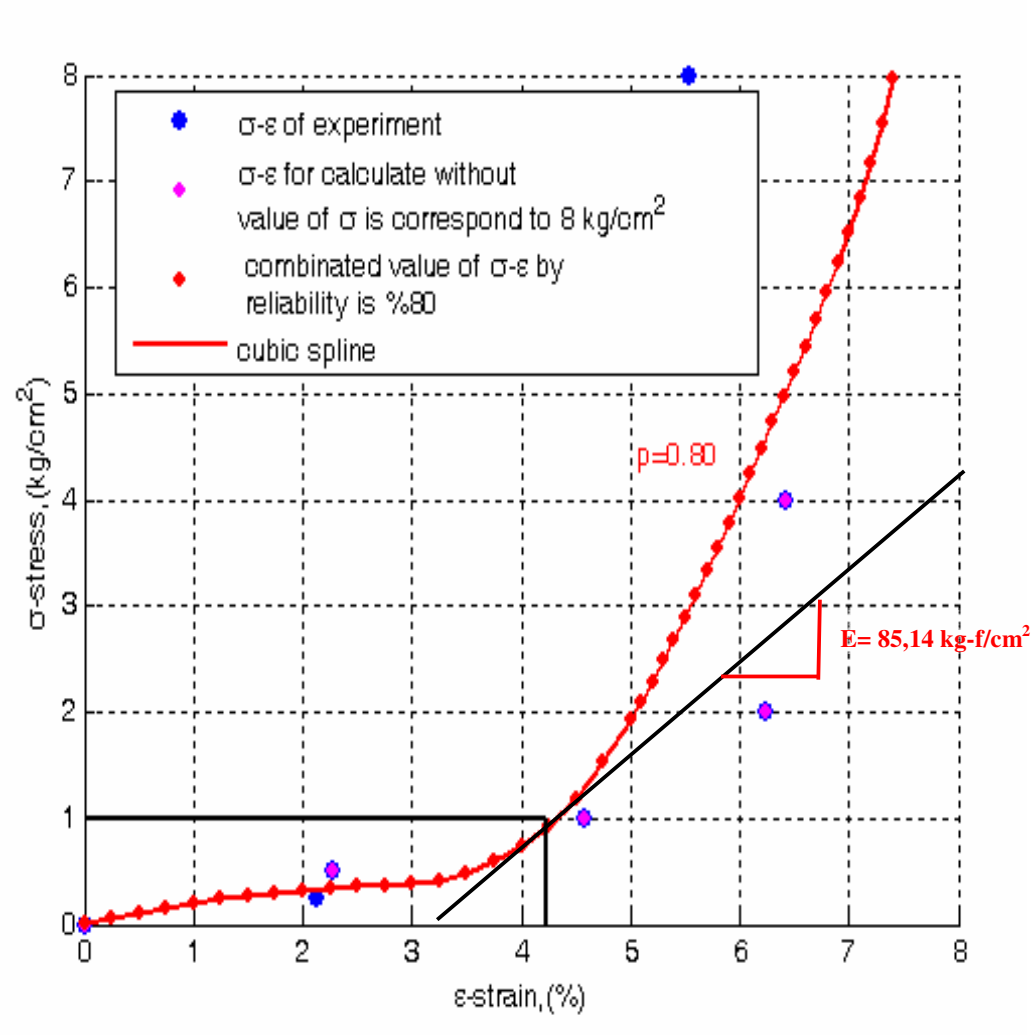

Figure B.2. 8 The oedometer test of B.08-1 is evaluated to find the E_{oed}^{ref} by the MATLAB, for translating the PLAXİS.

Table B.2. 8 The new values of evaluated odeometer test of specimen B08-1.

B.08-1		
Loading (kN/ m^2)	**Found ε (%) by Experiment**	**Found ε (%) by Matlab**
0	0.00	0.00
25	2.13	1.50
50	2.28	3.60
100	4.59	4.23
200	6.24	5.10
400	6.42	6.00
800	5.55	7.45

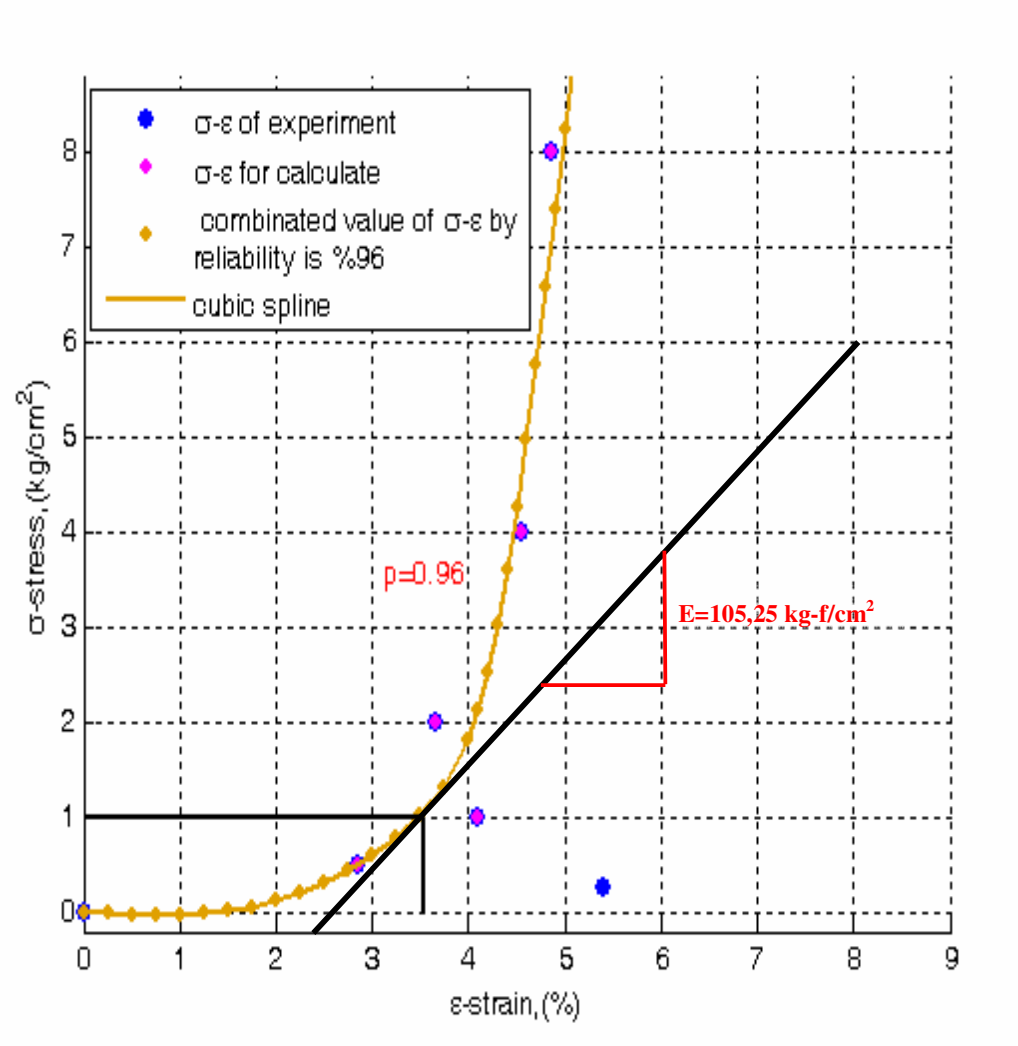

Figure B.2. 9 The oedometer test of B.09-1 is evaluated to find the E_{oed}^{ref} by the MATLAB, for translating the PLAXİS.

Table B.2. 9 The new values of evaluated odeometer test of specimen B09-1.

B.09-1		
Loading (kN/ m^2)	**Found ε (%) by Experiment**	**Found ε (%) by Matlab**
0	0.00	0.00
25	5.40	2.30
50	2.84	2.90
100	4.09	3.54
200	3.66	4.05
400	4.56	4.50
800	4.86	5.00

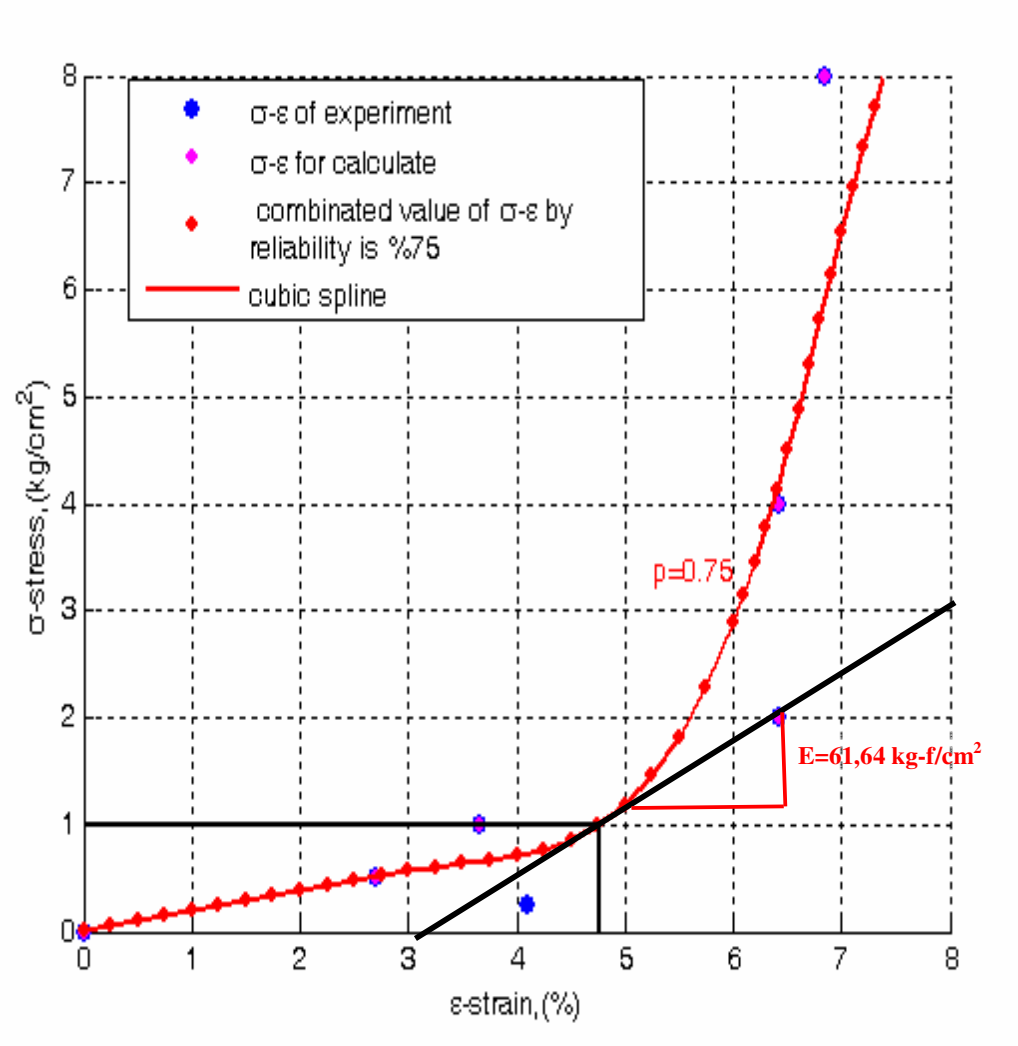

Figure B.2. 10 The oedometer test of B.09-2 is evaluated to find the E_{oed}^{ref} by the MATLAB, for translating the PLAXİS.

Table B.2. 10 The new values of evaluated odeometer test of specimen B09-2.

B.09-2		
Loading (kN/ m^2)	**Found ε (%) by Experiment**	**Found ε (%) by Matlab**
0	0.00	0.00
25	4.11	1.27
50	2.71	2.73
100	3.65	4.76
200	6.43	5.60
400	6.42	6.30
800	6.84	7.40

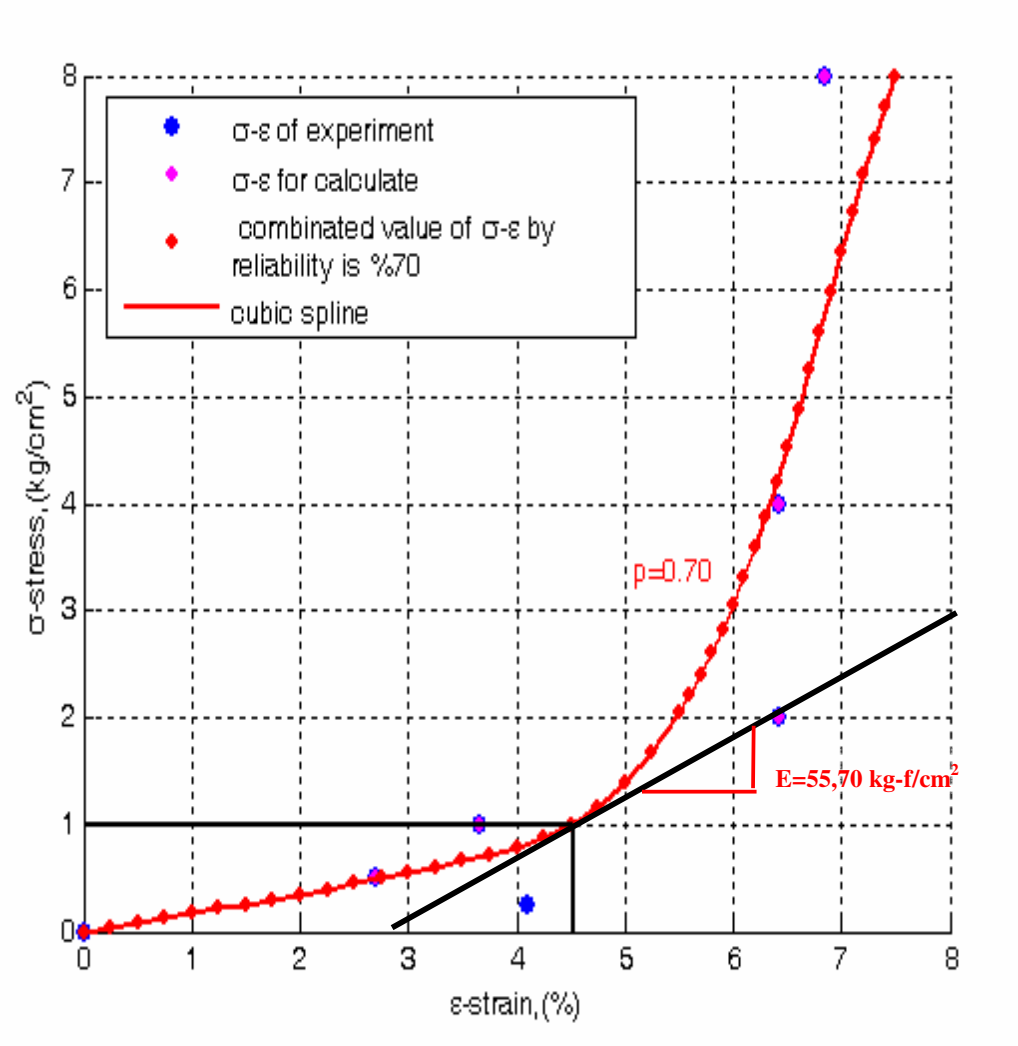

Figure B.2. 11 The oedometer test of B.10-1 is evaluated to find the E_{oed}^{ref} by the MATLAB, for translating the PLAXİS.

Table B.2. 11 The new values of evaluated odeometer test of specimen B10-1.

B.10-1		
Loading (kN/ m^2)	**Found ε (%) by Experiment**	**Found ε (%) by Matlab**
0	0.00	0.00
25	3.58	1.50
50	2.26	2.76
100	3.61	4.52
200	4.39	5.45
400	5.32	6.35
800	5.74	7.60

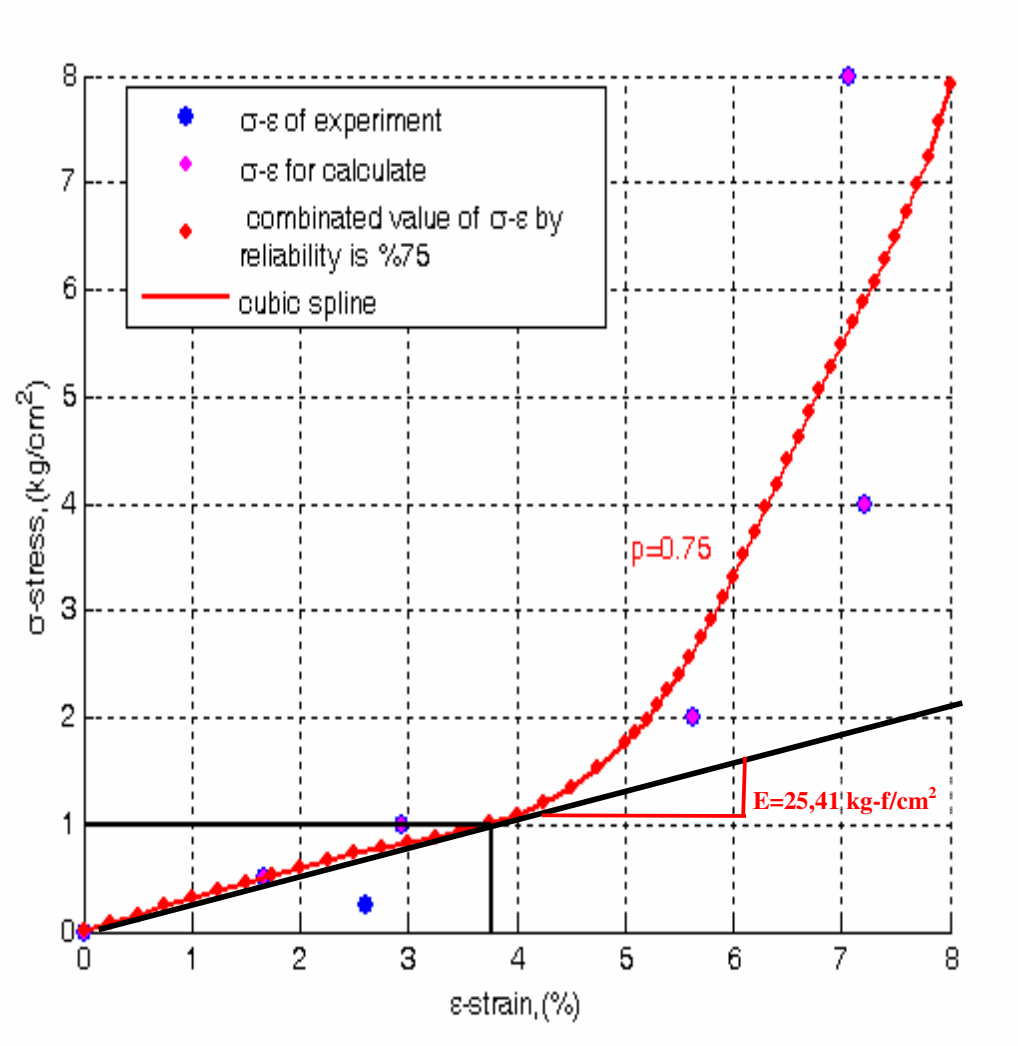

Figure B.2. 12 The oedometer test of B.10-2 is evaluated to find the E_{oed}^{ref} by the MATLAB, for translating the PLAXİS.

Table B.2. 12 The new values of evaluated odeometer test of specimen B10-2.

B.10-2		
Loading (kN/ m^2)	**Found ε (%) by Experiment**	**Found ε (%) by Matlab**
0	0.00	0.00
25	2.60	0.80
50	1.66	1.60
100	2.95	3.77
200	5.63	5.21
400	7.21	6.30
800	7.07	8.05

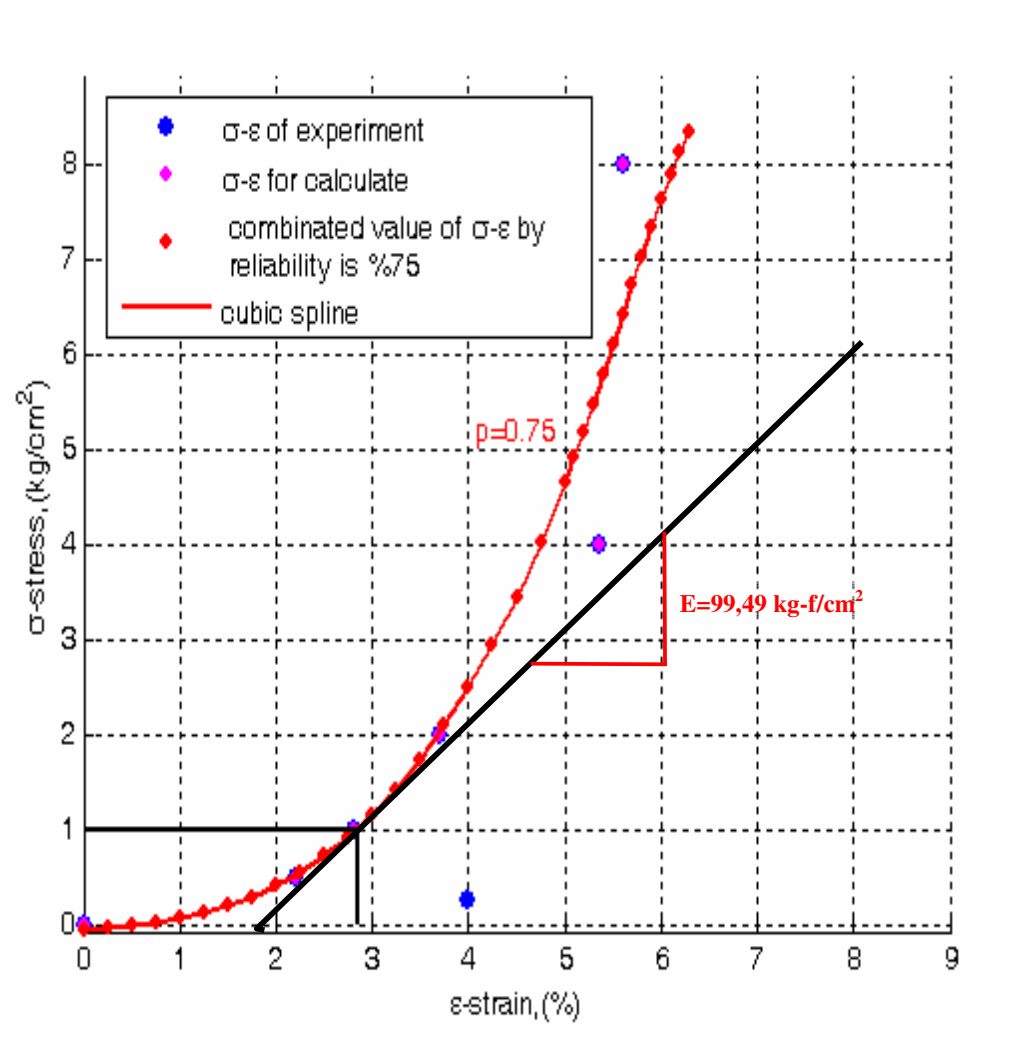

Figure B.2. 13 The oedometer test of B.11-1 is evaluated to find the E_{oed}^{ref} by the MATLAB, for translating the PLAXİS.

Table B.2. 13 The new values of evaluated odeometer test of specimen B11-1.

B.11-1		
Loading (kN/ m^2)	**Found ε (%) by Experiment**	**Found ε (%) by Matlab**
0	0.00	0.00
25	4.00	1.70
50	2.21	2.23
100	2.81	2.85
200	3.69	3.70
400	5.37	4.75
800	5.60	6.20

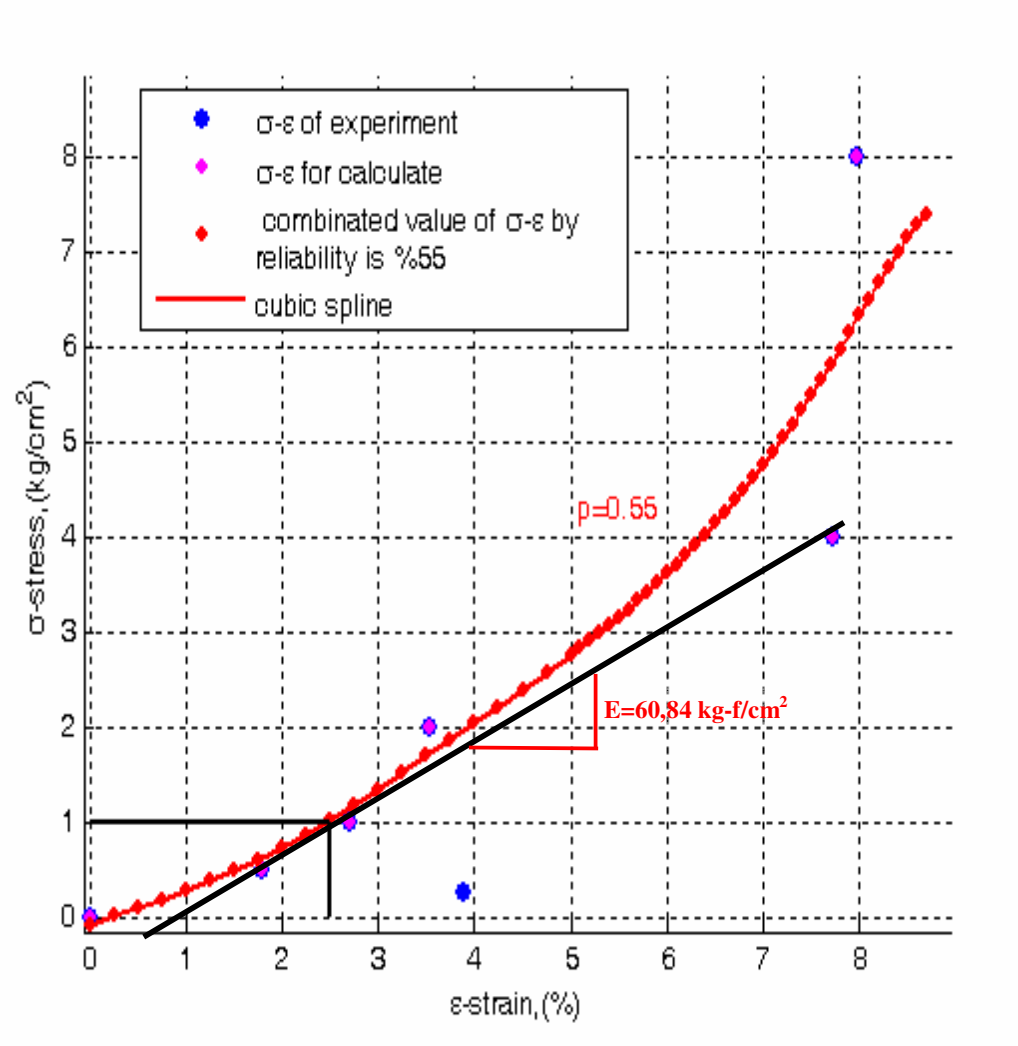

Figure B.2. 14 The oedometer test of B.11-2 is evaluated to find the E_{oed}^{ref} by the MATLAB, for translating the PLAXİS.

Table B.2. 14 The new values of evaluated odeometer test of specimen B11-2.

B.11-2		
Loading (kN/ m^2)	**Found ε (%) by Experiment**	**Found ε (%) by Matlab**
0	0.00	0.00
25	3.89	0.98
50	1.79	1.60
100	2.72	2.50
200	3.53	3.95
400	7.73	6.40
800	7.97	9.10

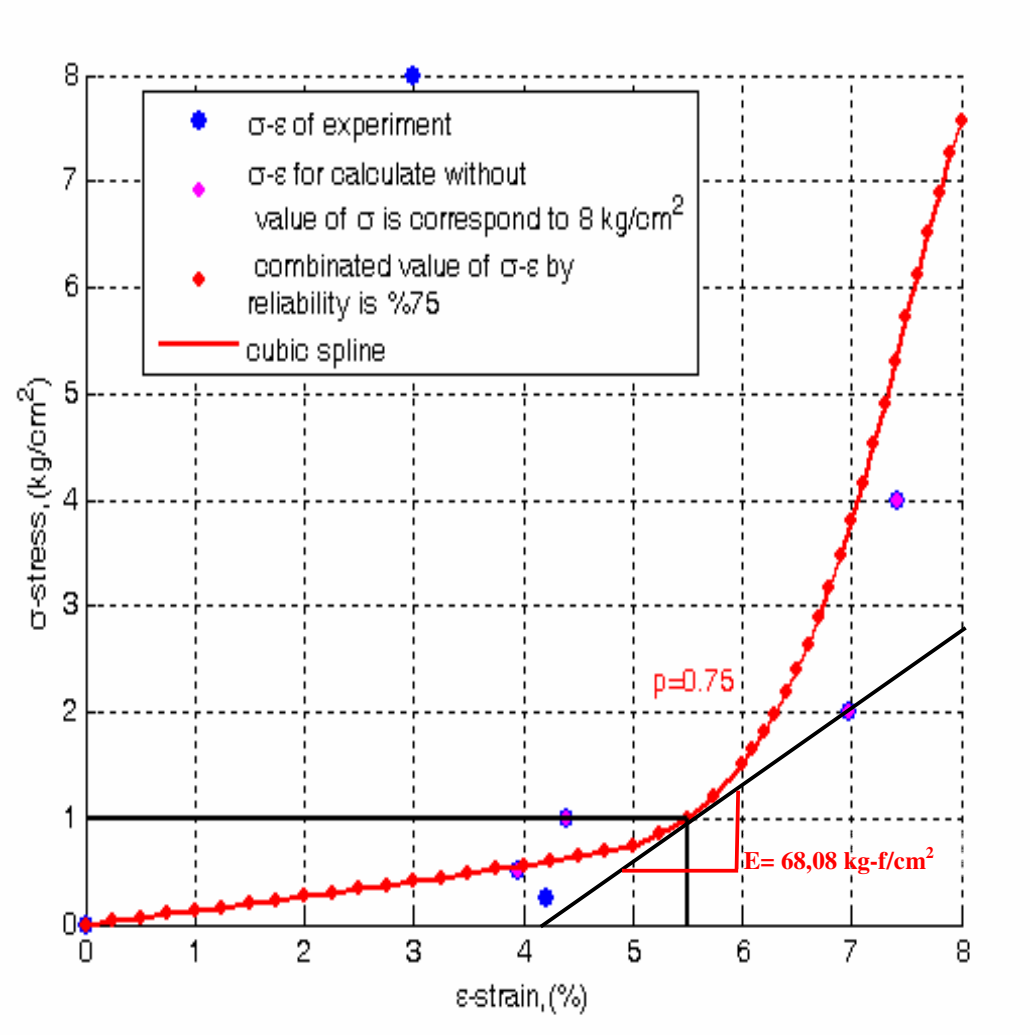

Figure B.2. 15 The oedometer test of B.12-1 is evaluated to find the E_{oed}^{ref} by the MATLAB, for translating the PLAXİS.

Table B.2. 15 The new values of evaluated odeometer test of specimen B12-1.

B.12-1		
Loading (kN/ m^2)	**Found ε (%) by Experiment**	**Found ε (%) by Matlab**
0	0.00	0.00
25	4.21	1.90
50	3.95	3.70
100	4.39	5.51
200	6.98	6.30
400	7.42	7.05
800	3.00	8.20

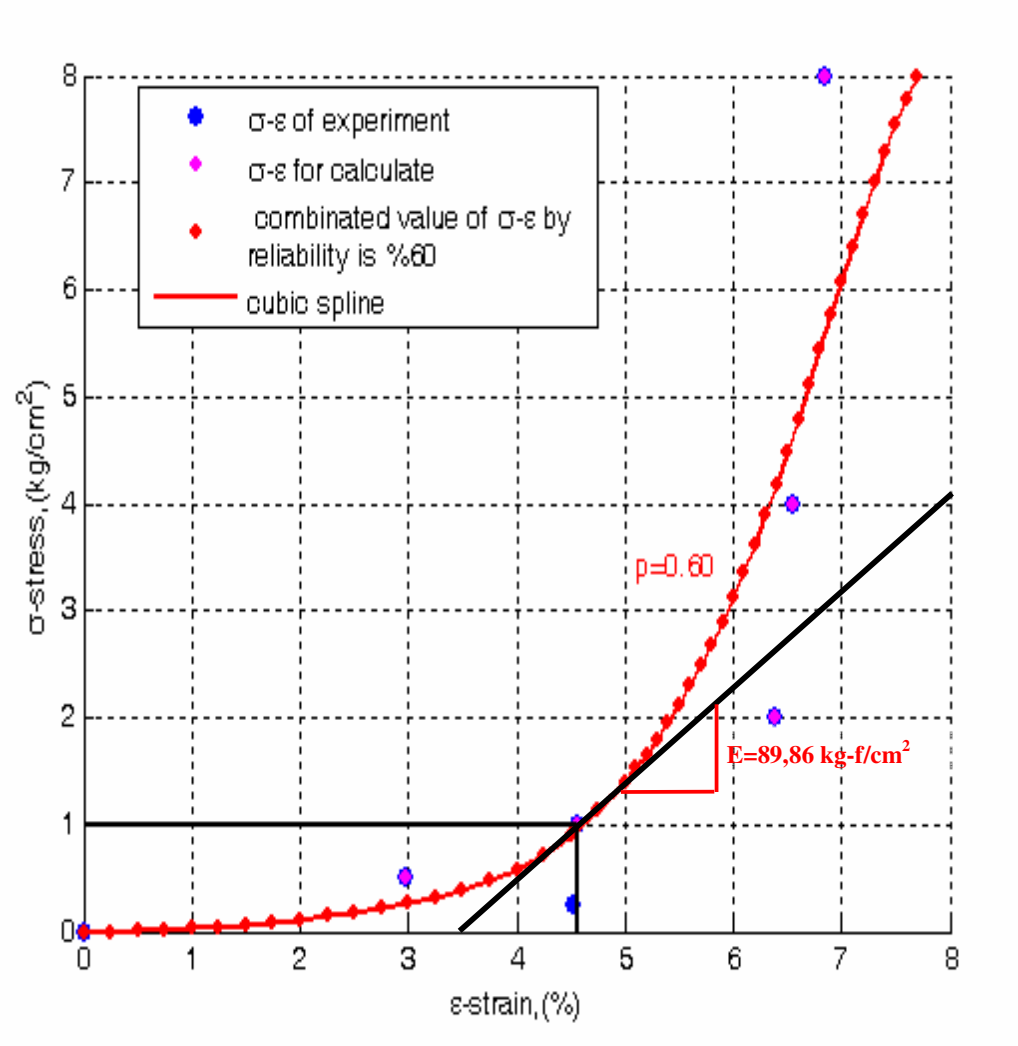

Figure B.2. 16 The oedometer test of B.12-2 is evaluated to find the E_{oed}^{ref} by the MATLAB, for translating the PLAXİS.

Table B.2. 16 The new values of evaluated odeometer test of specimen B12-2.

B.12-2		
Loading (kN/ m^2)	**Found ε (%) by Experiment**	**Found ε (%) by Matlab**
0	0.00	0.00
25	4.53	2.95
50	2.98	3.80
100	4.57	4.57
200	6.38	5.50
400	6.55	6.40
800	6.84	7.75

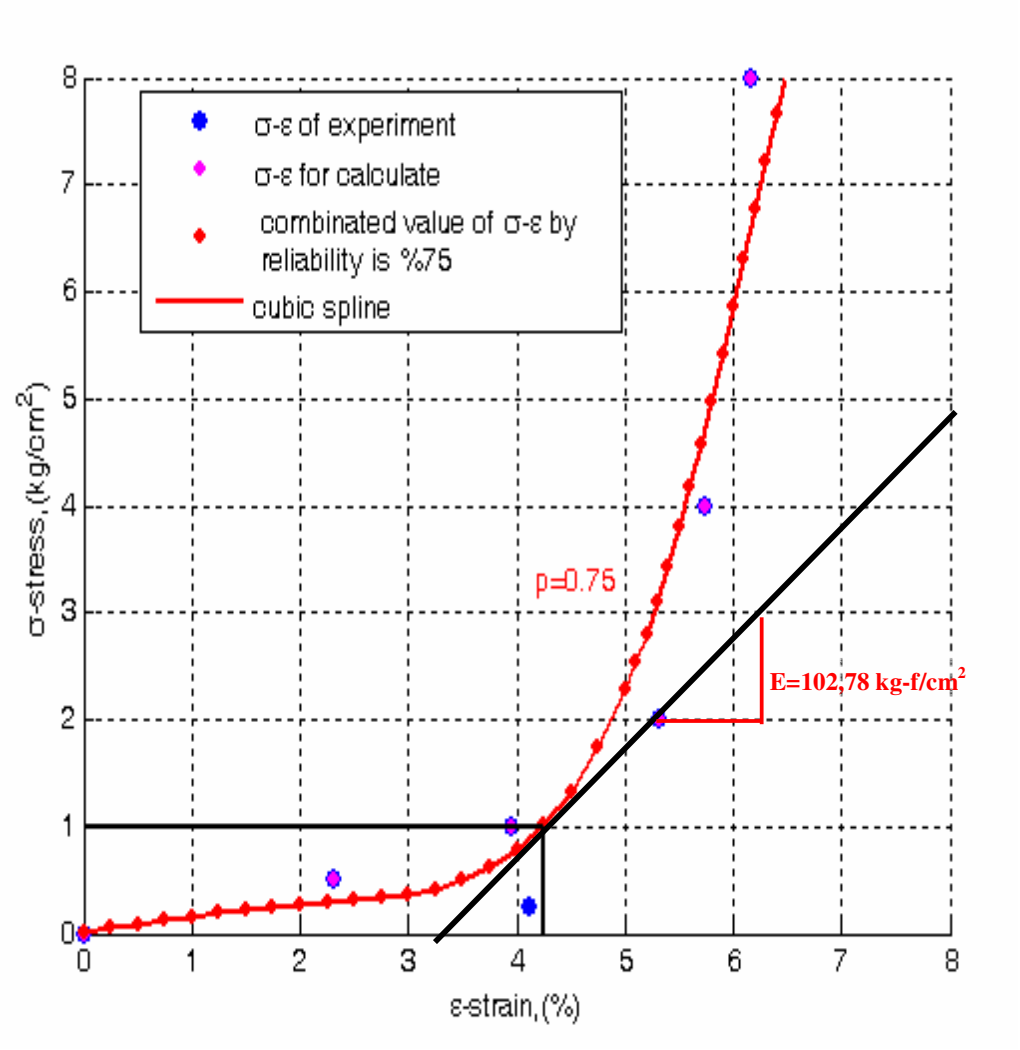

Figure B.2. 17 The oedometer test of B.13-1 is evaluated to find the E_{oed}^{ref} by the MATLAB, for translating the PLAXİS.

Table B.2. 17 The new values of evaluated odeometer test of specimen B13-1.

B.13-1		
Loading (kN/ m^2)	**Found ε (%) by Experiment**	**Found ε (%) by Matlab**
0	0.00	0.00
25	4.12	1.80
50	2.31	3.50
100	3.95	4.25
200	5.32	4.85
400	5.74	5.55
800	6.16	6.50

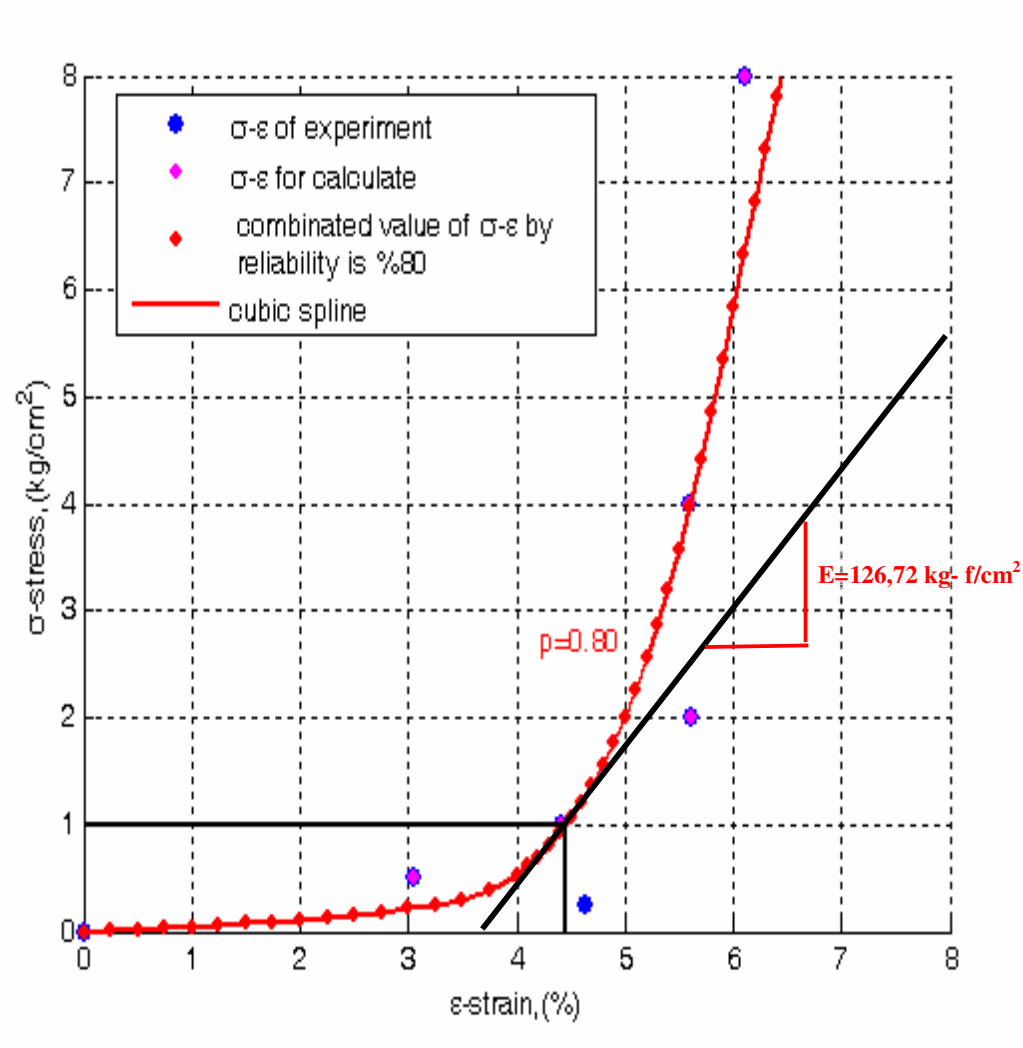

Figure B.2. 18 The oedometer test of B.13-2 is evaluated to find the E_{oed}^{ref} by the MATLAB, for translating the PLAXİS.

Table B.2. 18 The new values of evaluated odeometer test of specimen B13-2.

B.13-2		
Loading (kN/ m^2)	**Found ε (%) by Experiment**	**Found ε (%) by Matlab**
0	0.00	0.00
25	4.63	3.25
50	3.05	3.95
100	4.42	4.46
200	5.61	5.00
400	5.60	5.60
800	6.11	6.45

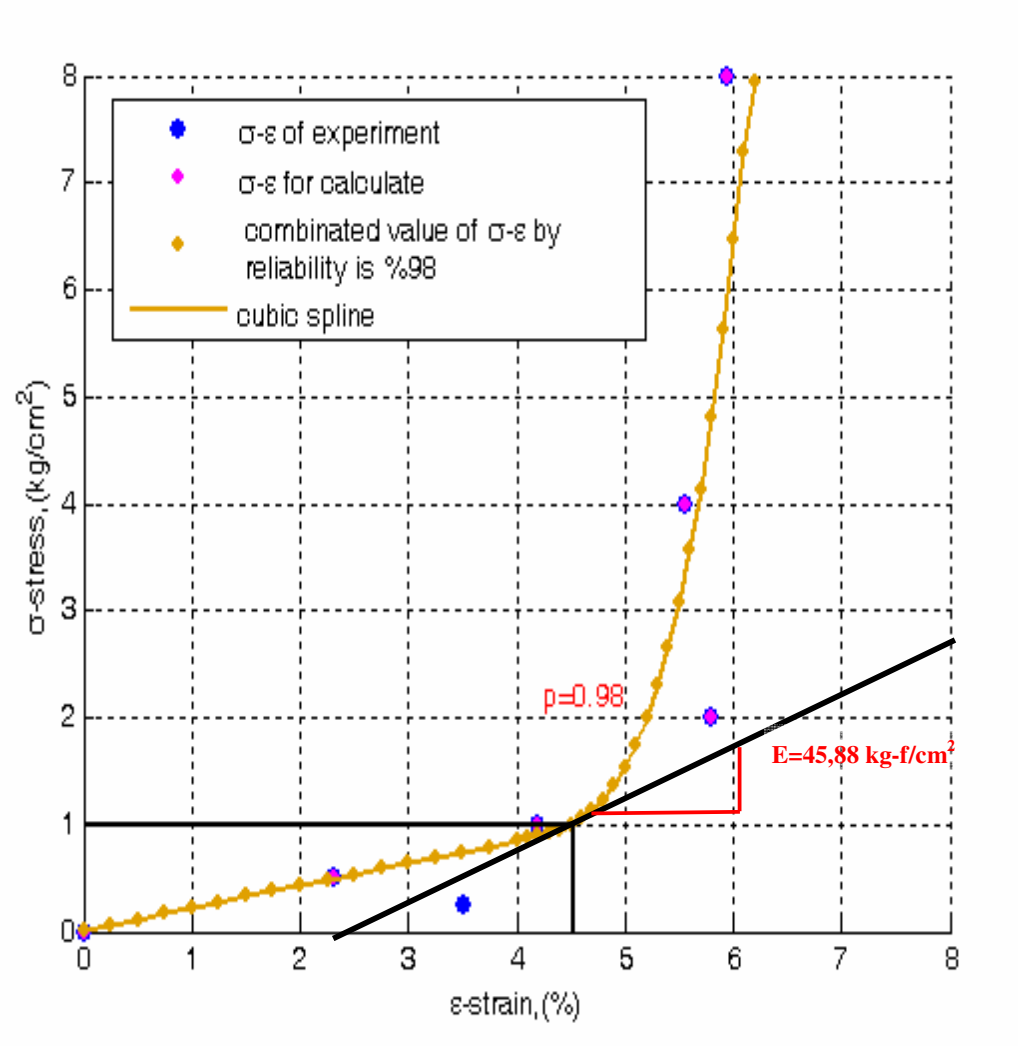

Figure B.2. 19 The oedometer test of B.14-1 is evaluated to find the E_{oed}^{ref} by the MATLAB, for translating the PLAXİS.

Table B.2. 19 The new values of evaluated odeometer test of specimen B14-1

B.14-1		
Loading (kN/ m^2)	**Found ε (%) by Experiment**	**Found ε (%) by Matlab**
0	0.00	0.00
25	3.51	1.15
50	2.32	2.25
100	4.20	4.53
200	5.79	5.20
400	5.56	5.67
800	5.95	6.20

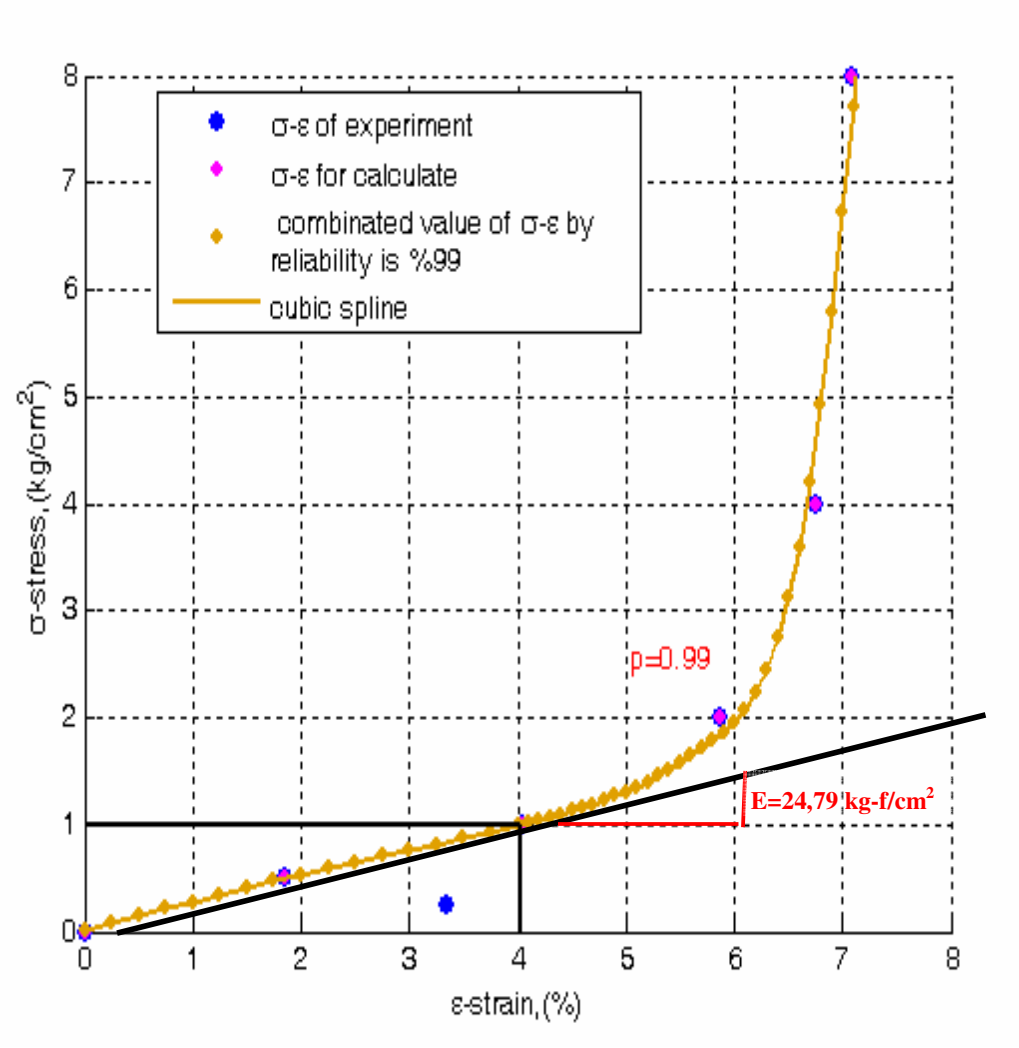

Figure B.2. 20 The oedometer test of B.15-1 is evaluated to find the E_{oed}^{ref} by the MATLAB, for translating the PLAXİS.

Table B.2. 20 The new values of evaluated odeometer test of specimen B15-1

B.15-1		
Loading (kN/ m^2)	**Found ε (%) by Experiment**	**Found ε (%) by Matlab**
0	0.00	0.00
25	3.34	0.95
50	1.85	1.90
100	4.04	4.03
200	5.87	6.05
400	6.76	6.66
800	7.08	7.13

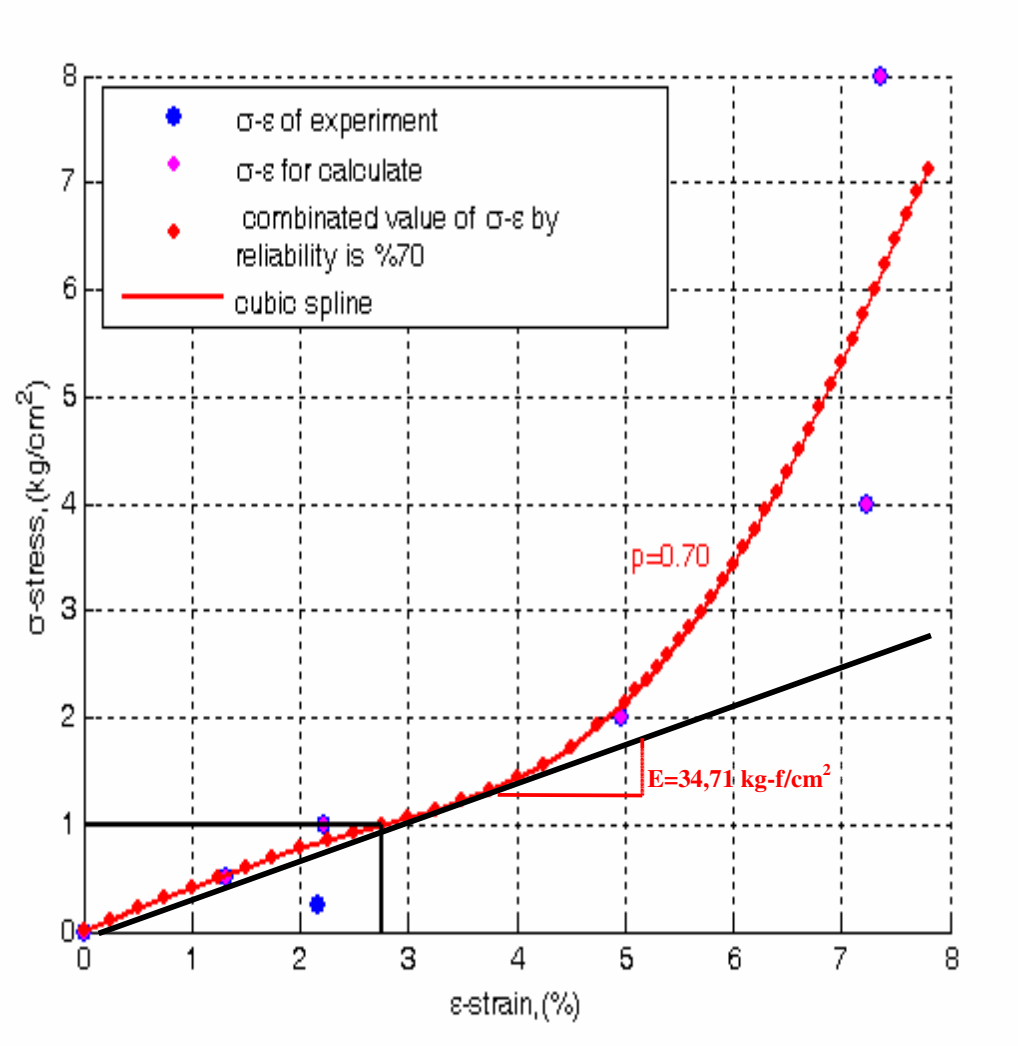

Figure B.2. 21 The oedometer test of B.16-1 is evaluated to find the E_{oed}^{ref} by the MATLAB, for translating the PLAXİS.

Table B.2. 21 The new values of evaluated odeometer test of specimen B16-1.

B.16-1		
Loading (kN/ m^2)	**Found ε (%) by Experiment**	**Found ε (%) by Matlab**
0	0.00	0.00
25	2.16	0.52
50	1.32	1.25
100	2.22	2.75
200	4.97	4.80
400	7.23	6.33
800	7.37	8.10

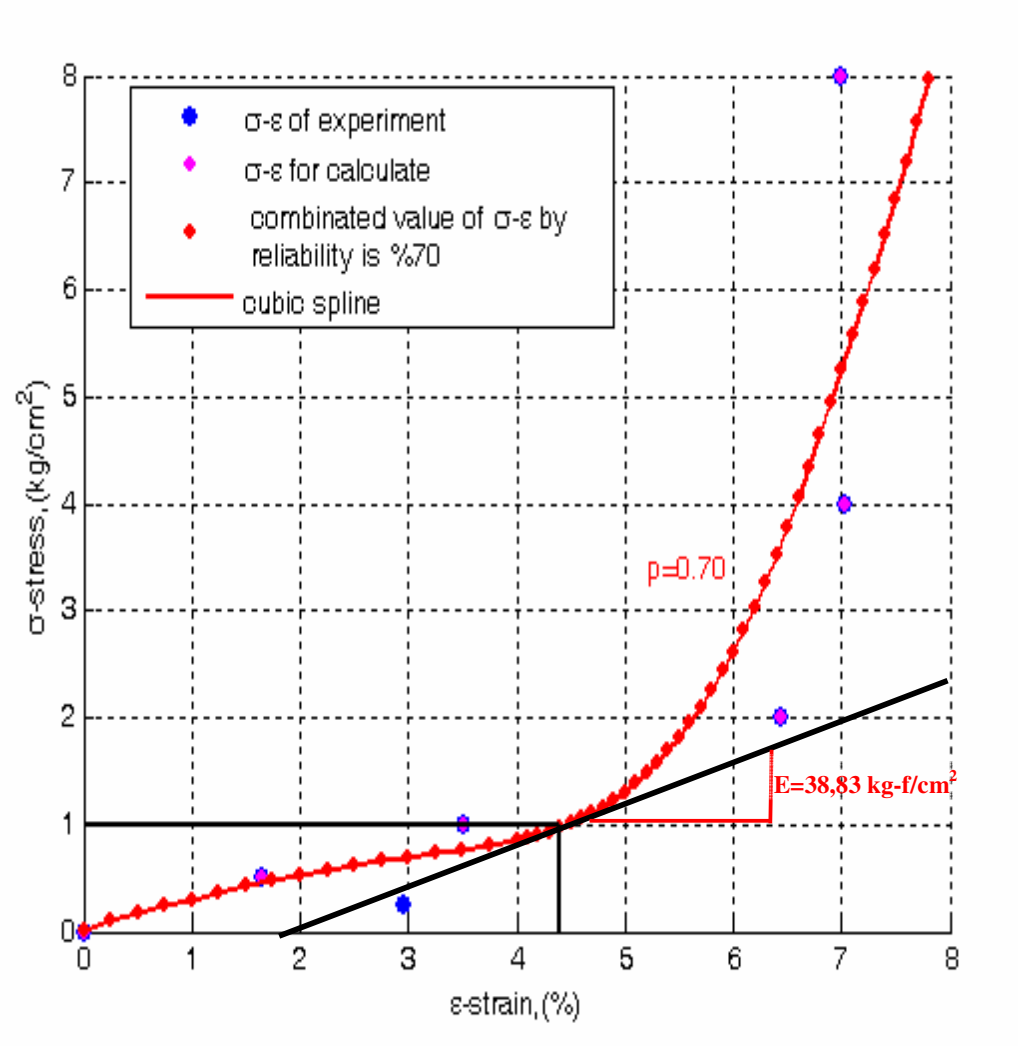

Figure B.2. 22 The oedometer test of B.16-2 is evaluated to find the E_{oed}^{ref} by the MATLAB, for translating the PLAXİS.

Table B.2. 22 The new values of evaluated odeometer test of specimen B16-2.

B.16-2		
Loading (kN/ m²)	**Found ε (%) by Experiment**	**Found ε (%) by Matlab**
0	0.00	0.00
25	2.96	0.80
50	1.64	1.85
100	3.51	4.40
200	6.44	5.65
400	7.03	6.58
800	7.00	7.82

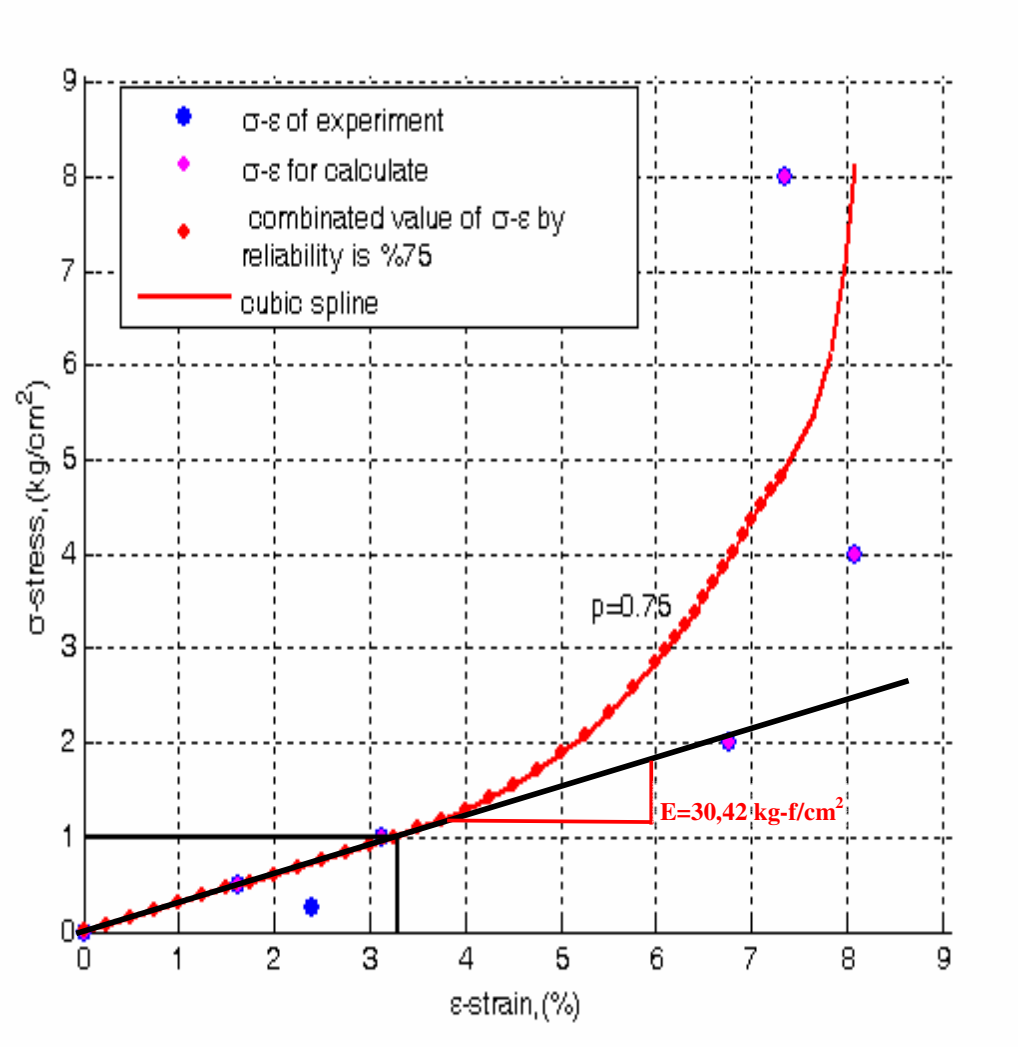

Figure B.2. 23 The oedometer test of B.17-1 is evaluated to find the E_{oed}^{ref} by the MATLAB, for translating the PLAXİS.

Table B.2. 23 The new values of evaluated odeometer test of specimen B17-1.

B.17-1		
Loading (kN/ m^2)	**Found ε (%) by Experiment**	**Found ε (%) by Matlab**
0	0.00	0.00
25	2.39	0.85
50	1.61	1.65
100	3.13	3.28
200	6.77	5.13
400	8.07	6.80
800	7.35	8.20

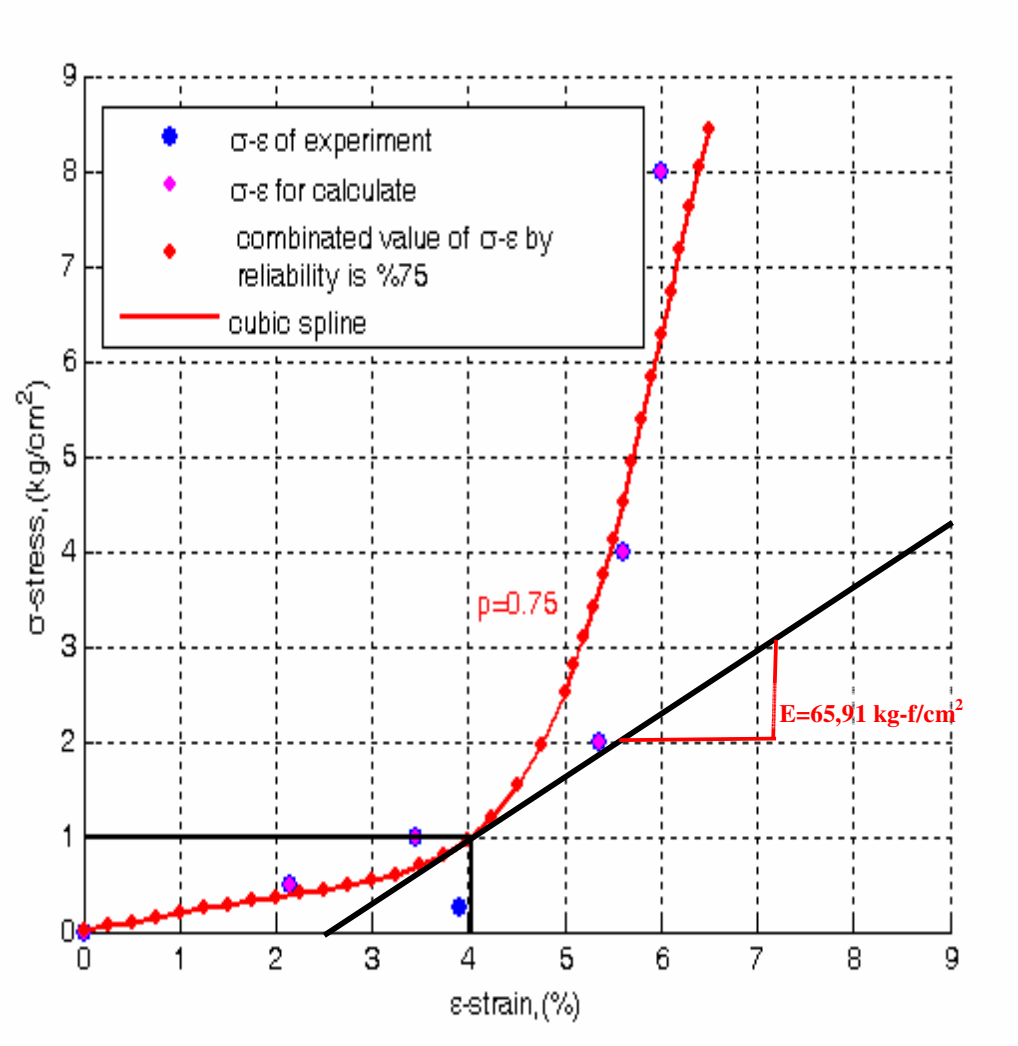

Figure B.2. 24 The oedometer test of B.17-2 is evaluated to find the E_{oed}^{ref} by the MATLAB, for translating the PLAXİS.

Table B.2. 24 The new values of evaluated odeometer test of specimen B17-2.

B.17-2		
Loading (kN/ m^2)	**Found ε (%) by Experiment**	**Found ε (%) by Matlab**
0	0.00	0.00
25	3.92	1.26
50	2.14	2.85
100	3.45	4.03
200	5.37	4.77
400	5.60	5.47
800	6.00	6.38

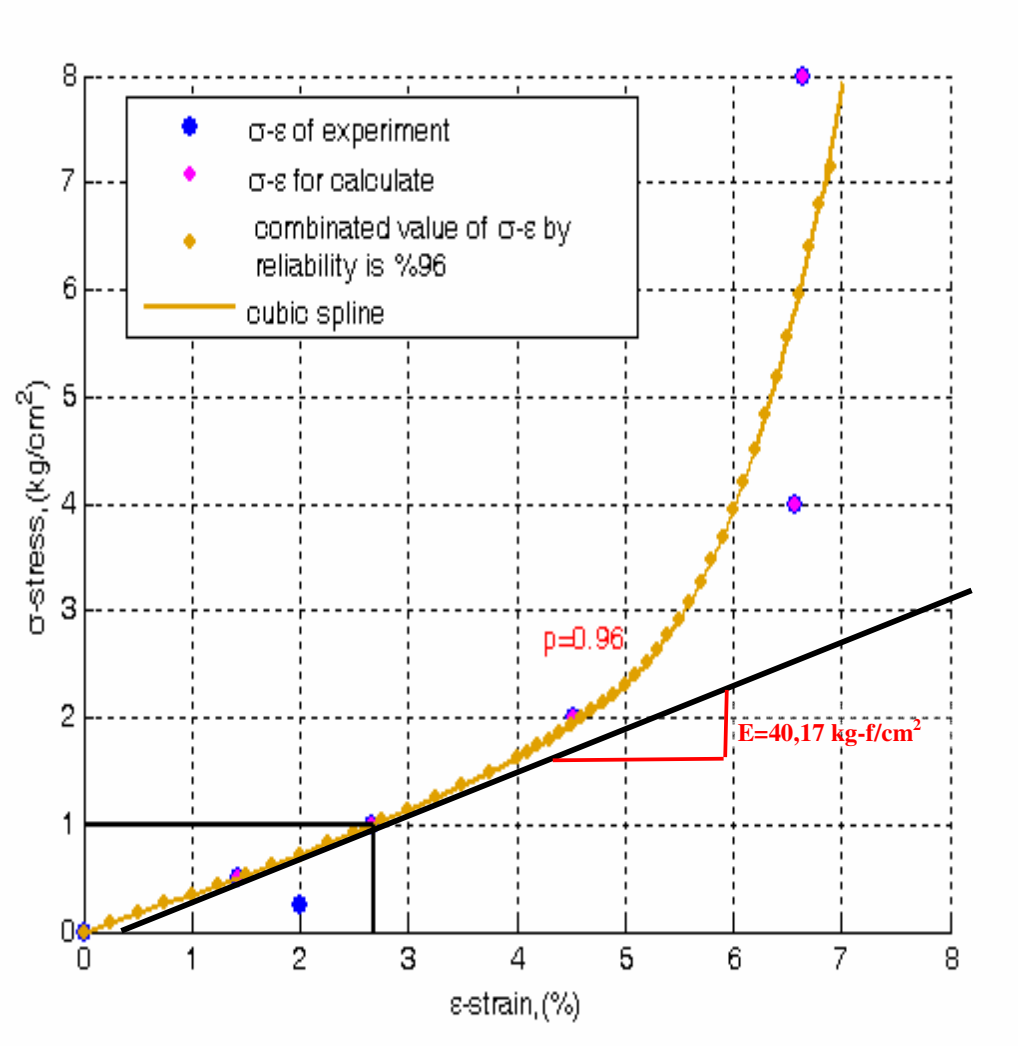

Figure B.2. 25 The oedometer test of B.18-1 is evaluated to find the E_{oed}^{ref} by the MATLAB, for translating the PLAXİS.

Table B.2. 25 The new values of evaluated odeometer test of specimen B18-1.

B.18-1		
Loading (kN/ m^2)	**Found ε (%) by Experiment**	**Found ε (%) by Matlab**
0	0.00	0.00
25	2.00	0.75
50	1.42	1.40
100	2.66	2.68
200	4.53	4.60
400	6.58	6.00
800	6.65	7.10

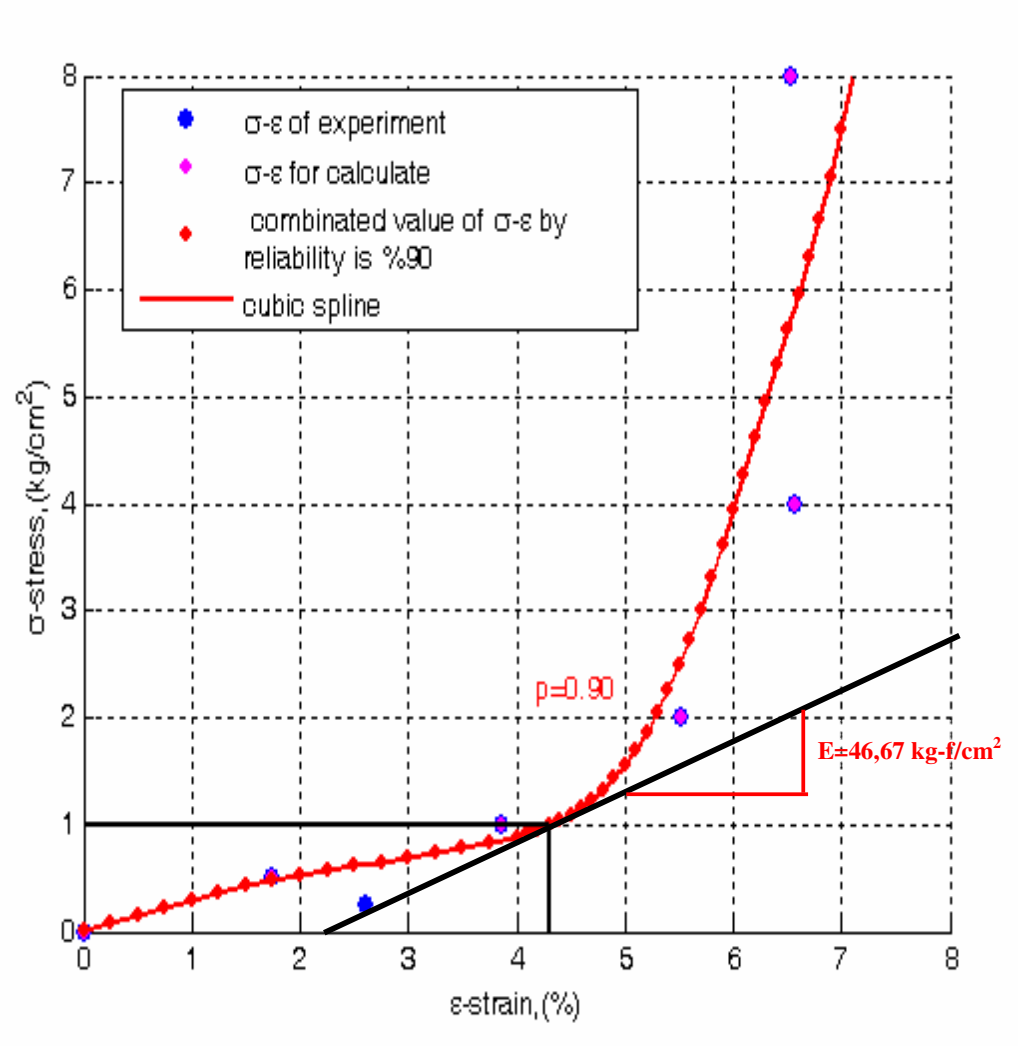

Figure B.2. 26 The oedometer test of B.18-2 is evaluated to find the E_{oed}^{ref} by the MATLAB, for translating the PLAXİS.

Table B.2. 26 The new values of evaluated odeometer test of specimen B18-2.

B.18-2		
Loading (kN/ m^2)	**Found ε (%) by Experiment**	**Found ε (%) by Matlab**
0	0.00	0.00
25	2.60	0.90
50	1.75	1.87
100	3.86	4.30
200	5.53	5.30
400	6.58	6.00
800	6.53	7.10

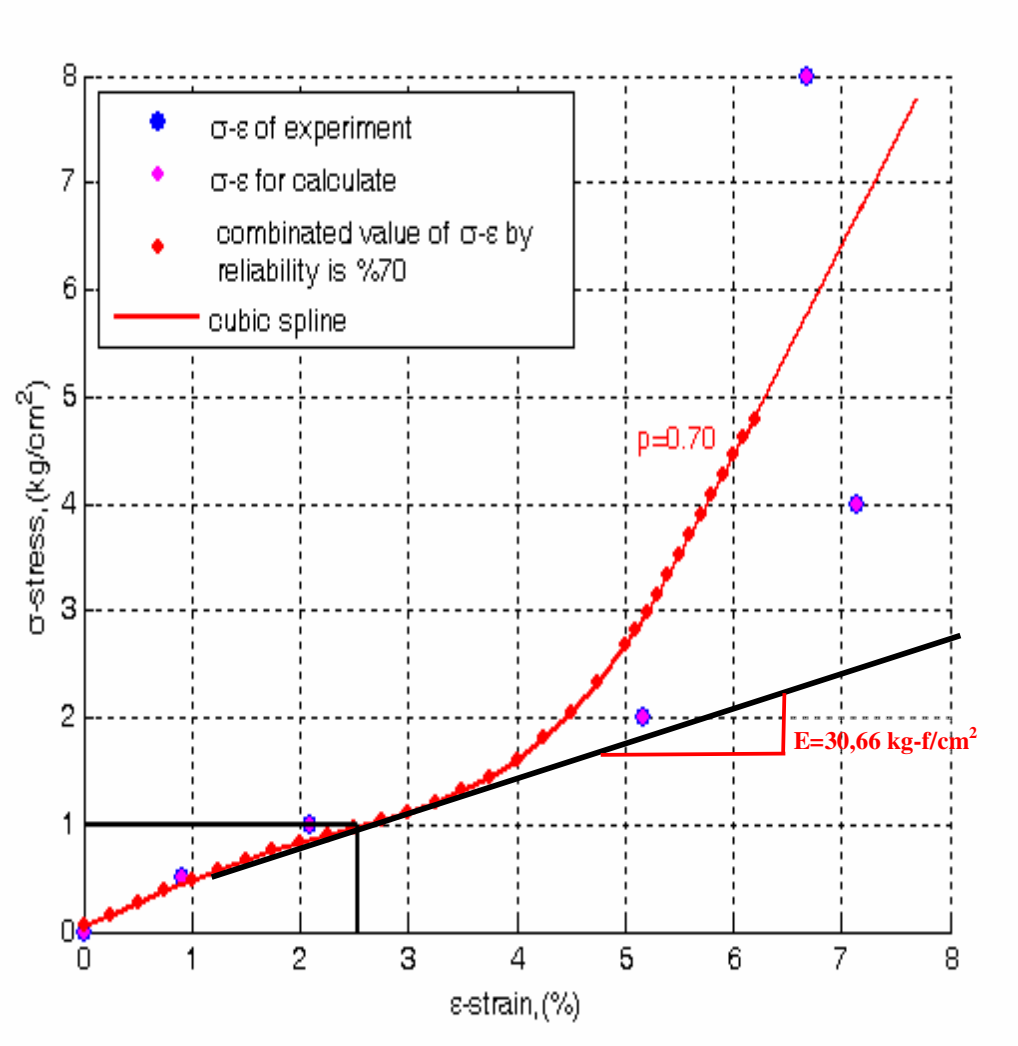

Figure B.2. 27 The oedometer test of B.19-1 is evaluated to find the E_{oed}^{ref} by the MATLAB, for translating the PLAXİS.

Table B.2. 27 The new values of evaluated odeometer test of specimen B19-1.

B.19-1		
Loading (kN/ m^2)	**Found ε (%) by Experiment**	**Found ε (%) by Matlab**
0	0.00	0.00
25	0.00	0.45
50	0.91	1.05
100	2.09	2.53
200	5.18	4.45
400	7.14	5.75
800	6.68	7.80

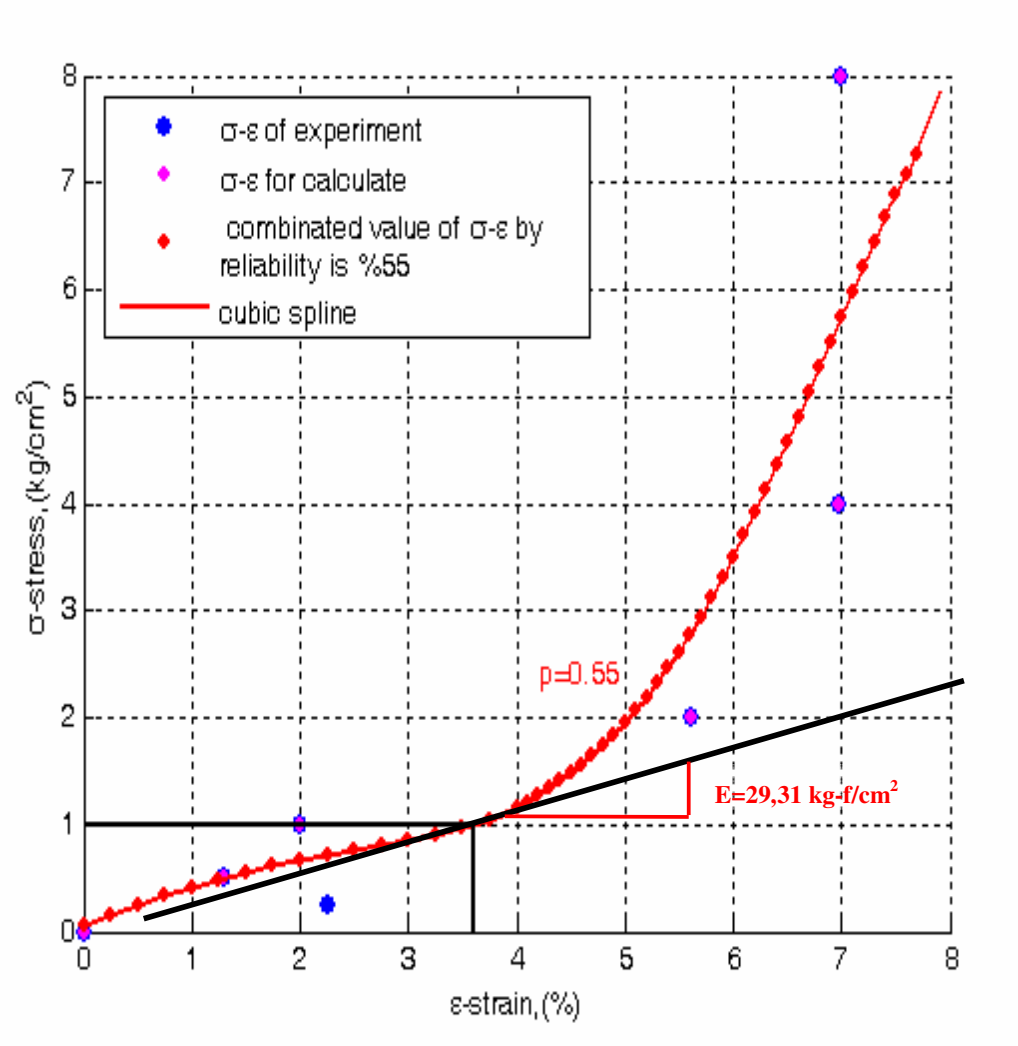

Figure B.2. 28 The oedometer test of B.20-1 is evaluated to find the E_{oed}^{ref} by the MATLAB, for translating the PLAXİS.

Table B.2. 28 The new values of evaluated odeometer test of specimen B20-1.

B.20-1		
Loading (kN/ m^2)	**Found ε (%) by Experiment**	**Found ε (%) by Matlab**
0	0.00	0.00
25	2.26	0.60
50	1.29	1.35
100	2.00	3.61
200	5.62	5.05
400	6.98	6.16
800	7.00	8.00

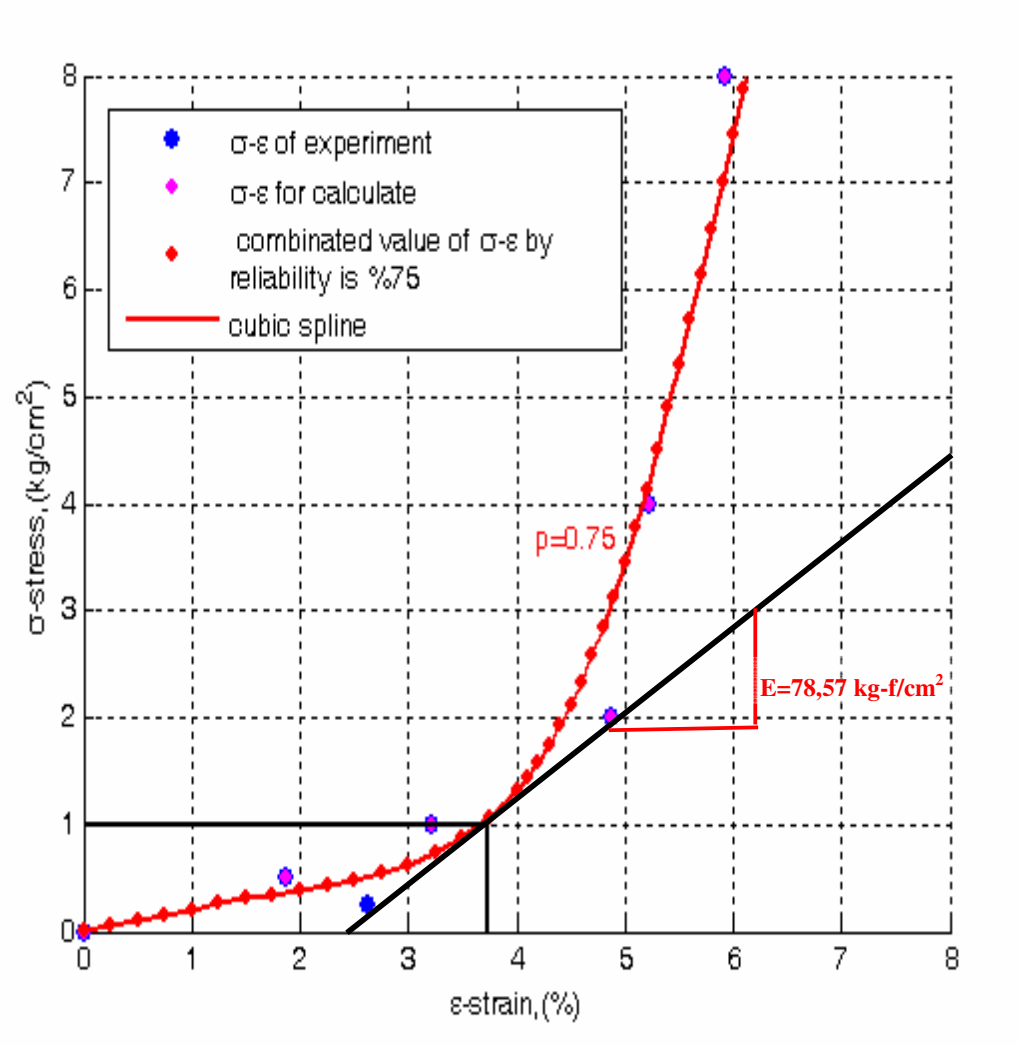

Figure B.2. 29 The oedometer test of B.20-2 is evaluated to find the E_{oed}^{ref} by the MATLAB, for translating the PLAXİS.

Table B.2. 29 The new values of evaluated odeometer test of specimen B20-2.

B.20-2		
Loading (kN/ m^2)	**Found ε (%) by Experiment**	**Found ε (%) by Matlab**
0	0.00	0.00
25	2.63	1.24
50	1.86	2.55
100	3.21	3.74
200	4.87	4.44
400	5.23	5.15
800	5.93	6.13

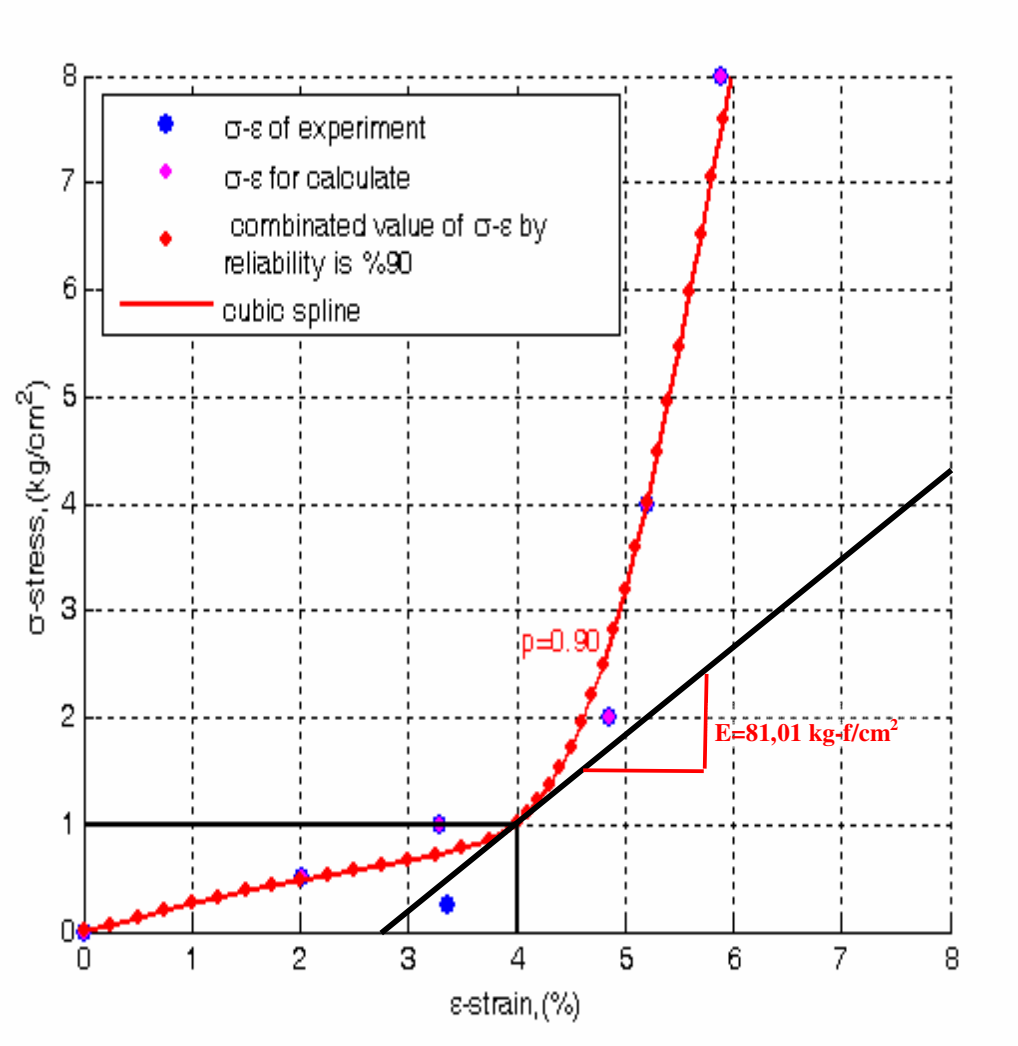

Figure B.2. 30 The oedometer test of B.21-1 is evaluated to find the E_{oed}^{ref} by the MATLAB, for translating the PLAXİS.

Table B.2. 30 The new values of evaluated odeometer test of specimen B21-1.

B.21-1		
Loading (kN/ m^2)	**Found ε (%) by Experiment**	**Found ε (%) by Matlab**
0	0.00	0.00
25	3.37	1.00
50	2.01	2.15
100	3.29	4.00
200	4.85	4.62
400	5.21	5.20
800	5.89	6.00

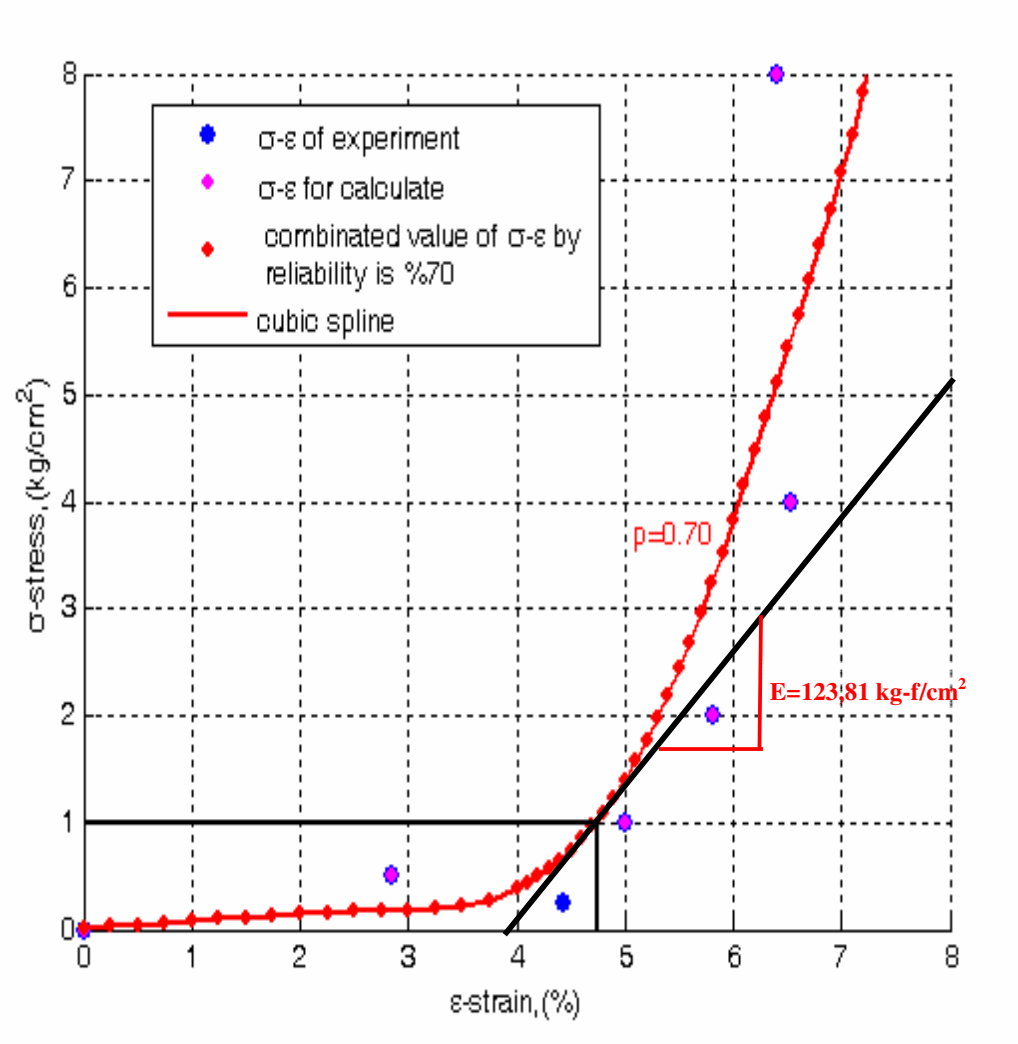

Figure B.2. 31 The oedometer test of B.23-1 is evaluated to find the E_{oed}^{ref} by the MATLAB, for translating the PLAXİS.

Table B.2. 31 The new values of evaluated odeometer test of specimen B23-1.

B.23-1		
Loading (kN/m^2)	**Found ε (%) by Experiment**	**Found ε (%) by Matlab**
0	0.00	0.00
25	4.44	3.65
50	2.84	4.22
100	5.00	4.75
200	5.82	5.30
400	6.53	6.07
800	6.40	7.25

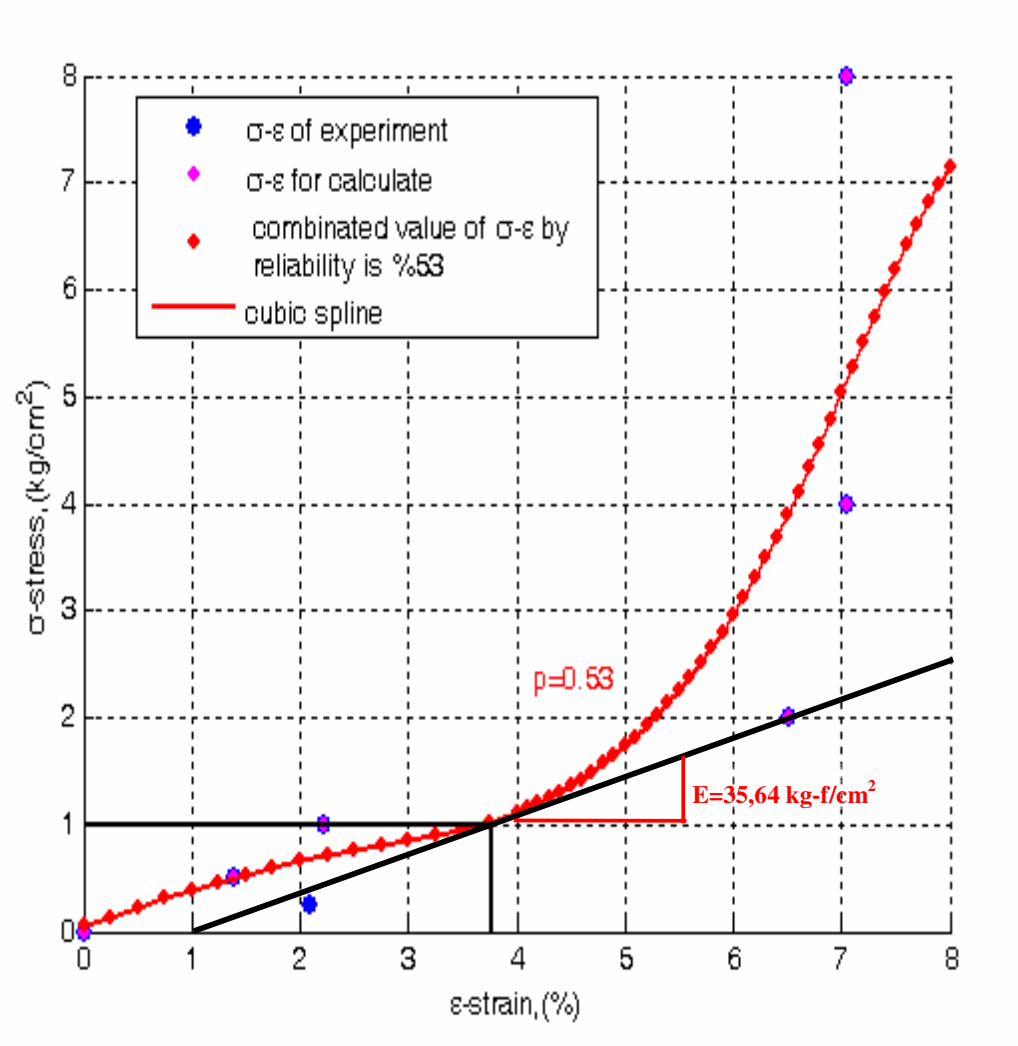

Figure B.2. 32 The oedometer test of B.24-1 is evaluated to find the E_{oed}^{ref} by the MATLAB, for translating the PLAXİS.

Table B.2. 32 The new values of evaluated odeometer test of specimen B24-1

B.24-1		
Loading (kN/ m^2)	**Found ε (%) by Experiment**	**Found ε (%) by Matlab**
0	0.00	0.00
25	2.08	0.85
50	1.39	1.45
100	2.22	3.78
200	6.52	5.30
400	7.05	6.55
800	7.05	8.50

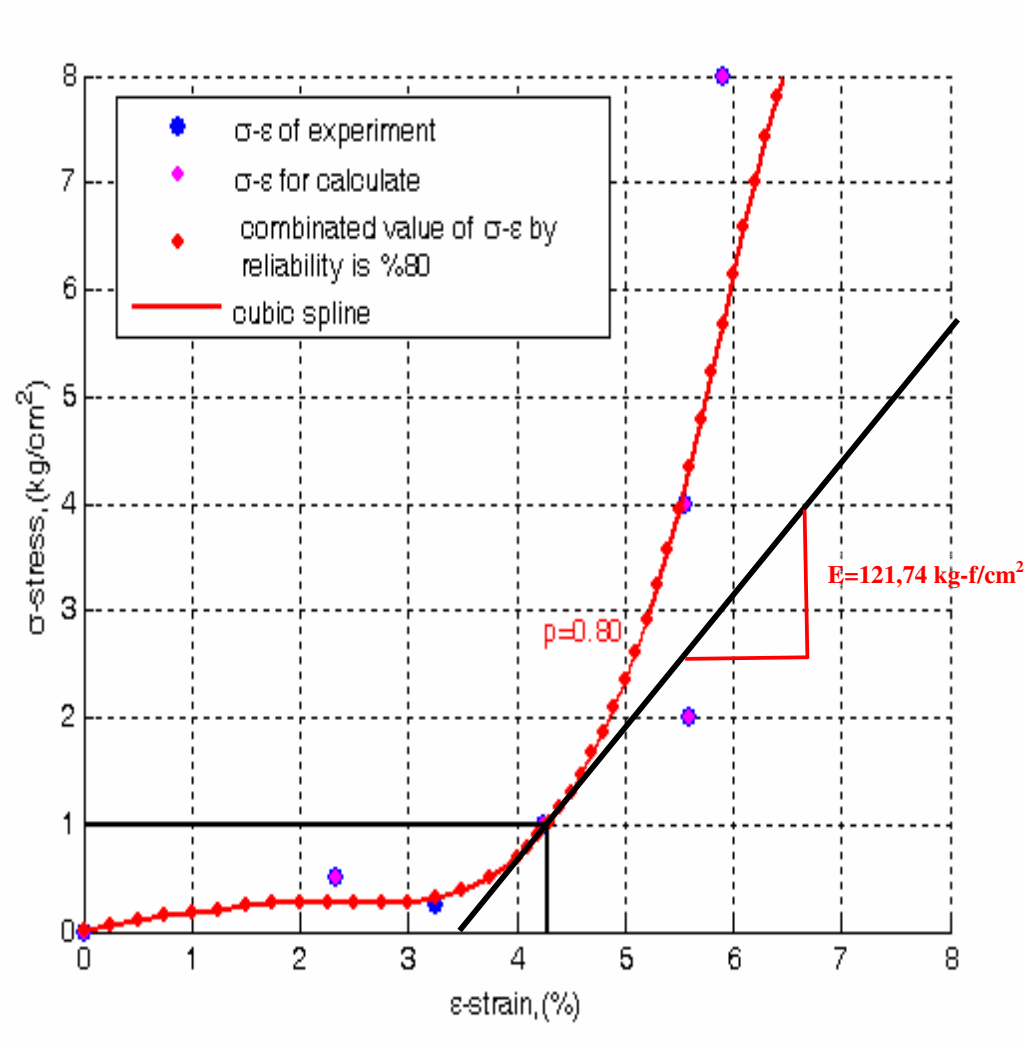

Figure B.2. 33 The oedometer test of B.25-1 is evaluated to find the E_{oed}^{ref} by the MATLAB, for translating the PLAXİS.

Table B.2. 33 The new values of evaluated odeometer test of specimen B25-1

B.25-1		
Loading (kN/ m^2)	**Found ε (%) by Experiment**	**Found ε (%) by Matlab**
0	0.00	0.00
25	3.25	1.75
50	2.33	3.75
100	4.24	4.30
200	5.60	4.84
400	5.56	5.50
800	5.92	6.45

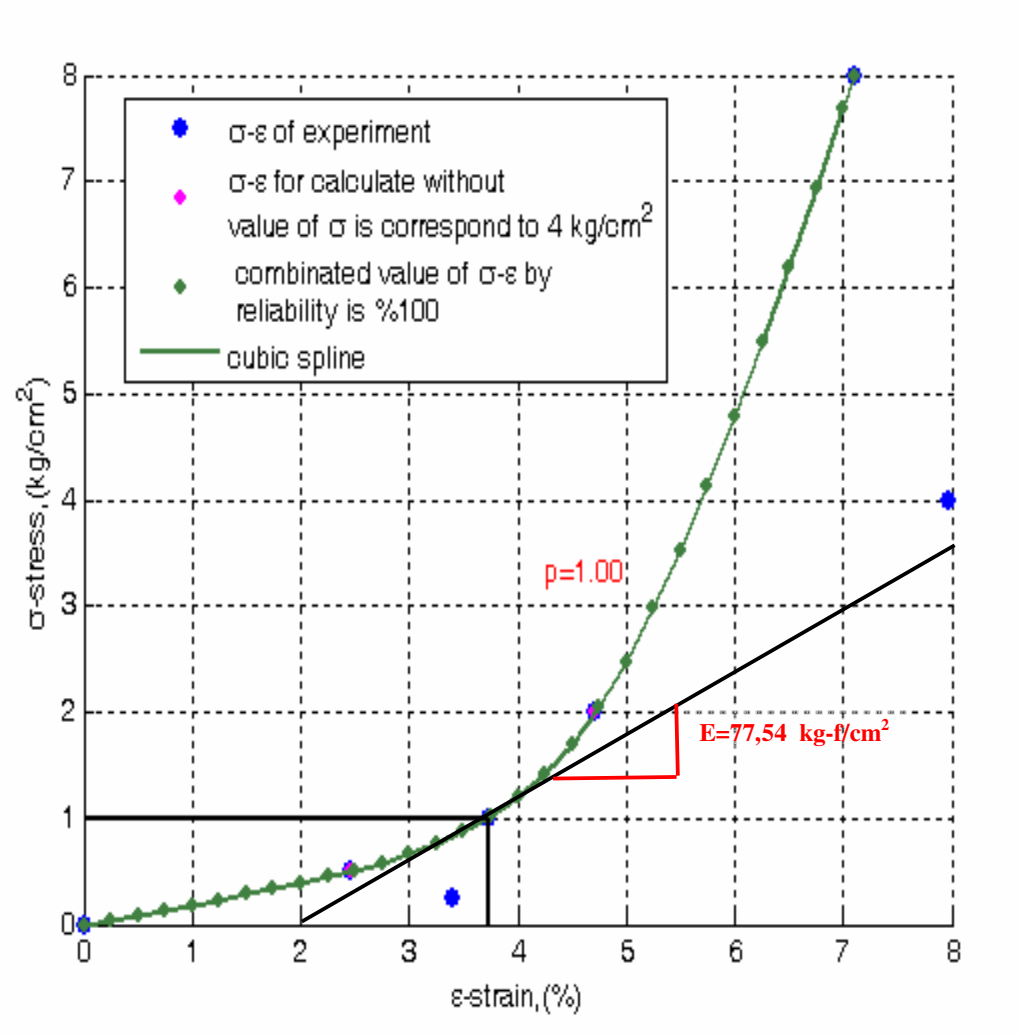

Figure B.2. 34 The oedometer test of B.26-1 is evaluated to find the E_{oed}^{ref} by the MATLAB, for translating the PLAXİS.

Table B.2. 34 The new values of evaluated odeometer test of specimen B26-1.

B.26-1		
Loading (kN/m^2)	**Found ε (%) by Experiment**	**Found ε (%) by Matlab**
0	0.00	0.00
25	3.40	1.40
50	2.45	2.45
100	3.73	3.73
200	4.72	4.73
400	7.98	5.70
800	7.11	7.10

Table B. 3 The relation of the specimens of oedometer test is given as

	LOAD (kN/m^2)					
Specimen name	**25**	**50**	**100**	**200**	**400**	**800**
B01-1	3.684	1.105	1.337	1.611	1.895	2.137
B01-2	5.789	3.495	4.632	5.411	6.074	5.600
B02-1	3.947	1.368	1.863	2.242	2.611	3.158
B02-2	1.895	1.263	2.221	3.568	5.221	5.832
B03-1	0.000	2.842	1.368	2.495	3.242	4.211
B05-1	5.895	3.947	5.558	6.074	6.211	6.105
B07-1	4.958	3.158	4.411	5.158	5.811	6.337
B08-1	2.126	2.284	4.589	6.242	6.421	5.547
B09-1	5.400	2.842	4.095	3.663	4.558	4.863
B09-2	4.105	2.705	3.653	6.432	6.421	6.842
B10-1	3.579	2.263	3.611	4.389	5.316	5.737
B10-2	2.600	1.663	2.947	5.632	7.211	7.074
B11-1	4.000	2.211	2.811	3.695	5.368	5.600
B11-2	3.895	1.789	2.716	3.526	7.726	7.968
B12-1	4.211	3.947	4.389	6.979	7.421	3.000
B12-2	4.526	2.979	4.568	6.379	6.547	6.842
B13-1	4.116	2.305	3.947	5.316	5.737	6.158
B13-2	4.632	3.053	4.421	5.611	5.600	6.105
B14-1	3.505	2.316	4.200	5.789	5.558	5.947
B15-1	3.337	1.853	4.042	5.874	6.758	7.084
B16-1	2.158	1.316	2.221	4.968	7.232	7.368
B16-2	2.958	1.642	3.505	6.442	7.032	7.000
B17-1	2.389	1.611	3.126	6.768	8.074	7.347
B17-2	3.916	2.137	3.453	5.368	5.600	6.000
B18-1	2.000	1.421	2.663	4.526	6.579	6.653
B18-2	2.600	1.747	3.863	5.526	6.579	6.526
B19-1	0.000	0.905	2.095	5.179	7.137	6.684
B20-1	2.263	1.295	2.000	5.621	6.979	7.000
B20-2	2.632	1.863	3.211	4.874	5.232	5.926
B21-1	3.368	2.011	3.295	4.853	5.211	5.895
B23-1	4.442	2.842	5.000	5.821	6.526	6.400
B24-1	2.084	1.389	2.221	6.516	7.053	7.053
B25-1	3.253	2.326	4.242	5.600	5.558	5.916
B26-1	3.400	2.453	3.726	4.716	7.979	7.105

Table B. 4 The fitting curve of the specimens of oedometer test is given at MATLAB:

	LOAD (kN/m^2)						
Specimen name	**initial**	**25**	**50**	**100**	**200**	**400**	**800**
B01-1	0.00	0.90	1.10	1.33	1.60	1.90	2.10
B01-2	0.00	3.10	3.90	4.42	4.80	5.40	6.10
B02-1	0.00	0.86	1.37	1.86	2.24	2.61	3.16
B02-2	0.00	0.73	1.25	2.21	3.77	5.10	5.90
B03-1	0.00	0.40	0.70	1.44	2.50	3.20	4.20
B05-1	0.00	4.20	4.70	5.14	5.60	6.05	6.85
B07-1	0.00	1.80	3.20	4.47	5.20	5.80	6.30
B08-1	0.00	1.50	3.60	4.23	5.10	6.00	7.45
B09-1	0.00	2.30	2.90	3.54	4.05	4.50	5.00
B09-2	0.00	1.27	2.73	4.76	5.60	6.30	7.40
B10-1	0.00	1.50	2.76	4.52	5.45	6.35	7.60
B10-2	0.00	0.80	1.60	3.77	5.21	6.30	8.05
B11-1	0.00	1.70	2.23	2.85	3.70	4.75	6.20
B11-2	0.00	0.98	1.60	2.50	3.95	6.40	9.10
B12-1	0.00	1.90	3.70	5.51	6.30	7.05	8.20
B12-2	0.00	2.95	3.80	4.57	5.50	6.40	7.75
B13-1	0.00	1.80	3.50	4.25	4.85	5.55	6.50
B13-2	0.00	3.25	3.95	4.46	5.00	5.60	6.45
B14-1	0.00	1.15	2.25	4.53	5.20	5.67	6.20
B15-1	0.00	0.95	1.90	4.03	6.05	6.66	7.13
B16-1	0.00	0.52	1.25	2.75	4.80	6.33	8.10
B16-2	0.00	0.80	1.85	4.40	5.65	6.58	7.82
B17-1	0.00	0.85	1.65	3.28	5.13	6.80	8.20
B17-2	0.00	1.26	2.85	4.03	4.77	5.47	6.38
B18-1	0.00	0.75	1.40	2.68	4.60	6.00	7.10
B18-2	0.00	0.90	1.87	4.30	5.30	6.00	7.10
B19-1	0.00	0.45	1.05	2.53	4.45	5.75	7.80
B20-1	0.00	0.60	1.35	3.61	5.05	6.16	8.00
B20-2	0.00	1.24	2.55	3.74	4.44	5.15	6.13
B21-1	0.00	1.00	2.15	4.00	4.62	5.20	6.00
B23-1	0.00	3.65	4.22	4.75	5.30	6.07	7.25
B24-1	0.00	0.85	1.45	3.78	5.30	6,55	8,5
B25-1	0.00	1.75	3.75	4.30	4,84	5.50	6,45
B26-1	0.00	1.40	2.45	3.73	4.73	5,7	7.10

Appendix C: The correlation between φ' and *Ip* for normally consolidated (including marine) clays. (Bowles,1997, pp.108)

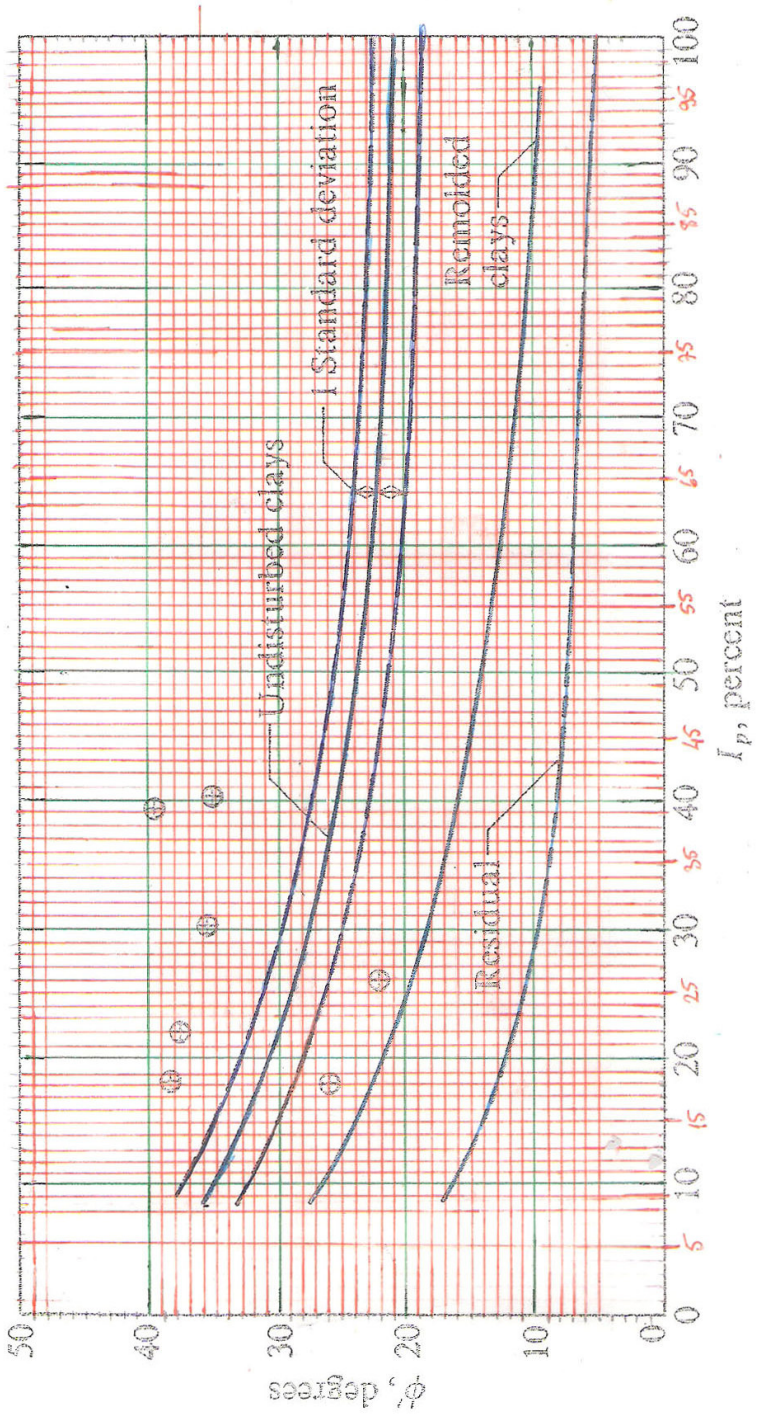

Figure C. 1 The relation between φ' and *Ip*

Appendix D: The Classification of the soil specimens due to E_{oed}^{ref}

Table D. 1 the soil properties of the specimens

Specimen name	E_eod (kN/m³)	class	IP	e_0	φ	γ nat (kN/m³)	γ dry (kN/m³)	
B02-2	4874	OH	32	1.29	27	17.63	12.33	
B10-2	2541	CH	41	1.5	25.1	16.74	10.66	
B14-1	4588	OH	36	1.45	26.1	16.82	10.70	very
B15-1	2479	OH	40	1.67	25.3	16.31	9.66	
B16-1	3471	OH	33	1.36	26.8	17.11	11.11	soft
B16-2	3883	CL	17	1.12	32	16.45	11.82	
B17-1	3042	CH	44	1.53	24.8	16.29	10.05	clay
B18-1	4017	OH	35	1.42	26.3	16.96	10.76	
B18-2	4667	OH	33	1.52	26.8	16.52	10.48	
B19-1	3066	OH	31	1.28	27.2	17.15	11.10	
B20-1	2931	OH	35	1.46	26.3	16.66	10.71	
B24-1	3564	CH	39	1.48	25.5	16.89	10.80	
B01-2	15385	OL	14	1.56	33.2	16.40	10.24	
B03-1	6709	CH	35	0.76	26.3	19.36	14.99	
B07-1	7432	CH	31	1.49	27.2	16.33	10.31	
B08-1	8514	CH	30	1.48	27.5	16.88	10.67	
B09-1	10525	CH	35	1.25	26.3	17.35	11.49	
B09-2	6164	CH	49	1.57	24	16.36	10.13	
B10-1	5570	CH	31	1.57	27.2	14.87	10.26	
B11-1	9949	OH	21	1.27	30.5	17.06	11.49	soft
B11-2	6084	OH	43	1.59	24.9	16.43	10.27	
B12-1	6803	OH	38	1.88	25.8	15.78	9.27	
B12-2	8986	OH	31	1.78	27.2	16.06	9.60	clay
B13-1	10278	OH	34	1.43	26.5	16.76	10.49	
B13-2	12672	OH	40	1.58	25.3	16.20	10.03	
B17-2	6591	OH	35	1.42	26.3	16.86	10.46	
B20-2	7857	OH	31	1.31	27.2	17.04	11.14	
B21-1	8101	OH	37	1.36	25.9	17.41	11.42	
B23-1	12381	CH	45	1.68	24.4	16.00	9.70	
B25-1	12174	CH	38	1.59	25.8	16.71	10.56	
B26-1	7754	CH	37	1.61	25.9	16.59	10.36	
B02-1	16735	SM	#	0.78		19.35	14.56	loose sand
B05-1	20714	CL	24	1.71	29.2	16.29	9.67	medium clay
B01-1	26250	SM	#	0.76		19.05	14.83	dense sand

Appendix E: The modelling of one-dimensional consolidation

In the general setting window, general model and general element are installed plain strain and 6-node, respectively, then geometry dimensions and units are determined. The geometry model of one dimensional consolidation is firstly drawn a square has 1m x 1m dimension. The type of soil material is set the experiment data. boundary conditions are defined. Also, load is determined to set at the initial condition. The Finite element mesh is applied to the soil. Water level and pore pressure are established before phases are set. Various load are set at each phases. The loads are stepped 0.25, 0.50, 1.00, 2.00, 4.00 and 8.00 kg/cm^2 at calculation window, respectively. Calculation type is selected consolidation. a node for determining load-displacement curve is selected before to beginning to the calculation stage. Especially, the node is selected at the top of the soil layer because load and displacement curve is similar to the stress-strain curve at 1m x 1m dimensional soil design.

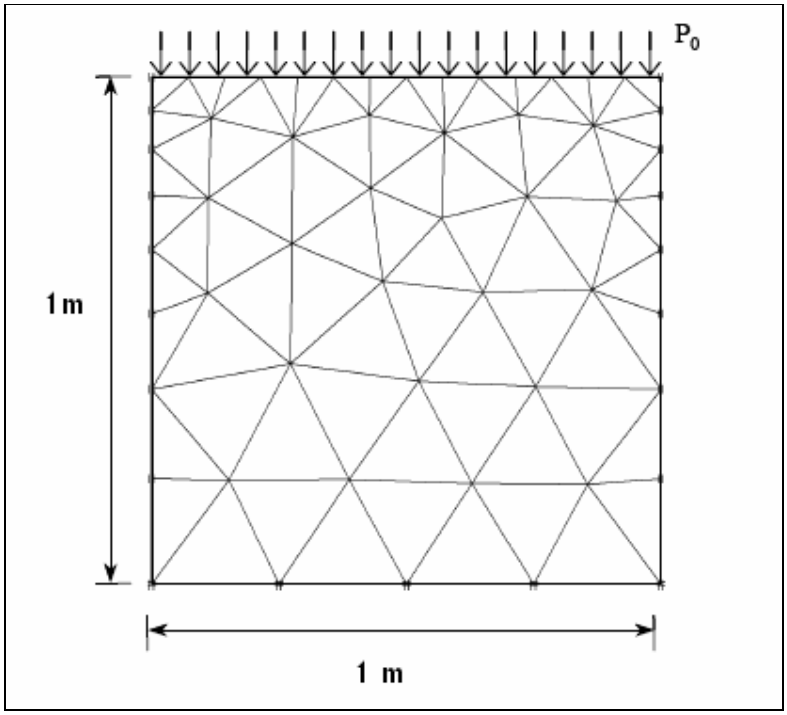

Figure E. 1 The modelling of odeometer by PLAXIS (Plaxis manual, 2002)

Appendix F: The names and properties of the derived models with using the trial and error method

Table F. 1 The derived models

Model name	**E_eod**	**E_50**	**E_ur (E_50*3)**	**φ**	**m**	***vur***	**ψ**	**c**
—	**(kN/m²)**	**(kN/m²)**	**(kN/m²)**	**(°)**	**—**	**—**	**—**	**—**
E models				□				
E5	E_oed_c	(E_oed*(1/0,5))	3*E_50	φ_c	1	0.20	0	0.005
E6	E_oed_c	(E_oed*(1/0,6))	3*E_50	φ_c	1	0.20	0	0.005
E7	E_oed_c	(E_oed*(1/0,7))	3*E_50	φ_c	1	0.20	0	0.005
E8	E_oed_c	(E_oed*(1/0,8))	3*E_50	φ_c	1	0.20	0	0.005
A models								
A1	E_oed_c	(E_oed*(1/0,8))	3*E_50	φ_c	0.8	0.20	0	0.005
A2	E_oed_c	(E_oed*(1/0,8))	3*E_50	φ_c	0.9	0.20	0	0.005
A3	E_oed_c	(E_oed*(1/0,8))	3*E_50	φ_c	0.7	0.20	0	0.005
A4	E_oed_c	(E_oed*(1/0,8))	3*E_50	φ_c	1	0.20	0	0.005
A5	E_oed_c	(E_oed*(1/0,8))	3*E_50	φ_c	1	0.15	0	0.005

The specimens are evaluated with different relationship through variables by decreasing sort due to E_{oed}^{ref} at the following page;

Table F. 2 Model name: E5

Specimen name	E_50 (Eoed*(1/0,5))	E_eod	E_ur (E_50*3)	φ	m	v_{ur}	ψ	c
—	(kN/m²)	(kN/m²)	(kN/m²)	(°)	—	—	—	(kN/m²)
B15-1	4959	2479	14876	25.3	1	0.2	0	0.005
B10-2	5082	2541	15246	25.1	1	0.2	0	0.005
B20-1	5862	2931	17586	26.3	1	0.2	0	0.005
B17-1	6083	3042	18250	24.8	1	0.2	0	0.005
B19-1	6132	3066	18396	27.2	1	0.2	0	0.005
B16-1	6942	3471	20826	26.8	1	0.2	0	0.005
B24-1	7129	3564	21386	25.5	1	0.2	0	0.005
B16-2	7766	3883	23298	32	1	0.2	0	0.005
B18-1	8033	4017	24100	26.3	1	0.2	0	0.005
B14-1	9176	4588	27529	26.1	1	0.2	0	0.005
B18-2	9333	4667	28000	26.8	1	0.2	0	0.005
B02-2	9748	4874	29244	27	1	0.2	0	0.005
B10-1	11139	5570	33418	27.2	1	0.2	0	0.005
B11-2	12168	6084	36503	24.9	1	0.2	0	0.005
B09-2	12329	6164	36986	24	1	0.2	0	0.005
B17-2	13182	6591	39545	26.3	1	0.2	0	0.005
B03-1	13418	6709	40253	26.3	1	0.2	0	0.005
B12-1	13607	6803	40820	25.8	1	0.2	0	0.005
B07-1	14865	7432	44595	27.2	1	0.2	0	0.005
B26-1	15507	7754	46522	25.9	1	0.2	0	0.005
B20-2	15714	7857	47143	27.2	1	0.2	0	0.005
B21-1	16203	8101	48608	25.9	1	0.2	0	0.005
B08-1	17027	8514	51081	27.5	1	0.2	0	0.005
B12-2	17971	8986	53913	27.2	1	0.2	0	0.005
B11-1	19899	9949	59696	30.5	1	0.2	0	0.005
B13-1	20556	10278	61667	26.5	1	0.2	0	0.005
B09-1	21050	10525	63150	26.3	1	0.2	0	0.005
B25-1	24348	12174	73043	25.8	1	0.2	0	0.005
B23-1	24762	12381	74286	24.4	1	0.2	0	0.005
B13-2	25344	12672	76031	25.3	1	0.2	0	0.005
B01-2	30769	15385	92308	33.2	1	0.2	0	0.005
B02-1	33469	16735	100408	#	1	0.2	0	0.005
B05-1	41429	20714	124286	29.2	1	0.2	0	0.005
B01-1	52500	26250	157500	#	1	0.2	0	0.005

Table F. 3 Model name: E6

Specimen name	E_50 (Eoed*(1/0,6))	E_eod	E_ur (E_50*3)	φ	m	v_{ur}	ψ	c
–	(kN/m²)	(kN/m²)	(kN/m²)	(°)	–	–	–	(kN/m²)
B15-1	4132	2479	12397	25.3	1	0.2	0	0.005
B10-2	4235	2541	12705	25.1	1	0.2	0	0.005
B20-1	4885	2931	14655	26.3	1	0.2	0	0.005
B17-1	5069	3042	15208	24.8	1	0.2	0	0.005
B19-1	5110	3066	15330	27.2	1	0.2	0	0.005
B16-1	5785	3471	17355	26.8	1	0.2	0	0.005
B24-1	5941	3564	17822	25.5	1	0.2	0	0.005
B16-2	6472	3883	19415	32	1	0.2	0	0.005
B18-1	6695	4017	20084	26.3	1	0.2	0	0.005
B14-1	7647	4588	22941	26.1	1	0.2	0	0.005
B18-2	7778	4667	23333	26.8	1	0.2	0	0.005
B02-2	8123	4874	24370	27	1	0.2	0	0.005
B10-1	9283	5570	27848	27.2	1	0.2	0	0.005
B11-2	10140	6084	30420	24.9	1	0.2	0	0.005
B09-2	10274	6164	30822	24	1	0.2	0	0.005
B17-2	10985	6591	32955	26.3	1	0.2	0	0.005
B03-1	11181	6709	33544	26.3	1	0.2	0	0.005
B12-1	11339	6803	34016	25.8	1	0.2	0	0.005
B07-1	12387	7432	37162	27.2	1	0.2	0	0.005
B26-1	12923	7754	38768	25.9	1	0.2	0	0.005
B20-2	13095	7857	39286	27.2	1	0.2	0	0.005
B21-1	13502	8101	40506	25.9	1	0.2	0	0.005
B08-1	14189	8514	42568	27.5	1	0.2	0	0.005
B12-2	14976	8986	44928	27.2	1	0.2	0	0.005
B11-1	16582	9949	49747	30.5	1	0.2	0	0.005
B13-1	17130	10278	51389	26.5	1	0.2	0	0.005
B09-1	17542	10525	52625	26.3	1	0.2	0	0.005
B25-1	20290	12174	60870	25.8	1	0.2	0	0.005
B23-1	20635	12381	61905	24.4	1	0.2	0	0.005
B13-2	21120	12672	63359	25.3	1	0.2	0	0.005
B01-2	25641	15385	76923	33.2	1	0.2	0	0.005
B02-1	27891	16735	83673	#	1	0.2	0	0.005
B05-1	34524	20714	103571	29.2	1	0.2	0	0.005
B01-1	43750	26250	131250	#	1	0.2	0	0.005

Table F. 4 Model name: E7

Specimen name	E_50 (Eoed*(1/0,7))	E_eod	E_ur (E_50*3)	φ	m	v_{ur}	ψ	c
—	(kN/m²)	(kN/m²)	(kN/m²)	(°)	—	—	—	(kN/m²)
B15-1	3542	2479	10626	25.3	1	0.2	0	0.005
B10-2	3630	2541	10890	25.1	1	0.2	0	0.005
B20-1	4187	2931	12562	26.3	1	0.2	0	0.005
B17-1	4345	3042	13036	24.8	1	0.2	0	0.005
B19-1	4380	3066	13140	27.2	1	0.2	0	0.005
B16-1	4959	3471	14876	26.8	1	0.2	0	0.005
B24-1	5092	3564	15276	25.5	1	0.2	0	0.005
B16-2	5547	3883	16641	32	1	0.2	0	0.005
B18-1	5738	4017	17215	26.3	1	0.2	0	0.005
B14-1	6555	4588	19664	26.1	1	0.2	0	0.005
B18-2	6667	4667	20000	26.8	1	0.2	0	0.005
B02-2	6963	4874	20888	27	1	0.2	0	0.005
B10-1	7957	5570	23870	27.2	1	0.2	0	0.005
B11-2	8691	6084	26074	24.9	1	0.2	0	0.005
B09-2	8806	6164	26419	24	1	0.2	0	0.005
B17-2	9416	6591	28247	26.3	1	0.2	0	0.005
B03-1	9584	6709	28752	26.3	1	0.2	0	0.005
B12-1	9719	6803	29157	25.8	1	0.2	0	0.005
B07-1	10618	7432	31853	27.2	1	0.2	0	0.005
B26-1	11077	7754	33230	25.9	1	0.2	0	0.005
B20-2	11224	7857	33673	27.2	1	0.2	0	0.005
B21-1	11573	8101	34720	25.9	1	0.2	0	0.005
B08-1	12162	8514	36486	27.5	1	0.2	0	0.005
B12-2	12836	8986	38509	27.2	1	0.2	0	0.005
B11-1	14213	9949	42640	30.5	1	0.2	0	0.005
B13-1	14683	10278	44048	26.5	1	0.2	0	0.005
B09-1	15036	10525	45107	26.3	1	0.2	0	0.005
B25-1	17391	12174	52174	25.8	1	0.2	0	0.005
B23-1	17687	12381	53061	24.4	1	0.2	0	0.005
B13-2	18103	12672	54308	25.3	1	0.2	0	0.005
B01-2	21978	15385	65934	33.2	1	0.2	0	0.005
B02-1	23907	16735	71720	#	1	0.2	0	0.005
B05-1	29592	20714	88776	29.2	1	0.2	0	0.005
B01-1	37500	26250	112500	#	1	0.2	0	0.005

Table F. 5 Model name: E8

Specimen name	E_50 (Eoed*(1/0,8))	E_eod	E_ur (E_50*3)	φ	m	v_{ur}	ψ	c
–	(kN/m²)	(kN/m²)	(kN/m²)	(°)	–	–	–	–
B15-1	3099	2479	9298	25.3	1	0.2	0	0.005
B10-2	3176	2541	9529	25.1	1	0.2	0	0.005
B20-1	3664	2931	10991	26.3	1	0.2	0	0.005
B17-1	3802	3042	11406	24.8	1	0.2	0	0.005
B19-1	3833	3066	11498	27.2	1	0.2	0	0.005
B16-1	4339	3471	13017	26.8	1	0.2	0	0.005
B24-1	4455	3564	13366	25.5	1	0.2	0	0.005
B16-2	4854	3883	14561	32	1	0.2	0	0.005
B18-1	5021	4017	15063	26.3	1	0.2	0	0.005
B14-1	5735	4588	17206	26.1	1	0.2	0	0.005
B18-2	5833	4667	17500	26.8	1	0.2	0	0.005
B02-2	6092	4874	18277	27	1	0.2	0	0.005
B10-1	6962	5570	20886	27.2	1	0.2	0	0.005
B11-2	7605	6084	22815	24.9	1	0.2	0	0.005
B09-2	7705	6164	23116	24	1	0.2	0	0.005
B17-2	8239	6591	24716	26.3	1	0.2	0	0.005
B03-1	8386	6709	25158	26.3	1	0.2	0	0.005
B12-1	8504	6803	25512	25.8	1	0.2	0	0.005
B07-1	9291	7432	27872	27.2	1	0.2	0	0.005
B26-1	9692	7754	29076	25.9	1	0.2	0	0.005
B20-2	9821	7857	29464	27.2	1	0.2	0	0.005
B21-1	10127	8101	30380	25.9	1	0.2	0	0.005
B08-1	10642	8514	31926	27.5	1	0.2	0	0.005
B12-2	11232	8986	33696	27.2	1	0.2	0	0.005
B11-1	12437	9949	37310	30.5	1	0.2	0	0.005
B13-1	12847	10278	38542	26.5	1	0.2	0	0.005
B09-1	13156	10525	39469	26.3	1	0.2	0	0.005
B25-1	15217	12174	45652	25.8	1	0.2	0	0.005
B23-1	15476	12381	46429	24.4	1	0.2	0	0.005
B13-2	15840	12672	47519	25.3	1	0.2	0	0.005
B01-2	19231	15385	57692	33.2	1	0.2	0	0.005
B02-1	20918	16735	62755	#	1	0.2	0	0.005
B05-1	25893	20714	77679	29.2	1	0.2	0	0.005
B01-1	32813	26250	98438	#	1	0.2	0	0.005

Appendix G: The first approach is E model that is evaluated with trial and error method by using decreasing sort due to E_{oed}.

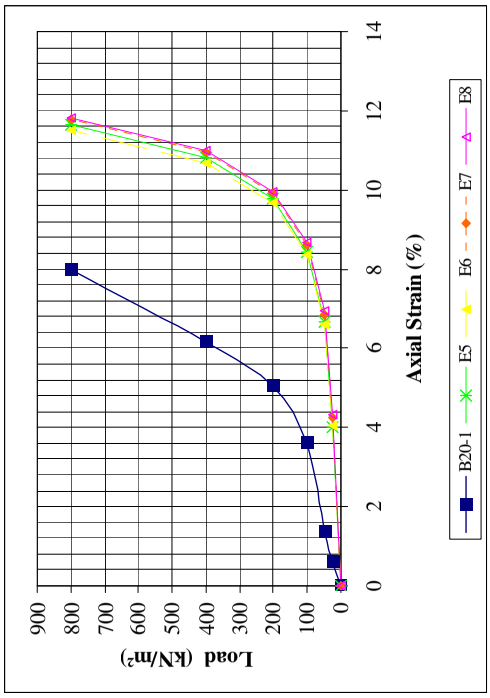

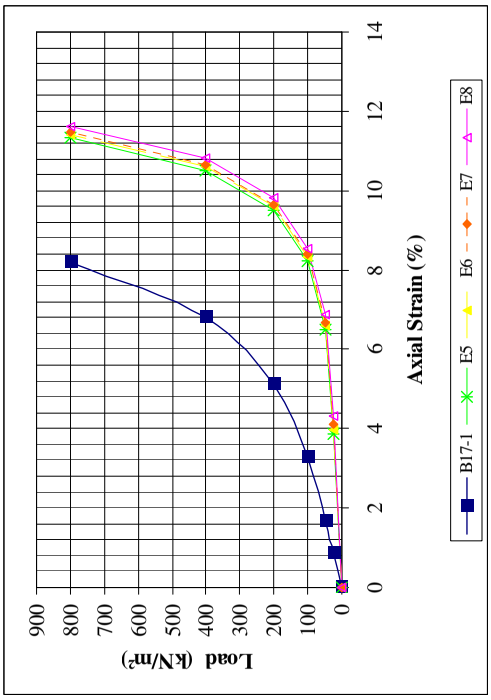

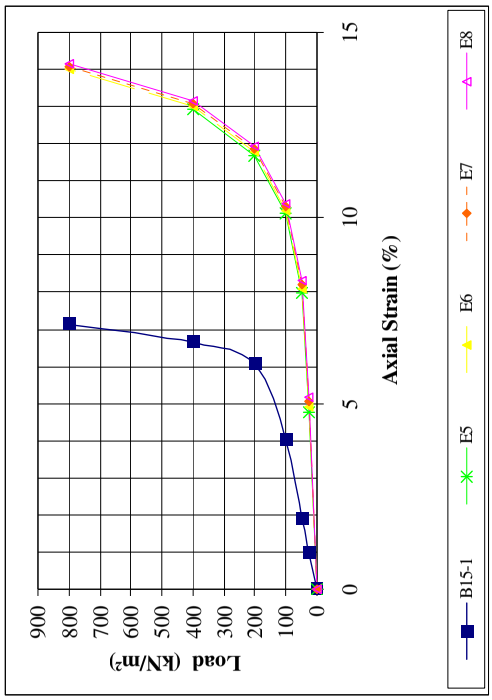

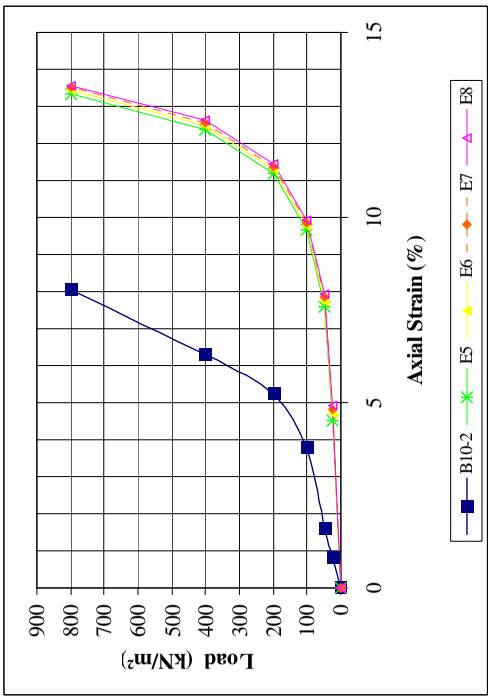

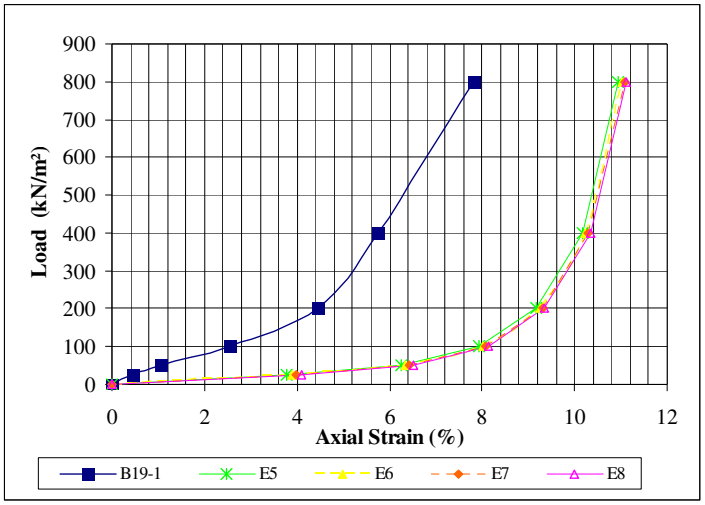
Load (kN/m²)
Axial Strain (%)
B19-1
E5
E6
E7
E8

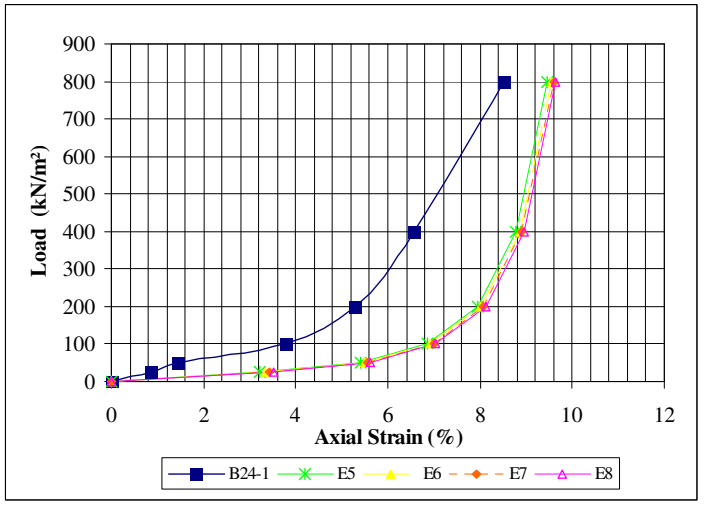
Load (kN/m²)
Axial Strain (%)
B24-1
E5
E6
E7
E8

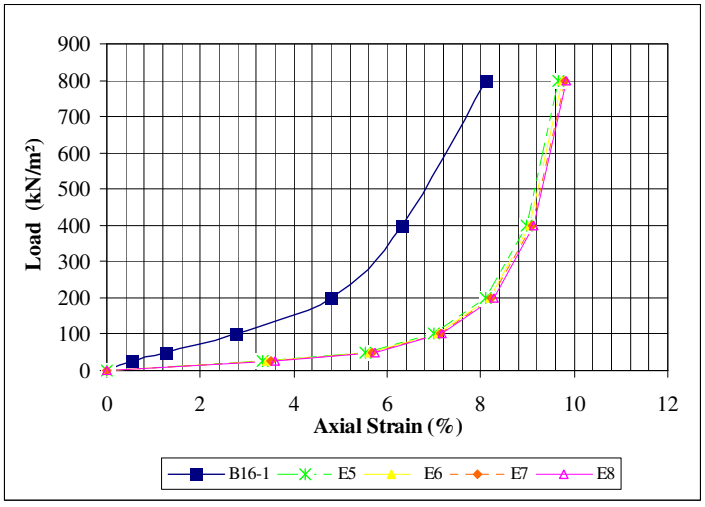
Load (kN/m²)
Axial Strain (%)
B16-1
E5
E6
E7
E8

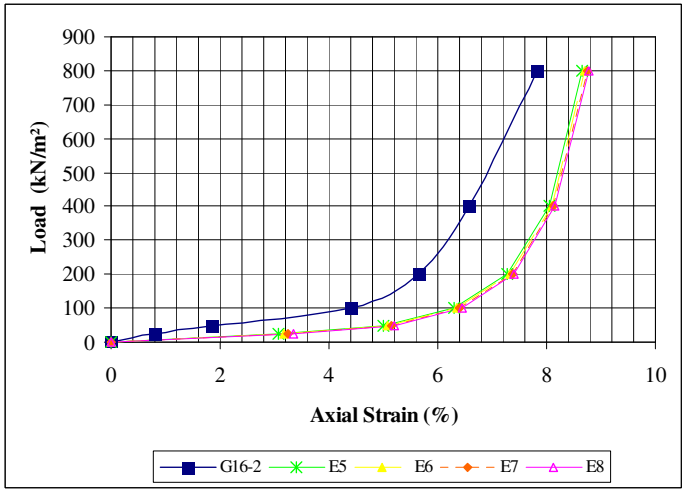
Load (kN/m²)
Axial Strain (%)
G16-2
E5
E6
E7
E8

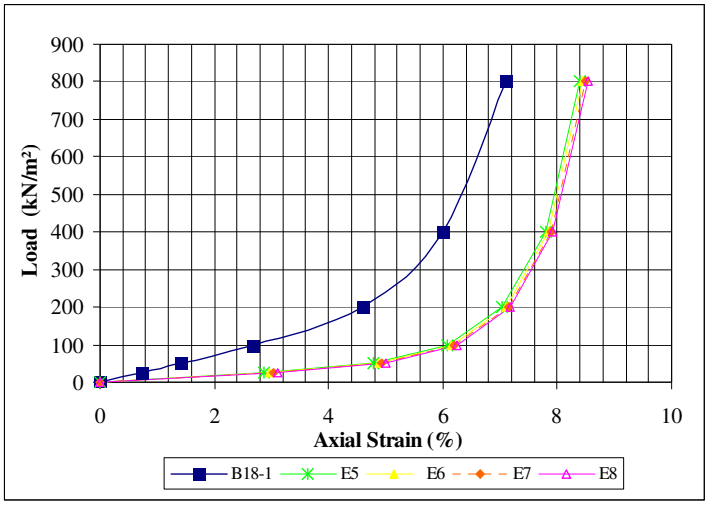
Load (kN/m²)
Axial Strain (%)
B18-1
E5
E6
E7
E8

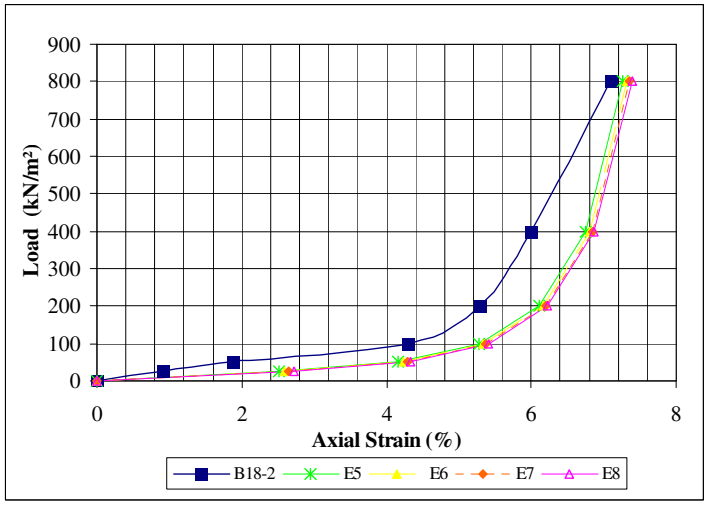
Load (kN/m²)
Axial Strain (%)
B18-2
E5
E6
E7
E8

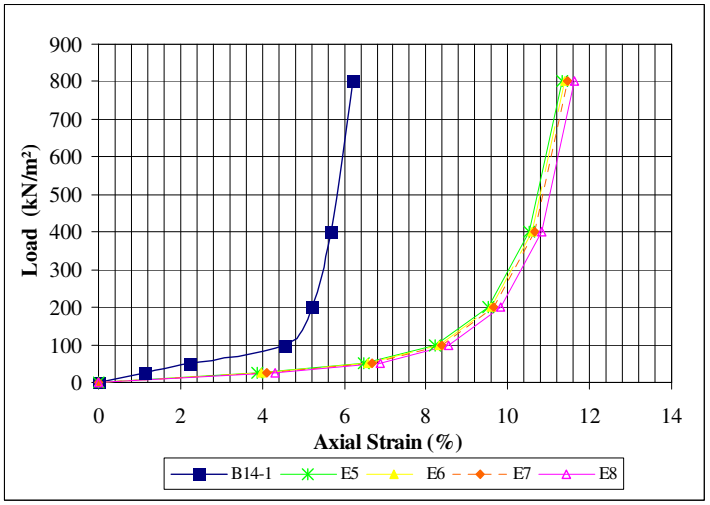
Load (kN/m²)
Axial Strain (%)
B14-1
E5
E6
E7
E8

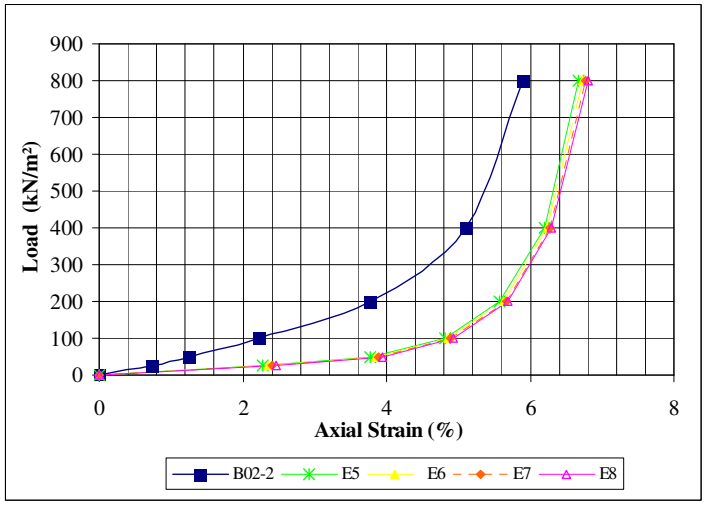
Load (kN/m²)
Axial Strain (%)
B02-2
E5
E6
E7
E8

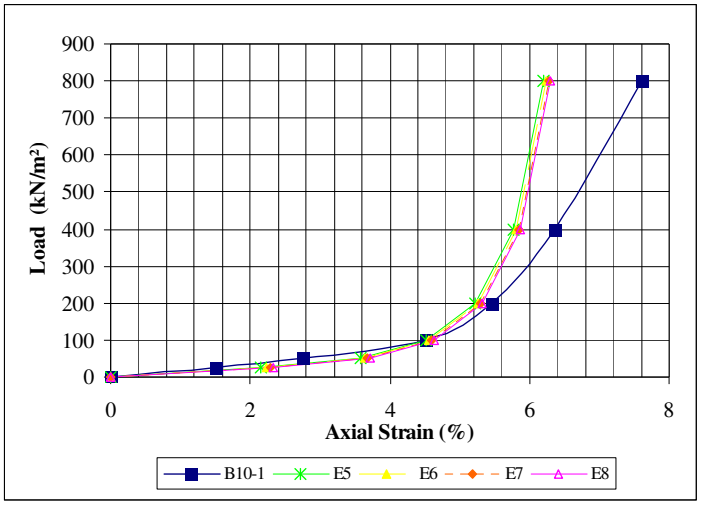
Load (kN/m²)
900
800
700
600
500
400
300
200
100
0
0
2
4
6
8
Axial Strain (%)
B10-1
E5
E6
E7
E8

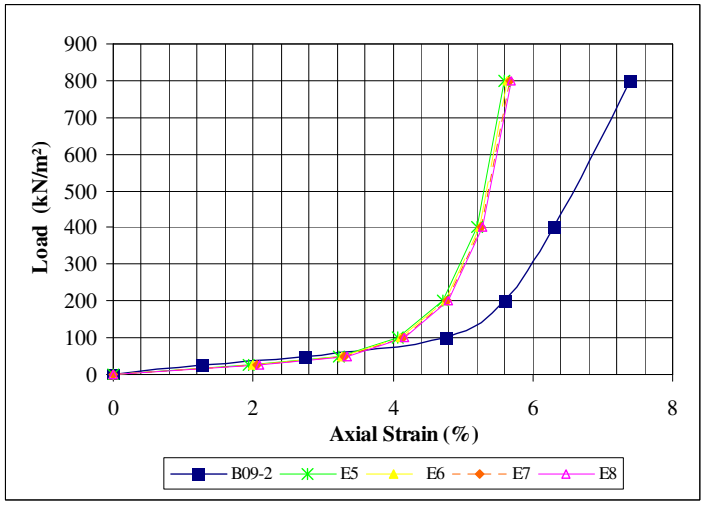
Load (kN/m²)
900
800
700
600
500
400
300
200
100
0
0
2
4
6
8
Axial Strain (%)
B09-2
E5
E6
E7
E8

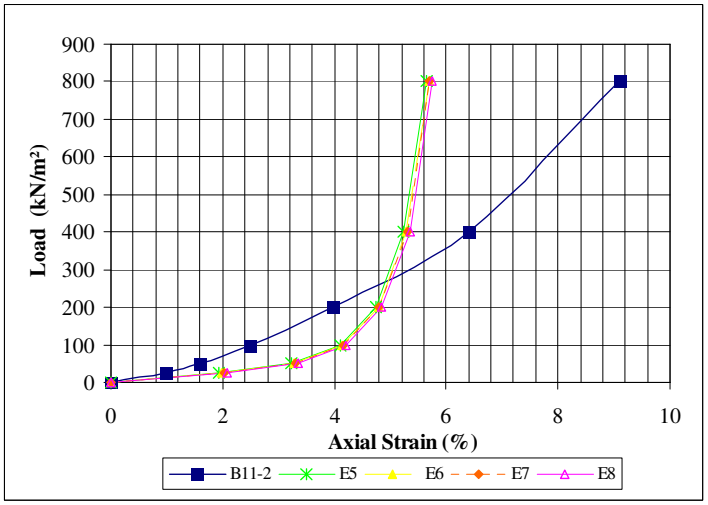
Load (kN/m²)
900
800
700
600
500
400
300
200
100
0
0
2
4
6
8
10
Axial Strain (%)
B11-2
E5
E6
E7
E8

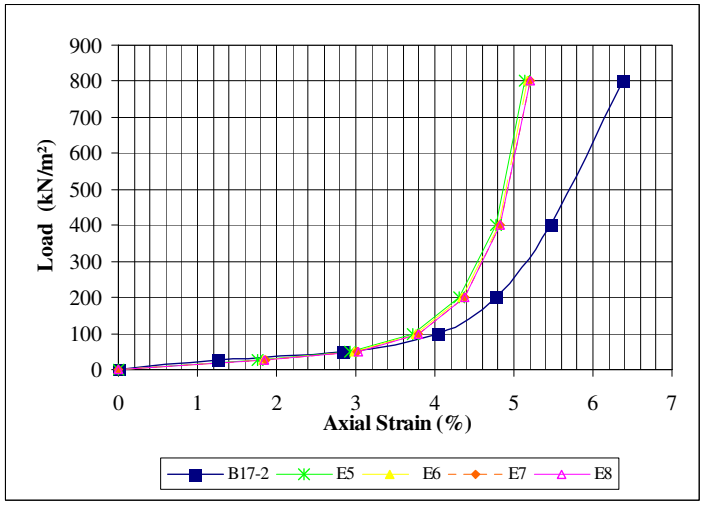
Load (kN/m²)
900
800
700
600
500
400
300
200
100
0
0
1
2
3
4
5
6
7
Axial Strain (%)
B17-2
E5
E6
E7
E8

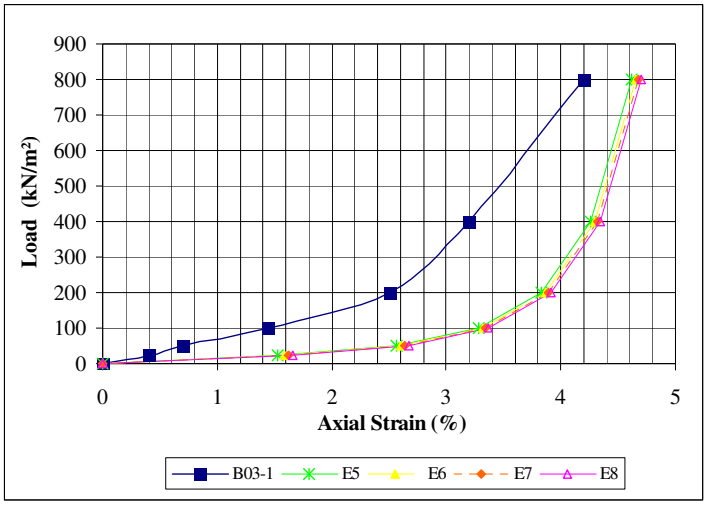
Load (kN/m²)
900
800
700
600
500
400
300
200
100
0
0
1
2
3
4
5
Axial Strain (%)
B03-1
E5
E6
E7
E8

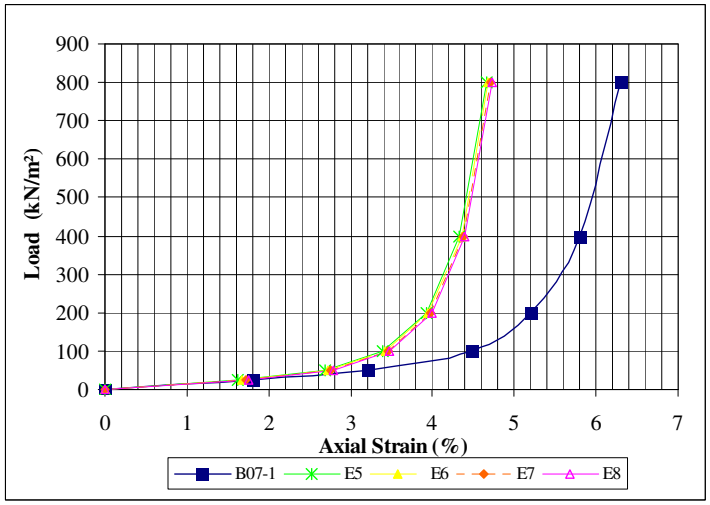
Load (kN/m²)
900
800
700
600
500
400
300
200
100
0
0
1
2
3
4
5
6
7
Axial Strain (%)
B07-1
E5
E6
E7
E8

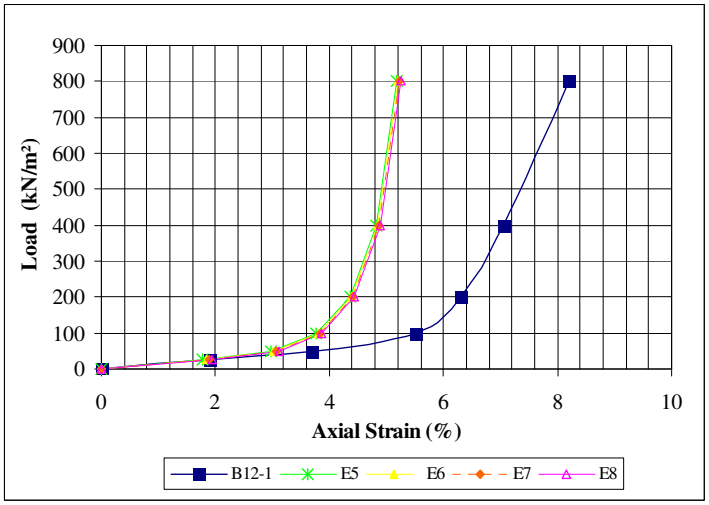
Load (kN/m²)
900
800
700
600
500
400
300
200
100
0
0
2
4
6
8
10
Axial Strain (%)
B12-1
E5
E6
E7
E8

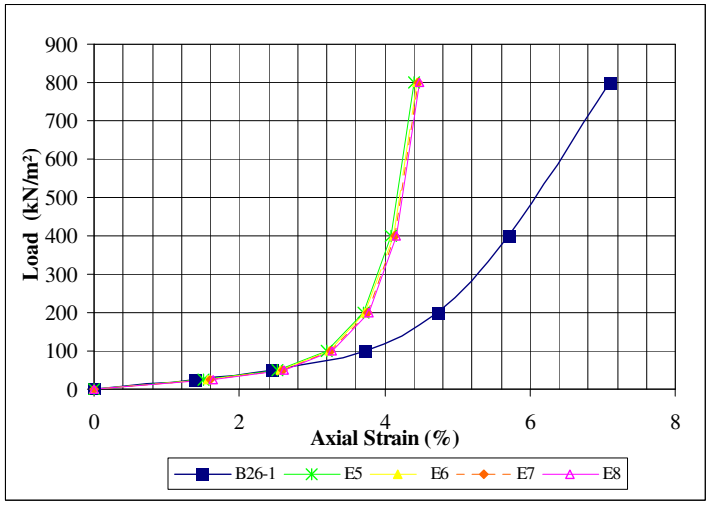
Load (kN/m²)
900
800
700
600
500
400
300
200
100
0
0
2
4
6
8
Axial Strain (%)
B26-1
E5
E6
E7
E8

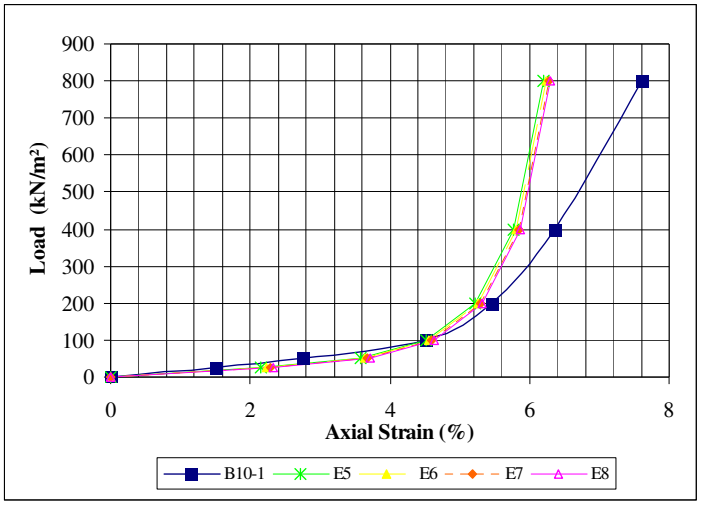
Load (kN/m²)
Axial Strain (%)
B10-1
E5
E6
E7
E8

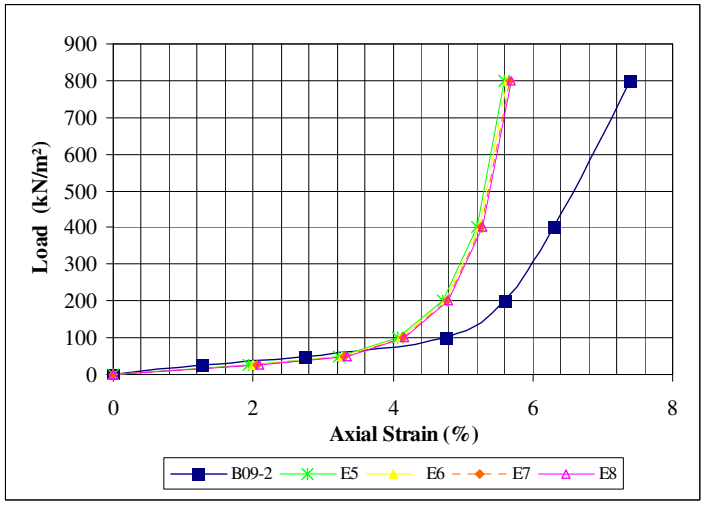
Load (kN/m²)
Axial Strain (%)
B09-2
E5
E6
E7
E8

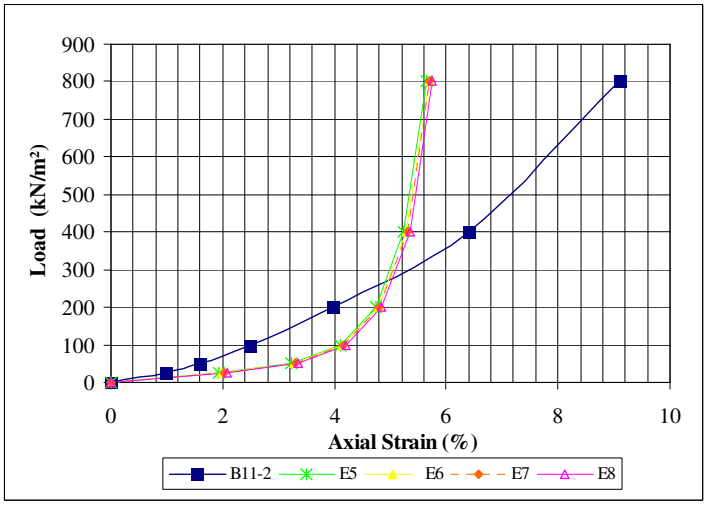
Load (kN/m²)
Axial Strain (%)
B11-2
E5
E6
E7
E8

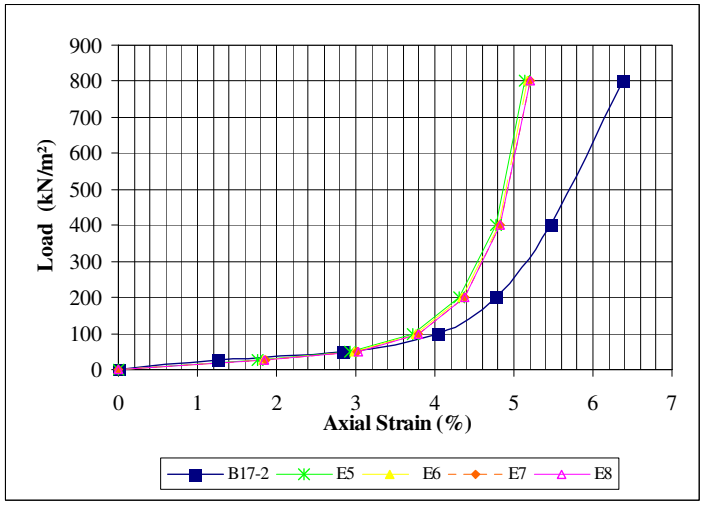
Load (kN/m²)
Axial Strain (%)
B17-2
E5
E6
E7
E8

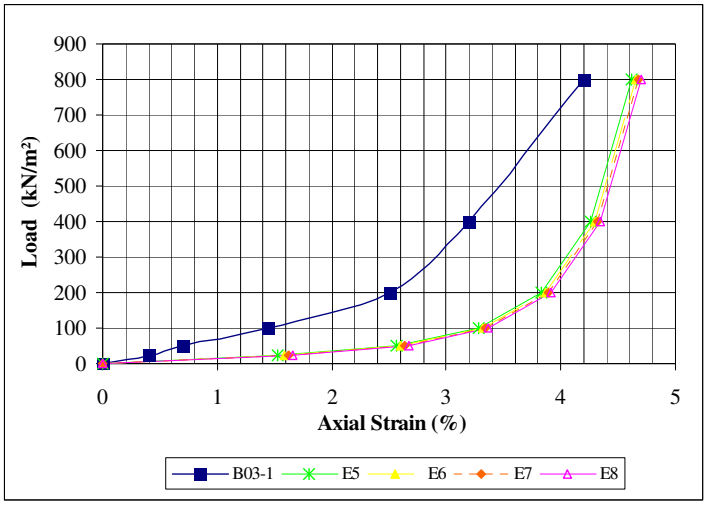
Load (kN/m²)
Axial Strain (%)
B03-1
E5
E6
E7
E8

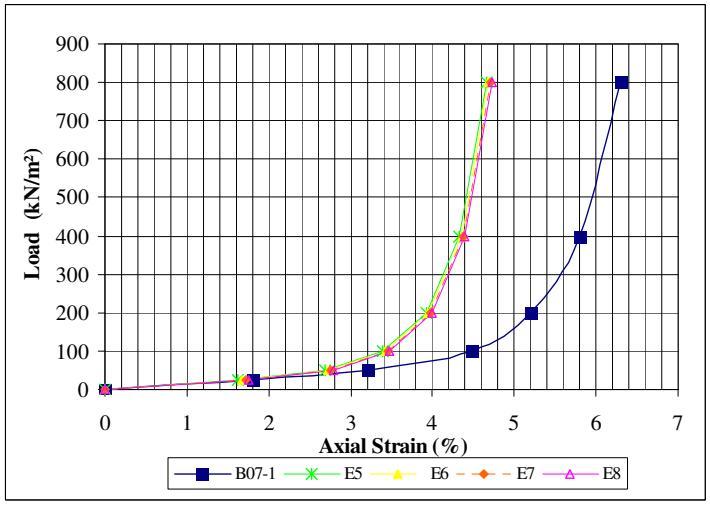
Load (kN/m²)
Axial Strain (%)
B07-1
E5
E6
E7
E8

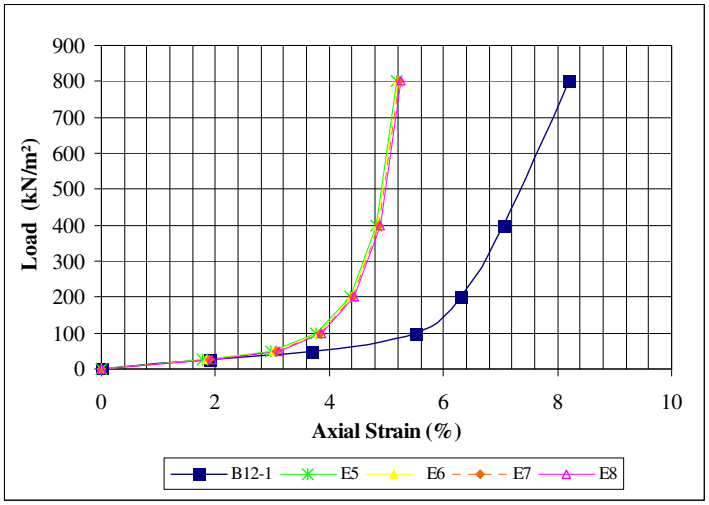
Load (kN/m²)
Axial Strain (%)
B12-1
E5
E6
E7
E8

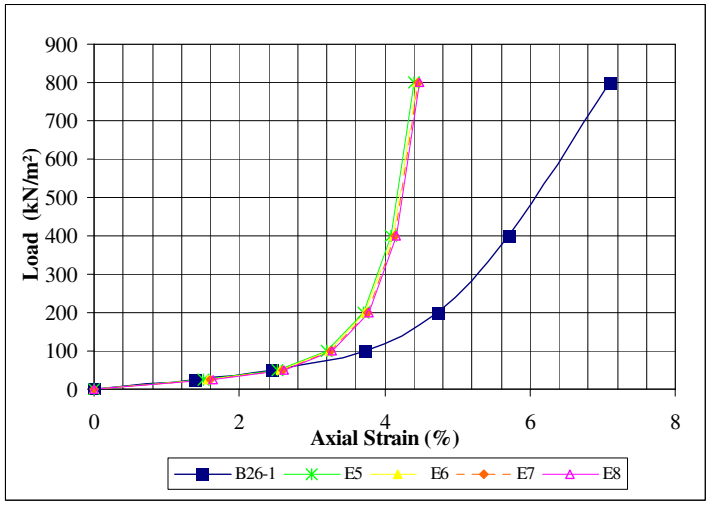
Load (kN/m²)
Axial Strain (%)
B26-1
E5
E6
E7
E8

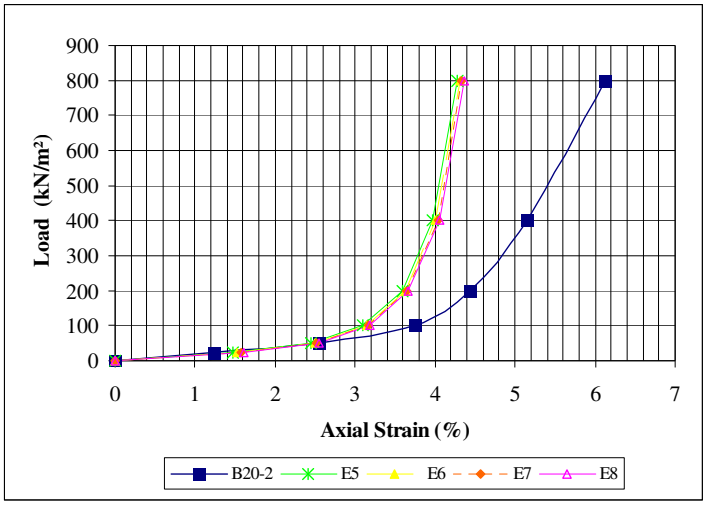
Load (kN/m²)
900
800
700
600
500
400
300
200
100
0
0 1 2 3 4 5 6 7
Axial Strain (%)
B20-2 E5 E6 E7 E8

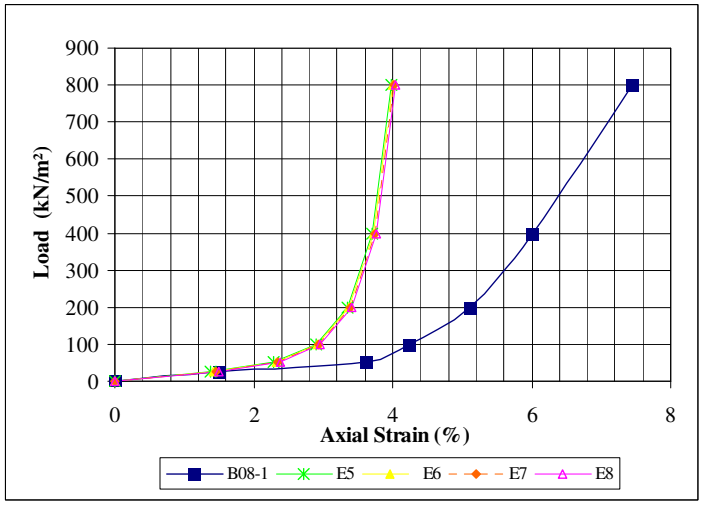
Load (kN/m²)
900
800
700
600
500
400
300
200
100
0
0 2 4 6 8
Axial Strain (%)
B08-1 E5 E6 E7 E8

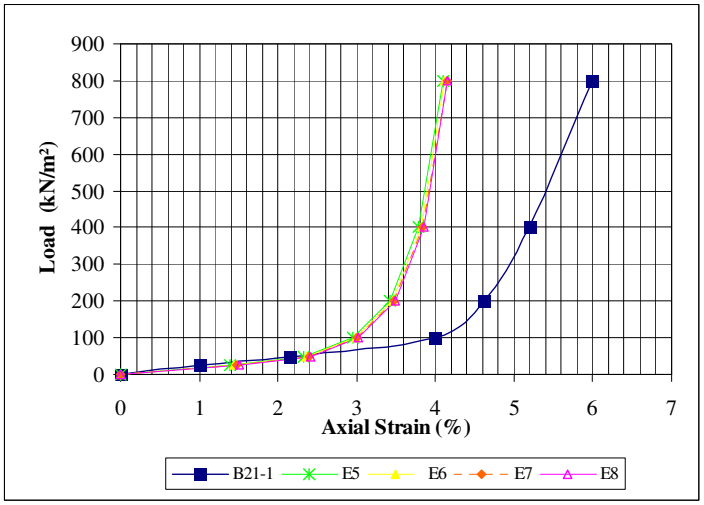
Load (kN/m²)
900
800
700
600
500
400
300
200
100
0
0 1 2 3 4 5 6 7
Axial Strain (%)
B21-1 E5 E6 E7 E8

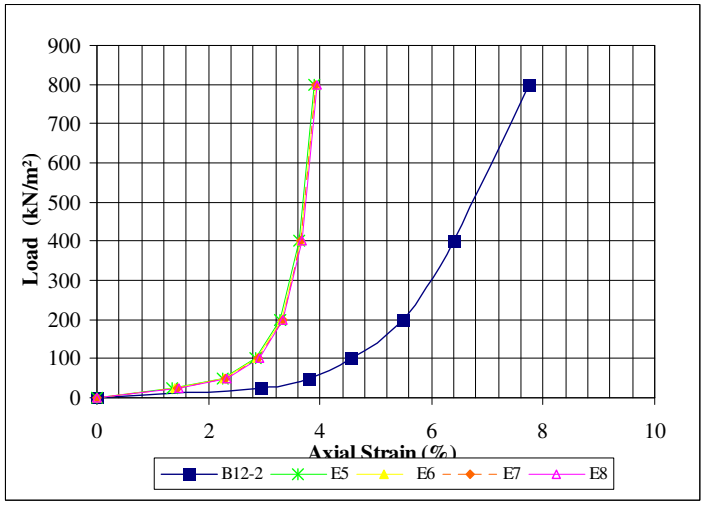
Load (kN/m²)
900
800
700
600
500
400
300
200
100
0
0 2 4 6 8 10
Axial Strain (%)
B12-2 E5 E6 E7 E8

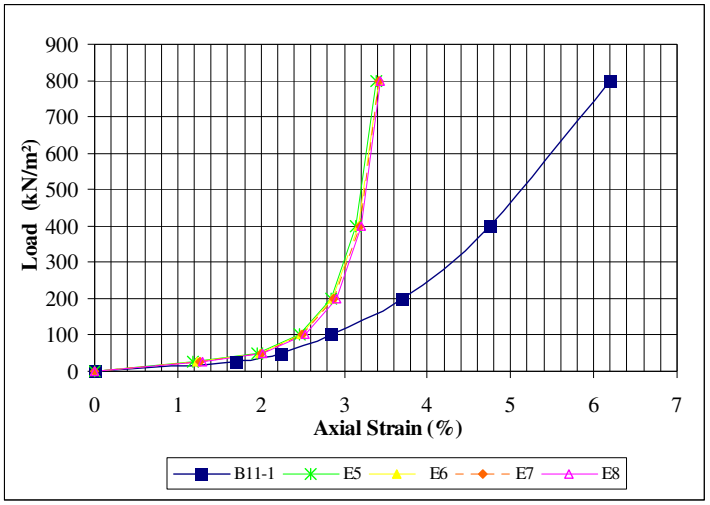
Load (kN/m²)
Axial Strain (%)
B11-1
E5
E6
E7
E8

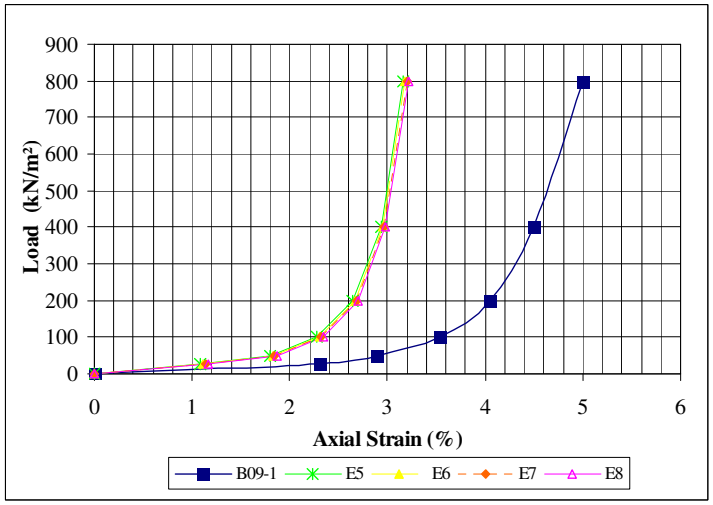
Load (kN/m²)
Axial Strain (%)
B09-1
E5
E6
E7
E8

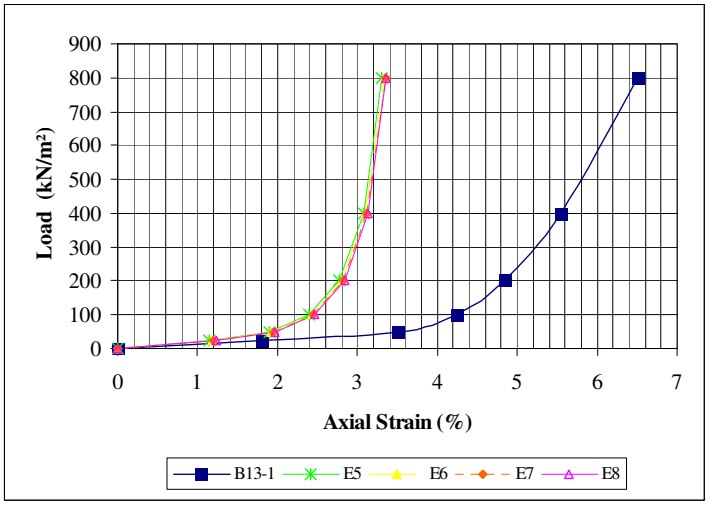
Load (kN/m²)
Axial Strain (%)
B13-1
E5
E6
E7
E8

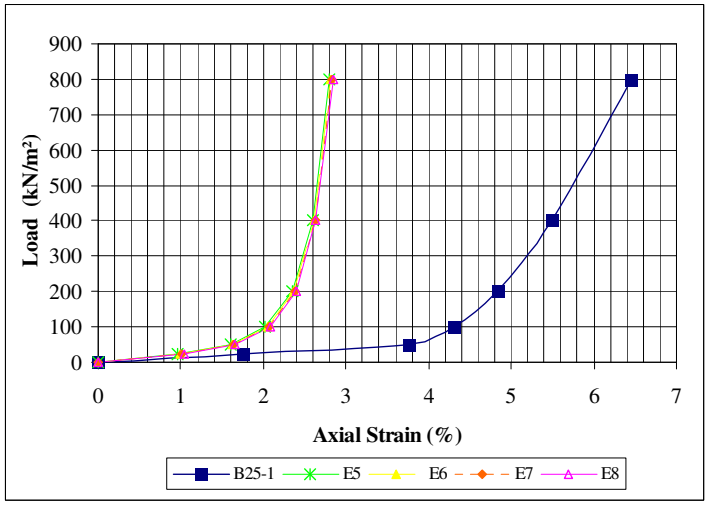
Load (kN/m²)
Axial Strain (%)
B25-1
E5
E6
E7
E8

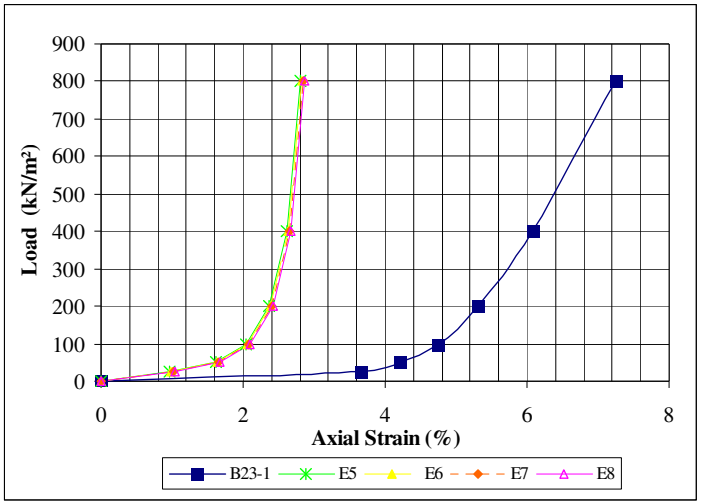
Load (kN/m²)
Axial Strain (%)
B23-1
E5
E6
E7
E8

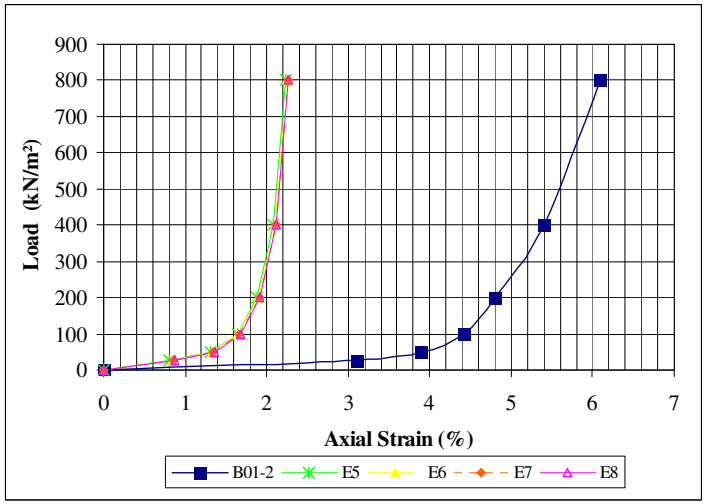
Load (kN/m²)
Axial Strain (%)
B01-2
E5
E6
E7
E8

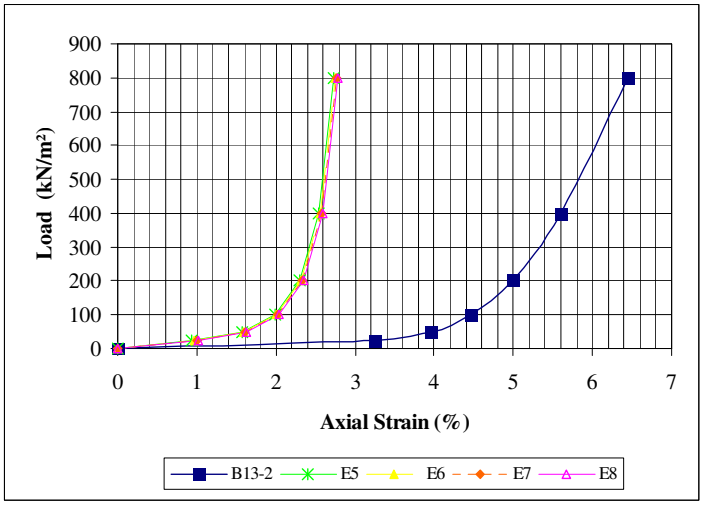
Load (kN/m²)
Axial Strain (%)
B13-2
E5
E6
E7
E8

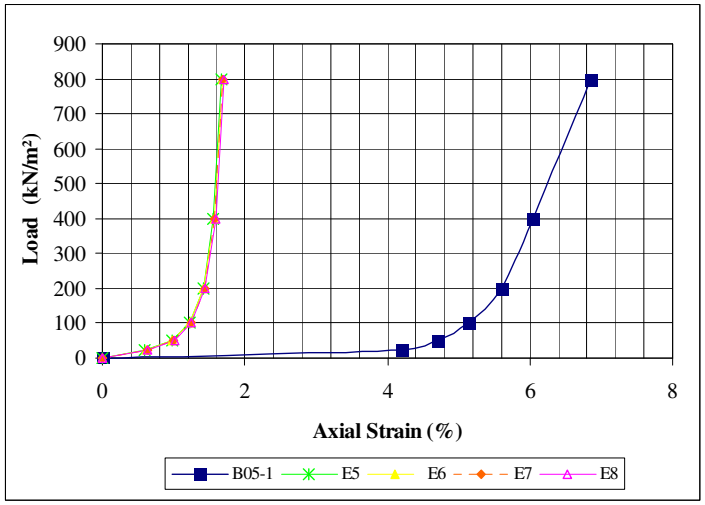
Load (kN/m²)
Axial Strain (%)
B05-1
E5
E6
E7
E8

Appendix H: The second approach is A model that is evaluated with trial and error method by using decreasing sort due to E_{oed}.

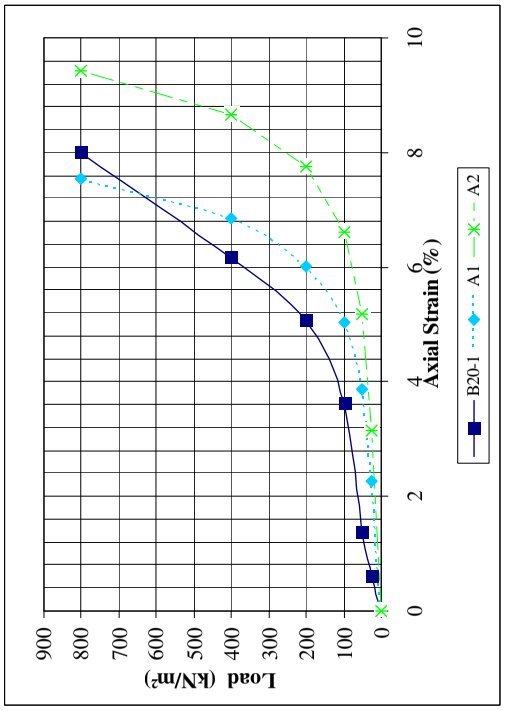

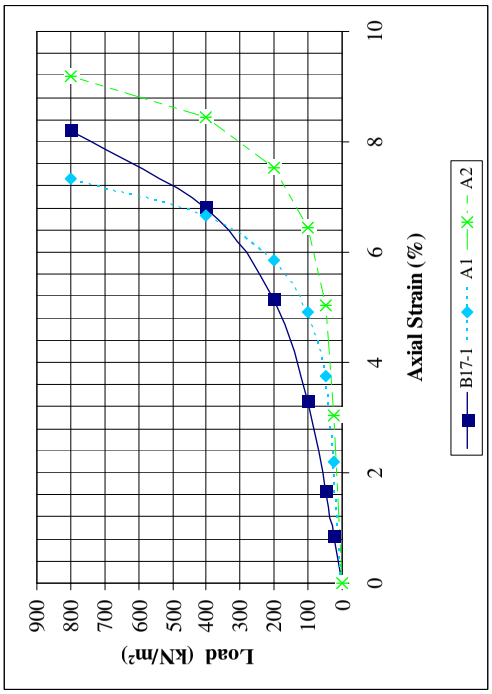

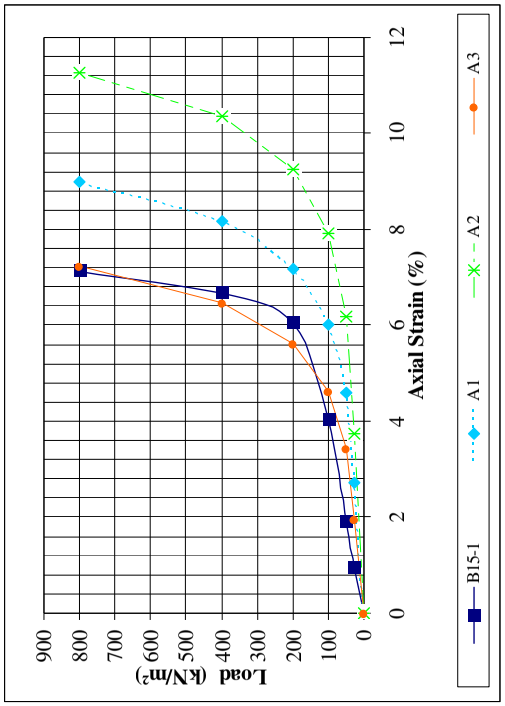

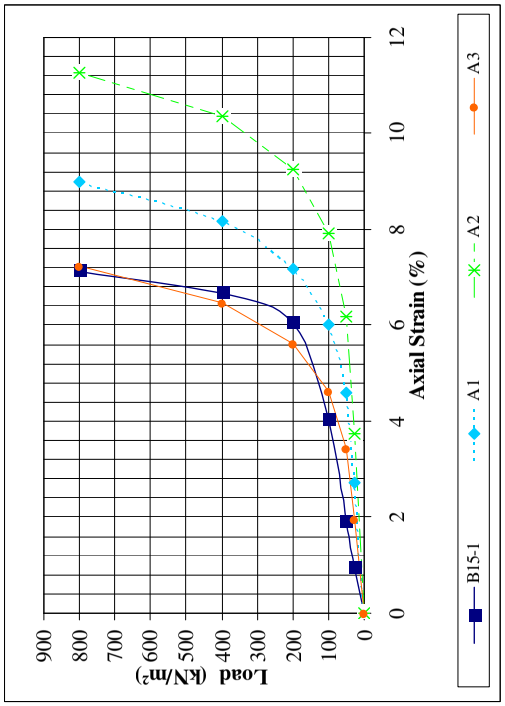

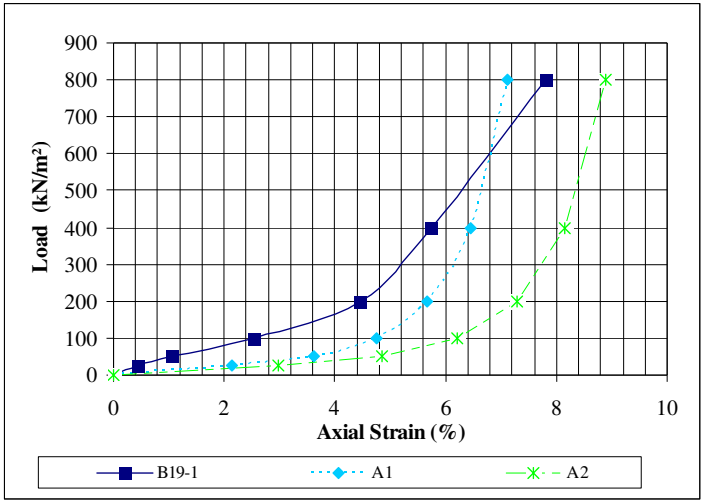
Load (kN/m²)
Axial Strain (%)
B19-1
A1
A2

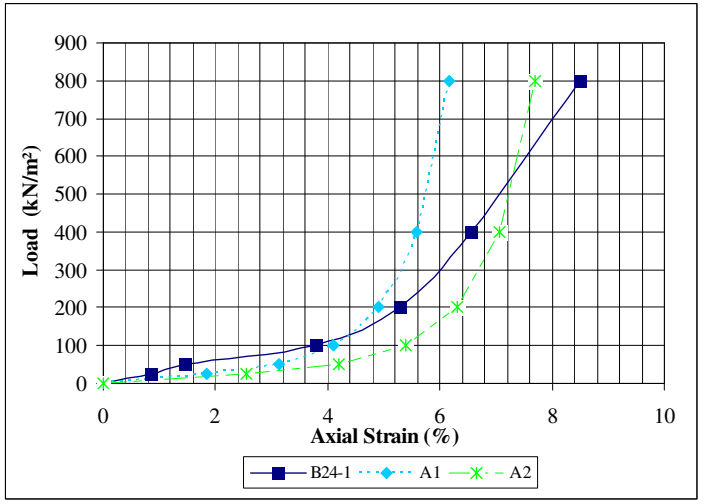
Load (kN/m²)
Axial Strain (%)
B24-1
A1
A2

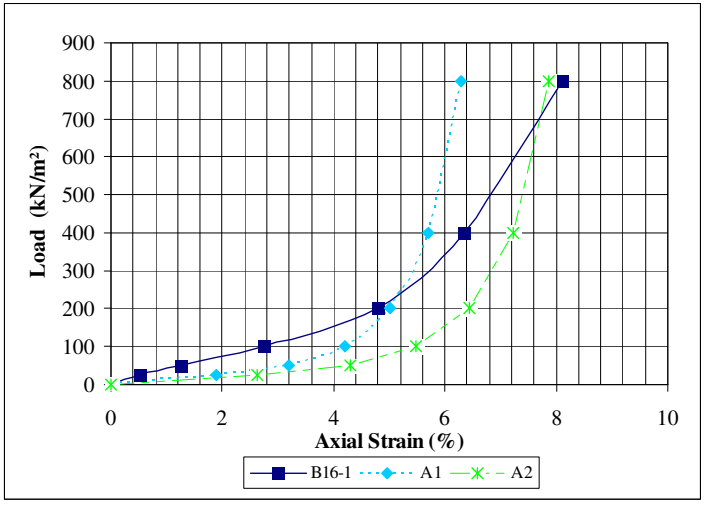
Load (kN/m²)
Axial Strain (%)
B16-1
A1
A2

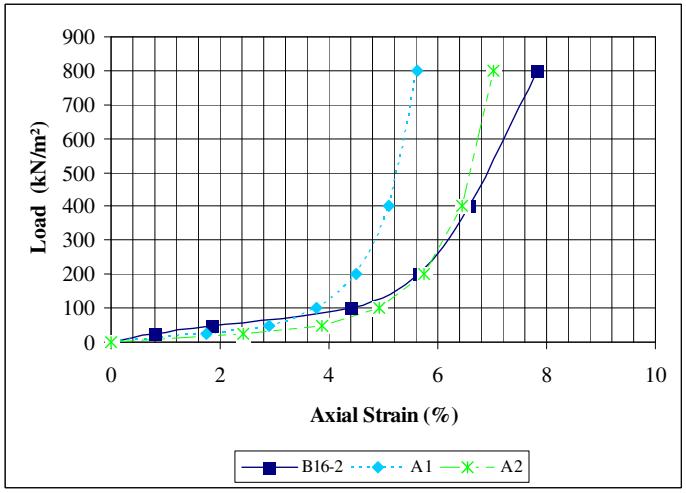
Load (kN/m²)
Axial Strain (%)
B16-2
A1
A2

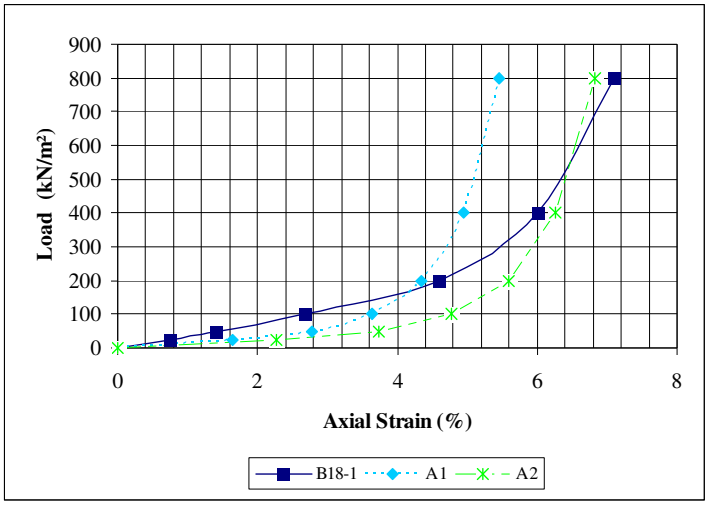
Load (kN/m²)
Axial Strain (%)
B18-1
A1
A2

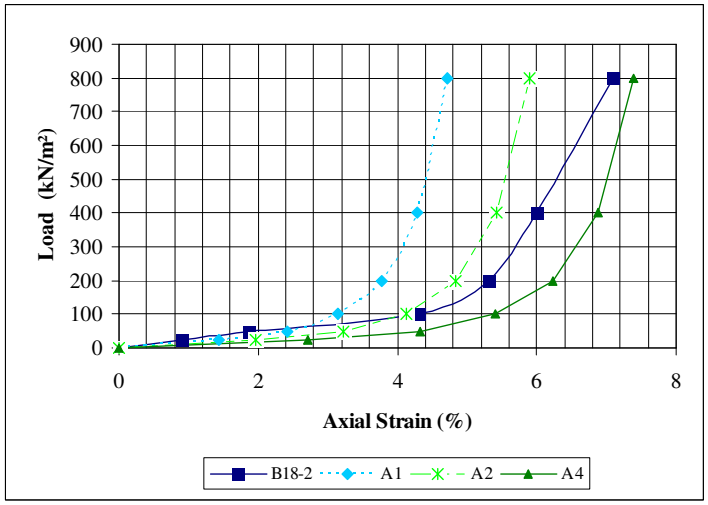
Load (kN/m²)
Axial Strain (%)
B18-2
A1
A2
A4

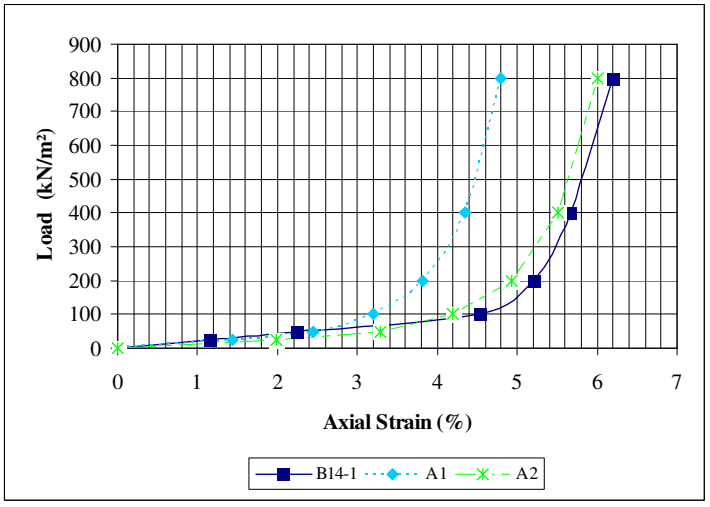
Load (kN/m²)
Axial Strain (%)
B14-1
A1
A2

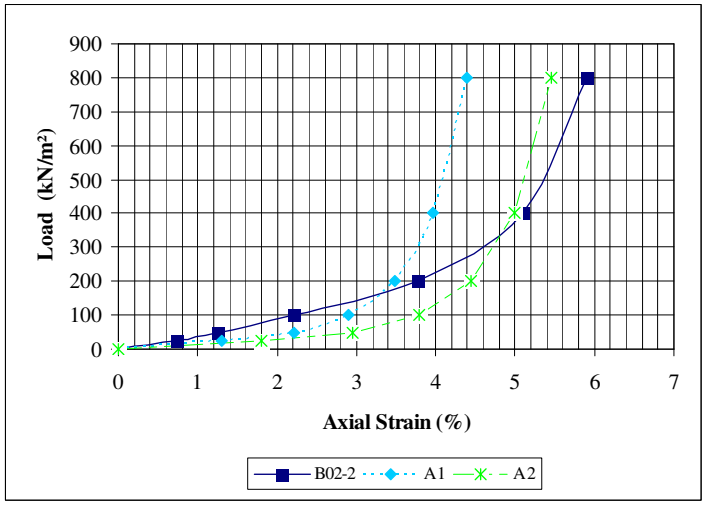
Load (kN/m²)
Axial Strain (%)
B02-2
A1
A2

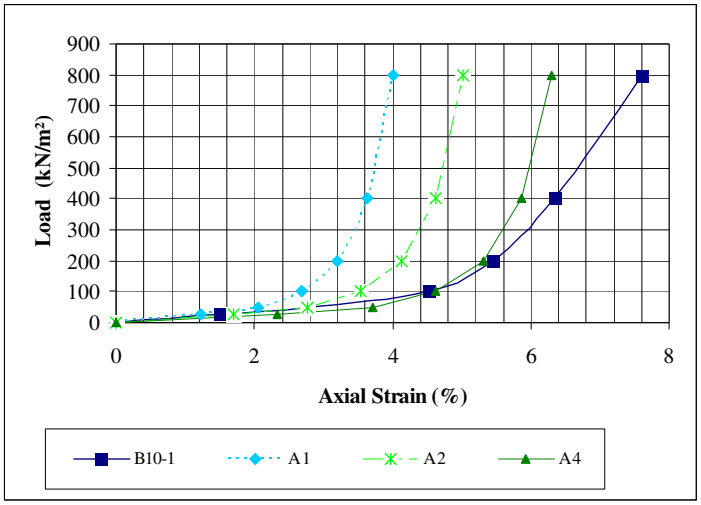
Load (kN/m²)
900
800
700
600
500
400
300
200
100
0
0
2
4
6
8
Axial Strain (%)
B10-1
A1
A2
A4

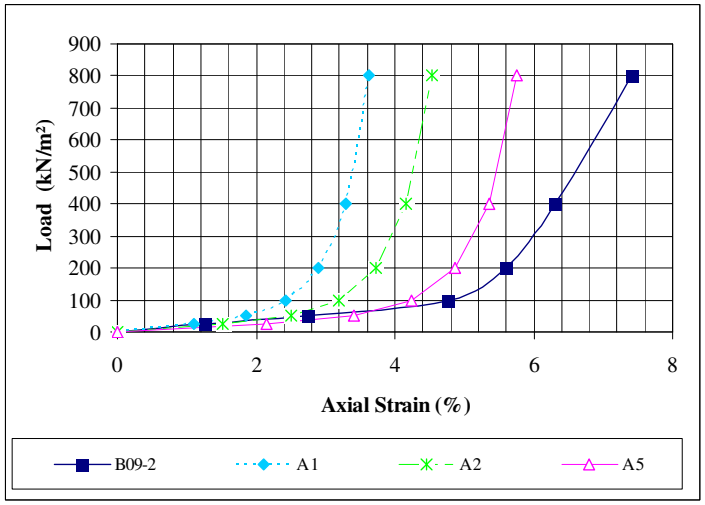
Load (kN/m²)
900
800
700
600
500
400
300
200
100
0
0
2
4
6
8
Axial Strain (%)
B09-2
A1
A2
A5

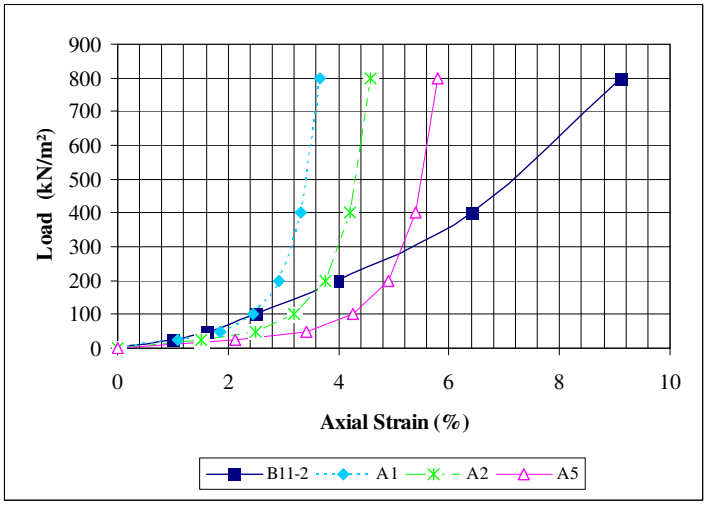
Load (kN/m²)
900
800
700
600
500
400
300
200
100
0
0
2
4
6
8
10
Axial Strain (%)
B11-2
A1
A2
A5

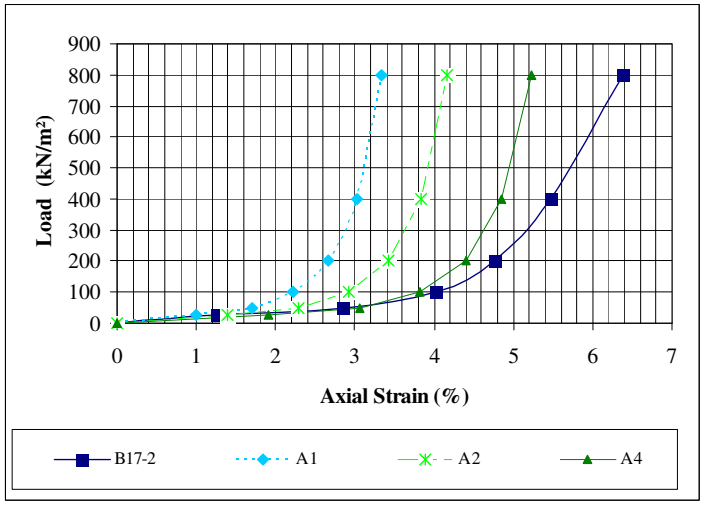
Load (kN/m²)
900
800
700
600
500
400
300
200
100
0
0
1
2
3
4
5
6
7
Axial Strain (%)
B17-2
A1
A2
A4

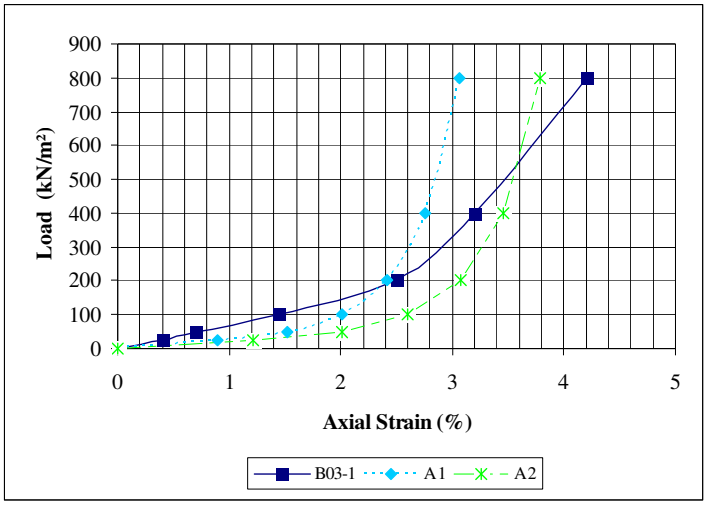
Load (kN/m²)
Axial Strain (%)
B03-1
A1
A2

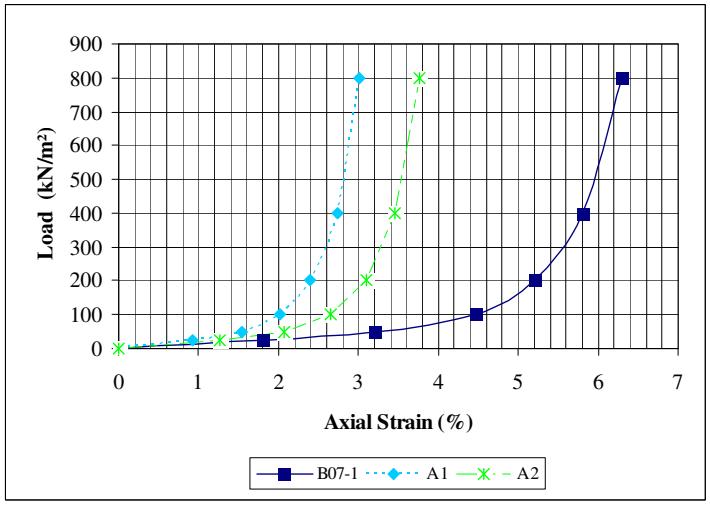
Load (kN/m²)
Axial Strain (%)
B07-1
A1
A2

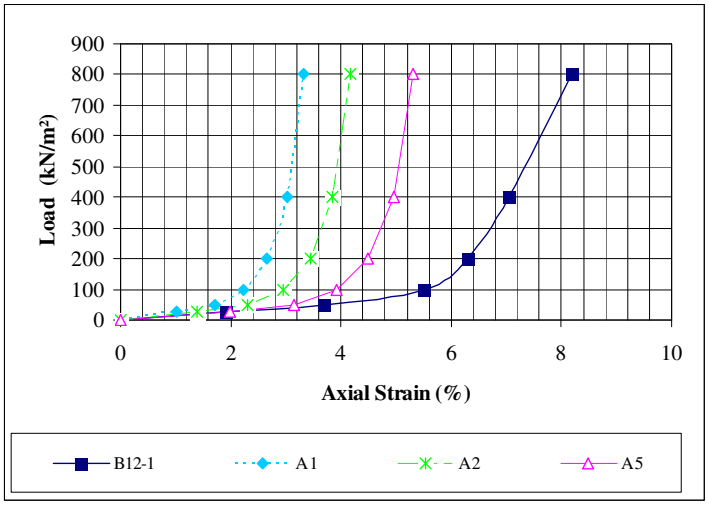
Load (kN/m²)
Axial Strain (%)
B12-1
A1
A2
A5

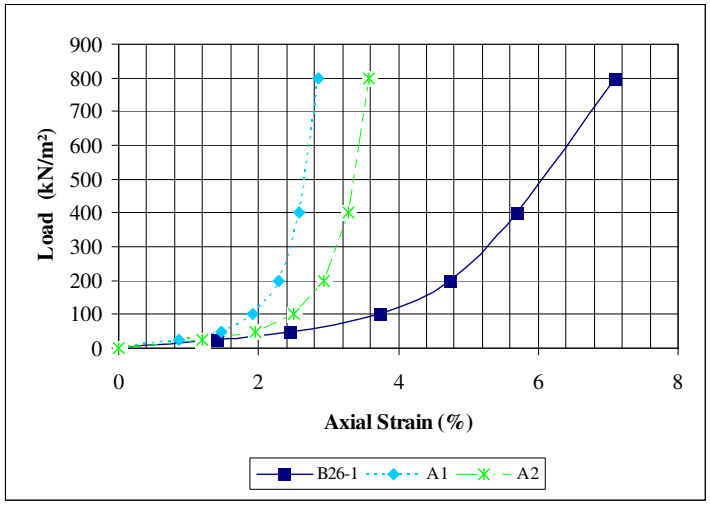
Load (kN/m²)
Axial Strain (%)
B26-1
A1
A2

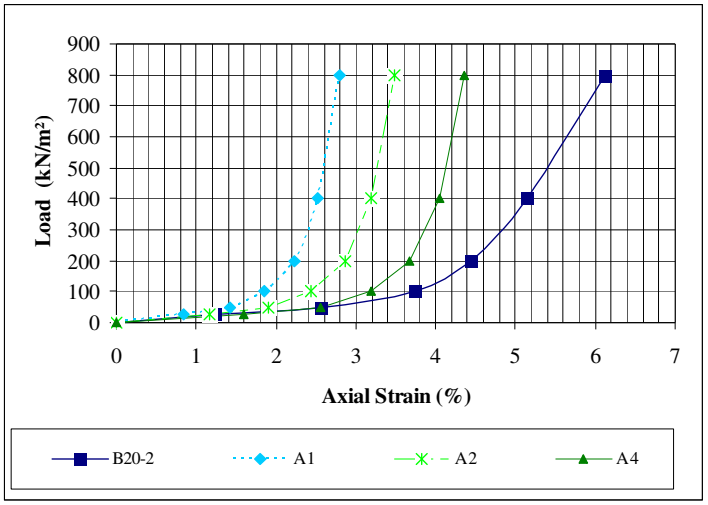
Load (kN/m²)
900
800
700
600
500
400
300
200
100
0
0 1 2 3 4 5 6 7
Axial Strain (%)
B20-2
A1
A2
A4

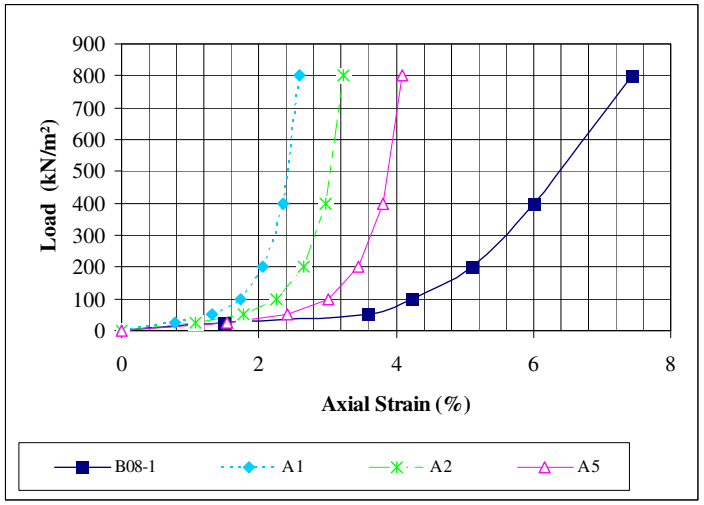
Load (kN/m²)
900
800
700
600
500
400
300
200
100
0
0 2 4 6 8
Axial Strain (%)
B08-1
A1
A2
A5

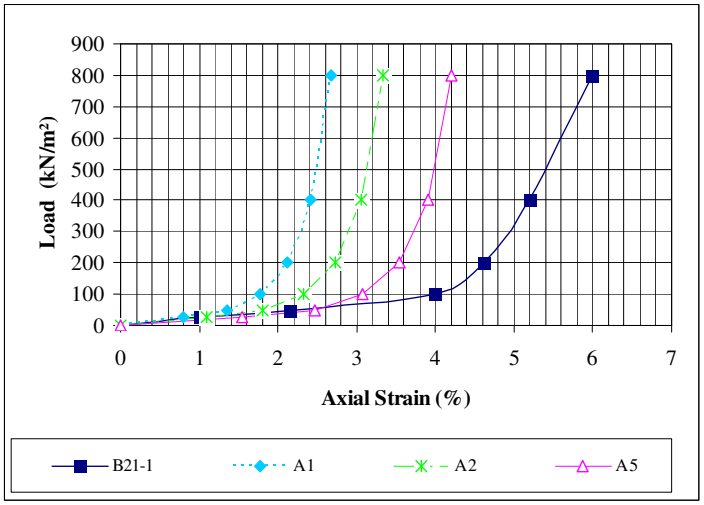
Load (kN/m²)
900
800
700
600
500
400
300
200
100
0
0 1 2 3 4 5 6 7
Axial Strain (%)
B21-1
A1
A2
A5

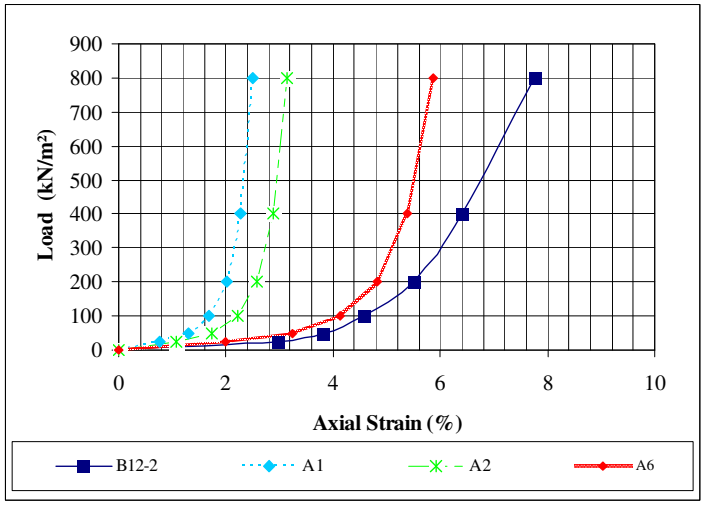
Load (kN/m²)
900
800
700
600
500
400
300
200
100
0
0 2 4 6 8 10
Axial Strain (%)
B12-2
A1
A2
A6

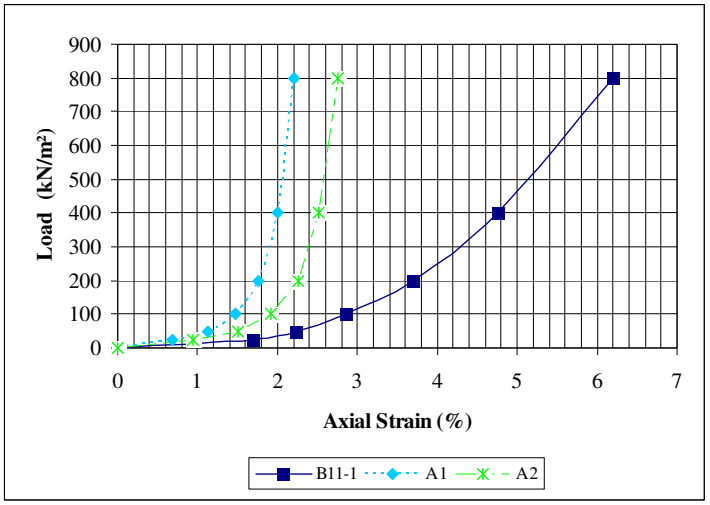
Load (kN/m²)
Axial Strain (%)
B11-1
A1
A2

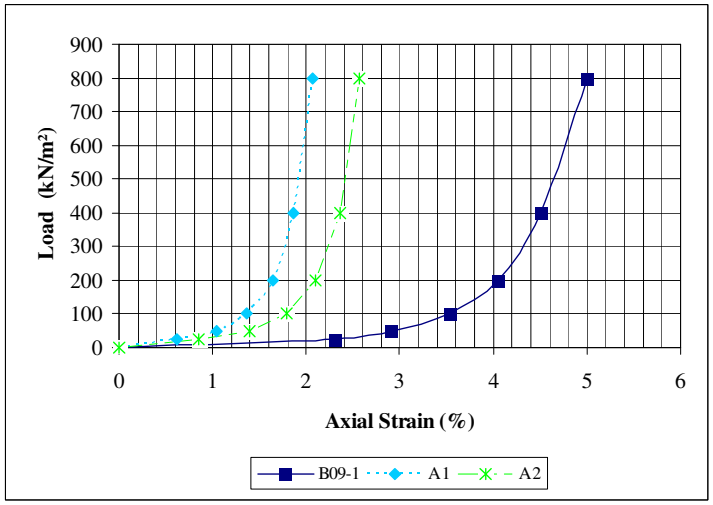
Load (kN/m²)
Axial Strain (%)
B09-1
A1
A2

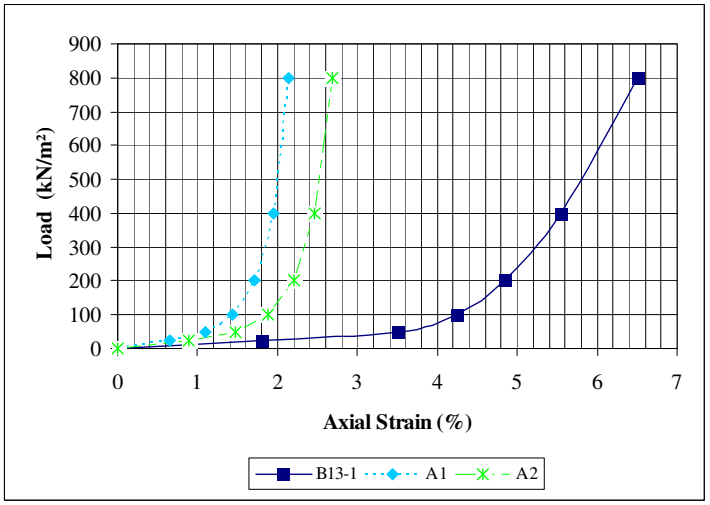
Load (kN/m²)
Axial Strain (%)
B13-1
A1
A2

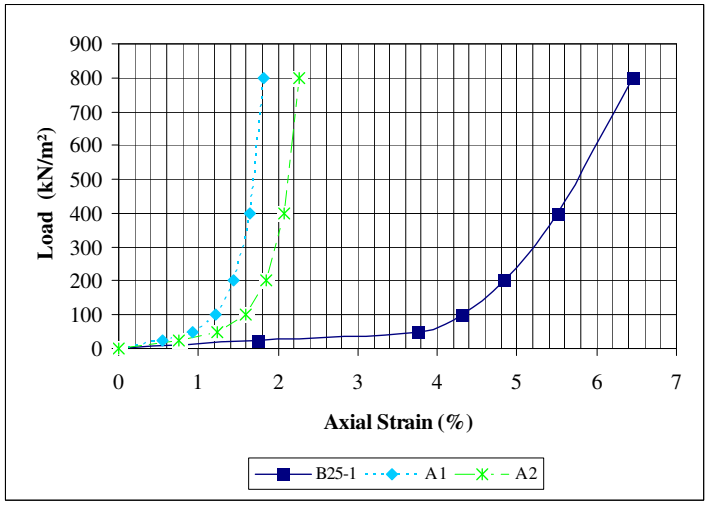
Load (kN/m²)
Axial Strain (%)
B25-1
A1
A2

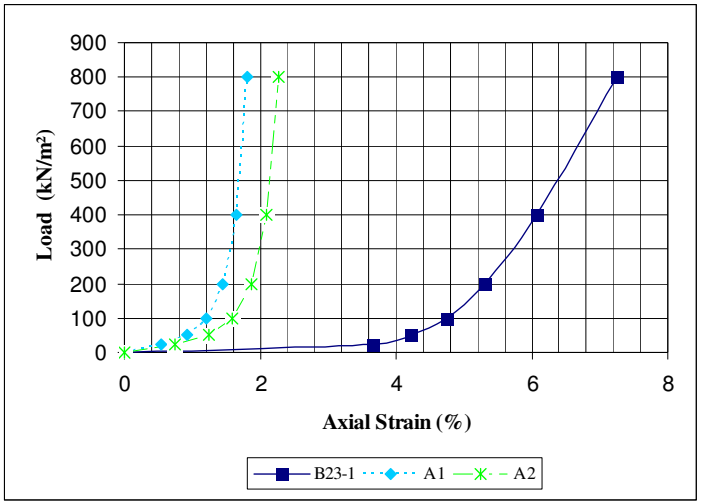
900
800
700
600
500
400
300
200
100
0
Load (kN/m²)
0
2
4
6
8
Axial Strain (%)
B23-1
A1
A2

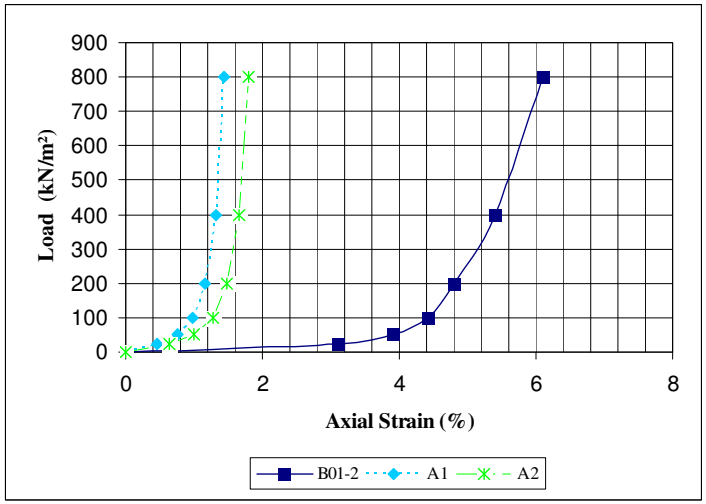
900
800
700
600
500
400
300
200
100
0
Load (kN/m²)
0
2
4
6
8
Axial Strain (%)
B01-2
A1
A2

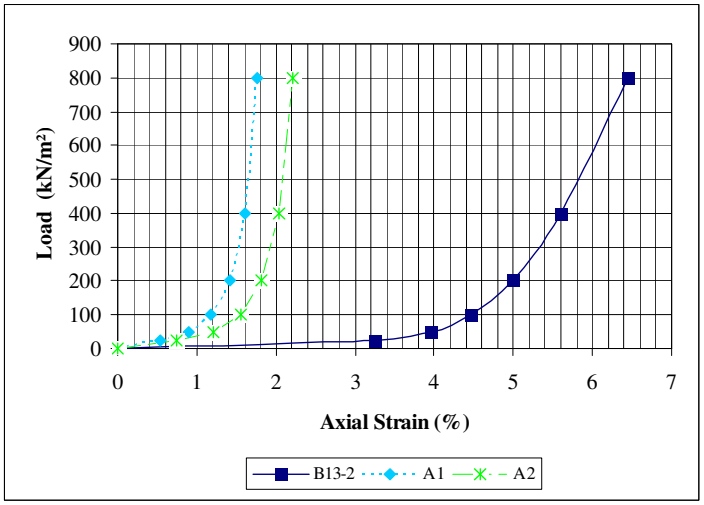
900
800
700
600
500
400
300
200
100
0
Load (kN/m²)
0
1
2
3
4
5
6
7
Axial Strain (%)
B13-2
A1
A2

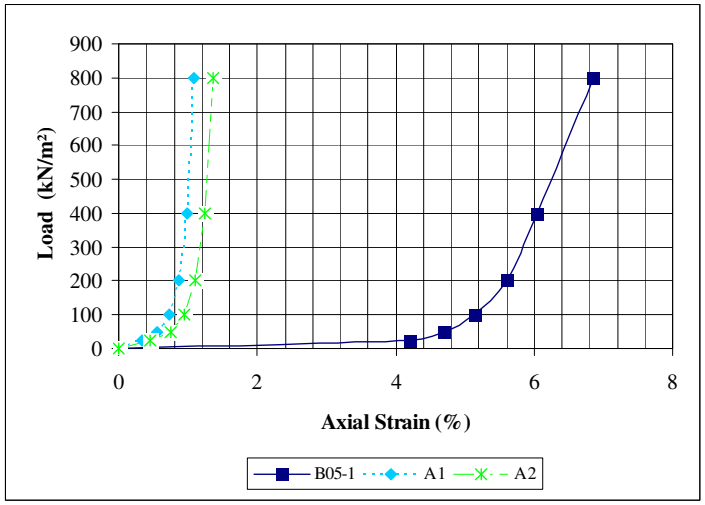
900
800
700
600
500
400
300
200
100
0
Load (kN/m²)
0
2
4
6
8
Axial Strain (%)
B05-1
A1
A2

Table H. 1 The found relations between the specimen and models

	Model name					
	E models	**A models**				
Specimen name	E*	A1	A2	A3	A4	A5
B15-1	–	–	–	+	–	–
B10-2	–	–	–	+	–	–
B20-1	–	+	–	–	–	–
B17-1	–	+	–	–	–	–
B19-1	–	+	–	–	–	–
B16-1	–	+	–	–	–	–
B24-1	–	–	+	–	–	–
B16-2	–	–	+	–	–	–
B18-1	–	–	+	–	–	–
B14-1	–	–	+	–	–	–
B18-2	+	–	+	–	–	–
B02-2	–	–	+	–	–	–
B10-1	+	–	–	–	+	–
B11-2	–	–	–	–	–	–
B09-2	+	–	–	–	–	+
B17-2	+	–	–	–	+	–
B03-1	–	–	+	–	–	–
B12-1	–	–	–	–	–	–
B07-1	–	–	–	–	–	–
B26-1	–	–	–	–	–	–
B20-2	+	–	+	–	–	–
B21-1	–	–	–	–	–	–
B08-1	–	–	–	–	–	–
B12-2	–	–	–	–	–	–
B11-1	–	–	–	–	–	–
B13-1	–	–	–	–	–	–
B09-1	–	–	–	–	–	–
B25-1	–	–	–	–	–	–
B23-1	–	–	–	–	–	–
B13-2	–	–	–	–	–	–
B01-2	–	–	–	–	–	–
B02-1	–	–	–	–	–	–
B05-1	–	–	–	–	–	–
B01-1	–	–	–	–	–	–

Table H. 2 The properties of Odeometer test of İZMİR bay areas soils

Speci-men name	Bore-hole No:	Tij	Depth(m):	USCS	γ nat (gr/cm³)	γ sat (gr/cm³)	γ dry (gr/cm³)	LL	PL	PI	e0	Cc	Loading States (kg/cm³)											
													0-0.25		0.25-0.50		0.50-1.00		1.00-2.00		2.00-4.00		4.00-8.00	
													cv	mv	cv	mv	cv	mv	cv	mv	cv	mv	cv	mv
B01-1	1	T1	3.00-3.45	SM	1.90	1.91	1.48	#	NP	#	0.76	0.24	684	150	255	46	441	28	241	17	302	10	289	6
B01-2	1	T7	13.50-13.95	OL	1.64	1.63	1.02	46	32	14	1.56	0.49	6.9	258	3.8	152	3.4	105	2.8	65	2.4	39	2.7	20
B02-1	2	T2	4.50-4.95	SM	1.94	1.90	1.46	#	NP	#	0.78	1.71	267	161	330	57	434	40	415	24	567	15	369	9
B02-2	2	T10	16.00-16.95	OH	1.76	1.80	1.23	72	40	32	1.29	0.42	15.9	77	11.3	52	10.9	46	7.7	38	5.8	30	6.1	18
B03-1	3	T10	18.50-18.95	CH	1.94	1.93	1.50	55	20	35	0.76	0.24	-	-	8.6	58	5.5	28	43	26	3	59	2.7	13
B05-1	5	T1	6.45-6.90	CL	1.63	1.60	0.97	50	26	24	1.71	0.55	27.9	243	15.1	171	13.6	127	9.9	74	10.1	41	8.5	22
B07-1	6	T4	18.50-18.95	CH	1.63	1.63	1.03	57	26	31	1.49	0.48	9.4	203	6.2	135	4.8	98	5.8	61	6.6	37	3.2	22
B08-1	8	T1	6.00-6.45	CH	1.69	1.66	1.07	61	31	30	1.48	0.52	68.7	86	47.3	94	33.9	98	24.9	71	166	39	96.7	18
B09-1	9	T1	5.50-5.95	CH	1.74	1.71	1.15	60	25	35	1.25	0.35	54.3	91	40.8	63	17.7	61	12.7	59	11.1	40	7.2	23
B09-2	9	T4	18.00-18.45	CH	1.64	1.62	1.01	74	25	49	1.57	0.57	73.1	222	44.1	122	17.9	91	43.6	43	39.6	28	44.2	16
B10-1	10	T1	8.00-8.45	CH	1.49	1.64	1.03	62	31	31	1.57	0.47	34.1	168	17.7	114	14.8	80	8.8	75	7.6	40	6.4	23
B10-2	10	T3	15.00-15.45	CH	1.67	1.67	1.07	64	23	41	1.5	0.59	71.5	146	37.5	95	37.9	78	38.5	50	38.2	32	27	18
B11-1	11	T1	10.50-10.95	OH	1.71	1.71	1.15	56	35	21	1.27	0.42	142	163	145	93	152	61	128	41	85	32	70	18
B11-2	11	T3	15.00-15.45	OH	1.64	1.64	1.03	79	36	43	1.59	0.69	23	159	19	75	205	58	16	39	9	47	6.5	26
B12-1	12	T1	8.00-8.45	OH	1.58	1.58	0.93	77	39	38	1.88	0.71	39	172	33	168	18	98	8.4	83	7.5	48	39.6	10
B12-2	12	T3	18.00-18.45	OH	1.61	1.60	0.96	66	35	31	1.78	0.63	31	185	12	127	9.6	101	9.8	75	8.4	42	8.3	24
B13-1	13	T2	12.00-12.45	OH	1.68	1.64	1.05	70	36	34	1.43	0.48	42.6	168	226	97	18.6	86	16.8	61	14.8	35	12.7	20
B13-2	13	T4	17.00-17.45	OH	1.62	1.62	1.00	74	34	40	1.58	0.52	17	190	7.8	190	7.2	98	5.6	66	6.4	35	5.7	21
B14-1	14	T4	17.00-17.45	OH	1.68	1.66	1.07	70	34	36	1.45	0.49	13.2	143	8.1	97	3.1	91	3	66	2.9	34	3.1	20

Table H. 2 The properties of Odeometer test of İZMİR bay areas soils (continued)

Speci-men name	Bore-hole No:	Tij	Depth(m):	USCS	γ nat (gr/cm^3)	γ sat (gr/cm^3)	γ dry (gr/cm^3)	LL	PL	PI	e0	Cc	Loading States (kg/cm^3)											
													0-0.25		0.25-0.50		0.50-1.00		1.00-2.00		2.00-4.00		4.00-8.00	
													cv	mv	cv	mv	cv	mv	cv	mv	cv	mv	cv	mv
B15-1	15	T1	6.50-6.95	OH	1.63	1.59	0.97	78	38	40	1.67	0.62	13.2	136	14.8	77	8.5	87	8.1	67	5.6	41	8.3	24
B16-1	16	T2	11.50-11.95	OH	1.71	1.69	1.11	63	30	33	1.36	0.57	21.8	87	24	54	20.2	47	7.1	54	6.5	42	7.3	23
B16-2	16	T3	17.50-17.95	CL	1.65	1.71	1.18	45	28	17	1.12	0.5	43.1	120	32.9	68	20.8	75	10.3	73	7.9	43	8	23
B17-1	17	T1	6.50-6.95	CH	1.63	1.61	1.00	69	25	44	1.53	0.65	37.8	97	40.6	71	26.4	66	10.9	56	7	49	7.5	25
B17-2	17	T3	17.50-17.95	OH	1.69	1.63	1.05	70	35	35	1.42	0.47	15.5	160	16.1	90	13.1	75	6.9	61	7.8	34	7.4	20
B18-1	18	T2	12.50-12.95	OH	1.70	1.66	1.08	70	35	35	1.42	0.53	96.7	81	62.3	58	47.5	56	29.9	49	13.9	38	12.3	21
B18-2	18	T3	19.00-19.45	OH	1.65	1.65	1.05	65	32	33	1.52	0.55	45.6	105	36.8	72	15.6	82	11.7	62	9.4	40	6.9	21
B19-1	19	T4	16.50-16.95	OH	1.72	1.67	1.11	70	35	35	1.28	0.52	-	-	147	18	142	43	32.9	56	21.9	40	16.8	21
B20-1	20	T1	11.00-11.45	OH	1.67	1.67	1.07	60	29	31	1.46	0.57	75.5	92	38.1	53	36	42	9.9	61	5.9	41	6.8	22
B20-2	20	T4	21.00-21.45	OH	1.70	1.68	1.11	65	34	31	1.31	0.43	49.4	107	23.6	77	12.1	68	11.1	54	9.8	31	10.2	19
B21-1	21	T3	15.50-15.95	OH	1.74	1.72	1.14	72	35	37	1.36	0.44	33	137	25	84	15.2	71	14.1	55	15.6	31	9.1	19
B23-1	23	T1	9.50-9.95	CH	1.60	1.60	0.97	76	31	45	1.68	0.58	37.8	182	19.7	121	17	111	12.8	69	9.3	41	-	22
B24-1	24	T2	10.00-10.45	CH	1.69	1.68	1.08	67	38	39	1.48	0.58	-	84	51.2	57	40	47	32.3	72	8.7	42	9	23
B25-1	25	T1	5.50-5.95	CH	1.67	1.67	1.06	68	30	38	1.59	0.49	55.6	132	29.5	96	18.5	92	22.4	75	14.5	34	11.8	20
B26-1	26	T4	13.50-13.95	CH	1.66	1.65	1.04	71	34	37	1.61	0.69	26.4	138	17	103	12.6	81	15.3	54	9.9	49	8.4	43

Table H. 3 The research of the fitting curve with using PLAXIS program in between initial curve and final curve

Curve	**γ sat**	**γ unsat**	**E-50**	**E-oed**	**E-ur**	**φ**	**m**	**ν ur**	**ψ**	Loading (kN/m^2)						
Name	kN/m^2	kN/m^2	kN/m^2	kN/m^2	kN/m^2	º	–	–	º	0	25	50	100	200	400	800
initial curve										0	0.60	1.15	2.25	4.00	5.05	5.75
final curve										0	2.60	3.70	4.95	5.95	6.80	8.10
M1	17	16	4000	2000	12000	27	1	0.2	0	0	5.81	9.64	12.22	14.15	15.66	16.86
M2	17	16	8000	4000	24000	27	1	0.2	0	0	2.97	4.90	6.19	7.15	7.90	8.51
M3	17	16	9000	4000	24000	27	1	0.2	0	0	2.819	4.745	6.043	7.009	7.764	8.365
M4	17	16	10000	6000	30000	27	1	0.2	0	0	2.002	3.267	4.117	4.757	5.253	5.656
M5	17	16	9500	5000	28500	27	1	0.2	0	0	2.344	3.874	4.905	5.676	6.275	6.759
M6	17	16	9600	4500	28500	27	1	0.2	0	0	2.547	4.257	5.403	6.258	6.926	7.465
M7	17	16	9510	4900	27000	27	1	0.2	0	0	2.406	3.974	5.022	5.806	6.42	6.916
M8	17	16	9510	4800	27000	27	1	0.2	3	0	2.446	4.048	5.126	5.924	6.55	7.055
M9	17	16	9510	4800	27000	27	1	0.2	10	0	2.446	4.048	5.126	5.924	6.55	7.055
M10	17	16	9500	5000	40000	27	1	0.2	0	0	1.178	2.227	3.018	3.634	4.128	4.538
M11	17	16	9000	4500	27000	27	0.75	0.2	0	0	1.146	2.041	2.74	3.32	3.816	4.244
M12	17	16	6000	4500	18000	27	0.75	0.2	0	0	1.239	2.137	2.836	3.425	3.924	4.358
M13	17	16	6000	4500	12000	27	0.75	0.2	0	0	1.299	2.22	2.932	3.529	4.033	4.47
M14	17	16	6000	4000	18000	27	0.85	0.15	0	0	1.925	3.233	4.191	4.963	5.597	6.134
M15	17	16	6000	3500	18000	27	0.85	0.2	0	0	2.088	3.573	4.666	5.546	6.274	6.881
M16	17	16	6000	3500	18000	27	0.75	0.2	0	0	1.526	2.683	3.58	4.333	4.977	5.535
M17	17	16	6000	3500	21000	27	0.75	0.2	0	0	1.487	2.627	3.523	4.269	4.908	5.462
M18	17	16	6000	3500	21000	27	0.75	0.15	0	0	1.534	2.69	3.592	4.348	4.989	5.545
M19	17	16	6000	3500	40000	27	0.75	0.2	0	0	0.318	0.479	0.637	0.788	0.933	1.068
M20	17	16	9000	5000	32000	27	0.75	0.2	0	0	1.018	1.812	2.437	2.959	3.405	3.791
M21	17	16	9000	5000	27000	27	0.75	0.2	0	0	1.057	1.866	2.498	3.027	3.475	3.863
M22	17	16	9000	5000	27000	27	0.75	0.15	0	0	1.09	1.909	2.544	3.075	3.529	3.917
M23	17	16	9000	5000	27000	27	0.85	0.15	0	0	1.506	2.56	3.332	3.946	4.455	4.884
M24	17	16	10000	5000	30000	27	0.85	0.15	0	0	1.468	2.522	3.296	3.911	4.418	4.845
M25	17	16	9000	5000	20000	27	0.85	0.15	0	0	1.553	2.623	3.4	4.021	4.534	4.96

Table H. 4 The properties of G model series

Curve name	γ sat kN/m^2	γ unsat kN/m^2	E-50 kN/m^2	E-oed kN/m^2	E-ur kN/m^2	φ º	m –	ν ur –	ψ º	Loading 0	25	50	100	200	400	800
initial curve	–	–	–	–	–	–	–	–	–	0	0.60	1.15	2.24	4.00	5.05	5.75
final curve	–	–	–	–	–	–	–	–	–	0	2.60	3.70	4.95	5.95	6.80	8.10
G1	17	16	9500	4990	28500	27	0.85	0.15	0	0	1.483	2.533	3.304	3.921	4.431	4.856
G2	17	16	8000	5000	24000	27	0.85	0.15	0	0	1.835	3.153	4.12	4.888	5.523	6.057
G3	17	16	9000	4500	20500	27	0.85	0.15	0	0	1.692	2.887	3.754	4.445	5.008	5.483
G4	17	16	9000	4500	20500	27	0.9	0.15	0	0	1.988	3.338	4.287	5.026	5.627	6.125
G5	17	16	9000	4500	20500	27	0.95	0.15	0	0	2.336	3.866	4.911	5.708	6.343	6.864
G6	17	16	9000	4500	20500	27	1	0.15	0	0	2.733	4.472	5.622	6.48	7.152	7.695